Experimental and Modeling Study on the Absorption of CO_2 in Aqueous Single and Blended Amines

Anirban Dey

Experimental and Modeling Study on the Absorption of CO_2 in Aqueous Single and Blended Amines

Thesis

Submitted in partial fulfillment of the
Requirements for the degree of

DOCTOR OF PHILOSOPHY

By

Anirban Dey
(Roll No. 146107017)

Department of Chemical Engineering

Indian Institute of Technology Guwahati

Guwahati-781039, Assam, India

November 2019

Dedicated to my Wife, Parents,

Mentor

And

Little Aayansh

Department of Chemical Engineering
Indian Institute of Technology Guwahati
Guwahati 781039, Assam, India

CERTIFICATE

It is certified that the work contained in this thesis entitled "***Experimental and Modeling study on the absorption of CO_2 in aqueous single and blended amines***" submitted by Mr. Anirban Dey for the award of the degree of Doctor of Philosophy has been carried out in the Department of Chemical Engineering, Indian Institute of Technology Guwahati under our supervision and this work has not been submitted elsewhere for the award of any other degree or diploma.

This thesis in our opinion, has reached the standard fulfilling the requirements for the award of the degree of Doctor of Philosophy in accordance with the regulations of the institute.

(Dr. Bishnupada Mandal)
Professor
Department of Chemical Engineering
Indian Institute of Technology Guwahati
Guwahati 781039, India

(Dr. Sukanta Kumar Dash)
Assistant Professor
Department of Chemical Engineering
Pandit Deendayal Petroleum University
Gandhinagar, Gujarat-32007,India

Acknowledgement

I take this opportunity to express my deep sense of respect and sincere gratitude to my thesis supervisors, **Prof. Bishnupada Mandal** and **Dr. Sukanta Kumar Dash** for giving me an opportunity to work under their supervision for my doctoral program at the Indian Institute of Technology Guwahati. I am indebted to Prof. Mandal and Dr. Dash for their valuable guidance and encouragement throughout this research program and instilling in me a relentless quest for perfection. Their expertise in the field of gas separation via chemical absorption gives me new insights towards my research work. The experience of working with them, I strongly believe, will have far-reaching influence in my future life.

I am also thankful to my doctoral committee members, **Prof. G. Pugazhenti, Prof. Chandan Das**, Department of Chemical Engineering and **Prof. Lal Mohan Kundu**, Department of Chemistry, for their valuable suggestions and instructions at each and every stage of this research program.

I must also thank my departmental colleagues at Pandit Deendayal Petroleum University for their constant support and motivation. I am thankful to **Dr. Swapnil Dharaskar**, HOD, **Dr. Pravin Kodgire**, **Dr. Manish Sinha, Dr. Surendra Sasikumar, Dr. Ashish Unnarkat** for their constant support and motivation throughout my research work. I would also like to thank the entire **PDPU** fraternity for providing me the platform for pursuing my doctoral research work and for extending help in every ways for the successful completion of thesis work.

I would also like to express my sincere gratitude to **Prof. S.S. Bandyopadhyay** and Dr**. Anurag Gupta**, Senior Mentors of our department, for their valuable suggestions to enhance my doctoral work.

I am also thankful to the technical staffs of our department for their sincere help and support during this work. I would like to thank all the staffs specially **Mr. Umang Soni**, **Mr. Prashant Patel, Mr. Rajesh Vanaspati** of PDPU **and Mr. Bhagya Boro** of IIT Guwahati, for their support in various forms

I would also like to extend special thanks to **Ms. Sweta Balchandani** and **Mrs. Bharti Saini**, my colleagues cum friends at PDPU, for their immense help and co-operation during my doctoral program. Various research based discussion with Ms. Sweta, my research group mate as well as her good analytical skills really helped me a lot in the modeling of current research problem undertaken. I am also thankful to my Research group colleagues / friends at IIT Guwahati for their support and contribution, **Ms. Rajashree, Mr. Rahul, Mr. Pradip, Mr. Surendra, Mr. Bhargav, Mr. Ramesh, and Ms. Mridusmita**. I am also fortunate enough to get excellent colleagues cum friends during my doctoral research tenure, **Mr. Darshit Shah, Mr. Manivel M, Mr. Akshay Jain, Mr. Vipin Shukla, Mrs. Anvita Sharma, Mrs. Niragi Dave, Mr. Abhishek Kumar Singh, Mr. Vikram Rathore, Mr. G. Vaitheeswaran.** I would like to thank all of them for their friendly co-operation during my research work. I am alo

I express my humble regards and respect to my **Parents and family members**. Their love, care, sacrifices and encouragement have made it possible for me to come so far. Finally, I would like to thank my beloved wife, **Tandra**, for her immense support, sacrifice and patience at all stages of this work all these years. She is not only a wonderful wife and mother to our beloved son, **Aayansh**, she is an exceptionally understanding and caring person. Her immense contributions to our home specially in bringing up Aayansh made my time at work easier and her companionship has made me a better person. I am also very much thankful to almighty God for blessing us with cute Aayansh in our life. Light moments with him really take away every bit of stress during the final stage of research work.

ANIRBAN

VITAE

Anirban Dey

Date of birth: March 04,1989

Email: Anirbanb4u@gmail.com, Anirban.dey@sot.pdpu.ac.in

Permanent Address
PO/Vill- Panchgram
Dist- Hailakandi
Assam,India
Pin-788802
Ph- 9435567691

Present Address
D-704, Shyam Shukan Residency
PDPU Cross-Road
Gandhinagar, Gujarat
Pin-382007
Ph: 82338654934

Education

- PhD (Thesis submitted)
  Department of Chemical Engineering
  Indian Institute of Technology Guwahati
  Guwahati, Assam, India

- M.Tech (Chemical Engineering)
  Department of Chemical Engineering
  Indian Institute of Technology Guwahati
  Guwahati, Assam, India
  (2011-2013)

- BE (Chemical Engineering)
  Department of Chemical Engineering
  Assam Engineering College
  Guwahati, Assam India
  (2007-2011)

Experience

- Lecturer
  July 2013- July 2019
- Assistant Professor
  July 2019-Till date

Department of Chemical Engineering,
Pandit Deendayal Petroleum University,
Gandhinagar, Gujarat, India

VITAE

Publications

Journal Papers

1. A. Dey, S.K. Dash, B. Mandal, Equilibrium CO_2 solubility and thermophysical properties of aqueous blends of (1-(2-aminoethyl) piperazine + N-methyldiethanolamine) for CO_2 absorption, ***Journal of Fluid Phase Equilibria***, 463 (2018 , 91-105.

2. A. Dey, S.K. Dash, S.C. Balchandani, B. Mandal, Investigation on the inclusion of 1-(2-aminoethyl) piperazine on the equilibrium CO_2 solubility of aqueous 2-amino-2-methyl-1-propanol, ***Journal of Molecular liquids***, 289 (2019), doi.org/10.1016/j.molliq.2019.111036.

3. A. Dey, S.K. Dash, B. Mandal, Analysis of Equilibrium CO_2 solubility in aqueous APDA and its potential blends with AMP/MDEA for Post- combustion CO_2 capture, ***International Journal of Energy Research***, (Accepted 05.03.20).

4. A. Dey, S.K. Dash, B. Mandal, Investigation on the vapour liquid equilibrium of CO_2 in aqueous blend of *N*-(3-Aminopropyl)-1,3-propanediamine (APDA) and 1-dimethylamino-2-propanol (1DMAP) (Submitted).

5. S.C. Balchandani, B. Mandal, **A. Dey**, A. Kumar, S. Garg, S. Dharaskar, Experimental investigation and KE modeling of CO2 solubility in reversible ionic liquid solvents for post combustion processes, ***Journal of Industrial and Engineering Chemistry*** (Under Review).

VITAE

Papers in Conferences

1. A. Dey, S.K. Dash, B. Mandal, Elucidating the effect of addition of 1-(2-aminoethyl) piperazine as an activator on the CO_2 solubility of aqueous *N*-methyldiethanoalmine, *IV International conference on "Sustainable Energy and Environmental Challenges"*, CSIR-NEERI, 27-29 November 2019.

2. A. Dey, S.K. Dash, B. Mandal, Effects of various key process parameters on the reboiler heat duty of CO_2 capture unit', *12th International conference on thermal Engineering: Theory and applications (ICTEA 2019)*, PDPU, 23 – 26 February 2019.

3. A. Dey, S.K. Dash, B. Mandal, Optimization of various process parameters on the % CO_2 removal of Post combustion CO_2 capture unit using aqueous single and blended amine solvent, *International conference on Renewable energy and climate change (REC 2019)*, IITRAM, 1-2 February 2019.

4. S.K.Dash, M. Firake, **A. Dey**, Post Combustion CO_2 Absorption into Potential Aqueous Blended Amines: Thermodynamic Study, Kinetics and Thermo-Physical Properties. *14th Greenhouse Gas Control Technologies Conference*, Melbourne 21 - 26 October 2018.

5. A. Dey, S.K. Dash, B. Mandal, Investigation of equilibrium CO_2 solubility in aqueous 1-(2-aminoethyl)piperazine (AEP) and its blend with monoethanolamine (MEA) , N-methyldiethanolamine (MDEA) and 2-Amino-2-methyl-1-propanol (AMP)', *Conference on Carbon Capture and Utilization*, NCL Pune, 14 – 15 December 2018.

6. A. Dey, S.K. Dash, B. Mandal, Equilibrium solubility measurement and performance study of aqueous 1-(2-aminoethyl) piperazine (AEP) over monoethanolamine (MEA) for carbon dioxide absorption, *International conference on advances in energy research (ICAER-2017*), IIT Bombay, 12 – 14 December 2017.

7. A. Dey, S.K. Dash, B. Mandal, Vapour liquid equilibrium measurement of CO_2 absorption in aqueous 1-(2-aminoethyl) Piperazine (AEP)), *19th International conference on Environmental pollution control and prevention*, Mumbai, Feb 2017.

8. A. Dey, S.K. Dash, B. Mandal, Density, viscosity and surface tension of aqueous solution of 2-MPZ, *CHEMCON 2015, IIT Guwahati*, 27 – 30 December 2015.

9. A. Dey, S.K. Dash, B. Mandal, Carbon dioxide absorption in monoethanolamine in a packed bed tower, *5th International conference on advances in energy research (ICAER-2015)*, IIT Bombay, 15 - 17 December 2011.

ABSTRACT

Experimental and Modeling Study on the Absorption of CO_2 in Aqueous Single and Blended Amines

In recent times the increase in global warming issue across the world motivates researchers to develop more improved technologies to reduce greenhouse gas such as carbon dioxide (CO_2) emission to the environment from thermal power plants and process industries. In this regard, regenerative CO_2 separation technology in which aqueous amine solutions absorb CO_2 or other acid gases proved to be an efficient technology to combat this issue. Polyamines consisting of more than one amine groups are considered as the potential activator in CO_2 and H_2S (hydrogen sulfide) gas removal technology.

The present work investigates two potential amine activators, 1-(2-aminoethyl) piperazine (AEP) and N-(3-aminopropyl)-1,3-propanediamine (APDA) for its applicability in efficient CO_2 capture from flue gas streams. The study reports new experimental CO_2 solubility data of absorption in various compositions of aqueous AEP and APDA system over the broad temperature and pressure range of (303.2-323.2) K and (3-300) kPa, respectively. Along with binary system, different blended system with non-carbamate forming amines such as N-methyldiethanolamine (MDEA), 2-amino-2-methyl-1-propanol (AMP) and 1-dimethylamino-2-propanol (1DMAP) have been also explored in the current work. The blended amine systems considered in this work are aqueous (AEP + MDEA), (AEP + AMP), (APDA + MDEA), (APDA + AMP) and (APDA + DMAP), respectively. The experimental solubility data is modeled using modified Kent-Eisenberg (KE) equilibrium model. The equilibrium constants related to amine deprotonation, and carbamate formation reactions are regressed as a function of important operating parameters such as, CO_2 partial pressure, amine concentration and temperature to fit the equilibrium CO_2 solubility data. The model predicted solubility results from KE model are in good agreement with the experimental data. The application of the modified KE model developed in this study can be further extended in estimating the concentrations of various ionic species at equilibrium conditions in the solvent phase. The distribution of various reaction species resulting from CO_2 –

amine reaction with the variation of α_{CO_2} has been estimated. The KE model can also be used to predict the pH of the CO_2 loaded amine solvents. Appropriate knowledge of pH of the loaded solvent is very important from the point of view of the design of CO_2 capture processes. The solubility data is also correlated using Feed forward Artificial Neural Network (ANN) model. The ANN architecture used in this work consists of Levenberg-Marquardt back propagation algorithm as training function. The transfer function implemented for hidden and output layers are hyperbolic tangent sigmoid functions and linear function, respectively. The predicted value from the feed forward neural network model shows very good agreement with the experimental data. In addition to this, ATR-FTIR and qualitative ^{13}C NMR have been also conducted to interpret the various important reaction products as well as to assess the reaction scheme of CO_2-amine reaction. A comprehensive comparison of CO_2 loading with other conventional solvents has been presented to assess the performance of studied solvents in the present work.

For detail characterization of the solvent, important thermophysical properties are measured and correlated throughout the experimental range. Thermophysical properties such as density, viscosity and surface tension of aqueous binary and ternary system have been measured in the temperature range of (303.2 to 343.2) K. The experimental binary and ternary density data as well as binary viscosity data were correlated by Redlich–Kister equation whereas ternary viscosity data were correlated by Grunberg and Nissan model. The density and viscosity data were modeled as a function of temperature and amine composition. The model results of these temperature dependent physical properties are also in good agreement with the experimental data. The surface tension data of the aqueous amine system has been correlated with temperature based correlation and multiple linear regression technique. The experimental viscosity data can be further utilized to analyze various thermodynamic properties such as Enthalpy (ΔH^o), Entropy (ΔS^o) and Gibbs energies (ΔG^o) of activation of viscous flow. The generated experimental solubility, thermophysical property data and the correlations developed in this work will allow for prediction of blend properties, thus significantly enhances the prediction capability of aqueous alkanolamines solutions for process design.

LIST OF CONTENTS

LIST OF TABLES

List of figures

Abbreviation

P_{CO_2}	Equilibrium CO_2 partial pressure, (kPa)
P^T	Total pressure in the equilibrium cell, (kPa)
P^v	Solution Vapour pressure in the equilibrium cell, (kPa)
P_{b1}	Initial buffer cell pressure, (kPa)
P_{b2}	Final buffer cell pressure, (kPa)
w	Mass fraction of amine
T	Temperature, (K)
V_b	Volume of buffer cell, (m^3)
V^g	Volume of gas phase in the equilibrium cell
R	Universal gas constant, (8.314 J. mole $^{-1}K^{-1}$)
n_{CO_2}	Moles of CO_2 transferred from buffer cell to equilibrium cell
$n^g{}_{CO_2}$	Moles of CO_2 corresponding to gas phase in the equilibrium cell
n_{am}	Moles of amine in the solvent mixture
Z_1	Compressibility factor corresponding to initial buffer cell pressure
Z_2	Compressibility factor corresponding to final buffer cell pressure
Z_{CO_2}	Compressibility factor corresponding to the equilibrium P_{CO2}
K	Reaction Equilibrium constant
H_{CO_2}	Henry's Law constant of CO_2 in the solvent
S	Error in objective function
N	Total set of data points
m_1	Initial AEP molar concentration, ($kmol.m^{-3}$)
m_2	Initial MDEA molar concentration, ($kmol.m^{-3}$)
X_i	Input variable
Y_i	Output variable
w_i	Weight coefficient
b_i	Bias associated with each weight coefficient
u	Standard uncertainty in the measured variable
V^E	Excess Molar volume, ($m^3.kmol^{-1}$)
A^p	Temperature based pair parameter for correlating excess molar volume.
V_i^o	Volume of pure component in the aqueous amine mixture, ($m^3.kmol^{-1}$)
V_m	Volume of aqueous amine mixture, ($m^3.kmol^{-1}$)
ρ_m	Experimentally measured density of aqueous amine mixture, ($Kg.m^{-3}$)
x_i	Mole fraction of pure component in the amine mixture
α_{CO2}	CO_2 loading in the solvent phase, (mole CO_2/ mole of amine)
μ_m	Experimentally measured viscosity of aqueous amine mixture, (mPa.s)

G_{ij}	Temperature based pair parameter for correlating viscosity data.
η	Kinematic viscosity of amine mixture, ($m^2.sec^{-1}$)
h	Planck's constant (6.6262×10^{-34}), joule.s
N_A	Avagadro's number (6.0225×10^{23}), mol^{-1}
M	Average molar mass of the amine mixture
ΔH°	Enthalpy of activation of viscous flow, ($kJ.mol^{-1}$)
ΔG°	Gibbs energy change of activation of viscous flow, ($kJ.mol^{-1}$)
ΔS°	Entropy change of activation of viscous flow, ($J.K^{-1}.mol^{-1}$)
Υ	Surface tension of the aqueous amine mixture ($mN.m^{-1}$)
MEA	Monoethanolamine
DEA	Diethanolamine
MDEA	*N*-Methyldiethanoalmine
AMP	2-Amino-2-methyl-1-propanol
AEP	1-(2-Aminoethyl) piperazine
APDA	*N*-(3-Aminopropyl)-1,3-propanediamine
1DMAP	1-Dimethylamino-2-propanol
AAD	Average absolute deviation
MSE	Mean square error

Chapter 1

INTRODUCTION, LITERATURE REVIEW AND OBJECTIVES

This chapter presents the current trends in global greenhouse gas emissions and its impact on the environment. The importance of adopting efficient CCS technologies along with a brief discussion on various carbon capture technologies has been presented. The chapter also presents an extensive literature review related to chemical absorption via aqueous single and blended amine systems. It elaborates on the background of research work as well as the importance and objectives of undertaken research work are also formulated.

1.1 Background

In recent years global warming and climate change issues resulting from the mass emission of greenhouse gases and other ozone-depleting substances, especially CO_2, has turn out to be a global concern. Driven by higher energy demand globally, the CO_2 emission from the energy-related sources increases 1.7 % to a historic high value of 33.1 Gt of CO_2 in 2018 [1]. This was the highest ever growth recorded since 2013 and also 70 % higher than the annual average rate since 2010. The higher emission is the result of higher energy demand and a robust global economy. Also due to extreme weather conditions in some parts of the world, the demand for excess energy for the extra cooling as well as heating also rises. While different sources contribute substantially to the higher emissions, the power sector accounted for nearly 2/3rd of total growth in the global greenhouse gas emission. Fossil-fueled power plants are responsible for nearly 40% of total CO_2 emissions, with coal-fired power plants being the main contributor [2]. As per the data compiled by the International energy agency (IEA), the four largest emitters of CO_2 globally consist of (i) China (9839 Mt CO_2) (ii) USA (5270 Mt CO_2) (iii) European Union (3544 Mt CO_2) (iv) India (2467 Mt CO_2), while the total

world emissions amounting to ≈36153 metric tons as of 2017 [3]. Fig. 1.1 presents the general trends of the total greenhouse gas emissions by the major emitter countries and the European Union. These major emitters contribute for nearly 70 % share in the emissions globally [4].

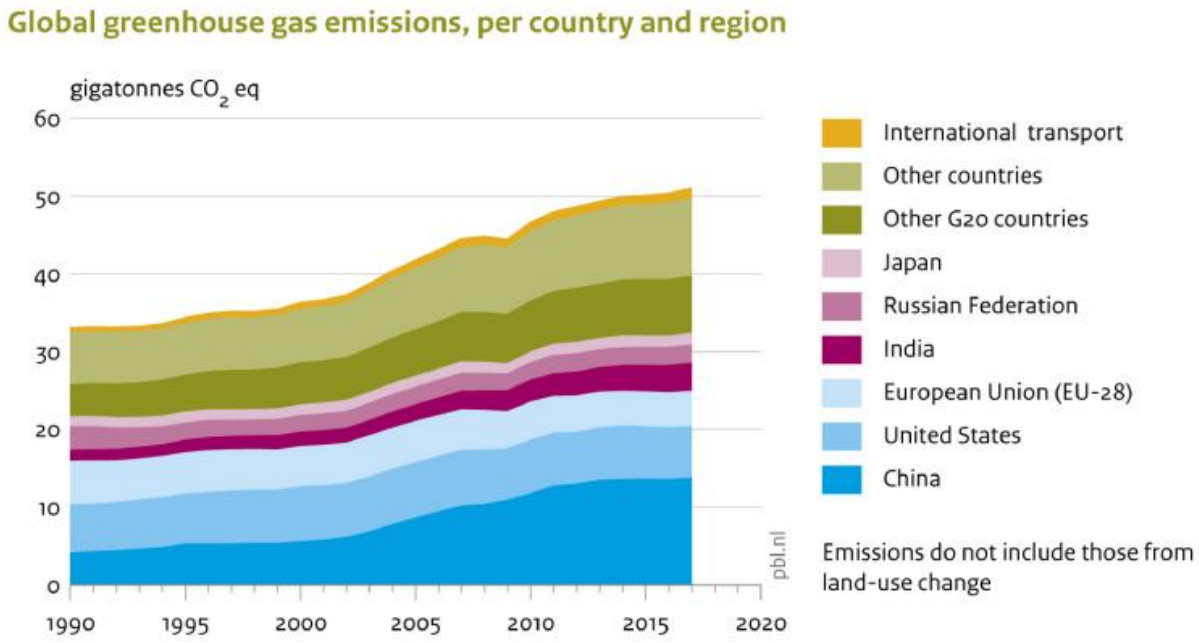

Fig. 1.1 Global greenhouse gas emissions, per country and region [4].

However, there are large inequalities observed globally in the case of yearly per capita emission of CO_2. The world largest per capita CO_2 emitters are the major oil producing nations. In 2017, Qatar recorded the highest emissions at 49 tonnes (t) per person, followed by Trinidad and Tobago (30 t), Kuwait (25 t), United Arab Emirates (25 t), Brunei (24 t), Bahrain (23 t) and Saudi Arabia (19 t) [5].

In the category of more populous nations, some of the highest per capita emitter can be observed in the case of Australia (17 t), USA (16.2 t) and Canada (15.6 t).This figures has been found to be more than 3 times higher than the global average, which in 2017 was 4.8 t. These trends directly indicate that countries with higher standard of living have higher carbon foot prints. In contrary some of the developed European nations show per capita emission close to the global average. In 2017 Portugal, France and UK recorded an emission of 5.3 t, 5.5 t and 5.8 t respectively [5]. The choice of energy source plays a key role here since major fraction of energy generation in these European countries are actually derived from nuclear

and renewable sources which results in the lower carbon foot print. India stands 61st globally with a total per capita emission of 1.7 t/yr [3]. However such continuous emissions worldwide have led to the immense rise in the concentration of carbon dioxide in the atmosphere which eventually crossed the 411 ppm mark in 2018 [4]. In view of this, there is great need to mitigate the problem of CO_2 emission to the atmosphere, while maintaining the faster economic growth. In this regard, efficient CO_2 capture strategies and its subsequent abatement such as carbon capture and storage (CCS) plays an important role in this regard [4]. IPCC in their annual report laid down the fact that the atmospheric CO_2 emissions could be brought down by 80-90 % for a modern conventional power plant equipped with efficient CCS technology.

1.2 Carbon capture and sequestration

Carbon capture and storage (CCS) includes a series of processes that are able to trap around 90 % of the carbon dioxide emitted via thermal power plants and other potential sources [6]. The CCS technology comprises of three different entities: (a) first capturing CO_2 from all the point sources (b) transportation of CO_2 for adequate storage and (c) secure storage of CO_2 underground into deep aquifers, or into deep unused oilfields. The capture of CO_2 can proceed via either of three methods: pre-combustion, post-combustion, and oxy-fuel combustion technique by adopting suitable methodologies based on available operating conditions [7]. After the suitable capture process, the trapped CO_2 is compressed, liquefied and transported for long distance for proper sequestration. The sequestration can be achieved by either deep underground storage or injecting into oil fields as part of enhanced oil recovery technique. Out of the total overall cost of CCS, CO_2 capture contributes to the 75 % fraction. Also, the cost of electricity production increases by around 50 % when CCS is employed in a conventional power plant [8]. Hence reducing the capture cost is the most important issue to be explored for the wide implementation of CCS process in thermal power plants.

1.2.1 Overview of CO_2 capture processes

The consideration of a particular CO_2 capture technique are basically based on a number of important factors including the application, the fixed cost as well the operating cost of technology deployment and if the existing system needs any retrofitting related to current

technology. There are mainly three approaches for CO_2 capture from industrial flue gas streams (Figs. 1.2 - 1.4).

1.2.1.1 Pre combustion

It refers to the capture of CO_2 prior to combustion. In this case, the fossil fuel such as coal is first partially oxidized in a gasifier to produce syngas. The syngas (mixture of CO and H_2) then undergoes steam reforming to form CO_2 and H_2 [8]. The concentrated volume of CO_2 then entered the scrubber column where it contacted with corresponding solvents for the absorption process. The rich solvent is then transferred into the regenerator column for stripping CO_2 and the separated H_2 stream can be used as a source of fuel for power generation. Based on the operating conditions of pressure, temperature, and CO_2 concentration, the separation of CO_2 can be accomplished by either chemical or physical solvent. Since this technology involves the substantial modifications in the design of power plant, this technique is most feasible for newer plants.

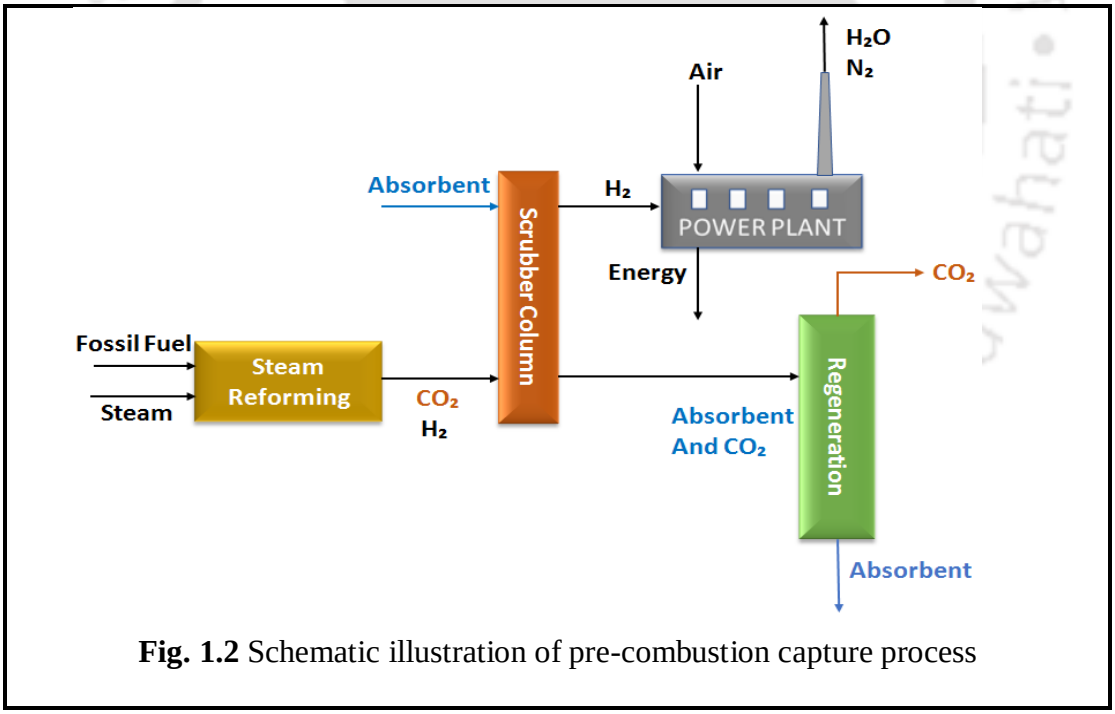

Fig. 1.2 Schematic illustration of pre-combustion capture process

1.2.1.2 Oxy-fuel combustion

The key features of oxyfuel combustion are that the combustion actually takes place with pure oxygen instead of air. This results in the generation of pure CO_2 as the major

combustion product. This technology requires a separate air separation unit which removes nitrogen and other constituents of air and generates purified oxygen. This stream is further admitted into the boiler where the combustion process takes place which results in steam generation to drive the turbine and produce electricity [9].

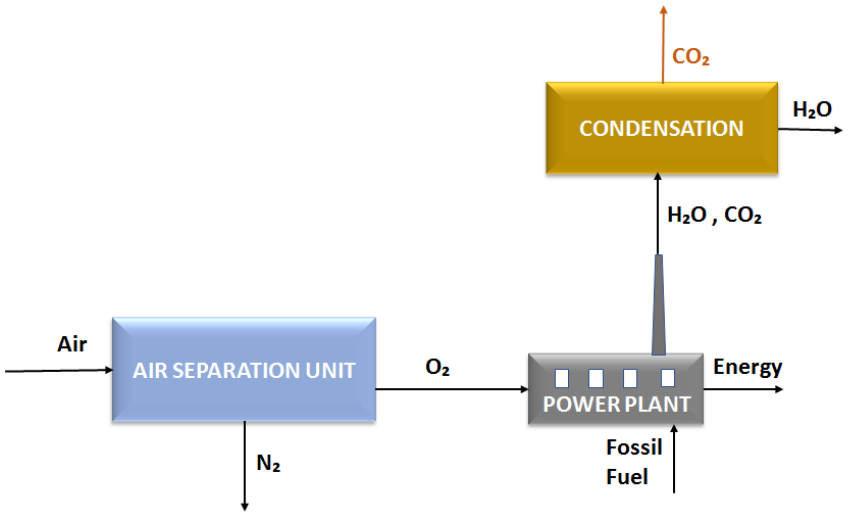

Fig. 1.3 Schematic illustration of oxy fuel combustion process

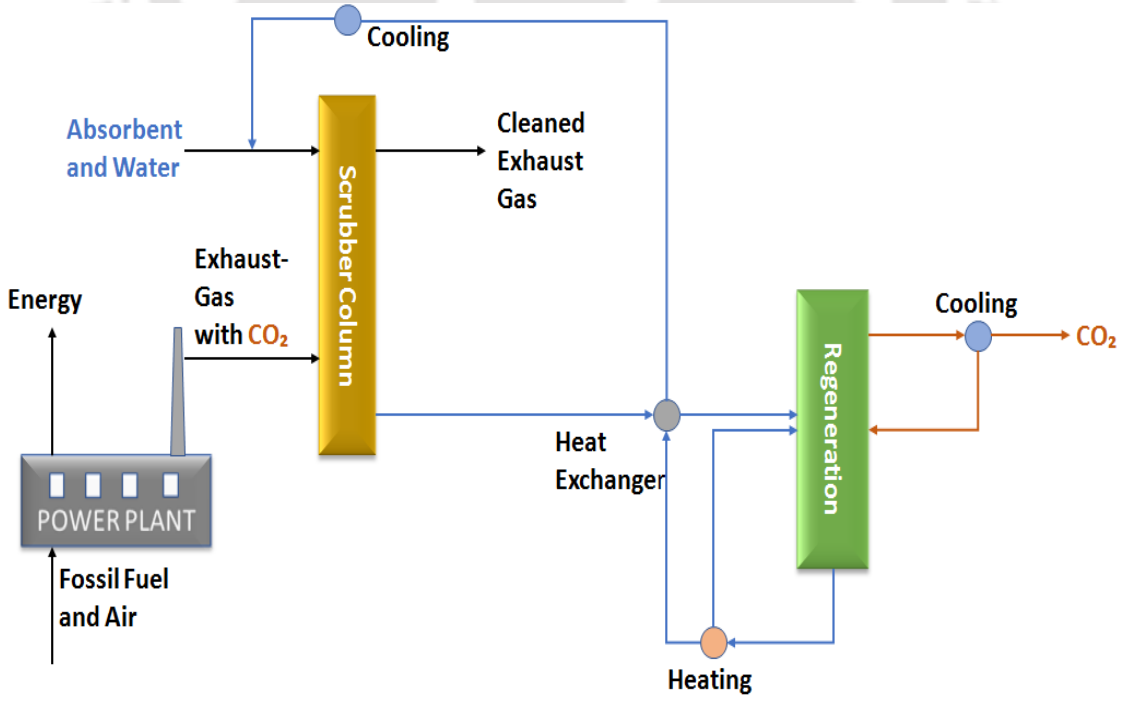

Fig. 1.4 Schematic illustration of post-combustion capture process

1.2.1.3 Post-combustion

In post-combustion capture technology, CO_2 is captured after the combustion process and is installed in thermal power plants or other large point sources as different separation unit. Large volume of gases needs to be treated since CO_2 in the exhaust stream is diluted by the nitrogen of the combustion air. Several separation techniques can be implemented such as membrane separation, adsorption, physical absorption, and chemical absorption. [10]

1.3 Post combustion carbon dioxide capture technologies

Within the PCC technology, there can be various CO_2 separation technologies, such as absorption, adsorption, cryogenic distillation and membrane separation [10]. Fig. 1.5 summarizes the various available technologies implemented in PCC applications. Out of all these available technologies, regenerative chemical absorption of CO_2 into aqueous alkanolamine solution is the most widely used technology practiced for bulk removal of acid gas from flue gas streams.

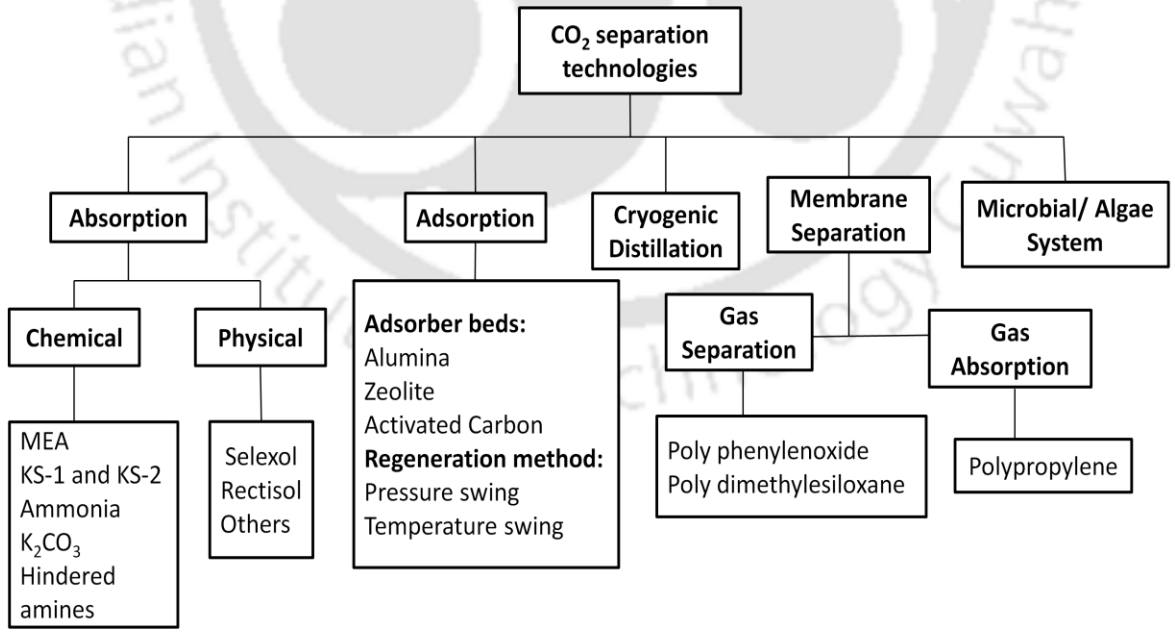

Fig. 1.5 Process technologies for post combustion CO_2 capture [10]

1.3.1 Chemical absorption

The main principle of chemical absorption process is based on the different reactivities of solute gases with the solvents. The reaction taking place in the system is mostly reversible one so that the CO_2 rich solvent can be regenerated simultaneously. Various basic absorbents such as aqueous ammonia, alkali carbonates, and alkanolamines are used as solvents in the absorption process. The interaction between the chemical solvents and CO_2 is very strong which results in the faster removal of CO_2 in a single stage of absorption process.

1.3.1.1 Alkanolamine based chemical absorption technology

The alkanolamine based chemical absorption technology acquainted with absorption and regeneration step is the most viable commercial technology employed in various natural gas processing facility for the efficient removal of CO_2. Alkanolamine consists of both amino group and hydroxyl group. The inherent hydroxyl group aids in the reduction of solvent vapour pressure as well as increases aqueous solubility, while the amino group provides the required alkalinity in aqueous solution to react with CO_2. Conventional alkanolamine used in the PCC process includes monoethanloamine (MEA), diethanolamine (DEA), N-methyldiethanoalmine (MDEA), 2-amino-2-methyl-1-propanol (AMP), piperazine (PZ), etc [8, 11-12]. The molecular structures of some important amines are shown in Fig. 1.6.

Amines are basically classified into primary, secondary, tertiary as well as sterically hindered amine. Primary and secondary amines are characterized by high reaction rate since they react rapidly with CO_2 to form intermediate carbamate ions [8]. However, since there is relatively large heat of absorption released with the formation of carbamate ions, the requirement of regeneration energy is high. Also, primary and secondary amines require two moles of amine solvent per mole of CO_2 absorbed and hence the theoretical CO_2 loading is restricted to 0.5. On the other hand, there exists no direct reaction between tertiary amine and CO_2, instead, it leads to the formation of protonated alkanolamine and bicarbonate species via hydrolysis reaction. Since it does not form intermediate carbamates, the reaction rate is very low in this case. The desirable traits associated with tertiary amines are its low regeneration heat duty, since the heat of reaction released with bicarbonate ion is to a large extent very less compared to the formation of carbamate ions. Apart from these the stochiometric CO_2 loading is 1:1 in the case of tertiary amine which accounts for higher CO_2 loadings. Another category of amine consists of sterically hindered amine. These amines can be either primary (AMP) or

secondary (diisopropylamine, DIPA) [11]. These amines exhibited highly reversible kinetics with CO_2 and thus requires lower regeneration energy requirement. Also hindered amines showcases better thermal stability than conventional amines.

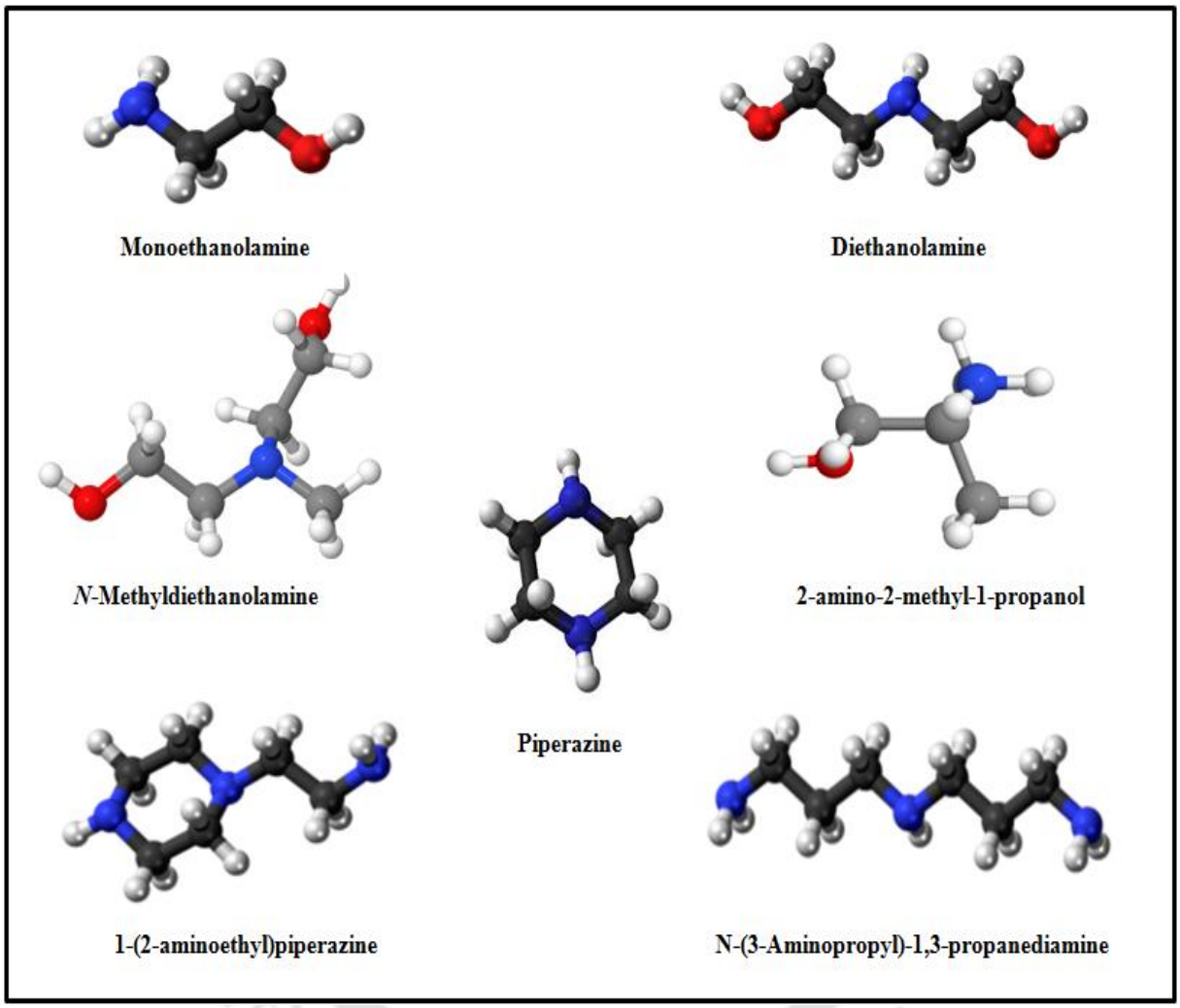

Fig. 1.6 Chemical structure of amines used in CO_2 capture application.

Alternatively, blended amine solvents which include a mixture of primary or secondary having higher reaction rates with tertiary or sterically hindered amines with better CO_2 loading can be also considered to be an attractive option for the post-combustion CO_2 capture application. Rate activators such as piperazine (PZ) has been also blended with slow reacting alkanolamines and shown very promising results [12]. PZ exhibits higher resistance to thermal and oxidative degradation compared to conventional amines and allows the use of lower concentration amines.

An amine based chemical absorption technology comprises of an absorption column and regenerator column (Fig 1.7). As part of post-combustion CO_2 separation method, first, the flue gas generated from the power plants enters a packed tower from the bottom where it undergoes a countercurrent contact with the CO_2-lean amine solvent.

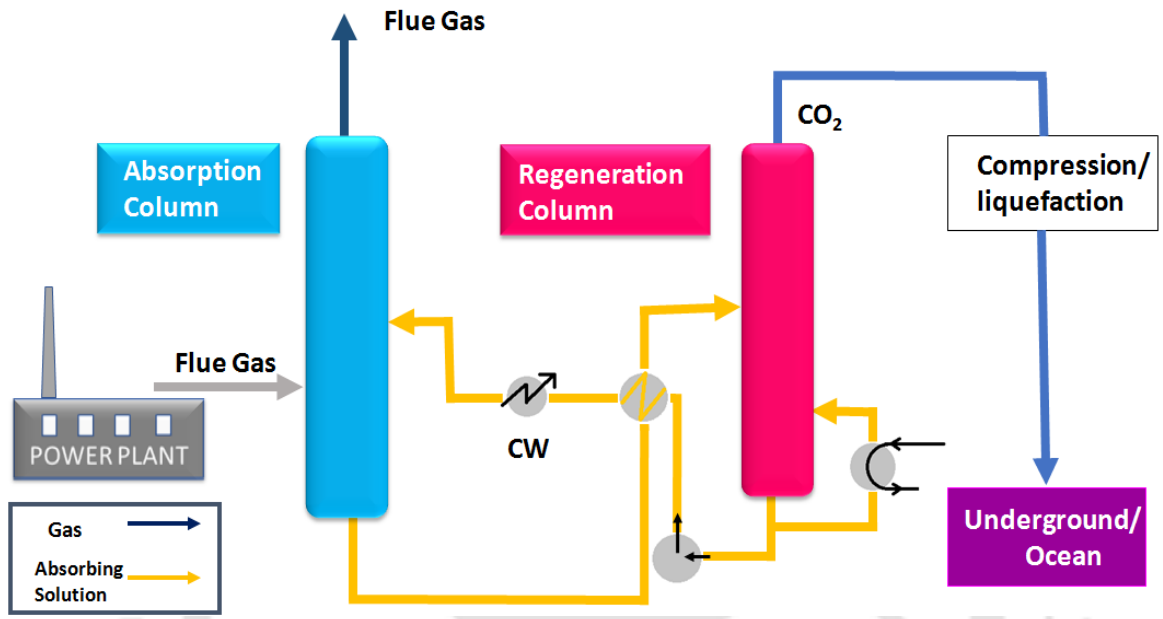

Fig. 1.7 Schematic of CO_2-amine absorption technology

After the subsequent chemical reaction aided absorption process, the CO_2-rich solvent enters the stripper column via a heat exchanger for the solvent regeneration. In the regenerator column, steam is used to strip the CO_2 from the solvent at temperatures between 120-130^oC. Pure CO_2 stream from the regenerator column can be further compressed for storage or other downstream application whereas the lean amine solvent is cooled to 40-60^oC and is pumped back to the absorption column via lean rich heat exchanger [13]. However, there are certain energy penalties associated with this process. First being the reboiler heat duty required to generate steam as well as to provide the necessary heat of desorption for stripping CO_2 from the solvent. Second relates to the energy required to compress the CO_2 to the conditions needed for storage and to operate the various intermediate metering devices.

1.3.2 Physical absorption

In physical absorption technique, the CO_2 gas molecules are absorbed in a liquid solvent in accordance with the Henry's law. Hence the complete absorption process is temperature and pressure-driven. The process uses organic solvents as the agent to physically absorb the solute component rather than reacting chemically. The necessary association between the solvent molecules and the solute CO_2 gas takes place by weak van der Waals or electrostatic force. These bonds are however weaker in nature as compared to chemical solvents. The volume of solute gas absorbed in the system can be proportionately related to the partial pressure of the gas. This process is favorable at higher partial pressure of CO_2 and lower temperature. The regeneration step can be facilitated by reducing the system pressure or by heating. Typical physical solvents commercially available are based on cold methanol (Rectisol), N-methyl-2-pyrollidone (Purisol), polyethylene, dimethyl ether of polyethylene glycol (Selexol), propylene carbonate (Fluor Process) and sulfolane [8]. However, since the partial pressure of CO_2 in flue gas is very low hence the sole application of physical solvent in the post-combustion capture technology is very limited. Hence some CO_2 capture unit explored the application of hybrid solvents which is a mixed blend of physical and chemical solvents. The most common example listed out here is the sulfinol process which employed a mixture of physical solvent such as sulfolane and chemically reacting amines such as DIPA or MDEA.

1.3.3 Physical adsorption

Adsorption technology depends on the inherent thermodynamic characteristics of a solute molecule to transfer from the gas phase to selectively adsorb itself on to the surface of the adsorbent. Adsorption can be physisorption or chemisorption. After adsorption the regeneration or desorption can be achieved either by pressure swing or temperature swing adsorption. Research is more focused on the amine coated active molecular sieves, metal-organic frameworks (MOF) as well as grafted zeolites [14-15]. Conventional used grafting agents for this sorbents includes polyethyleneimine or Na_2CO_3 based adsorbents to adsorb CO_2 from flue gas [16]. However, this process also requires extensive R & D for the application towards treatment of high volume flue gases in industries.

1.3.4 Cryogenic separation

The principle behind the cryogenic separation is that CO_2 can be separated from other gases by cooling and condensation. Cryogenic separation can be implemented for gas streams having high concentrations of CO_2 (> 90 %) but is not that much effective for the treatment of dilute CO_2 streams. It involves the refrigeration of gases to cool it down to very low temperature (lower than -73.3 ^oC) so that CO_2 can be either freezed out or liquefied and hence separated [17]. The significant feature of this process is that CO_2 is recovered /extracted in liquid phase which can be further transported conveniently to storage sites or can be pumped to the injection sites for enhanced oil recovery (EOR) applications. While the major disadvantages involved with this process is the high cost of refrigeration as well as removal of water traces from the streams to avoid condensate trap.

1.3.5 Membrane technologies

Gas separation membranes can be used for removing CO_2 from flue gas streams. Two types of membrane technologies can be used for separating CO_2 from other gases: gas separation membranes and gas absorption membranes. There are different grades of gas separation membranes used for PCC application which consist of either porous or non-porous organic polymeric or inorganic membrane (carbon, zeolite, ceramic or metallic) [18]. Another category of membranes is impregnated with reacting agents such as amine that selectively reacts with CO_2 [19]. Even though membranes showcases several desirable characteristics over the conventional absorption technology such as no regeneration energy requirement, simple modular system, however, it cannot achieve a higher degree of separation always which further necessitates the application of multiple stages recycling [20]. Other disadvantages involve with membrane includes its higher sensitivity to sulphur compounds and other trace elements. Recently researchers have integrated membrane separation processes with other approaches such as chemical absorption processes for availing the benefits of the processes.

The main point of concern for the amine-based chemical absorption technology is the high cost of solvent regeneration. In addition, the oxidative and thermal degradation of the solvent results in higher solvent make–up requirement. However, the major advantage of a chemical absorption technology is that it is the most mature technology for CO_2 capture and it is suitable for retrofitting of the existing plants. Thus, chemical absorption is considered as a reliable and relatively competitive method for reducing CO_2 emission [10] compared to the

available technologies for CO_2 capture from industrial flue gas streams. It can be also inferred that chemical absorption via energy-efficient aqueous amine solvent is the most viable solution for the industrial mass scale acid gas separation as the other methods are either developing or not economical. Hence absorption process with newer amine solvents, such as sterically hindered amines or tertiary amines facilitated by the amine activators which are having higher selectivity for CO_2, resistance to degradation as well as lower reboiler heat duty are currently the subject of global R&D.

1.4 Literature review

Amine based absorption-regeneration technology has been extensively used for several years for the bulk removal of acid gases from the flue gas as well as natural gas streams. Li et al. [21] in their study clearly inferred that CO_2 loading capacity can be increased by putting more hindrance to the amino functional groups present in the different categories of amines. The trends can be expressed as primary amines < hindered amines < secondary amines < tertiary amines < diamines. For the detail characterization of solvent with respect to its application in the PCC unit, the fundamental knowledge of acid gas solubility as well as thermophysical properties is very much important.

1.4.1 Absorption of CO_2 in single amine solvent

Solubility data of CO_2 in aqueous amine solutions at a wide experimental conditions viz. temperature, pressure and solvent concentration are very much essential for the rational design and optimization of acid gas removal units. Carbon dioxide solubility in aqueous single amines has been extensively studied by various researchers worldwide and the brief summary is presented in Table 1.1. Primary and secondary amine because of their stochiometric limitations with CO_2 depicts lower CO_2 loading capacity compared to tertiary and sterically hindered amines. However the higher loading can results from the hydrolysis of carbamate species at higher CO_2 partial pressure. A number of literatures are reported for the solubility of aqueous monoethanolamine solution [22-27]. Alongwith its application as a low cost conventional solvent in the acid gas treatment technology, it is also often used as a base case solvent in the comparative studies of new solvents for CO_2 absorption. Bouillon et al. [42] have shown that the usage of highly concentrated MEA can improve the CO_2 absorption performance.

Table 1.1 Summary of the literature review about the CO_2 solubility measurement in different single amine solvents

Amine	Concentration, wt%	Temperature, °C	CO_2 Partial Pressure, kPa	Reference
Monoethanolamine (MEA)	30	0-75	1.387 – 100.2	Mason et al. [22]
	15.3	40-140	0.56 – 4862	Jones et al. [23]
	30	0 – 60	0.0012-19954	Jou et al. [24]
	(15-30)	40-100	0.288 – 842.7	Lee et al. [25]
	30	120	7.3 – 191.9	Mamun et al. [26]
	(15-60)	40-120	0.001 - 20	Aronu et al. [27]
Diethanolamine (DEA)	(10-30)	100-200	105 - 2451	Kennard et al. [28]
	(20-30)	30-50	0.1-100.9	Benamor et al. [29]
	(25-35)	30 –50	0.098 - 100	Sulaiman et al. [30]
Diisopropanolamine (DIPA)	30	40-100	2.7 - 5888	Isaacs et al. [31]
N-Methyldiethanoalmine (MDEA)	30	40-100	1.2 - 1890	Shen et al. [32]
	50	55-85	65 - 754	Mamun et al. [26]
	50	25-100	8.27 – 140	Park et al. [33]
	50	100-200	138-4930	Chakma et al. [34]
	(5-75)	50-100	1-235	Rho et al. [35]
Triethanolamine (TEA)	(20-30)	30-50	1.62- 98	Chung et al. [36]
2-(diethylamino)-ethanol	(30-40)	60 – 80	3.7 - 192	Xu et al. [37]
2-amino-2-methyl-1-propanol (AMP)	(20-30)	30-50	4.05 -91	Kundu et al. [38]
	30	50	4.3 - 5645	Teng et al. [39]
	(30-40)	25-55	0.601-1450	Dash et al. [40]
1-dimethylamino-2-propanol (DMAP)	30	25-60	8.2- 100	Liang et al. [41]

Aronu et al. [27] in their work studied the CO_2 solubility in aqueous MEA system over a broad domain of experimental temperature and CO_2 partial pressure. It can be analyzed from their work that at higher laodings, the CO_2 solubility shows a strong dependency on the solvent concentration. The equilibrium CO_2 partial found to increase with the amine concentration and CO_2 loading. The extended Uniquac model was applied to correlate the

solubility data. The model was successfully employed to predict the ionic speciation profile, heat of absorption as well as amine volatility. MEA is characterized with high heat of absorption which can directly impact the heat duty. Benamor et al. [29] achieved a CO_2 loading of 0.786 and 0.671 at a CO_2 partial pressure of about 100 kPa for 2 M and 4 M aqueous diethanolamine (DEA) system. They have experimentally determined the carbamate ion concentration using titration analysis and compared with the model predicted results. The solubility data were fitted simultaneously to estimate the various binary interaction parameters required to calculate the activity coefficients featured in Deshmukh Mather Model [29].

Even though tertiary amines such as N-methyldiethanolamine (MDEA) are associated with slower kinetics but they are inherited with various significant features such as lower vapour pressure, excellent thermal and chemical stability. Also, since MDEA depicts lower corrosion behavior, it can be implemented at a high concentration in the gas sweetening technology. The usage of highly concentrated solvent can significantly reduces the solvent circulation rate in the absorption process and leads to good plant economics. Water plays a dominant role in the tertiary amine – CO_2 reaction system, since MDEA in absence of water generally does not react with CO_2 [43]. Further, the aqueous media facilitates the dissolution of MDEA through hydrogen bonding and this interaction promotes hydration reaction of CO_2 as suggested by Barth et al. [44]. In order to investigate the effect of solvent concentration, Rho et al. [35] measured and expressed the CO_2 solubility in the varied concentration range of (5 to 75) wt %. It can be interpreted from their results that the CO_2 loading decreases upon increasing the mass concentration of MDEA at a fixed operating temperature and CO_2 partial pressure. The solubility results were also expressed in terms of absorption capacity plot (mol of CO_2 per volume of solution). From the plot it can be observed that at pressure below 10 kPa, it is quite desirable to employ a 20.5 wt % MDEA solution while at higher pressure 50 mass % MDEA gives better results. Along with this enthalpy of CO_2 absorption has been also estimated using Gibbs-Helmoltz equation and found to be 54.6 $kJ.mol^{-1}$ for 50 mass % MDEA. Moreover exploration of alternate tertiary amines having faster kinetics compared to MDEA leads to the investigation of 1-dimethylamino-2-propanol (1DMA2P), a new category of tertiary amine. The results obtained by Liang et al. [41] confirm that the equilibrium CO_2 solubility in 1DMAP is higher than other conventional amines such as MEA and MDEA. The mass transfer study in a packed column reveals that the overall mass transfer coefficient ($K_G a_v$) follows the order: MEA > 1DMA2P > MDEA. The CO_2 absorption heat from Gibbs-

Helmoltz equation has been estimated to be -30.5 $kJ.mol^{-1}$, quite lower compared to MEA and conventionally used tertiary amine MDEA.

Sartori and Savage [45] suggested that the sterically hindered amines can be also explored as a potential solvent for CO_2 capture applications. Among the class of sterically hindered amines, AMP is the most popular one owing to its various desirable traits such as the theoretical capacity is twice as much of MEA. From the ^{13}C NMR study of Chakraborty et al. [46], it can be clearly inferred that the AMP carbamate formed in a very minute quantity compared to its fast reacting unsubstituted analogue, MEA. Xu et al. [47] further quantified the intermediate carabamate species and found it to be in the order of only 10^{-4} of the total concentration of amine. This findings indicates that the unsatable carbamates formed during the reaction may undergo hydrolysis rapidly and dissociates into bicarbonate ions and free amine species. Dash et al. [40] presents a theoretical and experimental analysis of CO_2 solubility in varied concentration of aqueous AMP solution. As per their investigation, at a constant operating temperature and CO_2 loading, the CO_2 partial pressure rises upon increase in the concentration of aqueous AMP solution. The similar trends were also reported by Kundu et al. [38]. The experimental solubility data are modeled using thermodynamic model developed based on electrolyte non random two liquid (ENRTL) theory. The activity coefficients predicted as per the model was used to predict the liquid phase ionic speciation profile with respect to change in corresponding CO_2 loading. Speciation plot reveals that AMP disappears with increase in CO_2 loading and the protonated species and bicarbonate ions were the dominant species prevailing in the system. The thermodynamic model was further used to predict the volatility of AMP and has been found to be 0.001 kPa for 40 wt % aqueous amine solution at 338 K. Along with this the average heat of absorption between T = (313 - 373) K was also estimated to be 70 $kJ.mol^{-1}$ CO_2.

1.4.2 Absorption of CO_2 in blended amine solvent

In order to overcome the limitations of single amine solvent, the concept of suitable blending of amines is gaining popularity in the field of acid gas separation technology via chemical absorption. The blended amines are formulated based on the synergetic effect of superior reaction kinetics showcased by primary or secondary amines as well as higher CO_2 loading and lower regeneration energy characterized by tertiary or sterically hindered amines. A brief

summary of the literature review corresponding to the CO_2 solubility in blended amine system is reported in Table 1.2.

Table 1.2 Summary of the literature review about the CO_2 solubility measurement in different blended amine solvents

Amine blends	Concentration, wt%	Temperature, °C	CO_2 Partial Pressure, kPa	References
Monoethanolamine + *N*-Methyldiethanoalmine	MEA : (6 – 18) MDEA : (12 – 24)	40 - 100	1.12 - 2080	Li et al. [48]
	MEA : (12 – 24) MDEA : (6 – 18)	40 - 100	1- 2016	Shen et al. [32]
Monoethanolamine + 2-amino-2-methyl-1-propnaol	MEA : (6 – 24) AMP : (6 - 24)	40 - 100	0.86 - 199	Li et al. [49]
Diethanolamine + 2-Amino-2-methyl-1-propanol	DEA : (6 – 15) AMP : (15 - 24)	30 - 50	1.021 - 354	Kundu et al. [50]
Diethanolamine + *N*-Methyldiethanolamine	DEA : (1.5 – 4.5) MDEA : (25.5 – 28.5)	30 - 50	2.4 - 90	Kundu et al. [51]
2-amino-2-methyl-1-propnaol + N-Methyldiethanolamine	AMP : (8.9 – 17.7) MDEA : (11.8 – 23.4)	30 - 70	106.25 - 4110	Suleman et al. [30]
N‑Methyl-2-ethanolamine + N-Methyldiethanolamine	MAE : (3 - 24) MDEA : (6 - 27)	30 - 50	0.503 – 545.6	Kumar et al. [52]
2-amino-2-methyl-1-propnaol + N‑Methyl-2-	MAE : (1.5 - 21) AMP : (9 – 28.5)	30 - 50	0.511 – 515.7	Kumar et al. [52]

Blends of primary and tertiary amine, (MEA + MDEA) have been extensively studied as a preliminary amine blends for CO_2 absorption. Li et al. [48] have reported the solubility of CO_2 in aqueous (MEA + MDEA) over broad operating conditions of temperature and pressure. According to their investigation, CO_2 solubility reduces gradually upon increase in temperature from 40 to 80°C. Also the solubility curves cross each other at a point where the partial pressure of CO_2 is 45 kPa. Li et al [49] in another research work investigated the blend of MEA with sterically hindered AMP solvent for CO_2 absorption. The solubilities of CO_2 in higher AMP mass fraction solutions are higher than those of solutions with a high MEA mass

fraction. The solubilities are correlated with Kent-Eisenberg model. The equilibrium constants of amine based reactions are estimated as a function of reaction temperature, amine concentration and CO_2 loading. Kundu et al. [50-51] investigated the solubility of CO_2 in (DEA + AMP) and (DEA + MDEA) blends. They have observed a cross-over in the solubility curves of different blended composition. The reason can be attributed to the fact that at low to moderate loadings, DEA can react faster with CO_2 compared to MDEA on account of its faster kinetics. However as the CO_2 loading increases, the free DEA species gets decreased which results in an increased ratio of MDEA to DEA in the aqueous system. While at higher loadings, the equilibrium is closer to MDEA than that of DEA resulting in the curves to cross each other. The solubility data are correlated with the modified Clegg-Pitzer equations. Simulated annealing algorithm was applied for estimating the interaction parameters and to determine the equilibrium composition of various ionic species present in the liquid phase.

More recently, there has been a growing interest in the usage of improved and activated alkanolamine solvents, e.g., piperazine (PZ) activated MDEA or AMP [53-54], for CO_2 removal. These activated blended solvents posses the desirable traits of relatively higher reaction rates as well as higher solubility of activating agents. These activating agents are mostly blended with non carbamate forming amines which are characterized with higher loading capacity as well as lower regeneration heat duty. A brief summary pertaining to the CO_2 solubility measurement in activated amine system is presented in Table 1.3. From the comprehensive study of Dash et al. [54], it can be observed that the CO_2 loading increases with the increase in PZ concentration in the mixed amine solvents of (PZ + MDEA) up to a loading of 1.0. Beyond this threshold value, a crossover has been observed where the loading decreases upon further increase in PZ concentration at a constant CO_2 partial pressure. Bishnoi and Richelle [62] relates this phenomena to the formation of various intermediate reaction products such as PZ- carbamate, PZ-dicarabamte as well as protonated PZ carabamate. The formation of all these intermediates increases the overall carbamate stability and hence more number of amine molecules is tied for each incoming CO_2 molecule in the absorber column.

Table 1.3 Summary of the literature review about the CO_2 solubility measurement in different activated amine solvents

Amine Blends	Concentration, wt%	Temperature, °C	CO_2 Partial Pressure, kPa	Researchers
Piperazine + 2-amino-2-methyl-1-propanol	PZ : (2 - 8) AMP : (22 - 28)	40 – 120	5.7 – 463.5	Tong et al. [53]
Piperazine + N-Methyldietahanolamine	PZ : (2 - 8) MDEA : (22 - 28)	30 – 50	1.85 - 1246	Dash et al. [54]
	PZ : (8.5 – 16.8) MDEA : (11.8 – 23.4)	30 – 70	102.5 - 4490	Suleman et al. [30]
Piperazine + Diethylenetetramine	PZ : (5 - 15) DETA : (15 - 25)	40- 80	0.8 - 923	Chang et al. [55]
Hexamethylenediamine + N-Methyldiethanolamine	HMDA : (5 - 20) MDEA : (10 - 25)	30 - 60	0.5 - 111	Mondal et al. [56]
Hexamethylenediamine + 2-amino-2-methyl-1-propanol	HMDA : (5 - 20) AMP : (10 - 25)	30 – 60	1.04 -110.57	Mondal et al. [57]
Ethylenediamine + N-Methyldiethanolamine	EDA : (5 - 15) MDEA : (85 - 95)	20 - 40	40 - 180	Hafizi et al. [58]
Diethylenetetramine + N-Methyldiethanolamine	DETA : (5 - 15) MDEA : (85 - 95)	20 - 40	40 -180	Hafizi et al. [58]
Triethylenetetramine + N-Methyldiethanolamine	TETA : (5 - 15) MDEA : (85 - 95)	20 - 40	30 - 180	Hafizi et al. [58]
Tetraethylenepentamine + N-Methyldiethanolamine	TEPA : (5 - 15) MDEA : (85 - 95)	20 - 40	30 -190	Hafizi et al. [58]
1,3-diaminopropane + Monoethanolamine	DAP : (2.5 - 5) MEA : (10 – 12.5)	40 - 60	3 - 215	Khodadi et al. [59]
Piperazine + Potassium carbonate	PZ : (7.5 - 10) K_2CO_3 : (15 - 20)	40 - 90	1.8 - 675	Kim et al. [60]
2-methylpiperazine + Potassium carbonate	2-MPZ : (7.5 - 10) K_2CO_3 : (15 - 20)	40 - 90	1.8 - 675	Kim et al. [60]
2-((2-aminoethyl)amino)ethanol + N-Methyldiethanolamine	AEEA : 5 MDEA: 30	35 - 95	103 - 4445	Zoghi et al. [61]

Dash et al. [63] further implemented ENRTL model to explain the thermodynamics of the CO_2 absorption in the mixed amine system of (AMP + PZ). The model has been used to adequately represent the solubility data within the AAD value of 12 %. The estimated speciation plot shows a considerable difference than the single AMP or PZ system. The

mixed blend concentration of 50 wt % shows the highest cyclic capacity compared to 30 and 40 wt % system. The mixed system having the composition (42 wt % AMP + 8 wt % PZ) corresponds to the highest capacity of 1.8 among the studied system. The thermodynamic model has been further applied to assess the amine volatility which has been also found to be less as compared to the single amines. The above key outcomes are also supported by the findings of Tong et al. [53] where the CO_2 solubility has been evaluated for two different mixed amine composition. The solubility data are well correlated with non–rigorous equilibrium based modified Kent-Eisenberg model, giving an average absolute relative deviation The studied amine system possesses twice as much of the CO_2 loading capacity compared to the conventional 30 wt % MEA solvent. In spite of its desirable features, the utility of PZ in concentrated form is limited due to solid precipitation at both the conditions of lean and rich CO_2 loading. At room temperature of (295 ^{o} K), concentrated PZ solution (8 mol.kg^{-1}) needs a net CO_2 loading of 0.25 mol of CO_2 per mol of alkalinity to remain prevalent in the aqueous solution without precipitation. Also formation of solids can be observed at higher CO_2 loading [64].

Another promising category of activators which includes derivative of piperazine have been also tested for its possible application in the CO_2 absorption from acid gas streams. Kim et al. [60] in their work have blended K_2CO_3, an inorganic solvent with 2-methylpiperazine (2-MPZ) and piperazine (PZ) and reported the CO_2 absorption rate and capacity. Since 2-MPZ consists of a methyl group associated with the cyclic diamine structure of PZ, it poses steric hindrance effect. This result in the formation of unsatable carabamte as well as a large amount of bicarbonate and carbonate species which may further reduces the overall regeneration cost compared to piperazine (PZ). They have observed that the aqueous blend of (20 wt % K_2CO_3 + 10 wt % 2-MPZ) and (20 wt % K_2CO_3 + 10 wt % PZ) had the lowest equilibrium CO_2 partial pressure for any corresponding CO_2 loading at the same conditions of temperature. However at temperature lower than 313 K, these solutions witnessed a large amount of $KHCO_3$ crystals. Also the aqueous system separates into two liquid phases before the commencement of reaction with CO_2.

Recently, another potential piperazine derivative, 1-(2-aminoethyl) piperazine (AEP) shows superior absorption characteristics compared to PZ. Paul et al. [65] investigated the kinetics of dilute aqueous AEP solution and the second-order rate constants k_2, were obtained as 31867.6, 56354.2, and 100946 $m^3.kmol^{-1}.s^{-1}$ at 303, 313 and 323K, respectively. The

observed second order reaction rate constant is slightly higher than the aqueous PZ solution. Du et al. [64] blended less concentrated PZ solution with AEP in order to remediate the precipitation issue keeping all the desired features of PZ solutions intact for PCC applications. The thermodynamics of the mixed solvent system was successfully assessed by ENRTL model and the CO_2 solubility, speciation as well as amine volatility were represented with better accuracy. The model predicts a cyclic capacity of 0.86 $mol.kg^{-1}$ for the mixed system compared to 0.50 $mol.kg^{-1}$ for 7 $mol.kg^{-1}$ MEA system. The promotion effect of the addition of 1-(2-aminoethyl) piperazine on the equilibrium CO_2 solubility of monoethanolamine can be observed from the work of Ramazani et al. [66]. The loading capacity of the blended solution increases as the concentration of AEP rises in the blend with maximum loading achieved at a molar ratio of 0.8 corresponding to (0.5 M AEP + 2.5 M MEA) system. The response surface methodology based on central composite design was employed to assess the relationship between the different independent variables on the CO_2 loading capacity.

Another potential activator explored in the recent literatures is hexamethylenediamine (HMDA). Singh et al. [67] compared the CO_2 loading capacity of different amines consisting of multiple amine groups. They have investigated the CO_2 loading capacity of various straight chain diamines and inferred that the absorption performance of HMDA is better than other straight chain diamines. The investigations were further extended by Mondal et al. [56-57]. Their study covers both the binary and blended system with AMP and MDEA as a base amine. The CO_2 loading increases significantly upon the addition of HMDA into the mixed amine system. For (15 wt % HMDA + 15 wt % AMP) system, the CO_2 loading has been enhanced by 30 % compared to 30 wt % AMP system. Along with the solubility study, the authors also measured the heat of absorption in the aqueous HMDA as well as (HMDA + MDEA) system [68]. Heat of absorption is the prime criteria which should be taken into consideration in the solvent selection as it directly relates to the energy penalty in regeneration step. Since highly reacting amines are characterized with higher enthalpy of CO_2 absorption, hence the reaction rate improvement due to blending is also linked with the higher heat of absorption. Hence the blending ratio should be optimized based on the appropriate kinetic, solubility and enthalpy data. At CO_2 partial pressure of 15 kPa and temperature of 313 K, the aqueous blend of (15 wt % HMDA + 15 wt % MDEA) corresponds to ΔH_{abs} = 79 $kJ.mol^{-1}$ as compared to 84 $kJ.mol^{-1}$ for 30 wt % MEA solution.

The chain length of alkylamines also plays a considerable role in the CO_2 absorption capacity. Increase in the chain length results in the reduction of initial absorption rate, while the CO_2 loading rises. The effect can be analyzed from the work of Hafizi et al. [58] where the MDEA has been blended with various Polyamines consisting of varying number of alkyl and amine groups viz. EDA, DETA, TETA and TEPA. According to their findings, the CO_2 loading is increased from 0.91 for pure MDEA to 0.94, 0.99, 1.01 and 1.05 for 15 wt % EDA, DETA, TETA and TEPA promoted solvent system. The cyclic capacity of the solvents was also studied through continuous absorption- desorption processes. The stability of formed ions is ordered as primary carbamate > primary - primary dicarbamate > primary−secondary dicarbamate, respectively. The desorption study further confirms the fact that amine blends comprising of higher numbers of secondary to primary amine groups leads to the formation of more secondary carbamate and dicarabamate species resulting in their better or complete regeneration.

1.5 Importance and objectives of present work

From the introductory discussion and the subsequent literature review it is evident that both experimental and theoretical studies are essential for the rational design of CO_2 capture plant. Amine based absorption cum regenerator technology have been widely practiced for several years for CO_2 absorption from acid gases present in flue gas as well as natural gas streams. However, the applicability of the amine technology for post combustion technology faces some serious economical and technological constraints. Firstly, the CO_2 partial pressure in the exhaust streams of flue gases is low and hence more power is needed to compress the gases for the absorption process. Secondly, the flue gases generated from the thermal power plants are too much in volume that it requires a large diameter absorption column [69]. To overcome these difficulties the solvent should be fast reacting with CO_2 and should have higher capacity and lower rate of degradation [9]. The conventional amines are associated with various limitations such as high regeneration energy requirement, solvent losses as well as environmental impact due to various solvent degradation products [70].

Various researchers investigated and recommended the usage of 2-amino-2-methyl-1-propanol (AMP) and N-methyldiethanolamine (MDEA) [32-35, 38-40] based solvents to overcome the limitations exhibited by the conventional amines in post-combustion carbon capture (PCC) unit. While MDEA is a tertiary amine, AMP belongs to the category of

sterically hindered amines. These category of amines posseses various desirable traits such as higer CO_2 loading, lower reboiler heat duty requirement, better thermal and chemical stability [71-73]. However, the rate of reaction of CO_2 absorption in AMP and MDEA is low ($k_{2,\ AMP}$ = 740 $m^3.kmol^{-1}s^{-1}$ at room temperature, $k_{2,\ MDEA}$ = 2.8 $m^3.kmol^{-1}s^{-1}$ at 313K) [73-74] compared to other conventional solvents such as MEA. In order to improve the reaction kinetics, AMP or MDEA is mixed with rate enhancer solvent such as polyamines. Over the years continuous effort has been laid down in exploring energy efficient solvent that have better performance than the conventional MEA based solvent system. In the category of rate activators researchers got very promising results upon blending polyamines with non-carbamate forming amines.

Recently, 1-(2-aminoethyl) piperazine (AEP), a piperazine derivative which is also a cyclic amine, can be explored as a rate activator and a solvent for the absorption of CO_2 [75]. The AEP molecule has several advantageous inherent properties, such as a high boiling point, low vapor pressure and good solubility in water [62]. The kinetic study of CO_2 absorption in aqueous (AEP + MDEA) has been reported by Paul et al. [76]. Their study revealed that in a 1 molar total (AEP + MDEA) solution, a replacement of 30 mole % MDEA by 30 mole % AEP in the aqueous solution had increased the CO_2 reaction rate by about 1470 times when the experiments were conducted at 303 K. Due to this rate enhancement property, AEP can be considered as a rate promoter in the CO_2-amine reaction. Similarly, N-(3-Aminopropyl)-1,3-propanediamine (APDA), which is an aliphatic polyamine containing two primary amine groups and one secondary group, has been also prove to be an superior activator having second-order rate constant k_2 for aqueous APDA to be 35775 $m^3kmol^{-1}s^{-1}$ which is substantially higher as compared to conventional PZ activator [77]. Although aqueous AEP and APDA as well as its blends with MDEA, AMP and 1DMAP are potentially important formulations for CO_2 capture, there is very limited information in the open literature on equilibrium solubility and thermo physical property measurements. For the detail characterization of the solvent, precise information on the thermo physical properties are also very much essential for the designing of any gas separation system. These properties are unique for any alkanolamine system and are basically represented as a function of temperature and composition. The primary objective of this work is to investigate the energy efficient solvent for the purpose of cost reduction of CO_2 capture process.

To achieve this objective, the following work has been undertaken for single as well as AEP and APDA activated amine solvents.

- Generation of equilibrium solubility data of CO_2 in aqueous 1-(2-aminoethyl)piperazine (AEP), aqueous N-(3-aminopropyl)-1,3-propanediamine (APDA), (AEP + MDEA + H_2O), (AEP + AMP + H_2O), (APDA + MDEA + H_2O), (APDA + AMP + H_2O) and (APDA + 1DMAP + H_2O) with various relative amine compositions over the temperature range of (303.2 -333.2 K) and within the CO_2 partial pressure range of 250 kPa.

- Development of modified Kent – Eisenberg equilibrium based thermodynamic model to represent the equilibrium solubility data over single and blended solvent system. Estimation of important reaction equilibrium constants via data regression and validation of the model using experimental results of this work.

- Development of Feed-forward Neural Network models for validating the experimentally generated CO_2 solubility data for the binary as well as ternary system. The network architecture is optimized by implementing Levenberg-Macquerdt (LM) back propagation algorithm.

- Measurement of important thermophysical properties (density, viscosity, and surface tension) of the aqueous single and blended amine solutions over wide range of temperature (303.2 -343.2 K) and amine concentration.

- Development and correlation of experimentally measured thermophysical properties using various well-established empirical models such as Redlich-Kister, and Grunberg-Nissan.

1.6 Thesis organization

The thesis mostly focuses on the investigation of various aqueous single and blended novel amine formulations for post combustion capture application with special emphasis to experimental and theoretical analysis of equilibrium CO_2 solubility.

Chapter 1: Background of the work, comprehensive literature survey, objectives and outline of the thesis have been discussed in this chapter

Chapter 2: The reaction mechanism of various categories of amines with CO_2**,** solubility modelling approaches adopted in the present work are reported here

Chapter 3: This chapter is devoted to the measurement of important thermo-physical properties such as density, viscosity and surface tension of (AEP+H_2O), (APDA+ H_2O), (AEP + MDEA + H_2O), (AEP + AMP + H_2O), (APDA + MDEA + H_2O), (APDA + AMP + H_2O) systems and their correlation using Redlich Kister and Grunberg Nissan type equation. The viscosity data have been further extended to estimate various thermodynamic parameters such as ΔG^o, ΔS^o, ΔH^o over all the temperature and composition range.

Chapter 4: This chapter presents the experimental measurement of solubility data of CO_2 absorption in aqueous AEP as well as aqueous (AEP + MDEA) and (AEP+ AMP) over a wide range of composition, temperature and CO_2 partial pressure. The solubility data are further correlated using modified Kent-Eisenberg model.

The equilibrium constant related to amine deprotonation and carbamate hydrolysis reaction are regressed to correlate the solubility data. The thermodynamic equilibrium model has been further applied to estimate the pH and liquid phase speciation of the CO_2 loaded solvent. FTIR-ATR and ^{13}C NMR analysis is also performed to assess the reaction scheme. An optimized Feed forward neural network model employing Levenberg- Marquardt algorithm has been also developed to correlate the solubility data.

Chapter 5: Experimental and theoretical analysis of equilibrium CO_2 solubility in aqueous N-(3-aminopropyl)-1, 3-propanediamine (APDA) and its potential blend with (MDEA/AMP) over broad domain of operating parameters has been reported in this chapter. Along with these blends the possibility of another grade of tertiary amine, 1-dimethylamino-2-propanol (1DMAP) has been also assessed for CO_2 absorption. The equilibrium solubility data are also modeled using modified KE and ANN models as discussed in the previous chapter. At the end a comprehensive comparison of the performance of the studied blend with conventional solvent blend used in PCC processes is presented in this chapter.

Chapter 6: In an ending note**,** general conclusions of this work and the directions for future work have been discussed in this chapter.

References

[1] V.M. Delmotte, P. Zhai, H.O. Pörtner, D. Roberts, J. Skea, P.R. Shukla, A. Pirani, W. Moufouma-Okia, C. Péan, R. Pidcock, S. Connors, J.B.R. Matthews, Y. Chen, X. Zhou, M.I. Gomis, E. Lonnoy, T. Maycock, M. Tignor, T. Waterfield. IPCC, (Inter Governmental panel for climate change) 2018. World Meteorological Organization, Geneva, Switzerland, 32 pp.

[2] International Energy outlook 2018 Highlights, US Energy information administration, https://www.eia.gov/outlooks/ieo/.

[3] http://www.globalcarbonatlas.org/en/CO_2-emissions

[4] J.G. Oliver, A.H.W. Peters, Trends in global CO_2 and total greenhouse gas emissions, 2018, PBL Netherlands Environmental assessment agency.

[5] https://ourworldindata.org/per-capita-CO_2

[6] Carbon capture and storage association report. http://www.ccsassociation.org/

[7] Z. Liang, W. Rongwong, H. Liu, K. Fu, H. Gao, F. Cao, Z. Zhang, T. Sema, A, Henni, Recent progress and new developments in post-combustion carbon-capture technology with amine based solvents, Int. J. Greenh. Gas Control 40 (2015) 26-54.

[8] A.A. Olajire, CO_2 capture and separation technologies for end-of-pipe applications-A review, Energy 35 (2010) 2610-2628.

[9] I. Sreedhar, T. Nahar, A. Venugopal, B. Srinivas, Carbon capture by absorption – Path covered and ahead, Renew. Sustain. Energy Rev. 76 (2017) 1080–1107.

[10] A.B. Rao, E.S. Rubin, A technical, economic, and environmental assessment of amine-based CO_2 capture technology for power plant greenhouse gas control, Env. Sci. Tech. 36 (2002) 4467-4475.

[11] S.K. Dash, A.N. Samanta, S.S. Bandyopadhyay, Simulation and parametric study of the post combustion CO_2 capture using aqueous 2-amino-2-methyl-1propanol and piperazine, Int. J. Greenh. Gas Control 21(2014) 130-139.

[12] J.T. Cullinane, G.T. Rochelle, Thermodynamics of aqueous potassium carbonate, piperazine, and carbondioxide, Fluid Phase Equilib. 227 (2005) 197-213.

[13] C. Stewart, M. Hessami, A study of methods of carbon dioxide capture and sequestration -the sustainability of a photosynthetic bioreactor approach, Energ. Convers. Manage. 46 (2005) 403-420.

[14] X.C. Xu, C.S. Song, J.M. Andresan, B.G. Miller, A.W. Scaroni, Novel Polyethyleneimine-modified mesoporous molecular sieve of MCM-41 Type as high-capacity adsorbent for CO_2 capture, Energ. Fuel 16 (2002) 1463-1469.

[15] S. Ullah, M.A. Bustam, M.A. Assiri, A.G. Al-Sehemi, M. Sagir, F.A. Abdul Kareem, A.E.I. Elkhalifah, A. Mukhtar, G. Gonfa, Synthesis, and characterization of metal-organic frameworks -177 for static and dynamic adsorption behavior of CO_2 and CH_4, Micropor. Mesopor. Mat. (2019) 109844.

[16] M.G. Plaza, C.Pevida, A. Arenillas, F. Rubiera, J.J. Pis, CO_2 capture by adsorption with nitrogen enriched carbons, Fuel 86 (2007) 2204-2212.

[17] A. Hart, N. Gnanendran, Cryogenic CO_2 capture in natural gas, Energy Procedia (2009) 697-706.

[18] Y. Han, W.S. W. Ho, Recent advances in polymeric membranes for CO_2 capture, Chi. J. Chem. Eng. 26 (2018) 2238 – 2254.

[19] L. Ansaloni, R. Rennemo, H.K. Knuutila, L. Deng, Development of membrane contactors using volatile amine-based absorbents for CO_2 capture: amine permeation through the membrane, J. Memb. Sci. 537 (2017) 272 – 282.

[20] V. Sluis, C.A. Hendriks, K. Blok, Feasibility of polymer membranes for carbon dioxide recovery from flue gas, Energ. Convers. Manage. 33(1992) 429-436.

[21] J. Li, A. Henni, P. Tontiwachwuthikal, Reaction kinetics of CO_2 in aqueous ethylenediamine, ethyl ethanolamine, and diethyl monoethanolamine solutions in the temperature range of 298-313 K, using the stopped-flow technique, Ind. Eng. Chem. Res. 46 (2207) 4426 – 4434.

[22] J.W. Mason, B.F. Dodge, Equilibrium absorption of carbon dioxide by solutions of the ethanolamines, Trans. Amer. Inst. Chem. Eng. 32 (1936) 27- 48.

[23] J.H. Jones, H.R. Froning, E.E. Claytor, Solubility of acidic gases in aqueous monoethanolamine, J. Chem. Eng. Data 4 (1959) 85-92.

[24] F. Jou, A.E. Mather, F.D. Otto, The solubility of CO_2 in a 30 mass percent monoethanolamine solution, Can. J. Chem. Eng. 73 (1995) 140 – 147.

[25] J.I. Lee, F.D. Otto, A.E. Mather, The solubility of H_2S and CO_2 in aqueous monoethanolamine solutions, Can. J. Chem. Eng. 52 (1974) 803 – 805.

[26] S. Mamun, R. Nilsen, H.F. Svendsen, Solubility of carbon dioxide in 30 mass % monoethanolamine and 50 mass % methyldiethanolamine solutions, J. Chem. Eng. Data 50 (2005) 630-634.

[27] U.E. Aronu S. Gondal , E.T. Hessen , T.H. Warberg , A. Hartono, K.A. Hoff , H.F. Svendsen, Solubility of CO_2 in 15,30,45 and 60 mass % MEA from 40 to120^oC and model representation using the extended UNIQUAC framework. Chem. Eng. Sci. 66 (2011) 6393 – 6406.

[28] M.L. Kennard, A. Melsen, Solubility of carbon dioxide in aqueous diethanolamine solutions at elevated temperatures and pressures, J. Chem. Eng. Data 29 (1984) 309-312.

[29] A. Benamor, M.K. Aroua, Modeling of CO_2 solubility and carbamate concentration in DEA, MDEA and their mixtures using the Deshmukh-Mather model, Fluid Phase Equilib. 231 (2005) 150 – 162.

[30] H. Suleman, A.S. Maulud, Z. Man, Experimental measurements and modelling of carbon dioxide solubility in aqueous AMP/MDEA and Piperazine/MDEA blends, Fluid Phase Equilib. 463 (2018) 142 – 148.

[31] E.E. Isaacs, F.D. Otto, A.E. Mather, Solubility of hydrogen sulfide and carbondioxide in an aqueous diisopropanolamine solution, J. Chem. Eng. Data 22 (1977) 71 – 73.

[32] K.P. Shen, M.H. Li, Solubility of carbon dioxide in aqueous mixtures of monoethanolamine with methyldiethanolamine, J. Chem. Eng. Data 37 (1992) 96-100.

[33] M.K. Park, O.C. Sandall, Solubility of carbon dioxide and nitrous oxide in 50 mass % methyldiethanolamine, J. Chem. Eng. Data 46 (2001) 166 – 168.

[34] A.Chakma, A. Meisen, Solubility of CO_2 in aqueous methyldiethanolamine and N,N-Bis(hydroxyethyl)piperazine solutions, Ind. Eng. Chem. Res. 26 (1987) 2461 – 2466.

[35] S.W. Rho, K.P. Yoo, Solubility of CO_2 in aqueous methyldiethanolamine solutions, J. Chem. Engg. Data 42 (1997) 1161 – 1164.

[36] P.Y. Chung, A.N. Soriano, R.B. Leron, M.H. Li, Equilibrium solubility of carbon dioxide in the amine solvent system of (triethanolamine + piperazine + water), J. Chem. Thermodyn 42 (2010) 802 – 807.

[37] Z. Xu, S. Wang, G. Qi, A.A. Trollebo, H.F. Svendsen, C. Chen, Vapour liquid equilibrium and heat of absorption of CO_2 in aqueous 2-(diethylamino)-ethanol solutions, Int. J. Greenh. Gas Control 29 (2014) 92 – 103.

[38] M. Kundu, B. P. Mandal, and S. S. Bandyopadhyay, Vapor-liquid equilibrium of CO_2 in aqueous solutions of 2-amino-2-methyl-1-propanol, J. Chem. Eng. Data 48 (2003) 789 – 796.

[39] T.T. Teng, A.E. Mather, Solubility of H_2S, CO_2 and their mixtures in an AMP solution, Can. J. Chem. Eng. 67 (1989) 846 – 850.

[40] S.K. Dash, A.N. Samanta, S.S. Bandyopadhyay, Experimental and theoretical investigation of solubility of carbon dioxide in concentrated aqueous solution of 2-Amino-2-methyl-1-propanol and piperazine, J. Chem. Thermodyn. 51 (2012) 120-125.

[41] Y. Liang, H. Liu, W. Rongwong, Z. Liang, R. Idem, P. Tontiwachwuthikul, Solubility, absorption heat and mass transfer studies of CO_2 absorption into aqueous solution of 1-dimethylamino-2-propanol, Fuel 144 (2015) 121 – 129.

[42] P.A. Bouillon, E. Lemaire, A. Mangiaracina, C. Tabasso, First results of the 2.25 t/h post-combustion CO_2 capture pilot plant of ENEL at the Brindisi coal power plant with MEA from 20 to 40% wt. In: Proceedings of the first post-combustion capture conference (PCCC1), 2011, 17–19May, Abu Dhabi.

[43] G.F. Versteeg, W.P.M. Van Swaaij, On the Kinetics between CO_2 and alkanolamines both in aqueous and non-aqueous solutions-II. tertiary amines, Chem. Eng. Sci. 43 (1988) 587 – 591.

[44] D. Barth, C. Tondre, G. Lappal, J.J. Delpuech, Kinetic study of carbon dioxide reaction with tertiary amines in aqueous solutions, J. Phys. Chem. 85 (1981) 3660 – 3679.

[45] G. Sartori, D.W. Savage, Sterically hindered amines for carbon dioxide removal from gases, Ind. Eng. Chem. Fundamen. 22 (1983) 239 – 249.

[46] A.K. Chakraborty, G. Astarita, K.B. Bischoff, CO_2 absorption in aqueous solutions of hindered amines, Chem. Eng. Sci. 41 (1986) 997 – 1003.

[47] S. Xu, Y.W. Wang, F.D. Otto, A.E. Mather, Kinetics of the reaction of carbon dioxide with 2-amino-2-methyl-1-propanol solutions, Chem. Eng. Sci. 51 (1996) 841 – 850.

[48] M.H. Li, K.P. Shen, Densities and solubilities of solutions of carbon dioxide in water + monoethanolamine + N-methyldiethanolamine, J. Chem. Eng. Data 37 (1992) 288–290.

[49] M.H. Li, B.C. Chang, Solubilities of carbondioxide in water + monoethanolamine + 2-amino-2-methyl-1-propanol, J. Chem. Eng. Data 39 (1994) 448 – 452.

[50] M. Kundu, S.S. Bandyopadhyay, Solubility of CO_2 in water + diethanolamine + 2-amino-2-methyl-1-propanol, J. Chem. Eng. Data 51 (2006) 398 – 405.

[51] M. Kundu, S.S. Bandyopadhyay, Solubility of CO_2 in water + diethanolamine + N-methyldiethanolamine, Fluid Phase Equilib. 248 (2006) 158 – 167.

[52] G. Kumar, M. Kundu, Solubility of CO_2 in aqueous blends of (N-methyl-2-ethanolamine + N-methyldiethanolamine) and (N-methyl-2-ethanolamine + 2-amino-2-methyl-1-propanol), J. Chem. Eng. Data 57 (2003) 3203-3209.

[53] D. Tong, G.C. Maitland, M.J.P. Trusler, P.S. Fennell, Solubility of carbondioxide in aqueous blends of 2-amino-2-methyl-1-propanol and piperazine, Chem. Eng. Sci. 101 (2013) 851 – 864.

[54] S.K. Dash, S.S. Bandyopadhyay, Studies on the effect of addition of piperazine and sulfolane into aqueous solution of N-methyldiethanolamine for CO_2 capture and VLE modelling using eNRTL equation, Int. J. Greenh. Gas Control 44 (2016) 227–237.

[55] Y.C. Chang, R.B. Leron, M.H. Li, Equilibrium solubility of carbon dioxide in aqueous solutions of (diethylenetriamine + piperazine), J. Chem. Thermodyn. 64 (2013) 106 – 113.

[56] B.K. Mondal, S.S. Bandyopadhyay, A.N. Samanta, Equilibrium solubility measurement and Kent-Eisenberg modeling of CO_2 absorption in aqueous mixture of N-methyldiethanolamine and hexamethylenediamine, Greenh. Gas Sci. Technol. (2016) 1-13.

[57] B.K. Mondal, S.S. Bandyopadhyay, A.N. Samanta, Experimental measurement and Kent-Eisenberg modelling of CO_2 solubility in aqueous mixture of 2-amino-2-methyl-1-propanol and hexamethylenediamine, Fluid Phase Equilib. 437 (2017) 118–126.

[58] A. Hafizi, M.H. Mokari, R. Khalifeh, M. Farsi, M.R. Rahimpour, Improving the CO_2 solubility in aqueous mixture of MDEA and different polyamine promoters: The effects of primary and secondary functional groups, J. Mol. Liq. (2019) 111803.

[59] M.J. Khodadadi, S. Riahi, M. Abbasi, Experimental modeling of the solubility of carbon dioxide in aqueous solution of monoethanolamine +1, 3-diaminopropane, J. Mol. Liq. 281 (2019) 415 – 422.

[60] Y.E. Kim, J.H. Choi, S.C. Nam, Y.I. Yoon, CO_2 absorption capacity using aqueous potassium carbonate with 2-methylpiperazine and piperazine, J. Ind. Eng. Chem. 18 (2012) 105 – 110.

[61] A.T. Zoghi, F. Feyzi, Equilibrium solubility of carbon dioxide in aqueous 2-((2-aminoethyl) amino) ethanol and N-methyldiethanolamine solution and modeling by electrolyte mPR-CPA EoS, J. Chem. Thermodyn. 67 (2013) 153 – 162.

[62] S. Bishnoi, G.T. Rochelle, Thermodynamics of piperazine / methyldiethanolamine / water/ carbon dioxide, Ind. Eng. Chem. Res. 41 (2002) 604 – 612.

[63] S.K. Dash, A.N. Samanta, S.S. Bandyopadhyay, Experimental and theoretical investigation of solubility of carbon dioxide in concentrated aqueous solution of 2-amino-2-methyl-1-propanol and piperazine, J. Chem. Thermodyn. 51 (2012) 120 -125.

[64] Y. Du, Le. Li, O. Namjoshi, K.A. Voice, A.N. Fine, G.T. Rochelle, Aqueous piperazine/N-(2-aminoethyl) piperazine for CO_2 capture, Energy Procedia 37 (2013) 1621-1638.

[65] S. Paul, A. K. Ghoshal, B. Mandal, Kinetics of absorption of carbon dioxide into aqueous solution of 2-(1-piperazinyl)-ethylamine, Chem. Eng. Sci. 64 (2009) 313-321.

[66] R. Ramazani, S. Mazinani, A. Hafizi, A. Jahanmiri, Equilibrium solubility of carbon dioxide in aqueous blend of monoethanolamine (MEA) and 2-1-piperazinyl-ethylamine (PZEA) solutions: Experimental and optimization study, Process Saf. Environ. Prot. 98 (2015) 325–332.

[67] P. Singh, J.P.M. Niederer, G.F. Versteeg, Structure and activity relationships for amine-based CO_2 absorbents-II, Chem. Eng. Res. Des. 7 (2008) 135–144.

[68] B.K. Mondal, S.S. Bandyopadhyay, A.N. Samanta, Measurement of CO_2 absorption enthalpy and heat capacity of aqueous hexamethylenediamine and its aqueous mixture with N-methyldiethanolamine, J. Chem. Thermodyn. 113 (2017) 276 – 290.

[69] S.K. Dash, L. Wadibhasme, Retrofitting a CO_2 capture unit with a coal based power plant: process simulation and parametric study, J. Clean Energy Tech. 5 (2017) 248 – 253.

[70] B.P. Spigarelli, S.K. Kawatra, Opportunities and challenges in carbon dioxide capture. J.CO_2.Util. 1 (2013) 69-87.

[71] H. Arcis, L. Rodier, J.Y. Coxam, Enthalpy of solution of CO_2 in aqueous solutions of 2-amino-2-methyl-1-propanol, J. Chem. Thermodyn. 39 (2007) 878–887.

[72] G.T. Rochelle, Thermal degradation of amines for CO_2 capture, Curr. Opin. Chem. Eng. 1 (2012) 183–190.

[73] A.K. Saha, S.S. Bandyopadhyay, A.K. Biswas, Kinetics of absorption of CO_2 into aqueous solutions of 2-amino-2-methyl-1-propanol, Chem. Eng. Sci. 50 (1995) 3587–3598.

[74] S. Kadiwala, A.V. Rayer, A. Henni, Kinetics of carbon dioxide (CO_2) with ethylenediamine, 3-amino-1-propanol in methanol and ethanol, and with 1-dimethylamino-2-propanol and 3-dimethylamino-1-propanol in water using stopped-flow technique, Chem. Eng. J. 179 (2012) 262– 271.

[75] J. Choi, Y. Kim, S. Nam, S. Yun, Y. Yoon, J. Lee, CO_2 absorption characteristics of a piperazine derivative with primary, secondary, and tertiary amino groups, Kor. J Chem. Engg. 33 (2016) 3222-3230.

[76] S. Paul, A.K. Ghoshal, B. Mandal, Kinetics of absorption of carbon dioxide into aqueous blends of 2-(1-piperazinyl)-ethylamine and N-methyldiethanolamine, Chem. Eng. Sci. 64 (2009) 1618–1622.

[77] B. Das, B. Deogam, B. Mandal, Absorption of CO_2 into novel aqueous bis (3-aminopropyl)amine and enhancement of CO_2 absorption into its blends with N-methyldiethanolamine, Int. J. Greenh. Gas Control 60 (2017) 172–185.

Chapter 2

REACTION MECHANISM AND MODELING APPROACHES FOR CO_2-AQEOUS AMINE SYSTEM

This chapter presents a comprehensive review of the basic reaction chemistry of aqueous amine solution with CO_2. Kinetics and thermodynamic concepts pertaining to the CO_2 absorption in aqueous amine solution have been briefly outlined here. The discussion includes reaction mechanism corresponding to various amine groups, developing rate expression and the interpretation of possible reaction products. The second part of the chapter mostly deals with the thermodynamics and the detail explanation on the various modeling strategies adopted in the present work to correlate the CO_2 solubility data.

2.1 Introduction

Absorption of CO_2 in alkanolamine solutions involves the chemical reaction of the CO_2 with the amines and hence the reaction scheme is also different for different categories of amines. The chemical reaction taking place in the aqueous amine phase results in the enhancement of overall liquid phase mass transfer coefficient compared to physical absorption case. In the case of slow reactions, the gas molecules first penetrate well into the bulk liquid phase prior to the commencement of reaction, hence the net effect of chemical reactions is not pronounced in the enhancement of overall mass transfer coefficient. Whereas in the case of very fast reaction, within a short distance from the gas-liquid interface, both the solute molecules and the reactants are instantaneously consumed by the reaction. In between slow and very fast reaction regime, there exist moderately fast and fast categories which again showcase different absorption kinetics. Hence to establish the appropriate reaction mechanism, the proper knowledge of reaction mechanism as well as reaction regimes are very much essential in the gas-liquid absorption system.

Along with the reliable solubility measurement techniques, appropriate mathematical models are also very much needed to predict the gas solubility over a varied range of operating conditions of temperature and acid gas loading. Equilibrium thermodynamics prevailing in the aqueous amine system can be expressed as the amalgamation of physical equilibrium prevailing in the gas-liquid phase and the reaction equilibrium corresponding to various intermediate reactions existing in aqueous alkanolamine systems. The thermodynamic framework as well as the development of accurate process model development pertaining to non-rigorous modified Kent Eisenberg models has been discussed in the subsequent sections. The chapter also discusses the development of ANN model, model architecture as well as optimization of the ANN network.

2.2 Reaction mechanism of CO_2-aqueous alkanolamine system

Two reaction mechanisms are generally used to articulate the reaction of CO_2 with a primary or secondary alkanolomaine: namely the zwitter ion mechanism and the termolecular mechanism, while the reaction of tertiary amines is described by the base catalyzed hydration of CO_2 [1].

2.2.1 Zwitterion mechanism

This mechanism was first introduced by Caplow [2] and later few amendments are introduced by Danckwerts [3]. According to the mechanism, CO_2 first reacts with amine functional group and forms an intermediate zwitterion compound. In the second step, this intermediate species undergo deprotonation upon reacting with any base molecules. According to Caplow [3] prior to CO_2-amine reaction, hydrogen bonding prevails in the aqueous system, however, later this assumption is neglected in the works of Danckwerts [3], Versteeg [4], Kumar [5]. Hence the reaction of CO_2 with primary and secondary amine can be explained as follows:

$$CO_2 + Am \underset{k_{-1}}{\overset{k_2}{\rightleftharpoons}} Am^+COO^- \qquad \text{(R 2.1)}$$

The intermediate zwitterion is a short lived species and it readily reacts with a base molecule b which results in its subsequent deprotonation. This results in the formation of carbamate species:

$$Am^+COO^- + b \xrightarrow{k_b} AmCOO^- + bH^+ \qquad \text{(R 2.2)}$$

In the above reaction, the component b can be the species ranging from an amine group, hydroxyl ion or water molecule. Since the presence of OH^- ion in the aqueous reaction phase is very less compared to the dominant species such as amine and H_2O molecule. On account of this, the net contribution of OH^- to the overall reaction rate can be neglected. Steady state principle to the intermediately formed zwitterion species can be used to estimate the rate of reaction existing in the CO_2-aqueous amine solutions.

$$r_{CO_2-amine} = \frac{k_2[CO_2][Am]}{1+\frac{1}{\sum\left(\frac{k_b}{k_{-1}}\right)[b]}} \tag{2.1}$$

Where,

k_2 = forward reaction rate constant for the formation of zwitterion

k_{-1} = reverse reaction rate constant for the formation of zwitterion

k_b = forward reaction rate constant for the deprotonation reaction

[Am] = concentration of amine

[CO_2] = concentration of carbon dioxide

[b] = concentration of base

The above equation can be further analyzed based on two asymptotic analysis approach.We can consider two cases:

Case 1: $\frac{k_{-1}}{k_b[b]} << 1$: At this condition, it can be interpreted that the zwitterion deprotonation reaction is faster as compared to the reverse reaction of zwitterion to form CO_2 and amine. As a result, the overall reaction can be considered to be second order and the equation can be simplified to:

$$r_{CO_2-amine} = k_2[CO_2][Am] \tag{2.2}$$

Case 2: $\frac{k_{-1}}{k_b[b]} >> 1$: At this condition, it can be considered that zwitterion deprotonation is the rate determining step, which results in a more complex form of equation

$$r_{CO_2-amine} = \frac{k_2[CO_2][Am](k_b[b])}{k_{-1}} \quad (2.3)$$

It can be inferred from the simplified equation deduced above that in the transition region between two asymptotic case, the reaction order changes between two and three. In the case of base molecule considered in reaction (R 2.2) to be amine itself, the carbamate formation reaction can be described by:

$$Am^+COO^- + Am \rightarrow AmCOO^- + AmH^+ \quad (R\ 2.3)$$

Hence in this case the overall reaction can be described based on the carbamate formation and can be represented by reactions (R 2.1) and (R 2.3):

$$CO_2 + 2Am \rightleftharpoons AmCOO^- + AmH^+ \quad (R\ 2.4)$$

Now in the case of sterically hindered amine, the formed zwitterion species reacts more conveniently with water molecules which lead to the formation of bicarbonate species.

$$AmCOO^- + H_2O \rightarrow HCO_3^- + AmH^+ \quad (R\ 2.5)$$

Similarly, the overall reaction related to the formation of bicarbonate species in the case of sterically hindered amine can be described by reactions (R 2.1) and (R 2.5):

$$CO_2 + Am + H_2O \rightleftharpoons HCO_3^- + AmH^+ \quad (R\ 2.6)$$

Since the AMP forms unstable carbamate hence it readily undergoes hydrolysis resulting in the formation of free amine molecules and bicarbonate species. The reaction scheme can be described by:

$$Am^+COO^- + H_2O \rightleftharpoons HCO_3^- + Am \quad (R\ 2.7)$$

The free amine molecule liberated as per the previous equati on again reacts with CO_2 and hence the chances of bicarbonate formation are predominantly higher compared to carbamate ions. Along with the fundamental amine-CO_2 reactions described here, the other important reactions taking place in the aqueous amine medium consists of the reactions involving water molecules and its dissociation products. The water dissociation reaction can be expressed as:

$$H_2O \rightleftharpoons H^+ + OH^- \qquad \text{(R 2.8)}$$

Similarly, the following simultaneous reactions having different kinetics are also taking place in the aqueous amine solution.

$$Am + H_2O \rightleftharpoons AmH^+ + OH^- \qquad \text{(R 2.9)}$$

$$CO_2 + H_2O \rightleftharpoons HCO_3^- + H^+ \qquad \text{(R 2.10)}$$

$$CO_2 + OH^- \rightleftharpoons HCO_3^- \qquad \text{(R 2.11)}$$

Reaction (R 2.10) can be neglected considering a very low reaction rate (k= 0.026 s^{-1} at 298 K). However, the reaction (R 2.11) contributes essentially to the overall reaction rate. The forward reaction rate of (R 2.11) is described by:

$$r_{CO_2-OH^-} = k^*_{OH^-}[CO_2][OH^-] \qquad (2.4)$$

Hence the overall reaction rate is given by:

$$r_{ov} = \frac{k_2[CO_2][Am]}{1 + \frac{1}{\sum\left(\frac{k_b}{k_{-1}}\right)[b]}} + k^*_{OH^-}[OH^-][CO_2] \qquad (2.5)$$

$$= k_{ov}[CO_2]$$

Where,

$[OH^-]$ = Concentration of hydroxyl ion in the reaction medium

$k^*_{OH^-}$ = Reaction rate constant for water hydration, $m^3.kmol.s^{-1}$

r_{ov} = Overall rate pertaining to CO_2-aqueous alkanolamine reaction.

k_{ov} = Overall reaction rate constant

2.2.2 Termolecular mechanism

According to termolecular mechanism [6], amine present in the aqueous solution reacts simultaneously with CO_2 and one molecule of base, b. According to this mechanism, the proton transfer and the necessary bond formation between the amine molecules and CO_2 takes place simultaneously.

$$CO_2 + Am \cdots\cdots b \rightleftharpoons AmCOO^- \cdots\cdots bH^+ \qquad \text{(R 2.12)}$$

The reaction witnesses the formation of an unstable short lived intermediate chemical complex. The complex further dissociates into free amine molecule and CO_2, while a small fraction of intermediate reacts with an water molecule or amine molecule to form ionic products.

2.2.3 Base catalyzed hydration mechanism

There is no as such direct reaction exist between tertiary amines (represented here as R_3N) and CO_2. Instead in aqueous medium, it facilitates the hydrolysis reaction of CO_2 to generate bicarbonate species. The reaction scheme can be expressed as [7]:

$$CO_2 + R_3N + H_2O \xrightarrow{k_2} R_3NH^+ + HCO_3^- \qquad \text{(R 2.13)}$$

Since the reaction with tertiary amines results in the generation of protonated amines and bicarbonate ions in aqueous solutions, it results in higher CO_2 loading and lower heat of absorption compared to primary and secondary amines.

2.3 Modeling of CO_2 solubility data

For the rational design of CO_2 capture unit, both experimental and theoretical analysis of solubility data is equally essential. The CO_2 solubility or VLE data in the aqueous amine systems are generally expressed in the form of total concentration of CO_2 prevailing in the aqueous amine solution vs the total partial pressure of the gas phase at equilibrium conditions. However,

appropriate correlations are always necessary for interpolating and extrapolating the data to the desired range of operating conditions [8].

In an absorber unit CO_2-amine reaction leads to the generation of various ionic species. Various thermodynamic models have been implemented to assess the reaction equilibrium prevailing in the CO_2 – amine system. In this regard, numerous studies have been performed and reported in the open literature for predicting equilibrium solubility data corresponding to both single and blended amine solvents. The thermodynamic models which are applied to predict or model the solubility data of CO_2 in aqueous alkanolamine solutions can be broadly classified into following heads [1]:

- Rigorous models based on excess Gibbs energy (gamma-phi models): The model uses the application of excess Gibbs energy. Electrolyte-NRTL and e-UNIQUAC are some of the widely used models in this category [9 - 10]. Faramarzi et al. [11] used e-UNIQUAC equation to model the binary aqueous solution of MEA and MDEA as well as ternary amine blends of MEA and MDEA.
- Equation of state model (phi-phi approach): In this category various equation of state (EOS) are used which can precisely assess the molecular interactions can be used to correlate the solubility data, eg. PR-EOS, PC-SAFT, electrolyte EOS [12], etc.
- Non-rigorous Empirical models: These models apply the reaction equilibrium constant to estimate the solubility data. It neglects the system non-ideality and hence fugacity, as well as, activity coefficient is considered as unity. The Kent –Eisenberg model is one of the preliminary models which is used till today in various modified forms with improved accuracy [13]

2.3.1 Modified Kent-Eisenberg model

The first practical and versatile model was proposed by Kent and Eisenberg [13]. This model neglects the non-ideality that exists between the aqueous amine-CO_2 systems. Thus compared to other rigorous models, the only parameter to estimate is the equilibrium reaction constants. The equilibrium reaction constants can be easily determined by estimating it as a function of important operating parameters. Also in rigorous models, the failure to provide a good estimate

of the initial guess values can lead to the convergence problems in the solubility estimation. As a result, the KE model reduces the computation time to a great extent. Lee et al. [14] reported that KE model has been found to provide a good prediction between the experimental and predicted over a wide range of experimental conditions.

2.3.1.1 Thermodynamic framework

The equations describing the CO_2 - primary or secondary / tertiary amines aqueous system equilibrium can be represented as follows: (where RNH_2 represents Primary amine and R_3N represents tertiary amine)

$$RNH^{3+} \overset{K_{11}}{\rightleftharpoons} H^+ + RNH_2 \quad \text{(R 2.14)}$$

$$R_3NH^+ \overset{K_{11}}{\rightleftharpoons} H^+ + R_3N \quad \text{(R 2.15)}$$

$$RNHCOO^- + H_2O \overset{K_2}{\rightleftharpoons} RNH_2 + HCO_3^- \quad \text{(R 2.16)}$$

$$H_2O + CO_2 \overset{K_3}{\rightleftharpoons} H^+ + HCO_3^- \quad \text{(R 2.17)}$$

$$H_2O \overset{K_4}{\rightleftharpoons} H^+ + OH^- \quad \text{(R 2.18)}$$

$$HCO_3^- \overset{K_5}{\rightleftharpoons} H^+ + CO_3^{2-} \quad \text{(R 2.19)}$$

Where,

K_{11} = Equilibrium constant of de-protonation of amine
K_2 = Equilibrium constant of carbamate hydrolysis of amine
K_3 = Equilibrium constant of formation of bicarbonate ion
K_4 = Equilibrium constant of dissociation of water
K_5 = Equilibrium constant of dissociation of bicarbonate ion

The concentration of CO_2 in liquid phase can be obtained from Henry's Law,

$$P_{CO_2} = H_{CO_2}[CO_2] \quad (2.6)$$

Where, P_{CO_2} is the equilibrium CO_2 partial pressure and H_{CO_2} is the Henry's law constant for CO_2 in aqueous amine solutions. The overall amine mass and electro neutrality balance equation for the primary amine can be written as:

$$m_1 = [RNH_2] + [RNH_3^+] + [RNHCOO^-] \quad (2.7)$$

$$m_1 \times \alpha_{CO_2} = [CO_2] + [HCO_3^-] + [CO_3^{2-}] + [RNHCOO^-] \quad (2.8)$$

$$[RNH_3^+] + [H^+] - [RNHCOO^-] + [HCO_3^-] + 2[CO_3^{2-}] + [OH^-] = 0 \quad (2.9)$$

Where, all the terms in third bracket represented in equation (2.7) – (2.8) stands for the ionic concentrations of all the species prevailing in the reaction phase.

Procedure for the modeling of CO_2 solubility can be expressed as [15]:

- Development of a non-linear equation that can be able to describe the chemical and physical equilibria existing in CO_2-aqueous amine systems. Also the charge balance equation of all the ions can be also considered.
- Estimation of concentration of all the ionic species expressed in the reaction equilibria by solving the non-linear equation formed in the above step
- Determination of the unknown equilibrium constants, K_i corresponding to the amine based chemical reactions by minimizing the AAD between the estimated and experimental CO_2 loading data.

The equilibrium constant pertaining to reactions (R 2.17) - (R 2.19) are generalized and can be obtained from open literature. While the solvent specific equilibrium constants represented in reactions (R 2.14 – R 2.16) needs to be regressed and estimated to fit the experimental solubility data. Kent-Eisenberg in their original work expressed the equilibrium constant as well as Henry's law constant in terms of temperature alone

$$\ln K = l + \frac{m}{T} + n.\ln T + o.T \quad (2.10)$$

where, T is temperature and l, m and n are the coefficients. Later, Chakma and Meisen [16] proposed a modified model expression in which the equilibrium constants of important amine reactions are represented as a function of other important process variables such as amine concentration and acid gas partial pressure along with the operating temperature. They obtained satisfactory results with the CO_2 solubility prediction in (AMP + DGA) solutions.

Several correlations were proposed in the open literature related to equilibrium constant K_i for modeling the experimental data. Li and Shen [17] represented the equilibrium constants of amine deprotonation as well as carbamate hydrolysis reaction in terms of temperature, CO_2 loading, and concentration. Recently, Khodadadi et al. [18] also employed the similar expression for modeling CO_2 solubility in a mixture of monoethanolamine and 1,3-diaminopropane.

$$\ln K_i = p_i + \frac{p_i}{T} + \frac{p_i}{T^3} + q_i \alpha_{CO_2} + \frac{q_i}{\alpha_{CO_2}} + \frac{q_i}{\alpha^2_{CO_2}} + q_i \ln m \tag{2.11}$$

Where, T, α_{CO_2} and m represents temperature, CO_2 loading and solvent concentration repectively. And p, q relates to the corresponding coefficients. Mondal et al. [19] regressed equilibrium constant as a function of CO_2 loading and temperature for (HMDA+MDEA+H_2O+CO_2) system. The equilibrium constant corresponding to HMDA bicarbamate formation and zwitterion deprotonation has been regressed to predict the solubility data.

$$\ln K_i = a_i + b_i \alpha + \frac{c_i}{T} + d_i \alpha^2 + \frac{e_i}{T^2} + f_i \frac{\alpha}{T} \tag{2.12}$$

Garg et al. [20] expressed the equilibrium constant in terms of partial pressure of CO_2, temperature and concentration of CO_2 in the solvent phase in order to predict the solubility. The equilibrium constant pertaining to amine deprotonation reaction of phenylalanine salts as well as its carbamate hydrolysis reaction are expressed as:

$$K_i = A_i + B_i m + C_i T + D_i m^2 + E_i (m \times T) + F_i (T^2) + G_i (P_{CO_2}) + H_i (P_{CO_2}{}^2) \tag{2.13}$$

Where, P_{CO_2} expressed in equation (2.13) stands for Partial pressure of CO_2 and the K_i used in equation (2.10 -2.13) stands for apparent equilibrium constant.

2.3.2 Artificial neural network model

Neural networks are considered as one of the versatile and widely used computation tools for the estimation of various properties compared to usual mathematical correlations, since it does not require a pre-assumption of the input-output relationship. Artificial neural network (ANN) platform has been already applied in correlating equilibrium solubility data of CO_2 with various solvent systems [21-24].

2.3.2.1 Multilayer feed-forward networks

Neural networks are classified depending on various parameters such as the algorithm adopted in the network, type of network architecture input transformation. Out of various ANN model described in literature, feed-forward multilayer neural network (FNN) is the most popular choice among researchers since it can represent effectively the non-linearity between the different variables representing many complex systems [25]. Fig. 2.2 represents an arrangement of a typical multiple layer neural network for the prediction of CO_2 solubility in a blended aqueous amine solution.

The network consists of an input layer, one or more hidden layers and an output layer which are again connected by neurons, where the information is getting processed. In order to improve the prediction accuracy of the network handling more number of neural interactions, multiple hidden layers can be employed. The data pertaining to all the input parameters for a corresponding system are introduced into the input layer. The data are then transferred to the one or more hidden layers via neurons for processing and then it is sent to output layers for the final projection.The neurons in the hidden layer and output layer must be trained to determine the output of the network. Information at the input layer is processed at each neuron in the hidden layer using a transfer function and then transferred to the output layer as given by:

$$Y_i = f\left(\sum_{i=1}^{n}(w_i X_i + b_i)\right) \qquad (2.14)$$

Where, X_i and Y_i represent the input and output of the i^{th} neuron, respectively, f is the transfer function, w_i is the weight coefficient and b_i is the bias associated with each weight coefficient. For a network to simulate a certain task, weights and biases are adjusted automatically. This

process is called training, in which a suitable training algorithm is used to process the weights and biases of the network. The objective of the training is to minimize the error between the modeled output and the actual or experimental value. The ANN architecture used in this work consists of Levenberg-Marquardt (LM) back-propagation algorithm as training function [26-27].

The LM algorithm is considered as the fastest algorithm for moderate size networks and it is characterized by an exclusive feature of memory reduction when the network functions having large number of data sets. The transfer function implemented for hidden and output layers are hyperbolic tangent sigmoid functions and linear function, respectively.

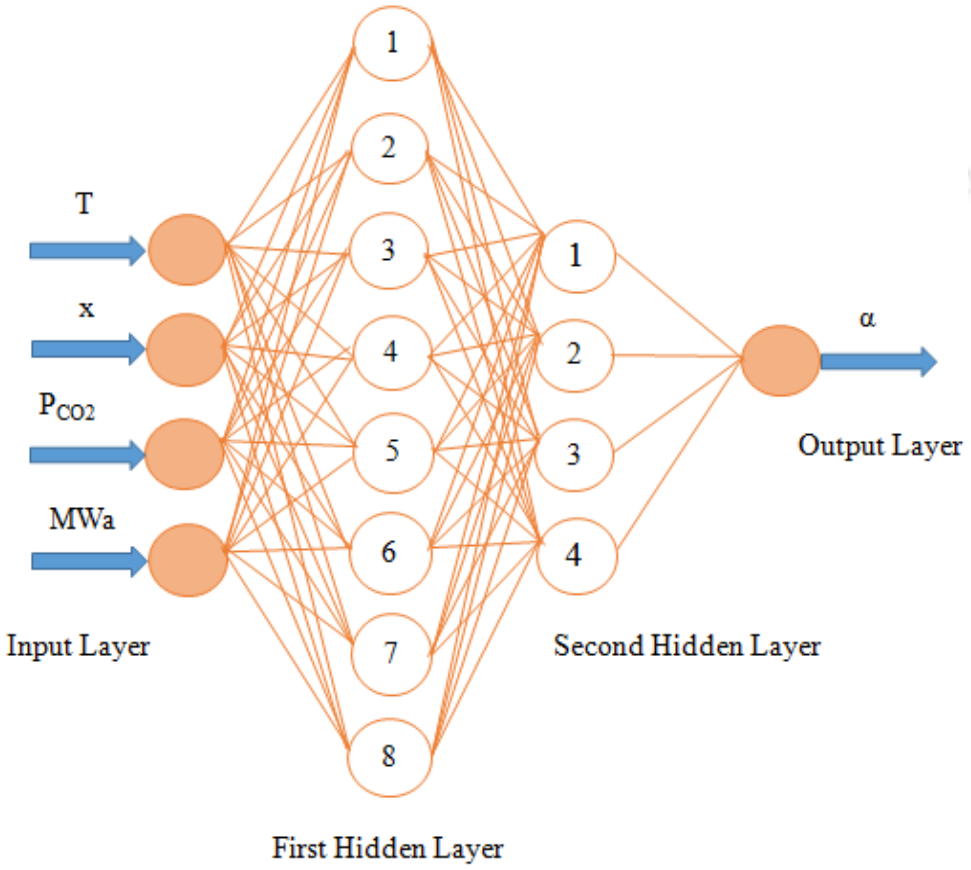

Fig. 2.1 Network structure of the multilayer feed-forward network with two hidden layers, consisting of 8 and 4 neurons

$$f_{hid}(x) = \frac{2}{1+e^{-2x}} - 1 \qquad (2.15)$$

$$f_{out}(x) = x \tag{2.16}$$

Where, $f_{hid}(x)$ and $f_{out}(x)$ represents the transfer function employed for hidden layer and output layer respectively. The transfer function used in hidden layer is hyperbolic tangent sigmoid function and the linear function is used in output layer.The prime objective of the training procedure is to minimize the error between experimental and predicted value. The performance and the validation of the developed network is analyzed using the statistical parameter as expressed below:

$$\text{Mean square error } (MSE) = \frac{1}{N}\sum_{i=1}^{N}\left(Y_i^{\exp} - Y_i^{pre}\right)^2 \tag{2.17}$$

Where 'N' stands for the number of data points, $Y_i^{\exp}$ is the experimental value of output variable, Y_i^{pre} is the network predicted value of output variable.

2.3.3.2 Analysis and acquirement of solubility data

Precise experimental CO_2 solubility data at different operating conditions are very much essential for optimizing particular neural network. The total data sets entered into the network can be further divided into three parts:

Training data sets: These are provided to the network through the training procedure and the network is optimized according to the generated error

Validation data sets: These are employed to compute the network generalization, and to stop the training process when there is no further improvement in the generalization

Testing data sets: These have no direct influence on the training process and hence give an independent measurement of the network performance during and after training.

Most of the researchers in this domain used 70 % of the total data sets for training. So in the present system, the networks are developed keeping 70 % data for training, 15 % for validation and 15% for testing [28]. Before the training of the ANN network, the input and output data sets are normalized in the range of 0-1, since all the input and output property data sets are acquainted with different units and range.

$$Y_i = \frac{X_i - X_{\min}}{X_{\max} - X_{\min}} \tag{2.18}$$

The maximum value of different input variables, X_i is represented by $X_{\max}$ and the minimum value is expressed as $X_{\min}$ respectively in the training and test data sets. Y_i is the normalized value of the input and output variable in the range of (0-1). The optimal design of the ANN was figured out by the trial and error method with the variation in the number of neurons. A low number of neurons may result in large errors in the network while a large number may lead to over-fitting [29, 30]. Optimum structure of the network is considered based on the minimum error criteria (% AAD and MSE).

The main limitation of the artificial neural network model is its black box nature and the unexplained behavior of the network. Also there is no specific rule for determining the structure of artificial neural network. Appropriate network structure is achieved through experience and trial and error. Moreover, ANN modeling requires much more data compared to conventional models for better prediction.

References

[1] Z. Liang, W. Rongwong, H. Liu, Recent progress and new developments in post-combustion carbon-capture technology with amine based solvents, Int. J. Greenh. Gas Control 40 (2015) 26-54.

[2] P. Danckwerts, The reaction of CO_2 with ethanolamines, Chem. Eng. Sci. (1979) 443-446.

[3] M. Caplow, Kinetics of carbamate formation and breakdown, J. American Chem. Soc. 90 (1968) 6795-6803.

[4] G. Versteeg, L.V. Dijck, W.P.M. Swaaij, On the kinetics between CO_2 and alkanolamines both in aqueous and non-aqueous solutions- An overview, Chem. Eng. Com. 144 (1996)113-158.

[5] P. Kumar, J. Hogendoorn,, G. Versteeg,, P. Feron, Kinetics of the reaction of CO_2 with aqueous potassium salt of taurine and glycine, AIChE Journal 49(2003)203-213.

[6] J.E. Crooks, J.P. Donnellan, Kinetics and mechanism of the reaction between carbon dioxide and amines in aqueous solution, J. Chem. Soc. Perkin Transactions 2 (1989) 331-333.

[7] T.L. Donaldson, Y.N. Nguyen. Carbon dioxide reaction kinetics and transport in aqueous amine membranes, Ind. Eng. Chem. Fund. 19 (1980) 260-266.

[8] G. Kumar, Vapour liquid equilibrium of carbon dioxide in newly proposed blends of alkanolamine, (2013) Ph D dissertation. NIT Rourkela

[9] S.K. Dash, A.N. Samanta, S.S. Bandyopadhyay, Vapour liquid equilibria of carbon dioxide in dilute and concentrated aqueous solutions of piperazine at low to high pressure, Fluid Phase Equilib. 300 (2011) 145-154.

[10] A. Haghtalab, H. Eghbali, A. Shojaeian, Experiment and modeling solubility of CO_2 in aqueous solutions of diisopropanolamine + 2-amino-2-methyl-1-propano + piperazine at high pressures, J. Chem. Thermodyn. 71 (2014) 71–83.

[11] L. Faramarzi, G.M. Kontogeorgis, K. Thomsen, E.H. Stenby, Extended UNIQUAC model for thermodynamic modeling of CO2absorption in aqueous alkanolamine solutions, Fluid Phase Equilib. 282 (2009)121–132.

[12] F. Diab, E. Provost, N. Laloue, P. Alix, W. Furst, Effect of the incorporation of speciation data in the modeling of CO_2–DEA–H_2O system, Fluid Phase Equilib. 353 (2013) 22–30.

[13] R.L. Kent, B. Eisenberg, Better data for amine treating, Hydrocarbon Process. 55 (1976) 87-90

[14] I.J. Lee, F.D. Otto, A.E. Mather, The measurement and prediction of the solubility of the mixtures of carbon dioxide and hydrogen sulphide in a 2.5 N monoethanolamine solutions, Can. J. Chem. Eng., 54 (1976) 803-805.

[15] S.J. Hwang, H.K. Kwang, S. Lee, Prediction of VLE for aqueous blended amines using VLE models of single amines, Int. J. Greenh. Gas Control 49 (2016) 250–258

[16] A. Chakma, A. Meisen, Improved Kent-Eisenberg model for predicting CO_2, solubilities in aqueous diethanolamine (DEA) solutions, Gas Sep. Pur. 4 (1990) 37-40.

[17] M.H. Li, K.P. Shen, Calculation of equilibrium solubility of carbon dioxide in aqueous mixtures of monoethanolamine with methyldiethanolamine, Fluid Phase Equilib. 85 (1993) 129-140

[18] M. Khodadadi, S. Riahi, M. Abbasi, Experimental modeling of the solubility of carbon dioxide in aqueous solution of monoethanolamine +1, 3-diaminopropane, J. Mol. Liq. 281 (2019) 415 – 422.

[19] B.K. Mondal, S.S. Bandyopadhyay, A.N. Samanta, Equilibrium solubility measurement and Kent-Eisenberg modeling of CO_2 absorption in aqueous mixture of N-methyldiethanoalmine and hexamethylenediamine, Greenh. Gas Sci. Tech. (2016) 1-13.

[20] S. Garg, A.M. Shariff, M.S. Shaikh, B. Lal, H. Suleman, N. Faiqa, Experimental data , thermodynamic and neural network modeling of CO_2 solubility in aqueous sodium salt of L -phenylalanine, J. CO_2 Util. 19 (2017) 146–156.

[21] R.S. Abdul, A.A. Omar, B. Lal, Performance of aqueous tetrabutylammonium hydroxide, piperazine and their blends for carbon dioxide capture, J. Mol. Liq. 214 (2016) 522-528.

[22] S. Babamohammadi, A. Shamiri , T.N.G. Borhani , M.S. Shafeeyan , M.K. Aroua , R. Yusof, Solubility of CO_2 in aqueous solutions of glycerol and monoethanolamine, J. Mol. Liq. 249 (2018) 40-52.

[23] C. Li, H. Liu, M. Xiao, X. Luo, H. Gao, Z. Liang, Thermodynamics and ANN models for predication of the equilibrium CO_2 solubility in aqueous 3-dimethylamino-1-propanol solution, Int. J. Greenh. Gas Control 63 (2017) 77–85.

[24] H. Yarveicya, M. M. Ghiasi, A. H. Mohammadi, Performance evaluation of the machine learning approaches in modeling of CO_2 equilibrium absorption in Piperazine aqueous solution, J. Mol. Liq. 255 (2018) 375-383.

[25] M.E. Hamzehie, S. Mazinani , F. Davardoost , A. Mokhtare , H. Najibi ,B.V. Bruggen, S. Darvishmanesh, Developing a feed forward multilayer neural network model for prediction of CO_2 solubility in blended aqueous amine solutions, J. Nat. Gas Sci. Eng. 21 (2014) 19-25.

[26] M. Mirarab, M. Sharifi, M.A. Ghayyem, F. Mirarab, Prediction of solubility of CO_2 in ethanol-[EMIM][Tf2N] ionic liquid mixtures using artificial neural networks based on genetic algorithm, Fluid Phase Equilib. 371 (2014) 6–14.

[27] M. Mirarab, M. Sharifi, B. Behzadi, M.A. Ghayyem, Intelligent prediction of CO_2 capture in propyl amine methyl imidazole alanine ionic liquid: an artificial neural network model, Sep. Sci. Technol. 50 (1) (2014) 26–37.

[28] H. Pahlavanzadeh , S. Nourani, M. Saber, Experimental analysis and modeling of CO_2 solubility in AMP (2-amino-2-methyl-1-propanol) at low CO_2 partial pressure using the models of Deshmukh–Mather and the artificial neural network, J. Chem. Thermodyn. 43 (2011) 1775-1783

[29] G. Chen, X. Luo, H. Zhang, K. Fu, Z. Liang, W. Rongwong, P. Tontiwachwuthikul, R. Idem, Artificial neural network models for the prediction of CO_2 solubility in aqueous amine solutions, Int. J. Greenh. Gas Control 39 (2015) 174-184.

Chapter 3

THERMOPHYSICAL PROPERTIES OF AQUEOUS SINGLE AND BLENDED AMINES

This chapter reports thermophysical properties such as density, viscosity and surface tension data of aqueous 1-(2-aminoethyl) piperazine and N-(3-aminopropyl)-1,3-propanediamine as well as their potential blends with N-methyldiethanoalmine and 2-amino-2-methyl-1-propanol. All the measurement were conducted over the temperature range of (303.2 to 343.2) K. The density and viscosity results were further correlated as a function of temperature and concentration of amine with Redlich - Kister and Grunberg - Nissan models, respectively. The experimental surface tension data were correlated by using temperature based correlation and multiple linear regression technique. The experimental viscosity data were further utilized to analyze various thermodynamic properties such as enthalpy (ΔH^o), entropy (ΔS^o) and Gibbs energies (ΔG^o) of activation of viscous flow.

3.1 Introduction

A comprehensive knowledge of thermophysical properties of solvents over a broad domain of experimental conditions is very much essential for the rational design of industrial as well as lab-scale gas-liquid absorption system [1-3]. Density is necessary for the determination of physical solubility of CO_2 in the solvent, mass transfer, and solvent kinetics. Viscosity is often required to estimate diffusivity using modified Stoke – Einstein equation, which is necessary in the calculation of mass transfer and kinetic properties. Along with this, surface tension also has great importance in analyzing the behavior and hydrodynamics in a gas-liquid system [4]. It directly relates the mass transfer processes between gas and liquid phases because it affects the size of bubbles in bubbling reactors and the wettability of the solvent in the packed bed contactors.

The density, viscosity and surface tension of the aqueous single amine solution have been reported in the literature such as (MEA + H_2O) [5 - 8], (DEA + H_2O) [5, 9 - 11], (MDEA + H_2O) [5, 6 , 9, 12 - 14], (TEA + H_2O) [11], (AMP + H_2O) [5 - 7, 15], (PZ + H_2O) [16 - 20], (2-PE + H_2O) [21 , 22], (AEPD + H_2O) [23], (DMPA + H_2O) [24], (DMEDA + H_2O) [25], (DEEA + H_2O) [26]. The thermophysical property measurements of the blended amine system such as (MEA + MDEA + H_2O) [5, 10, 13, 27], (MEA + AMP + H_2O) [5, 7, 10, 27], (DEA + MDEA + H_2O) [5, 9, 10] , (DEA + AMP + H_2O) [5, 10, 28] , (PZ + AMP + H_2O) [18, 19, 29, 32], (PZ + MDEA + H_2O) [20, 30, 32], (MAE + AMP) [33] and (MAE + MDEA) [33]. The detail summary of the corresponding literature review has been presented in Tables I.1 – I.6 of Appendix I

The present work focuses on the determination of the density, viscosity and surface tension of aqueous solutions of 1-(2-aminoethyl)piperazine (AEP) and N-(3-aminopropyl)-1,3-propanediamine (APDA) as well as different aqueous blends of (AEP + MDEA), (AEP + AMP), (APDA + MDEA) and (APDA + AMP) at atmospheric conditions and within the broad temperature range of (303.2 to 343.2) K. The concentrations of aqueous binary mixture are varied from 0.10 to 0.40 mass fractions while the AEP and APDA activated aqueous ternary blends are studied for 0.40 and 0.30 mass fraction, respectively. The experimental density and viscosity data are correlated using Redlich–Kister equation [34] and Grunberg - Nissan model [35], and the experimental surface tension data with temperature-based correlations and multiple linear regression techniques [36].

3.2 Experimental

3.2.1 Materials

All the reagents used in the present work were obtained from Sigma Aldrich Co. Ltd and used without further purification (Table 3.1). Double distilled deionized water was used for making all the amine solutions. The total amine contents of the solutions were determined by titration with standard HCl using methyl orange indicator.

3.2.2 Measurement of density

The densities of the aqueous amine solutions were measured using oscillating tube digital density meter (Make: Anton-Paar, Model: DMA 4500). It has an inherent Peltier temperature controller

and aided with automatic viscosity correction across the entire viscosity range of samples. The density meter was calibrated using deionized water throughout the experimental temperature range at atmospheric pressure condition. Each reported experimental density value in the present study is taken as the mean of at three measurements. The water density corresponding to various temperatures was taken from the NIST database [37]. The maximum standard uncertainty associated with the measurement of density and temperature can be taken as ± 0.05 $kg.m^{-3}$ and ± 0.02 K, respectively.

3.2.3 Measurement of viscosity and surface tension

The viscosities of amine solutions were obtained using U-tube Ostwald viscometer [9], which uses a capillary flow method for measuring viscosity and surface tension of the solution simultaneously. The measurement was done through viscous flow time (VFT) and pendant drop number (PDN) technique, respectively as described by Kumar et al. [39]. Prior to measurement, the viscometer was washed with Millipore® water and dried completely before each set of experiment. The viscometer was immersed in a water bath where a circulating temperature controller (Make: JULABO F32 FRG) was used to control the desired temperature. Once the thermal equilibrium is established, the viscous flow time was measured with an electronic stopwatch having an accuracy of ±0.1 s, while the PDN was recorded with an electronic counter. Each reported viscosity and surface tension data are taken as the average of at least three measurements. For the viscosity measurement, the combined expanded uncertainty was estimated to be within ±0.03 mPa·s for all the aqueous amine solutions. Similarly, the approximate uncertainty in the measured surface tension data was estimated to be within ±0.3 $mN.m^{-1}$

3.3 Results and discussion

3.3.1 Measurement and correlation of density

For the validation of the experimental methodology adopted in the present system for density measurements, the densities of (0.10, 0.20 and 0.30) mass fraction aqueous MDEA were measured from (303.2 to 333.2) K and the experimental results were compared with the literature

data [6, 12]. These comparisons are reported in Table 3.2. The average absolute deviations (% AAD) of the density data are 0.07, 0.04 and 0.07 for the amine solution having the composition of (0.10, 0.20 and 0.30) mass fraction of MDEA, respectively. The low AAD value indicates that the experimental results are in excellent agreement with the literature data. The experimentally measured density values of aqueous binary and ternary solution were evaluated by varying the temperature from (303.2 to 343.2) K. These are reported in Tables 3.3-3.8 and elsewhere [40 – 41].

The experimental density data measured in this work has been further correlated using the Redlich- Kister type equation as suggested by Paul et al. [42]. A semi-empirical Redlich-Kister equation was used to determine the excess properties of amine solutions like excess molar volume as a function of molar composition. The Redlich-Kister equation can be expressed as:

$$V^{E}{}_{jk} = x_j x_k \sum_{p=0}^{N} A_p (x_j - x_k)^p \qquad (3.1)$$

In equation (3.1), V^E is the excess molar volume of the amine mixture, x_j and x_k are the mole fraction of the pure components in the amine mixture, A_p is the optimized pair parameter and N represents total number of optimized pair parameters. The temperature dependency of the pair parameter can be expressed in terms of temperature dependent coefficients l, m and n respectively:

$$A_p = l + m.T + n.T^2 \qquad (3.2)$$

For the binary system, the excess volume is then calculated using equation (3.3).

$$V_E = V^{E}{}_{12} \qquad (3.3)$$

For the ternary system, the excess volume is calculated from the individual contributions as expressed below.

$$V_E = V^{E}{}_{12} + V^{E}{}_{13} + V^{E}{}_{23} \qquad (3.4)$$

Further the experimental measured density is used to determine the excess volume of the amine solution

$$V_E = V_m - \sum x_i V_i^o \tag{3.5}$$

Where, V_i^o and V_m represents the volume of the pure constituent and amine mixture at a specified temperature in molar scale. V_m is then calculated from the experimental measured density by

$$V_m = \frac{\sum x_i M_i}{\rho_m} \tag{3.6}$$

Where, M_i represents the molar mass of pure constituent i, ρ_m corresponds to the experimentally calculated density of the amine mixture, and x_i represents the mole fraction of the pure constituent i.

The temperature dependent binary interaction parameters of equation (3.2) for the amine mixtures have been calculated by regression of experimental data within the temperature range of (303.2 to 343.2) K and are reported in Tables 3.9-3.14. The pure component densities of all the constituents used in the present work can be obtained from various literature sources [12, 37, 43 - 44] but pure component density of AEP over the experimental temperature range were determined experimentally in the present work and reported elsewhere [40] as this data is not available in the open literature. The % (AAD) between the correlated and experimental results are determined by using equation (3.7)

$$\%AAD = \frac{1}{N}\sum_{i=1}^{N}\frac{\left|X_{cal,i} - X_{\exp,i}\right|}{X_{\exp,i}} \times 100 \tag{3.7}$$

Where N is the total number of data points, $X_{cal,i}$ and $X_{\exp,i}$ represents the correlated and experimental results. The % (AAD) between the experimental and correlated results for (AEP + H_2O) as well as (AEP + MDEA + H_2O) and (AEP + AMP + H_2O) systems are 0.04, 0.04 and

0.08, respectively. Whereas binary and ternary system of (APDA + H_2O), (APDA + MDEA + H_2O) and (APDA+ AMP + H_2O) shows an average absolute deviation of 0.06, 0.07 and 0.05, respectively. The lower values of AAD across all the solvent systems studied in this work indicate that experimental results are in well agreement with the model calculated data. The comparison between the correlated and experimental results is represented in Figs. 3.1 - 3.6.

It shows a decreasing trend in the measured density with increase in temperature since the volume of solution increases. Excess volume of the amine mixtures can be calculated using equation (3.5) and it is compared with the model calculated value. The excess volume (V_E) for the binary mixture of (AEP + H_2O) shows negative value for all the composition and temperature range studied. While for the (AEP+ MDEA/AMP +H_2O), the V_E shows positive sign. The sign convention for the excess volume can be analyzed on the basis of three kinds of interactions between the individual constituent of a solution [45] forces resulting in +ve contribution, (b) –ve contribution can be the results of various kinds of chemical interactions such as charge transfer, the formation of H-bonds and other complex interactions (c) variation in size and shape of the individual component of the mixtures, results in structural variation and due to the random packing of molecules into each other's structure leads to the reduction of the overall molar volume and compressibility of the solution mixtures, which also results in a – ve value of V_E. The –ve excess value of the binary system understudied reflects strong interactions among unlike molecules. Taking into account the sign and magnitude of V_E, It can be inferred that there are strong interactions such as hydrogen bonding prevailing in the blends [25].

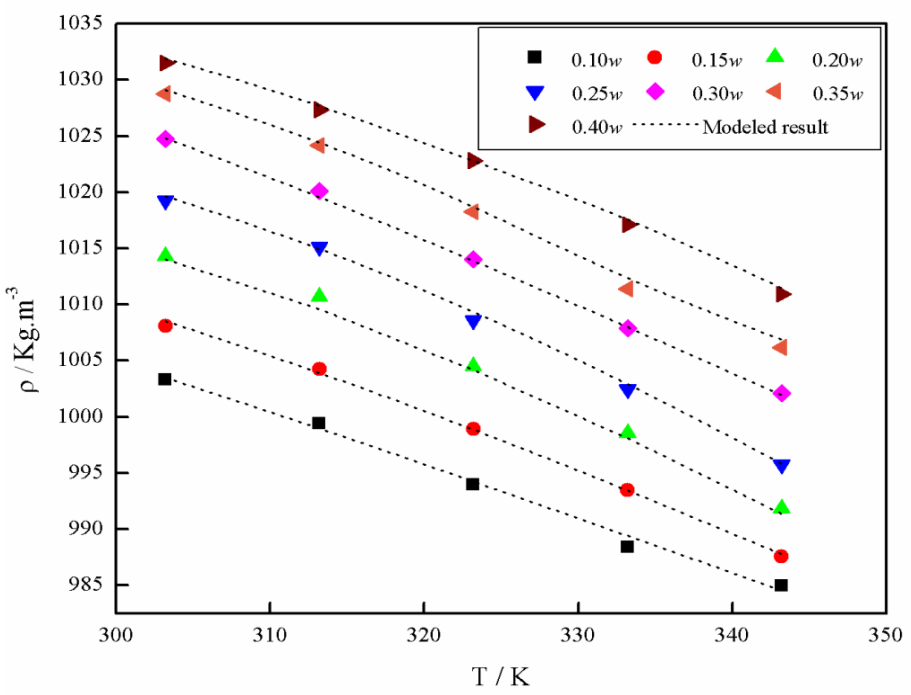

Fig. 3.1 Density of aqueous AEP system at various temperatures and composition (mass fraction)

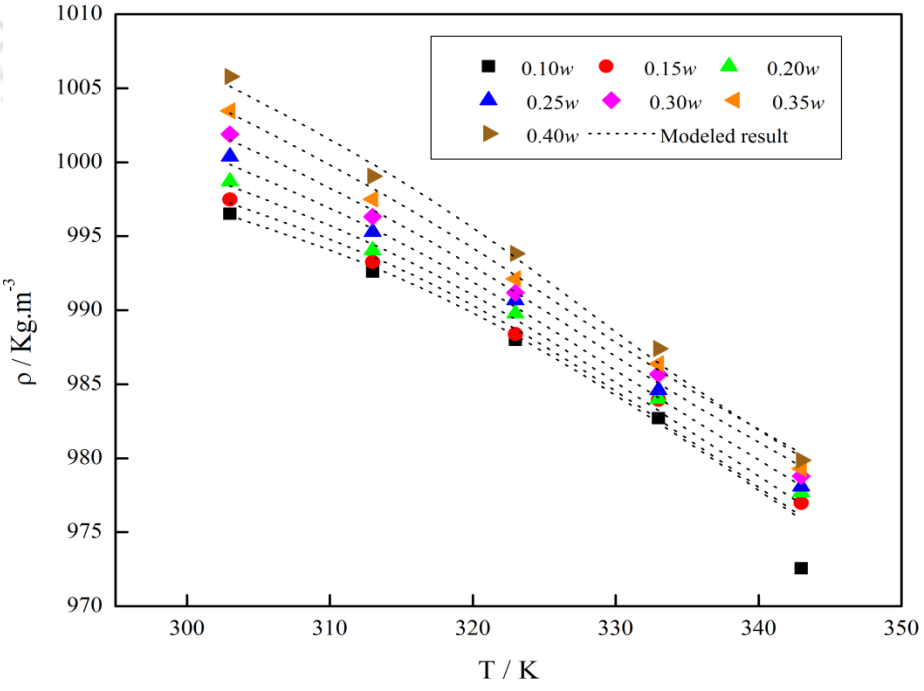

Fig. 3.2 Density of aqueous APDA system at various temperatures and composition (mass fraction)

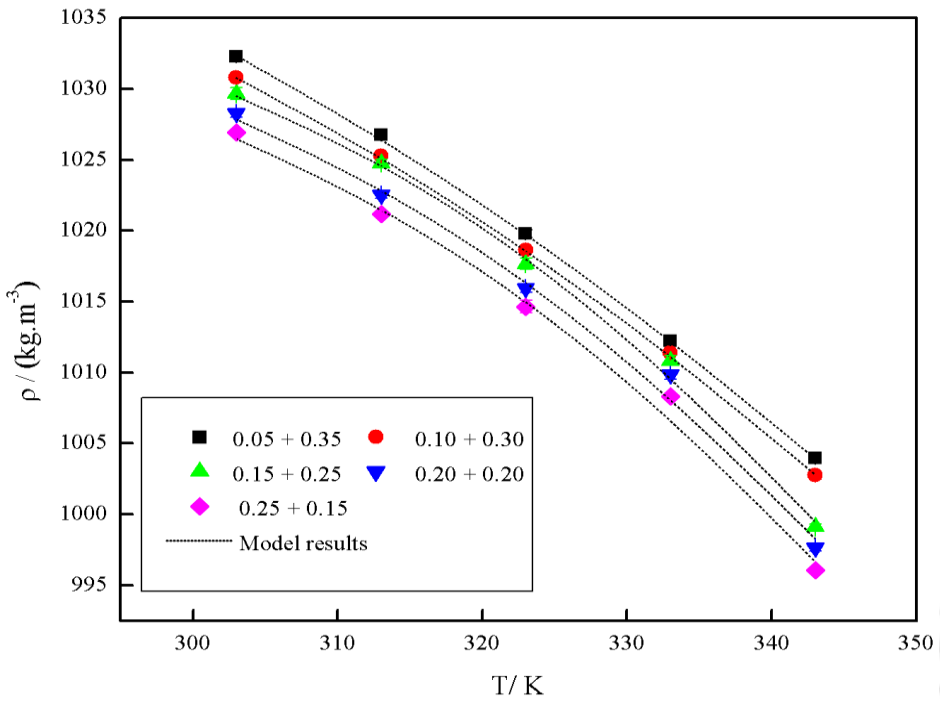

Fig. 3.3 Density of aqueous (AEP + MDEA) system at various temperatures and composition (mass fraction)

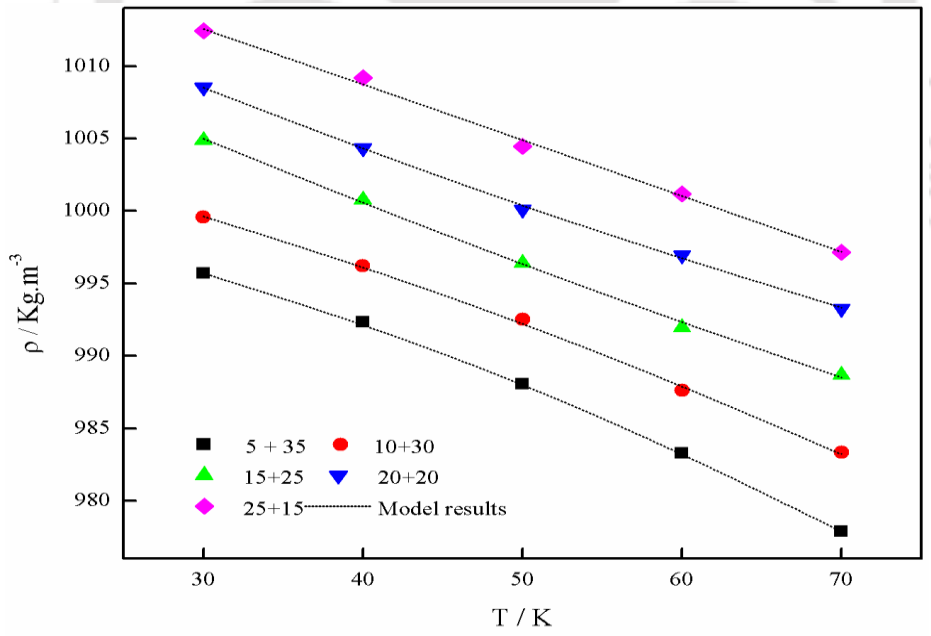

Fig. 3.4 Density of aqueous (AEP + AMP) system at various temperatures and composition (mass fraction)

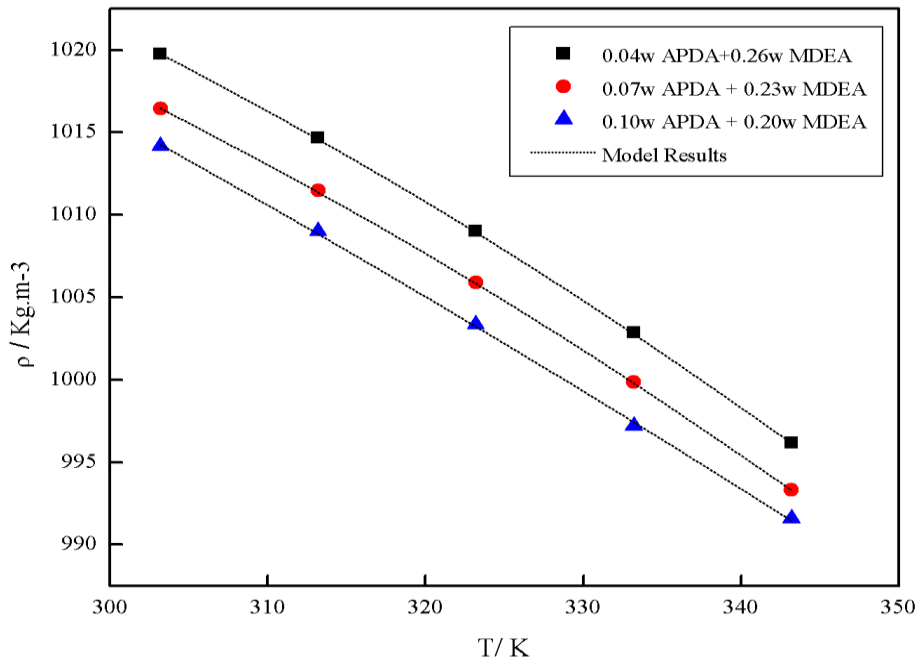

Fig. 3.5 Density of aqueous (APDA + MDEA) system at various temperatures and composition (mass fraction)

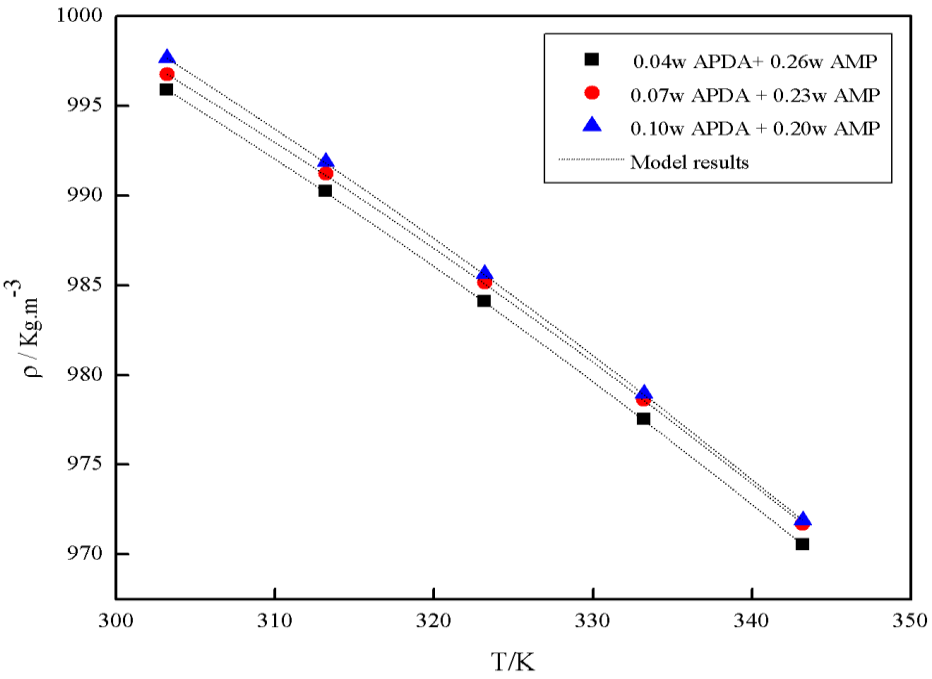

Fig. 3.6 Density of aqueous (APDA + AMP) system at various temperatures and composition (mass fraction)

3.3.2 Measurement and correlation of viscosity

The experimental methodology of the viscosity measurement has been also validated using the literature results [6, 12]. The experimental results are well-matched with the literature data (Table 3.15). The experimentally calculated viscosity values of binary solvents are presented in Tables 3.3 and 3.6 whereas the results pertaining to the ternary amine system over the temperature range of (303.2 -343.2) K are reported in Tables 3.16 - 3.19. It can be observed from these tables that the viscosity of all the binary and ternary system decreases with an increase in temperature which results from the decrease in molecular density and intermolecular forces.

To further check the thermodynamic consistency of the experimental viscosity data, a Redlich-Kister type equation is used to correlate the viscosity of the binary solution [42]. The modified expression using kinematic viscosity is defined as follows:

$$\delta\eta = x_j x_k \sum_{p=0}^{N} A_p (x_j - x_k)^p \tag{3.8}$$

Where, $\delta\eta$ is the relative deviation in the kinematic viscosity, x_j and x_k are the mole fraction of the pure components in the mixture, *N* is the total number of optimized pair parameters and A_p are temperature dependent pair parameters expressed as:

$$A_p = l + \frac{m}{T+n} \tag{3.9}$$

Where, *T* represents temperature of the solution and *l*, *m* and *n* are the coefficients of temperature dependent pair parameters. The relative deviation of the viscosity of amine solution can be obtained from the experimental viscosity data:

$$\delta\eta = \ln\eta_m - \sum_{i=1}^{n} x_i \ln\eta_i \tag{3.10}$$

In the above expression η_m represents the measured kinematic viscosity of the amine solution and η_i represents the kinematic viscosity of the pure components at the reference temperature. The kinematic viscosity of the aqueous mixture can be calculated by:

$\eta_m = \frac{\mu}{\rho}$, where μ amd ρ represents the dynamic viscosity and the density of the amine solution.

The % average absolute deviation between the correlated and the experimental data for the (AEP + H_2O) and (APDA + H_2O) system is about 2.18 and 8.19 which can be interpreted from Tables 3.9 and 3.12, respectively.

The Grunberg and Nissan model was used to correlate the experimental viscosity of the ternary system [5, 44]. The equation corresponding to the above mentioned model can be expressed as:

$$\ln \mu_m = \sum x_i \ln \mu_i + \sum\sum x_i x_j G_{ij} \tag{3.11}$$

Where, μ_m is the measured dynamic viscosity of the amine mixtures, μ_i represents the viscosity of the pure component and x_i is the mole fraction of the i^{th} component, in the solution.

For a ternary system the equation can be expressed as:

$$\ln \mu_m = x_1 \ln \mu_1 + x_2 \ln \mu_2 + x_3 \ln \mu_3 + x_1 x_2 G_{12} + x_1 x_3 G_{13} + x_2 x_3 G_{23} \tag{3.12}$$

G_{ij} in Eq. (3.11) are temperature based parameters and it is expressed in the form given below:

$$G_{ij} = l + m.T + n.T^2 \tag{3.13}$$

Where, l, m and n are the temperature-dependent constants and are calculated by regression analysis of the experimental data measured in the present work and are given in Tables 3.20 - 3.21. The % AAD between the experimental and the correlated data of (AEP + MDEA + H_2O) and (AEP + AMP + H_2O) systems are 2.03 and 1.16, respectively whereas for (APDA + MDEA + H_2O) and (APDA + AMP + H_2O) systems, the experimental results shows the deviation of 2.27 and 1.07 from the model calculated data.

The comparisons between the experimental and correlated viscosity results of both the binary and ternary system have been also presented in graphical form in Figs. 3.7 - 3.12. It can be seen that the correlated viscosity data from equations (3.8) and (3.11) are in good agreement with the experimental viscosity data.

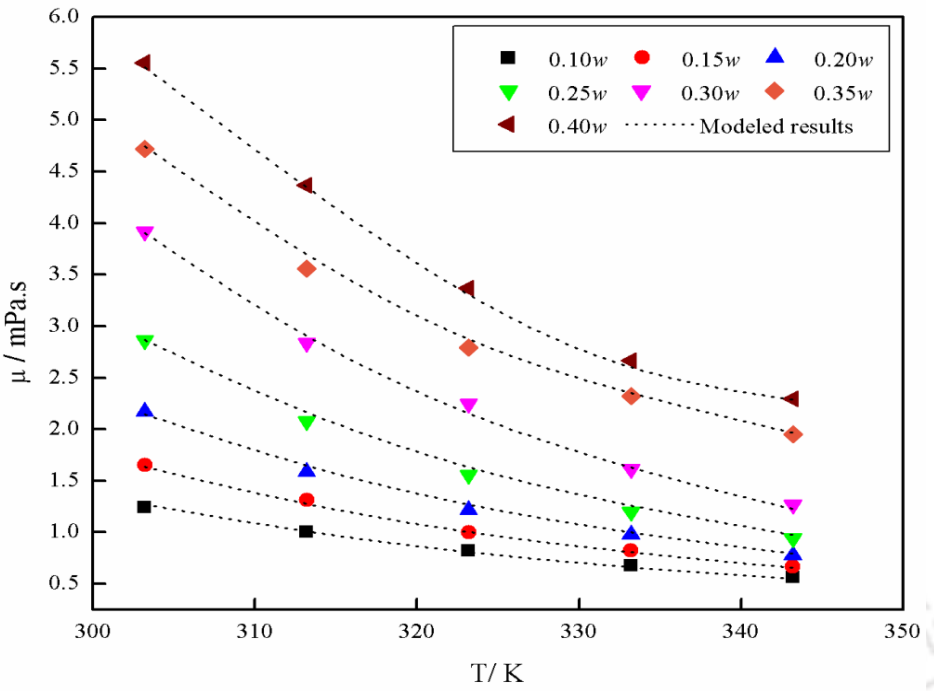

Fig. 3.7 Viscosity of aqueous AEP system at various temperatures and composition (mass fraction)

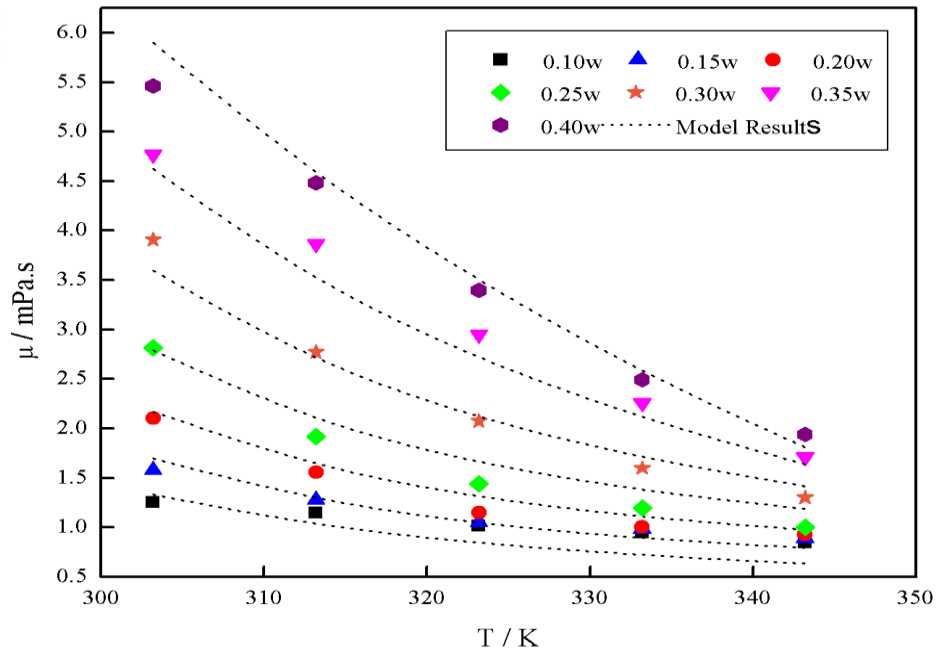

Fig. 3.8 Viscosity of aqueous APDA system at various temperatures and composition (mass fraction)

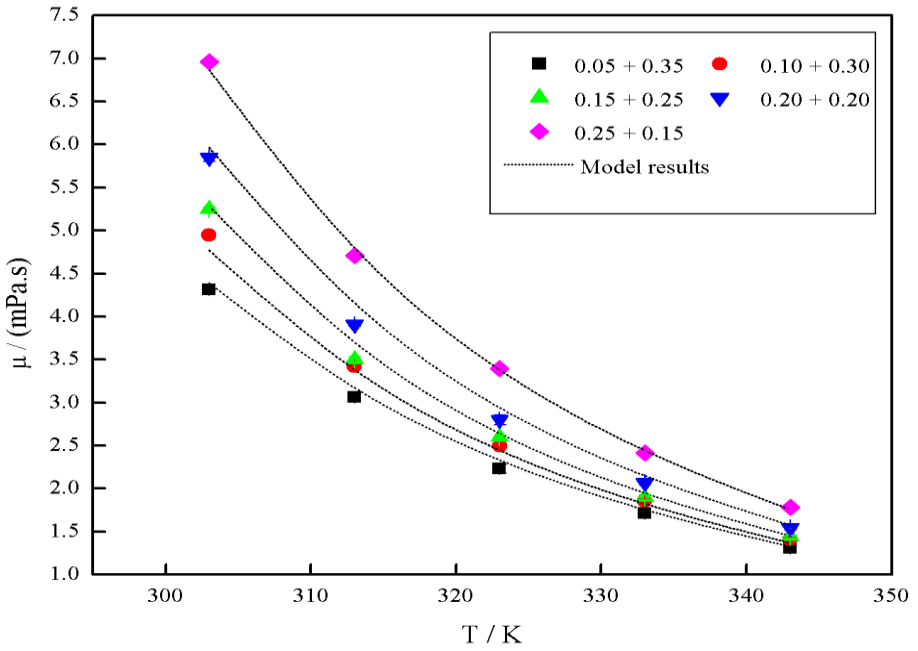

Fig 3.9 Viscosity of aqueous (AEP + MDEA) system at various temperatures and composition (mass fraction)

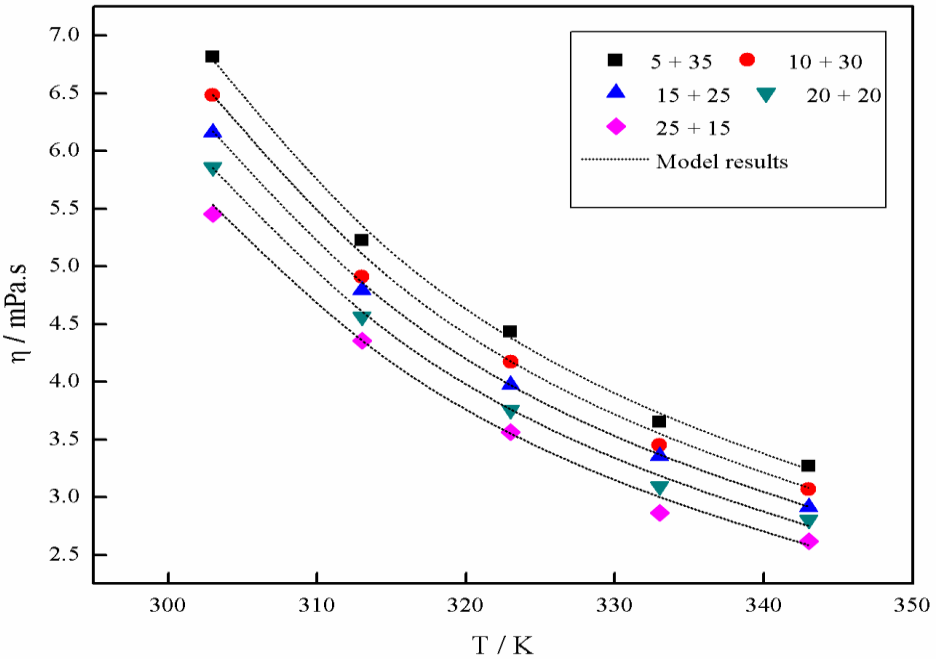

Fig 3.10 Viscosity of aqueous (AEP + AMP) system at various temperatures and composition (mass fraction

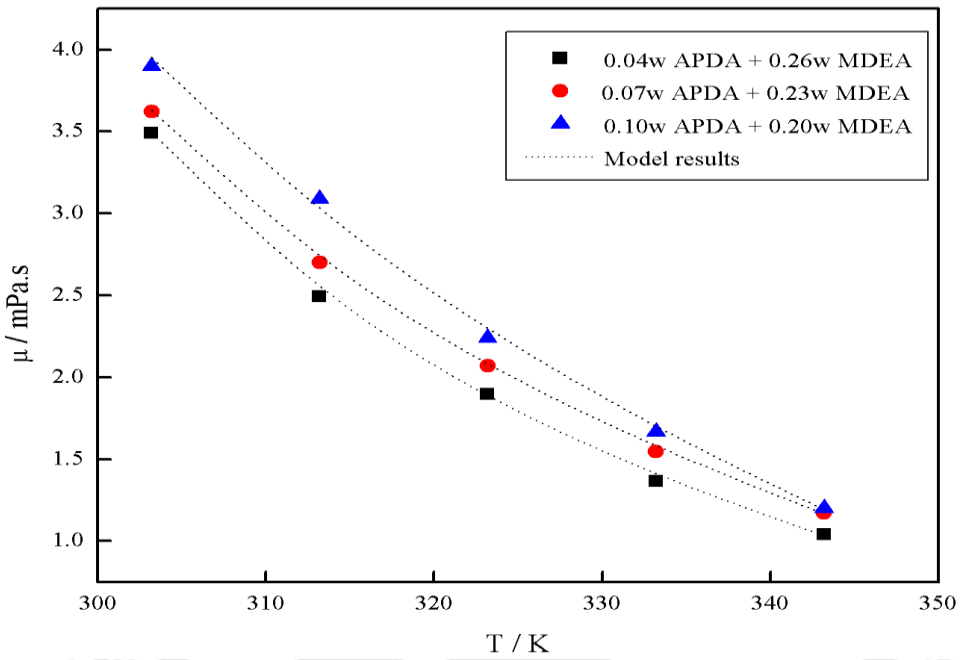

Fig. 3.11 Viscosity of aqueous (APDA + MDEA + H_2O) system at various temperatures and composition (mass fraction)

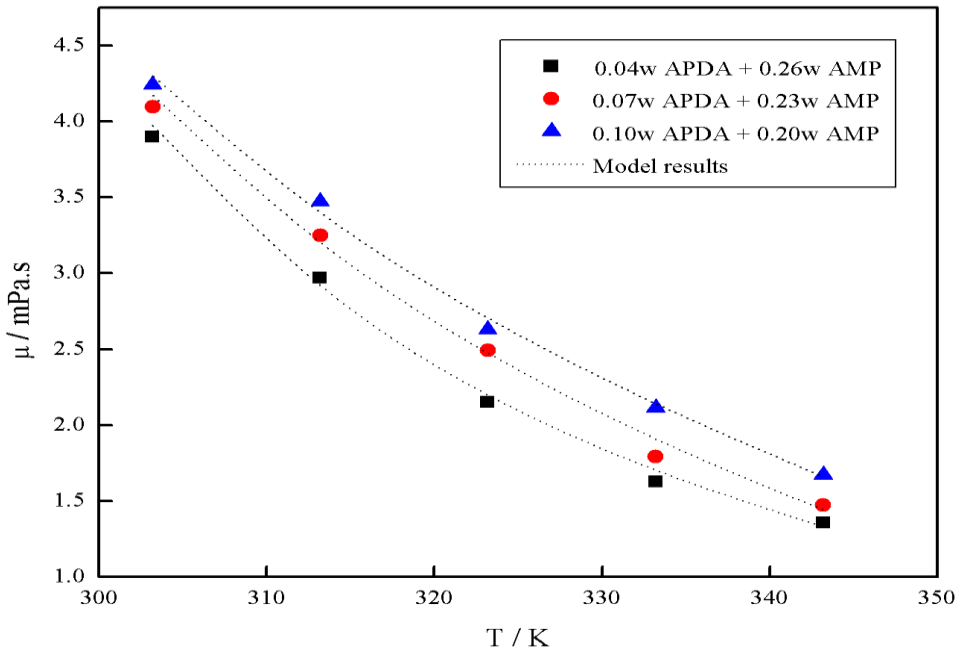

Fig. 3.12 Viscosity of aqueous (APDA + AMP + H_2O) system at various temperatures and composition (mass fraction)

3.3.2.1 Thermodynamic property estimation

Experimental viscosity data can be utilized to analyze various thermodynamic properties such as Enthalpy (ΔH^o), Entropy (ΔS^o) and Gibbs energies (ΔG^o) of activation of viscous flow. These properties are determined by applying Andrade's theory. According to this theory, the kinematic viscosity can be expressed as follows [46 - 47]:

$$\eta = \frac{hN_A}{M}\exp\left(\frac{\Delta G^o}{R.T}\right) \tag{3.14}$$

In the above equation, $M = \Sigma(x_i M_i)$ stands for average molecular mass of the amine system which can be calculated using mole fraction and the molar mass of pure component, x_i and M_i. Whereas h , R, N_A and T represents Planck's constant, Gas constant, Avogadro number, and absolute temperature, respectively. Taking into the consideration, the experimental values of kinematic viscosities of the binary and ternary solvent system at different temperatures, ΔG^0 values are calculated using equation (3.14) and are reported in Tables 3.22-3.24.

Also according to the solution thermodynamics, Gibbs free energy can be expressed as:

$$\Delta G^o = \Delta H^o - T.\Delta S^o \tag{3.15}$$

The other thermodynamic parameters such as ΔH^o and ΔS^o can be calculated from Eq. (3.15) using ΔG^o derived from the earlier equation and has been reported in Tables 3.25-3.27.

It can be observed from the reported results that the ΔG^o and ΔH^o values corresponding to the entire composition and temperature studied, are positive for the understudy system, which reflects a strong interaction between the individual components of the solution mixture. On the other hand, the values of ΔS^o are found to be negative indicating the absence of any disorderness in the viscous flow and confirms that the viscous flow is an ordered process and involve contiguous liquid layers which should retain their structural configuration even moving in a stationary steady state. [48].

3.3.3 Measurement and correlation of surface tension

Surface tension has great importance in analyzing the behavior and hydrodynamics in a gas-liquid systems. It directly relates the mass transfer processes between gas and liquid phases because it affects the size of bubbles in bubbling reactors and the wettability of the solvent in the packed bed contractors. The surface tension measurement procedure adopted in the present work has been validated by comparing the experimentally determined surface tension data of aqueous 0.10, 0.20 and 0.30 mass fraction diethanolamine (DEA) solutions with that of already available literature [49]. The results of the present experimental work are in good agreement with that of the literature data with average absolute deviation (AAD) of 0.02. The validation results have been reported in Table 3.28. In the present study, the surface tensions of the binary as well ternary solvent mixture were determined at (303.2 - 343.2) K and are given in Tables 3.29 – 3.32. It can be seen from the experimental results that the surface tension of the binary mixture decreases with temperature and concentration. The effect of temperature and concentration on the surface tension data of the binary as well as ternary system is presented in Figs. 3.13 - 3.18.

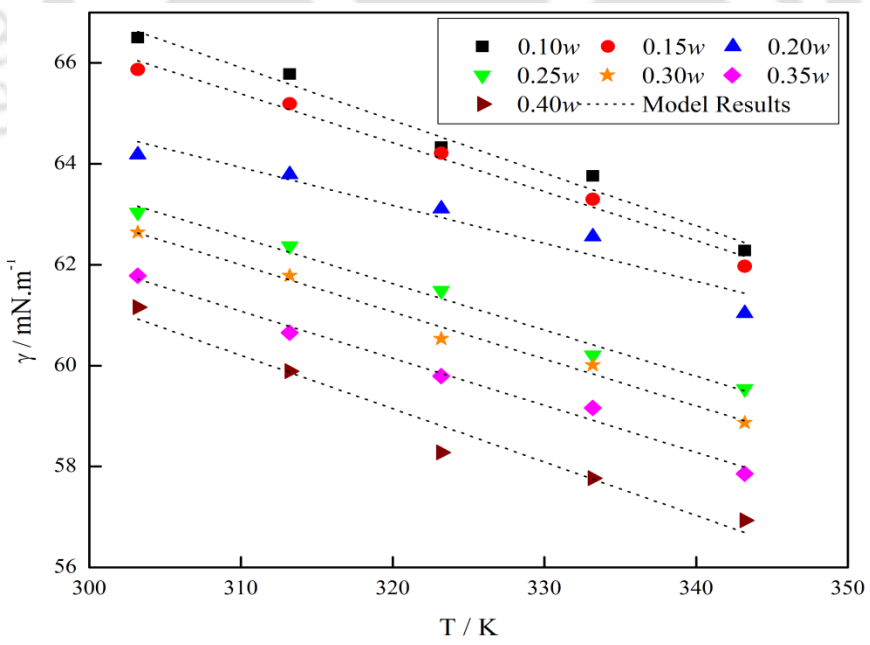

Fig. 3.13 Surface tension of aqueous AEP system at various temperatures and composition (mass fraction)

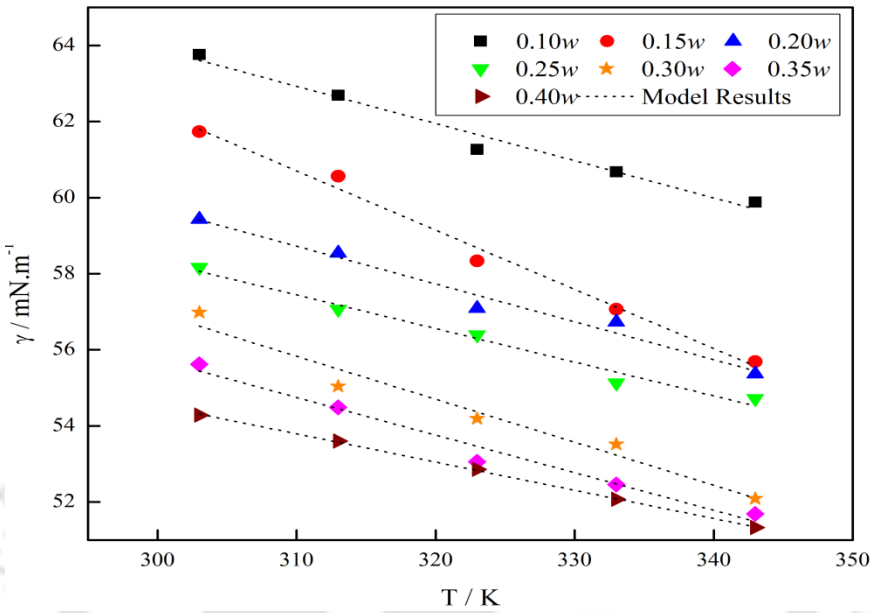

Fig. 3.14 Surface tension of aqueous APDA system at various temperatures and composition (mass fraction)

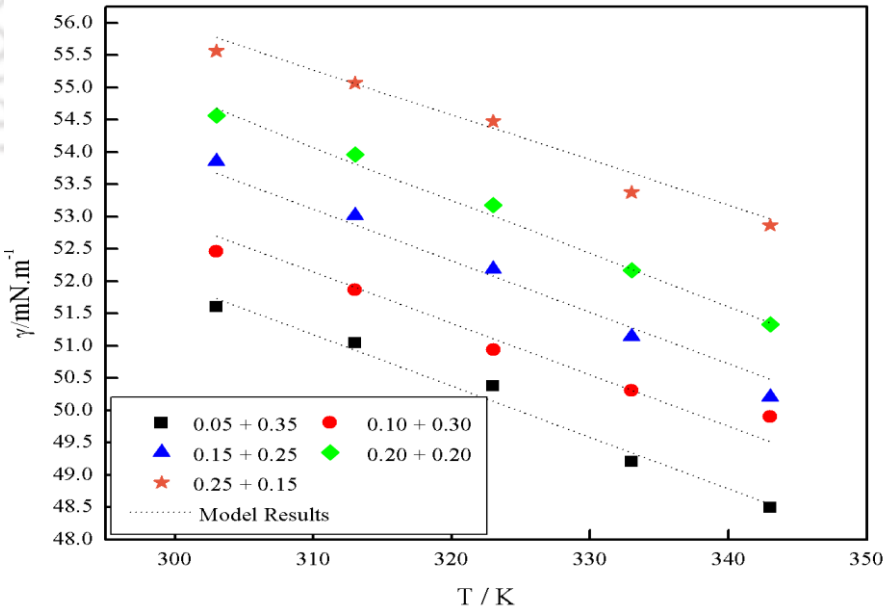

Fig. 3.15 Surface tension of aqueous (AEP+ MDEA) system at various temperatures and composition (mass fraction)

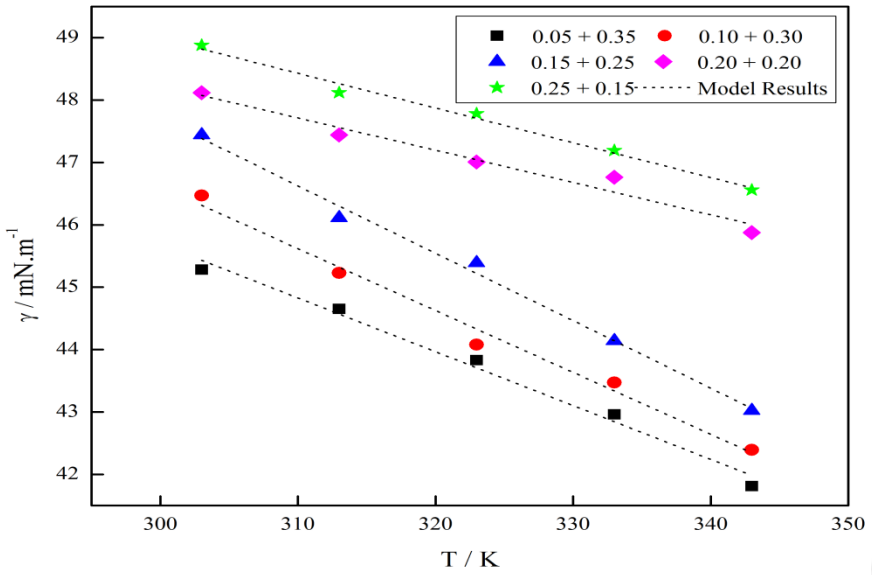

Fig. 3.16 Surface tension of aqueous (AEP+ AMP) system at various temperatures and composition (mass fraction)

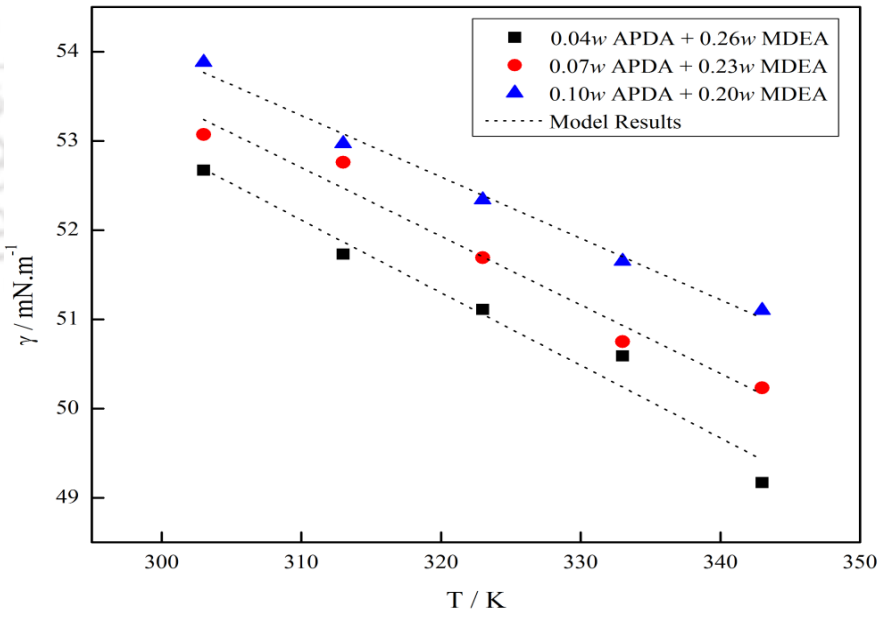

Fig. 3.17 Surface tension of aqueous (APDA+ MDEA) system at various temperatures and composition (mass fraction)

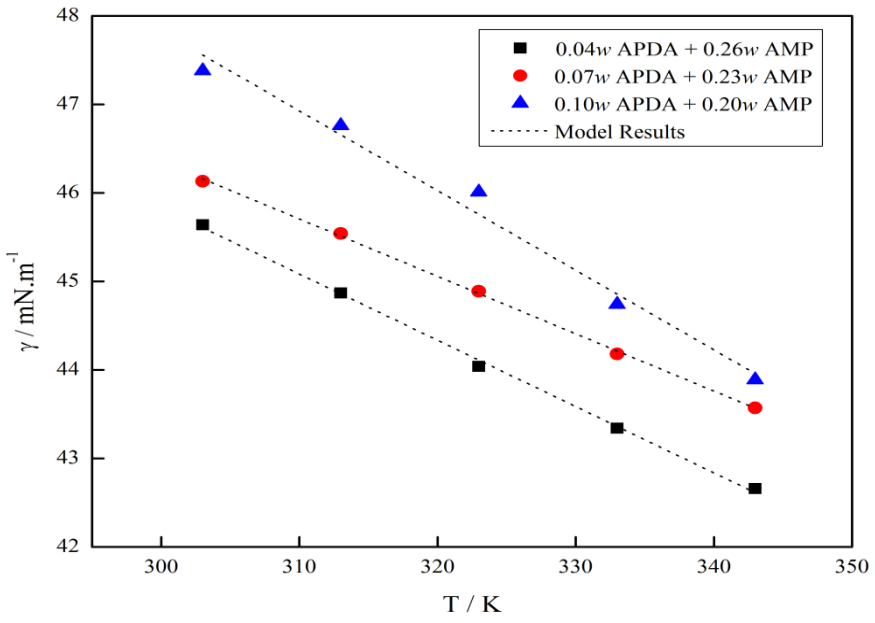

Fig. 3.18 Surface tension of aqueous (APDA+ AMP) system at various temperatures and composition (mass fraction)

This linear nature allows the use of equation. (3.16) that has been suggested by Venkat et al. [33] to predict the consistency of the effect of temperature on the experimental measured surface tension data.

$$\gamma = k_1 + k_2.T \tag{3.16}$$

Where, ϒ is the measured surface tension of the aqueous amine solution and T stands for solution tempearture. The constants k_1 and k_2 are the temperature dependent constants and have been calculated by regression of experimental data for all the amine system studied in the current work and are presented in Tables 3.33- 3.38. In addition to that a correlation for surface tension has been developed using multiple linear regression (MLR) technique [36] for aqueous (AEP + MDEA) system. The correlation as a function of reference temperature for the measurement and individual composition of amines can be represented as:

$$\gamma = A_1 + A_2T + A_3x_1 + A_4x_2 + A_5x_3 \tag{3.17}$$

Where, ($A_1 - A_5$) are the coefficients and x_1, x_2 and x_3 are the mole fraction of pure components. The % AAD between the experimental and correlated data of equation (3.17) for (AEP + MDEA + H_2O) systems is about 0.31. Rocha et al. [50] in their work described the influence of surface tension in calculating the effective mass transfer area in a column. The surface tension value in the present ternary system ranges from (48- 55) $mN.m^{-1}$, which can lead to higher mass transfer area between the gas and solvent phase in an absorption column [51].

3.4 Conclusions

In this work, the density, viscosity and surface tension of binary systems of aqueous AEP and APDA and ternary system of aqueous (AEP + MDEA + H_2O),(AEP + AMP + H_2O), (APDA + MDEA + H_2O) and (APDA + AMP + H_2O) were determined and correlated over the temperature range (303.2 to 343.2) K. The measured thermophysical property of amine systems shows very good similarity with the model calculated results over the entire domain of studied temperature and composition range. The –ve excess volume of the understudied binary system reflects strong interactions among unlike molecules. Moreover, the derived thermodynamic property from the kinematic viscosity data indicates that ΔG^o and ΔH^o values corresponding to the entire composition and temperatures studied are positive and ΔS^o are found to be negative for the understudy system. This further confirms the presence of stronger interactions between the individual components of aqueous amine mixture as well as the absence of any disorderness in the viscous flow.

Table 3.1 Provenance and purity of reagent

Alias	Chemical	Source	Purity (Mass fraction)	Method of Purification
DEA	Diethanolamine 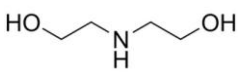	Sigma Aldrich Co.	99 %	None
MDEA	N-Methyldiethanolamine 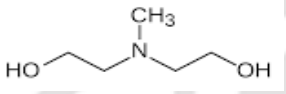	Sigma Aldrich Co.	95 %	None
AEP	1-(2-Aminoethyl) piperazine 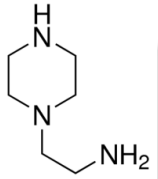	Sigma Aldrich Co.	99 %	None
AMP	2-Amino-2-methyl-1-Propanol 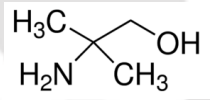	Sigma Aldrich Co.	95 %	None
APDA	N-(3-Aminopropyl)-1, 3-propanediamine 	Sigma Aldrich Co.	99 %	None

Table 3.2 Comparison of the densities (ρ) of aqueous MDEA solutions (mass fraction, w) measured in the present work with literature values at pressure P= 0.1 MPa

Mass Fraction (MDEA)	T/K	ρ/kg.m^{-3}			AAD%
		Ref. 37	Ref. 38	This work	
0.10	303.2	1004		1003.8	0.07
	313.2	1000.7		999.5	
	323.2	996		995.2	
	333.2	991.2		990.5	
0.20	303.2	1013.2	1013.3	1012.4	0.04
	313.2	1009.1	1008.9	1008.4	
	323.2	1004.7	1004	1003.5	
	333.2	999.3	998.3	998.6	
0.30	303.2	1022.9	1022.3	1024.5	0.07
	313.2	1018	1017.1	1019.5	
	323.2	1013	1011.6	1015.2	
	333.2	1006.9	1005.7	1008.2	

Table 3.3a Density (ρ), Viscosity (μ) and surface tension (Υ) of unloaded (AEP + H_2O) solution at P= 0.1 MPa

T/K	Mass Fraction (AEP)	ρ/Kg.m^{-3}	μ/mPa.s	Υ/mN.m
303.2	0.1	1003.3	1.24	66.5
313.2	0.1	999.4	1.00	65.78
323.2	0.1	993.9	0.82	64.33
333.2	0.1	988.4	0.67	63.76
343.2	0.1	984.9	0.56	62.28
303.2	0.15	1008.1	1.65	65.87
313.2	0.15	1004.2	1.31	65.19
323.2	0.15	998.9	1.00	64.21
333.2	0.15	993.5	0.83	63.3
343.2	0.15	987.5	0.67	61.97
303.2	0.2	1014.3	2.17	64.18
313.2	0.2	1010.7	1.59	63.79
323.2	0.2	1004.5	1.22	63.11
333.2	0.2	998.6	0.97	62.56
343.2	0.2	991.8	0.78	61.04
303.2	0.25	1019.2	2.86	63.04
313.2	0.25	1015.1	2.07	62.37
323.2	0.25	1008.6	1.55	61.49
333.2	0.25	1002.5	1.19	60.21
343.2	0.25	995.7	0.94	59.54

Table 3.3b Density (ρ), Viscosity (μ) and surface tension (Υ) of unloaded (AEP + H_2O) solution at P= 0.1 MPa

T/K	Mass Fraction (AEP)	ρ/Kg.m^{-3}	μ/mPa.s	ϒ/mN.m
303.2	0.3	1024.7	3.92	62.64
313.2	0.3	1020.1	2.84	61.78
323.2	0.3	1014.0	2.24	60.53
333.2	0.3	1007.9	1.61	60.01
343.2	0.3	1002.1	1.26	58.87
303.2	0.35	1028.8	4.72	61.78
313.2	0.35	1024.2	3.56	60.65
323.2	0.35	1018.3	2.79	59.79
333.2	0.35	1011.4	2.32	59.16
343.2	0.35	1006.2	1.95	57.86
303.2	0.4	1031.5	5.56	61.16
313.2	0.4	1027.3	4.37	59.89
323.2	0.4	1022.8	3.37	58.28
333.2	0.4	1017.1	2.66	57.77
343.2	0.4	1010.9	2.29	56.93

Table 3.4a Density (ρ) for (AEP + MDEA + H_2O) from 303.2 K to 343.2 K at pressure P=0.1 MPa

T/K	Mass Fraction (AEP)	Mass Fraction (MDEA)	ρ/Kg.m^{-3}
303.2	0.05	0.35	1032.3
313.2	0.05	0.35	1026.7
323.2	0.05	0.35	1019.8
333.2	0.05	0.35	1012.2
343.2	0.05	0.35	1003.9
303.2	0.1	0.3	1030.8
313.2	0.1	0.3	1025.3
323.2	0.1	0.3	1018.6
333.2	0.1	0.3	1011.4
343.2	0.1	0.3	1002.7
303.2	0.15	0.25	1029.7
313.2	0.15	0.25	1024.8
323.2	0.15	0.25	1017.7
333.2	0.15	0.25	1010.8
343.2	0.15	0.25	999.1

Table 3.4b Density (ρ) for (AEP + MDEA + H2O) from 303.2 K to 343.2 K at pressure P=0.1 MPa

T/K	Mass Fraction (AEP)	Mass Fraction (MDEA)	ρ/Kg.m^{-3}
303.2	0.2	0.2	1028.3
313.2	0.2	0.2	1022.5
323.2	0.2	0.2	1015.9
333.2	0.2	0.2	1009.8
343.2	0.2	0.2	997.7
303.2	0.25	0.15	1026.9
313.2	0.25	0.15	1021.2
323.2	0.25	0.15	1014.6
333.2	0.25	0.15	1008.3
343.2	0.25	0.15	996.1

Table 3.5a Density (ρ) for (AEP + AMP + H_2O) from 303.2 K to 343.2 K at pressure P=0.1 MPa

T/K	Mass Fraction (AEP)	Mass Fraction (AMP)	ρ/Kg.m^{-3}
303.2	0.05	0.35	998.7
313.2	0.05	0.35	991.9
323.2	0.05	0.35	984.8
333.2	0.05	0.35	977.7
343.2	0.05	0.35	970.1
303.2	0.1	0.3	1003.8
313.2	0.1	0.3	997.1
323.2	0.1	0.3	990.2
333.2	0.1	0.3	983.4
343.2	0.1	0.3	975.7
303.2	0.15	0.25	1009.4
313.2	0.15	0.25	1002.7
323.2	0.15	0.25	995.8
333.2	0.15	0.25	988.8
343.2	0.15	0.25	981.2

Table 3.5b Density (ρ) for (AEP + AMP + H_2O) from 303.2 K to 343.2 K at pressure P=0.1 MPa

T/K	Mass Fraction (AEP)	Mass Fraction (AMP)	ρ/Kg.m^{-3}
303.2	0.2	0.2	1014.4
313.2	0.2	0.2	1007.8
323.2	0.2	0.2	1000.9
333.2	0.2	0.2	994.6
343.2	0.2	0.2	987
303.2	0.25	0.15	1019.6
313.2	0.25	0.15	1013
323.2	0.25	0.15	1006
333.2	0.25	0.15	999.7
343.2	0.25	0.15	992.1

Table 3.6a Density (ρ), Viscosity (μ) and surface tension (Υ) of unloaded (APDA + H_2O) solution at pressure P= 0.1 MPa

T/K	Mass Fraction (APDA)	ρ/Kg.m^{-3}	μ/mPa.s	Υ/mN.m
303.2	0.1	996.5	1.25	63.76
313.2	0.1	992.6	1.14	62.69
323.2	0.1	988	1.01	61.27
333.2	0.1	982.7	0.94	60.68
343.2	0.1	972.6	0.85	59.88
303.2	0.15	997.5	1.58	61.73
313.2	0.15	993.2	1.28	60.56
323.2	0.15	988.4	1.05	58.34
333.2	0.15	983.9	0.98	57.07
343.2	0.15	976.9	0.89	55.69
303.2	0.2	998.7	2.10	59.43
313.2	0.2	994.1	1.56	58.54
323.2	0.2	989.8	1.15	57.09
333.2	0.2	984.0	1.00	56.73
343.2	0.2	977.7	0.93	55.37
303.2	0.25	1000.4	2.82	58.17
313.2	0.25	995.3	1.92	57.07
323.2	0.25	990.7	1.44	56.39
333.2	0.25	984.6	1.19	55.13
343.2	0.25	978.1	1.00	54.72

Table 3.6b Density (ρ), Viscosity (μ) and surface tension (Υ) of unloaded (APDA + H_2O) solution at pressure P= 0.1 MPa

T/K	Mass Fraction (APDA)	ρ/Kg.m-3	μ/mPa.s	ϒ/mN.m
303.2	0.3	1001.9	3.91	56.98
313.2	0.3	996.3	2.77	55.04
323.2	0.3	991.2	2.07	54.19
333.2	0.3	985.7	1.6	53.52
343.2	0.3	978.8	1.3	52.09
303.2	0.35	1003.5	4.77	55.62
313.2	0.35	997.5	3.87	54.49
323.2	0.35	992.1	2.95	53.06
333.2	0.35	986.4	2.26	52.46
343.2	0.35	979.3	1.71	51.69
303.2	0.4	1005.8	5.47	54.28
313.2	0.4	999.1	4.49	53.6
323.2	0.4	993.8	3.40	52.86
333.2	0.4	987.4	2.49	52.07
343.2	0.4	979.9	1.94	51.33

Table 3.7 Density (ρ) for (APDA + MDEA + H_2O) from 303.2 K to 343.2 K at pressure P=0.1 MPa

T/K	Mass Fraction (AEP)	Mass Fraction (MDEA)	ρ/Kg.m^{-3}
303.2	0.04	0.26	1019.8
313.2	0.04	0.26	1014.7
323.2	0.04	0.26	1009.0
333.2	0.04	0.26	1002.9
343.2	0.04	0.26	996.2
303.2	0.07	0.23	1016.5
313.2	0.07	0.23	1011.5
323.2	0.07	0.23	1005.9
333.2	0.07	0.23	999.9
343.2	0.07	0.23	993.3
303.2	0.1	0.2	1014.2
313.2	0.1	0.2	1009.0
323.2	0.1	0.2	1003.3
333.2	0.1	0.2	997.2
343.2	0.1	0.2	991.6

Table 3.8 Density (ρ) for (APDA + AMP + H_2O) from 303.2 K to 343.2 K at pressure P=0.1 MPa

T/K	Mass Fraction (AEP)	Mass Fraction (AMP)	ρ/Kg.m^{-3}
303.2	0.04	0.26	995.9
313.2	0.04	0.26	990.3
323.2	0.04	0.26	984.1
333.2	0.04	0.26	977.5
343.2	0.04	0.26	970.5
303.2	0.07	0.23	996.7
313.2	0.07	0.23	991.2
323.2	0.07	0.23	985.1
333.2	0.07	0.23	978.6
343.2	0.07	0.23	971.7
303.2	0.1	0.2	996.7
313.2	0.1	0.2	991.2
323.2	0.1	0.2	985.1
333.2	0.1	0.2	978.6
343.2	0.1	0.2	971.7

Table 3.9 Binary Redlich-Kister Parameters A_0, A_1, A_2 for the Excess Volume of density (ρ) and kinematic viscosity (η) for (AEP+H_2O) system

Parameters		Binary Pair	
		Binary pair (ρ)	Binary pair (η)
A_0	l	-133.06	-5483.096
	m	0.844	34.971
	n	-1.334×10^{-3}	-5.552×10^{-2}
A_1	l	-290.102	-6019.267
	m	1.841	37.77
	n	-2.909×10^{-3}	-5.923×10^{-2}
A_2	l	-158.057	
	m	1.003	
	n	-1.585×10^{-3}	
AAD %		0.04	2.18

Table 3.10 Binary Redlich-Kister Parameters A_0, A_1, A_2 for the Excess Volume of density (ρ) for (AEP + MDEA + H_2O) system

Parameters		Binary Pair		
		AEP + MDEA	AEP + H_2O	MDEA + H_2O
A_0	*l*	233.239	377.337	-437.605
	m	-1.476	-2.388	2.769
	n	2.329×10^{-3}	3.769×10^{-3}	-4.370×10^{-3}
A_1	*l*	-1672.13	-482.472	233.380
	m	10.582	-3.054	-1.477
	n	-1.669×10^{-2}	-4.819×10^{-3}	2.331×10^{-3}
A_2	*l*	-30793.92	-1154.760	933.123
	m	194.923	7.309	-5.906
	n	-3.077×10^{-1}	-1.153×10^{-2}	9.319×10^{-3}
AAD %			0.04	

Table 3.11 Binary Redlich-Kister Parameters A_0, A_1, A_2 for the Excess Volume of density (ρ) for (AEP + AMP + H_2O) system

Parameters		Binary Pair		
		AEP + AMP	AEP + H_2O	AMP + H_2O
A_0	*l*	-410.58	189.562	92.266
	m	2.442	-1.129	-0.551
	n	3.63×10^{-3}	1.682×10^{-3}	8.24×10^{-4}
A_1	*l*	20.839	4.163	598.745
	m	-0.154	-0.026	-3.569
	n	2.74×10^{-4}	3.80×10^{-5}	5.313×10^{-3}
A_2	*l*	7570.55	-275.3	626.5347
	m	-45.268	1.641	-3.73
	n	6.763×10^{-2}	-0.00244	5.547×10^{-3}
AAD %			0.08	

Table 3.12 Binary Redlich-Kister Parameters A_0, A_1, A_2 for the Excess Volume of density (ρ) and kinematic viscosity (η) for (APDA+ H_2O) system

Parameters		Binary Pair	
		Binary pair (ρ)	Binary pair (η)
A_0	l	128.228	-7579.069
	m	-0.815	47.776
	n	1.294×10^{-3}	-0.075
A_1	l	282.651	-8673.527
	m	-1.795	54.398
	n	2.851×10^{-3}	-0.086
A_2	l	155.856	
	m	-0.989	
	n	1.572×10^{-3}	
AAD %		0.06	8.19

Table 3.13 Binary Redlich-Kister Parameters A_0, A_1, A_2 for the Excess Volume of density (ρ) for (APDA + MDEA+ H_2O) system

Parameters		Binary Pair		
		APDA + MDEA	APDA + H_2O	MDEA + H_2O
A_0	*l*	12.427	-12.835	-10.173
	m	-7.749×10^{-2}	8.102×10^{-2}	6.447×10^{-2}
	n	1.195×10^{-4}	-1.248×10^{-4}	-9.929×10^{-5}
A_1	*l*	-1.223	-2.592	-5.849×10^{-1}
	m	7.629×10^{-3}	1.529×10^{-2}	2.722×10^{-3}
	n	-1.176×10^{-5}	-2.372×10^{-5}	-4.323×10^{-6}
A_2	*l*	3.918×10^{-2}	14.157	9.720
	m	-2.445×10^{-4}	-8.752×10^{-2}	-5.979×10^{-2}
	n	3.77×10^{-7}	1.351×10^{-4}	9.232×10^{-5}
AAD %		0.05		

Table 3.14 Binary Redlich-Kister Parameters A_0, A_1, A_2 for the Excess Volume of density (ρ) for (APDA + AMP + H_2O) system

Parameters		Binary Pair		
		APDA + AMP	APDA + H_2O	AMP + H_2O
A_0		0.756	-1.019	-0.190
	l	-4.299×10^{-3}	6.527×10^{-3}	1.974×10^{-3}
	m	4.885×10^{-6}	-7.206×10^{-6}	-1.995×10^{-6}
	n			
A_1		-9.201×10^{-2}	-0.434	-0.103
	l	5.272×10^{-4}	1.845×10^{-3}	-2.081×10^{-4}
	m	-5.979×10^{-7}	-2.278×10^{-6}	-1.254×10^{-3}
	n			
A_2		4.856×10^{-3}	1.407	-1.995×10^{-6}
	l	-2.788×10^{-5}	-7.465×10^{-3}	1.628×10^{-8}
	m	3.160×10^{-7}	8.637×10^{-6}	1.621×10^{-6}
	n			
AAD %			0.07	

Table 3.15 Comparison of the viscosities (μ) of aqueous MDEA solutions (mass fraction, w) measured in the present work with literature values at pressure P= 0.1 MPa

Mass Fraction (MDEA)	T/K	μ/mPa.s			AAD%
		Ref. 37	Ref. 38	This work	
0.10	303.2	1.14		1.16	1.12
	313.2	0.91		0.91	
	323.2	0.75		0.75	
	333.2	0.63		0.64	
0.20	303.2	1.69	1.70	1.64	0.89
	313.2	1.30	1.32	1.31	
	323.2	1.05	1.05	1.06	
	333.2	0.86	0.86	0.87	
0.30	303.2	2.61	2.62	2.63	0.97
	313.2	1.94	1.95	1.95	
	323.2	1.51	1.52	1.52	
	333.2	1.21	1.21	1.22	

Table 3.16a Viscosity (μ) for (AEP + MDEA + H_2O) from 303.2 K to 343.2 K at pressure P=0.1 MPa

T/K	Mass Fraction (AEP)	Mass Fraction (MDEA)	μ/mPa.s
303.2	0.05	0.35	4.31
313.2	0.05	0.35	3.06
323.2	0.05	0.35	2.23
333.2	0.05	0.35	1.71
343.2	0.05	0.35	1.31
303.2	0.1	0.3	4.95
313.2	0.1	0.3	3.42
323.2	0.1	0.3	2.50
333.2	0.1	0.3	1.86
343.2	0.1	0.3	1.41
303.2	0.15	0.25	5.25
313.2	0.15	0.25	3.50
323.2	0.15	0.25	2.6
333.2	0.15	0.25	1.90
343.2	0.15	0.25	1.44

Table 3.16 b Viscosity (μ) for (AEP + MDEA+ H_2O) from 303.2 K to 343.2 K at pressure P=0.1 MPa

T/K	Mass Fraction (AEP)	Mass Fraction (MDEA)	μ/mPa.s
303.2	0.2	0.2	5.85
313.2	0.2	0.2	3.91
323.2	0.2	0.2	2.80
333.2	0.2	0.2	2.07
343.2	0.2	0.2	1.54
303.2	0.25	0.15	6.96
313.2	0.25	0.15	4.71
323.2	0.25	0.15	3.39
333.2	0.25	0.15	2.42
343.2	0.25	0.15	1.78

Table 3.17a Viscosity (μ) for (AEP + AMP + H_2O) from 303.2 K to 343.2 K at pressure P=0.1 MPa

T/K	Mass Fraction (AEP)	Mass Fraction (AMP)	μ/mPa.s
303.2	0.05	0.35	6.82
313.2	0.05	0.35	5.23
323.2	0.05	0.35	4.43
333.2	0.05	0.35	3.65
343.2	0.05	0.35	3.27
303.2	0.1	0.3	6.49
313.2	0.1	0.3	4.91
323.2	0.1	0.3	4.17
333.2	0.1	0.3	3.45
343.2	0.1	0.3	3.07
303.2	0.15	0.25	6.16
313.2	0.15	0.25	4.79
323.2	0.15	0.25	3.97
333.2	0.15	0.25	3.36
343.2	0.15	0.25	2.91

Table 3.17b Viscosity (μ) for (AEP + AMP + H_2O) from 303.2 K to 343.2 K at pressure P=0.1 MPa

T/K	Mass Fraction (AEP)	Mass Fraction (AMP)	μ/mPa.s
303.2	0.2	0.2	5.86
313.2	0.2	0.2	4.56
323.2	0.2	0.2	3.75
333.2	0.2	0.2	3.09
343.2	0.2	0.2	2.80
303.2	0.25	0.15	5.45
313.2	0.25	0.15	4.35
323.2	0.25	0.15	3.56
333.2	0.25	0.15	2.86
343.2	0.25	0.15	2.62

Table 3.18 Viscosity (μ) for (APDA + MDEA + H_2O) from 303.2 K to 343.2 K at pressure P=0.1 MPa

T/K	Mass Fraction (APDA)	Mass Fraction (MDEA)	μ/mPa.s
303.2	0.04	0.26	3.49
313.2	0.04	0.26	2.49
323.2	0.04	0.26	1.89
333.2	0.04	0.26	1.36
343.2	0.04	0.26	1.04
303.2	0.07	0.23	3.62
313.2	0.07	0.23	2.70
323.2	0.07	0.23	2.07
333.2	0.07	0.23	1.55
343.2	0.07	0.23	1.17
303.2	0.10	0.20	3.90
313.2	0.10	0.20	3.09
323.2	0.10	0.20	2.24
333.2	0.10	0.20	1.67
343.2	0.10	0.20	1.20

Table 3.19 Viscosity (μ) for (APDA + AMP + H_2O) from 303.2 K to 343.2 K at pressure P=0.1 MPa

T/K	Mass Fraction (APDA)	Mass Fraction (AMP)	μ/mPa.s
303.2	0.04	0.26	3.90
313.2	0.04	0.26	2.97
323.2	0.04	0.26	2.15
333.2	0.04	0.26	1.63
343.2	0.04	0.26	1.35
303.2	0.07	0.23	4.10
313.2	0.07	0.23	3.25
323.2	0.07	0.23	2.49
333.2	0.07	0.23	1.79
343.2	0.07	0.23	1.47
303.2	0.10	0.20	4.24
313.2	0.10	0.20	3.47
323.2	0.10	0.20	2.63
333.2	0.10	0.20	2.11
343.2	0.10	0.20	1.67

Table 3.20 Parameters (G_{12}, G_{23}, and G_{13}) of the Grunberg-Nissan Model for (AEP + MDEA + H_2O) and (AEP + AMP +H_2O)

Parameters		Ternary Pairs	
		AEP + MDEA +H_2O	AEP + AMP +H_2O
G_{12}	*l*	9194.7	403.835
	m	-57.014	-2.487
	n	8.716 x 10^{-2}	4 x 10^{-3}
G_{23}	*l*	-41.53	47.872
	m	0.434	-0.208
	n	-8.221 x 10^{-4}	4 x 10^{-4}
G_{13}	*l*	-288.14	2.706
	m	2.166	0.103
	n	-3.673 x 10^{-3}	-2 x 10^{-4}
AAD %		2.03	1.16

Table 3.21 Parameters (G_{12}, G_{23}, and G_{13}) of the Grunberg-Nissan Model for (APDA + MDEA + H_2O) and (APDA+ AMP +H_2O)

Parameters		Ternary Pairs	
		APDA + MDEA +H_2O	APDA + AMP +H_2O
G_{12}	*l*	-1.564 x 10^5	8.331 x 10^4
	m	994.069	-569.884
	n	-1.575	0.966
G_{23}	*l*	598.849	-45.149
	m	-3.585	0.701
	n	5.468 x 10^{-3}	-1.6 x 10-3
G_{13}	*l*	6.339 x 10^3	-4.725 x 10^3
	m	-40.399	31.701
	n	6.453 x 10^{-2}	-0.052
AAD %		2.273	1.068

Table 3.22a Estimated Gibbs energies of activation of viscous flow (ΔG^{o}/kJ.mol^{-1}) of (AEP/APDA + H_2O) from 303.2 K to 343.2 K

T/K	Mass Fraction	ΔG^{o}/kJ.mol^{-1}	
		AEP + H_2O	APDA+H_2O
303.2	0.1	45.18	45.21
313.2	0.1	46.13	46.47
323.2	0.1	47.07	47.62
333.2	0.1	48.02	48.91
343.2	0.1	48.93	50.07
303.2	0.15	46.01	45.93
313.2	0.15	46.94	46.88
323.2	0.15	47.73	47.87
333.2	0.15	48.69	49.15
343.2	0.15	49.57	50.35
303.2	0.2	46.81	46.77
313.2	0.2	47.56	47.54
323.2	0.2	48.38	48.24
333.2	0.2	49.27	49.35
343.2	0.2	50.12	50.62
303.2	0.25	47.63	47.64
313.2	0.25	48.38	48.22
323.2	0.25	49.16	48.98
333.2	0.25	49.98	49.98
343.2	0.25	50.82	50.99

Table 3.22b Estimated Gibbs energies of activation of viscous flow (ΔG^o/kJ.mol^{-1}) of (AEP/APDA + H_2O) from 303.2 K to 343.2 K

T/K	Mass Fraction	ΔG^o/kJ.mol^{-1}	
		AEP + H2O	APDA+H2O
303.2	0.3	48.55	48.61
313.2	0.3	49.33	49.32
323.2	0.3	50.29	50.11
333.2	0.3	50.94	50.95
343.2	0.3	51.80	51.88
303.2	0.35	48.87	48.97
313.2	0.35	49.76	50.04
323.2	0.35	50.71	50.91
333.2	0.35	51.79	51.74
343.2	0.35	52.86	52.51
303.2	0.4	49.42	49.46
313.2	0.4	50.43	50.57
323.2	0.4	51.36	51.44
333.2	0.4	52.31	52.17
343.2	0.4	53.47	53.02

Table 3.23 Estimated Gibbs energies of activation of viscous flow (ΔG^{o}/kJ.mol^{-1}) of (AEP+ MDEA/AMP + H_2O) from 303.2 K to 343.2 K

Mass Fraction (AEP)	Mass Fraction (MDEA/AMP)	ΔG^{o}/kJ.mol^{-1}	
		AEP +MDEA+ H_2O	AEP+AMP+H_2O
0.05	0.35	49.15	50.25
0.05	0.35	49.88	51.22
0.05	0.35	50.62	52.43
0.05	0.35	51.46	53.53
0.05	0.35	52.24	54.83
0.1	0.3	49.50	50.13
0.1	0.3	50.17	51.06
0.1	0.3	50.93	52.27
0.1	0.3	51.69	53.37
0.1	0.3	52.45	54.65
0.15	0.25	49.65	49.99
0.15	0.25	50.24	51.00
0.15	0.25	51.04	52.14
0.15	0.25	51.74	53.30
0.15	0.25	52.51	54.50
0.2	0.2	49.93	49.87
0.2	0.2	50.52	50.87
0.2	0.2	51.24	51.98
0.2	0.2	51.99	53.07
0.2	0.2	52.71	54.39
0.25	0.15	50.37	49.69
0.25	0.15	51.01	50.75
0.25	0.15	51.76	51.85
0.25	0.15	52.42	52.85
0.25	0.15	53.12	54.19

Table 3.24 Estimated Gibbs energies of activation of viscous flow (ΔG^{o}/kJ.mol^{-1}) of (APDA+ MDEA/AMP + H_2O) from 303.2 K to 343.2 K

Mass Fraction (APDA)	Mass Fraction (MDEA/AMP)	ΔG^{o}/kJ.mol^{-1}	
		APDA +MDEA+ H_2O	APDA+AMP+H_2O
0.04	0.26	48.31	48.42
0.04	0.26	49.03	49.31
0.04	0.26	49.86	50.01
0.04	0.26	50.49	50.79
0.04	0.26	51.23	51.79
0.07	0.23	48.41	48.57
0.07	0.23	49.34	49.57
0.07	0.23	50.10	50.44
0.07	0.23	50.84	51.09
0.07	0.23	51.81	52.06
0.10	0.20	48.60	48.67
0.10	0.20	49.67	49.76
0.10	0.20	50.31	50.60
0.10	0.20	51.21	51.56
0.10	0.20	52.26	52.44

Table 3.25 Estimated entropy of activation ($\Delta S^o/JK^{-1}mol^{-1}$) and enthalpy of activation ($\Delta H^o/kJmol^{-1}$) for the viscous flow of (AEP/APDA $+H_2O$)

	AEP + H_2O		APDA + H_2O	
Mass fraction	ΔS^o /$JK^{-1}mol^{-1}$	ΔH^o /$kJmol^{-1}$	ΔS^o /$JK^{-1}mol^{-1}$	ΔH^o /$kJmol^{-1}$
0.1	-93.95	16.70	-121.535	8.38
0.15	-88.44	19.20	-110.676	12.26
0.2	-83.03	21.59	-94.2322	18.05
0.25	-79.57	23.47	-83.8371	22.06
0.3	-81.01	24.00	-81.4554	23.85
0.35	-99.76	18.56	-88.2168	22.32
0.4	-99.66	19.18	-87.756	22.97

Table 3.26 Estimated entropy of activation ($\Delta S^o/JK^{-1}mol^{-1}$) and enthalpy of activation ($\Delta H^o/kJmol^{-1}$) for the viscous flow of (AEP + MDEA/AMP + H_2O)

	AEP + MDEA+ H_2O		AEP + AMP + H_2O	
Mass fraction	ΔS^o /$JK^{-1}mol^{-1}$	ΔH^o /$kJmol^{-1}$	ΔS^o /$JK^{-1}mol^{-1}$	ΔH^o /$kJmol^{-1}$
0.05 + 0.35	-77.45	25.64	-114.36	15.49
0.10 + 0.30	-73.89	27.07	-113.25	15.69
0.15 + 0.25	-72.12	27.73	-112.78	15.74
0.20 + 0.20	-70.18	28.59	-111.98	15.85
0.25 + 0.15	-69.17	29.38	-110.85	16.04

Table 3.27 Estimated entropy of activation ($\Delta S^o/JK^{-1}mol^{-1}$) and enthalpy of activation ($\Delta H^o/kJmol^{-1}$) for the viscous flow of (APDA + MDEA/AMP + H_2O)

	APDA + MDEA+ H_2O		APDA+ AMP + H_2O	
Mass fraction	ΔS^o /$JK^{-1}mol^{-1}$	ΔH^o /$kJmol^{-1}$	ΔS^o /$JK^{-1}mol^{-1}$	ΔH^o /$kJmol^{-1}$
0.04 + 0.26	-73.17	26.14	-82.52	23.53
0.07 + 0.23	-83.06	23.25	-85.52	22.82
0.10 + 0.20	-89.02	21.64	-93.78	20.40

Table 3.28 Comparison of the surface tension (Υ) of aqueous DEA solutions (mass fraction, w) measured in the present work with literature values at pressure P= 0.1 MPa

Mass Fraction (DEA)	T/K	Υ/mN.m		AAD%
		Ref. 37	This work	
0.10	313.2	61.65	60.42	0.02
	323.2	60.69	59.18	
	333.2	60.48	58.85	
0.20	313.2	63.94	63.07	0.01
	323.2	62.62	62.23	
	333.2	61.73	60.56	
0.30	313.2	60.17	61.57	0.02
	323.2	58.57	60.13	
	333.2	57.27	58.43	

Table 3.29a Surface tension (ϒ) for (AEP + MDEA + H_2O) from 303.2 K to 343.2 K at pressure P=0.1 MPa

T/K	Mass Fraction (AEP)	Mass Fraction (MDEA)	ϒ/mN.m
303.2	0.05	0.35	51.60
313.2	0.05	0.35	51.03
323.2	0.05	0.35	50.37
333.2	0.05	0.35	49.21
343.2	0.05	0.35	48.49
303.2	0.1	0.3	52.46
313.2	0.1	0.3	51.87
323.2	0.1	0.3	50.94
333.2	0.1	0.3	50.31
343.2	0.1	0.3	49.91
303.2	0.15	0.25	53.86
313.2	0.15	0.25	53.02
323.2	0.15	0.25	52.18
333.2	0.15	0.25	51.14
343.2	0.15	0.25	50.20

Table 3.29b Surface tension (Υ) for (AEP + MDEA + H_2O) from 303.2 K to 343.2 K at pressure P=0.1 MPa

T/K	Mass Fraction (AEP)	Mass Fraction (MDEA)	Υ/mN.m
303.2	0.2	0.2	54.57
313.2	0.2	0.2	53.96
323.2	0.2	0.2	53.18
333.2	0.2	0.2	52.17
343.2	0.2	0.2	51.33
303.2	0.25	0.15	55.57
313.2	0.25	0.15	55.07
323.2	0.25	0.15	54.50
333.2	0.25	0.15	53.38
343.2	0.25	0.15	52.87

Table 3.30a Surface tension (Υ) for (AEP + AMP + H_2O) from 303.2 K to 343.2 K at pressure P=0.1 MPa

T/K	Mass Fraction (AEP)	Mass Fraction (AMP)	Υ/mN.m
303.2	0.05	0.35	45.28
313.2	0.05	0.35	44.65
323.2	0.05	0.35	43.83
333.2	0.05	0.35	42.96
343.2	0.05	0.35	41.81
303.2	0.1	0.3	46.47
313.2	0.1	0.3	45.23
323.2	0.1	0.3	44.08
333.2	0.1	0.3	43.47
343.2	0.1	0.3	42.39
303.2	0.15	0.25	47.44
313.2	0.15	0.25	46.11
323.2	0.15	0.25	45.39
333.2	0.15	0.25	44.14
343.2	0.15	0.25	43.02

Table 3.30b Surface tension (Υ) for (AEP + AMP + H_2O) from 303.2 K to 343.2 K at pressure P=0.1 MPa

T/K	Mass Fraction (AEP)	Mass Fraction (AMP)	Υ/mN.m
303.2	0.2	0.2	48.12
313.2	0.2	0.2	47.44
323.2	0.2	0.2	47.01
333.2	0.2	0.2	46.77
343.2	0.2	0.2	45.87
303.2	0.25	0.15	48.88
313.2	0.25	0.15	48.12
323.2	0.25	0.15	47.78
333.2	0.25	0.15	47.19
343.2	0.25	0.15	46.56

Table 3.31 Surface tension (Υ) for (APDA + MDEA + H_2O) from 303.2 K to 343.2 K at pressure P=0.1 MPa

T/K	Mass Fraction (APDA)	Mass Fraction (MDEA)	Υ/mN.m
303.2	0.04	0.26	52.67
313.2	0.04	0.26	51.73
323.2	0.04	0.26	51.11
333.2	0.04	0.26	50.59
343.2	0.04	0.26	49.17
303.2	0.07	0.23	53.07
313.2	0.07	0.23	52.76
323.2	0.07	0.23	51.69
333.2	0.07	0.23	50.75
343.2	0.07	0.23	50.23
303.2	0.1	0.2	53.88
313.2	0.1	0.2	52.97
323.2	0.1	0.2	52.34
333.2	0.1	0.2	51.65
343.2	0.1	0.2	51.1

Table 3.32 Surface tension (Υ) for (APDA + AMP + H_2O) from 303.2 K to 343.2 K at pressure P=0.1 MPa

T/K	Mass Fraction (APDA)	Mass Fraction (AMP)	Υ/mN.m
303.2	0.04	0.26	45.64
313.2	0.04	0.26	44.87
323.2	0.04	0.26	44.04
333.2	0.04	0.26	43.34
343.2	0.04	0.26	42.66
303.2	0.07	0.23	46.13
313.2	0.07	0.23	45.54
323.2	0.07	0.23	44.89
333.2	0.07	0.23	44.18
343.2	0.07	0.23	43.57
303.2	0.1	0.2	47.38
313.2	0.1	0.2	46.76
323.2	0.1	0.2	46.01
333.2	0.1	0.2	44.74
343.2	0.1	0.2	43.89

Table 3.33 Temperature based surface tension parameters for the (AEP + H_2O) system.

Mass fraction	k_1 ($mN.m^{-1}$)	k_2 ($mN.m^{-1}.K^{-1}$)	% AAD
0.1	98.33	-0.104	0.29
0.15	95.42	-0.0969	0.24
0.2	87.204	-0.0751	0.42
0.25	90.93	-0.0916	0.21
0.3	90.85	-0.0931	0.18
0.35	89.99	-0.0933	0.21
0.4	92.99	-0.1058	0.36

Table 3.34 Temperature based surface tension parameters for the (APDA + H_2O) system.

Mass fraction	k_1 ($mN.m^{-1}$)	k_2 ($mN.m^{-1}.K^{-1}$)	% AAD
0.1	93.22	-0.0977	0.25
0.15	108.99	-0.1557	0.31
0.2	89.52	-0.0933	0.29
0.25	84.86	-0.0884	0.28
0.3	90.87	-0.113	0.47
0.35	85.42	-0.0989	0.31
0.4	76.83	-0.0743	0.45

Table 3.35 Temperature based surface tension parameters for the (AEP + MDEA+ H_2O) system.

Mass fraction	k_1 ($mN.m^{-1}$)	k_2 ($mN.m^{-1}.K^{-1}$)	% AAD
0.05 + 0.35	76.184	-0.081	0.33
0.10 + 0.30	72.644	-0.067	0.29
0.15 + 0.25	81.75	-0.092	0.31
0.20 + 0.20	79.685	-0.083	0.17
0.25 + 0.15	76.973	-0.071	0.24

Table 3.36 Temperature based surface tension parameters for the (AEP + AMP+ H_2O) system.

Mass fraction	k_1 ($mN.m^{-1}$)	k_2 ($mN.m^{-1}.K^{-1}$)
0.05 + 0.35	71.59	-0.086
0.10 + 0.30	76.38	-0.099
0.15 + 0.25	80.152	-0.108
0.20 + 0.20	63.74	-0.052
0.25 + 0.15	65.705	-0.056

Table 3.37 Temperature based surface tension parameters for the (APDA + MDEA + H_2O) system.

Mass fraction	k_1 ($mN.m^{-1}$)	k_2 ($mN.m^{-1}.K^{-1}$)
0.04 + 0.26	77.35	-0.081
0.07 + 0.23	76.55	-0.077
0.10 + 0.20	74.62	-0.069

Table 3.38 Temperature based surface tension parameters for the (APDA + AMP+ H_2O) system.

Mass fraction	k_1 ($mN.m^{-1}$)	k_2 ($mN.m^{-1}.K^{-1}$)
0.04 + 0.26	68.31	-0.075
0.07 + 0.23	65.8	-0.065
0.10 + 0.20	74.83	-0.09

References

[1] U.E. Aronu, A. Hartono, H.F. Svendsen, Density, viscosity, and N_2O solubility of aqueous amino acid salt and amino acid salt solutions, J. Chem. Thermodyn. 45 (2012) 90–99.

[2] I. Khattab, F. Bandarkar, M. Fakhree, A. Jouyban, Density, viscosity, and surface tension of water + ethanol mixturesfrom 293 to 323K, Korean J. Chem. Eng. 29 (2012) 812–817.

[3] A.F. Portugal, P.W.J. Derks, G.F. Versteeg, F.D. Magalhaes, A. Mendes, Characterization of potassium glycinate forcarbon dioxide absorption purposes, Chem. Eng. Sci. 62 (2007) 6534–6547.

[4] T.Y. Wu, B.K. Chen, L. Hao, C.W. Kuo, I.W. Sun, Thermophysical properties of binary mixtures {1-methyl-3-pentylimidazoliumtetrafluoroborate + polyethylene glycol methyl ether}, J. Taiwan Inst. Chem. Eng. 43 (2012) 313–321.

[5] B. Mandal, M. Kundu, S.S. Bandyopadhyay, Density and viscosity of aqueous solutions of (N-methyldiethanolamine + monoethanolamine), (N-methyldiethanolamine + diethanolamine), (2-amino-2-methyl-1-propanol + monoethanolamine), and (2-amino- 2-methyl-1-propanol + diethanolamine), J. Chem. Eng. Data 48 (2003) 703 – 707.

[6] M.H. Li, Y.C. Li, Densities and viscosities of solutions of monoethanolamine + N-methyldiethanolamine + water and monoethanolamine + 2-amino-2-methyl-1-propanol + water, J. Chem. Eng. Data 39 (1994) 444 – 447.

[7] G. Vazquez, E. Alvarez, J.M. Navaza, R. Rendo, E. Romero, Surface tension of binary mixtures of water + monoethanolamine and water + 2-amino-2-methyl-1-propanol and tertiary mixtures of these amines with water from 25 °C to 50 °C, J. Chem. Eng. Data 42 (1997) 57 – 59.

[8] J. Han, J. Jin, D.A. Eimer, M.C. Melaaen, Density of water + monoethanolamine + CO_2 from (298.15 to 413.15) K and surface tension of water + monoethanolamine from (303.15 to 333.15) K, J. Chem. Eng. Data 57 (2012) 1095 – 1103.

[9] E.B. Rinker, D.W. Oelschlager, A.T. Colussi, K.R. Henry, O.C. Sandall, Viscosity, density, and surface tension of binary mixtures of water and N-methyldiethanolamine and water and diethanolamine and tertiary mixtures of these amines with water over the temperature range 20 – 100 ^{o}C, J. Chem. Eng. Data 39 (1994) 392 – 395.

[10] C.H. Hsu, M.H. Li, Densities of aqueous blended amines, J. Chem. Eng. Data 42 (1997) 502 – 507.

[11] G. Vazquez, E. Alvarez, R. Rendo, E. Romero, J.M. Navaza, Surface tension of aqueous solutions of diethanolamine and triethanolamine from 25 °C to 50 °C, J. Chem. Eng. Data 41 (1996) 806 – 808.

[12] H.A. Al-Ghawas, D.P. Hagewiesche, G. Ruiz-Ibanez, O.C. Sandall, Physicochemical properties important for carbon dioxide absorption in aqueous methyldiethanolamine, J. Chem. Eng. Data 34 (1989) 385 – 391.

[13] E. Alvarez, R. Rendo, B. Sanjurjo, M. Sanchezvilas, J.M. Navaza, Surface tension of binary mixtures of water + N-methyldiethanolamine and ternary mixtures of this amine and water with monoethanolamine, diethanolamine, and 2-amino-2-methyl-1-propanol from 25 to 50 °C, J. Chem. Eng. Data 43 (1998) 1027 – 1029.

[14] A. Muhammad, M.I.A. Mutalib, C.D. Wilfred, T. Murugesan, A. Shafeeq, Viscosity, refractive index, surface tension, and thermal decomposition of aqueous N-methyldiethanolamine solutions from (298.15 to 338.15) K, J. Chem. Thermodyn. 53 (2008) 2226 – 2229.

[15] S. Xu, F.D. Otto, A.E. Mather, Physical properties of aqueous AMP solutions, J. Chem. Eng. Data 36 (1991) 71 – 75.

[16] P.W. Derks, K.J. Hogendoorn, G.F. Versteeg, Solubility of N_2O in and density, viscosity, and surface tension of aqueous piperazine solutions, J. Chem. Eng. Data 50 (2005) 1947 – 1950.

[17] A. Samanta, S.S. Bandyopadhyay, Density and viscosity of aqueous solutions of piperazine and (2-amino-2-methyl-1-propanol + piperazine) from 298 to 333 K, J. Chem. Eng. Data 51 (2006) 467 – 470.

[18] W.C. Sun, C.B. Yong, M.H. Li, Kinetics of the absorption of carbon dioxide into mixed aqueous solutions of 2-amino-2-methyl-1-propanol and piperazine, Chem. Eng. Sci. 60 (2005) 503 – 516.

[19] G. Murshid, A.M. Shariff, L.K. Keong, M.A. Bustam, Physical properties of aqueous solutions of piperazine and (2-amino-2-methyl-1-propanol + piperazine) from (298.15 to 333.15) K, J. Chem. Eng. Data 56 (2011) 2660 – 2663.

[20] A. Muhammad, M.I.A. Mutalib, T. Murugesan, A. Shafeeq, Thermophysical properties of aqueous piperazine and aqueous (N-methyldiethanolamine + piperazine) solutions at temperatures (298.15 to 338.15) K, J. Chem. Eng. Data 54 (2009) 2317 – 2321.

[21] S. Xu, Y. Wang, F.D. Otto, A.E. Mather, Physicochemical properties of 2-piperidineethanol and its aqueous solutions, J. Chem. Eng. Data 37 (1992) 407 – 411.

[22] K.P. Shen, M.H. Li, S.M. Yi, Kinetics of carbon dioxide with sterically hindered 2-piperidineethanol aqueous solutions, Ind. Eng. Chem. Res. 30 (1991) 1811 – 1813.

[23] S.J. Yoon, H.S. Lee, H. Lee, Densities, viscosities, and surface tensions of aqueous 2-amino-2-ethyl-1, 3-propanediol solutions, J. Chem. Eng. Data 47 (2002) 30 – 32.

[24] K. Narayanaswamy, A.V. Rayer, S. Kadiwala, A. Henni, Volumetric properties, viscosities, refractive indices and surface tensions for (dimethylpropanolamine (DMPA) + water) mixtures from 298.15 K to 343.15 K, J. Chem. Eng. Data 543 (2012) 218 – 225.

[25] A. Blanco, A. Garciaabuin, D. Goimezdiaz, J.M. Navaza, Density, speed of sound, viscosity, and surface tension of dimethylethylenediamine + water and (ethanolamine + dimethylethanolamine) + water from T = (293.15 to 323.15) K, J. Chem. Eng. Data 61 (2016) 188 – 194.

[26] D. Fu, L. Wang, X.F. Tian, Experiments and model for the surface tension of DEAE-PZ and DEAE-MEA aqueous solutions, J. Chem. Thermodyn. 105 (2017) 71 – 75.

[27] M.H. Li, K.P. Shen, Densities and solubilities of solutions of carbon dioxide in water + monoethanolamine + N-methyldiethanolamine, J. Chem. Eng. Data 37 (1992) 288 –290.

[28] C.H. Hsu, M.H. Li, Viscosities of aqueous blended amines, J. Chem. Eng. Data 42 (1997) 714 – 720.

[29] A. Samanta, S.S. Bandyopadhyay, Density and viscosity of aqueous solutions of piperazine and (2-amino-2-methyl-1-propanol + piperazine) from 298 to 333 K, J. Chem. Eng. Data 51 (2006) 467 – 470.

[30] P.W.J. Derks, E.S. Hamborg, J.A. Hogendoorn, J.P.M. Niederer, G.F. Versteeg, Densities, viscosities, and liquid diffusivities in aqueous piperazine and aqueous (piperazine + N-methyldiethanolamine) solutions, J. Chem. Eng. Data 53 (2008) 1179 – 1185.

[31] S.Y. Horng, M.H. Li, Kinetics of absorption of carbon dioxide into aqueous solutions of monoethanolamine + triethanolamine, Ind. Eng. Chem. Res. 41 (2002) 257 – 266.

[32] S. Paul and B. Mandal, Density and viscosity of aqueous solutions of (2-Piperidineethanol + Piperazine) from (288 to 333) K and surface tension of aqueous solutions of (N-methyldiethanolamine + piperazine), (2-amino-2-methyl-1-propanol + piperazine), and (2-piperidineethanol + piperazine) from (293 to 323) K, J. Chem. Eng. Data 51 (2006) 2242 – 2245.

[33] A. Venkat, G. Kumar, and M. Kundu, Density and surface tension of aqueous solutions of (2-(methylamino)-ethanol +2-amino-2-methyl-1-propanol) and (2-(methylamino)-ethanol + N-methyldiethanolamine) from (298.15 to 323.15) K, J. Chem. Eng. Data 55 (2010) 4580 – 4585.

[34] O. Redlich, A.T. Kister, Algebraic representation of thermodynamic properties and the classification of solutions, Ind. Eng. Chem. Res. 40 (1948) 345-348.

[35] L. Grunberg, A.H. Nissan, Mixture law for viscosity, Nature 164 (1949) 799-800.

[36] J.S. Torrecilla, J. Palomer, J. Garcia, E. Rojo, F. Rodriguez, Modelling of carbon dioxide solubility in ionic liquids at sub and supercritical conditions by neural networks and mathematical regressions, Chemomet. Intelligent Lab. Sys. 93 (2008) 149–159.

[37] NIST Scientific and Technical Databases, Thermophysical properties of fluid systems, 2017. http://webbook.nist.gov/chemistry/fluid/.

[38] M. Singh, Survismeter Type I and II for Surface Tension, Viscosity measurements liquids for academic, research and development studies, J. Biochem. Biophys. Methods 67 (2006) 151−161.

[39] D. Kumar, A. Chandra, M. Singh, Influence of urea on shifting hydrophilic to hydrophobic interactions of Pr $(NO_3)_3$, Sm$(NO_3)_3$, and Gd$(NO_3)_3$ with BSA in aqueous citric Acid: A volumetric, viscometric, and surface tension study, J. Chem. Eng. Data 59 (2014) 3643−3651.

[40] A. Dey , S.K. Dash, B.P. Mandal, Equilibrium CO_2 solubility and thermophysical properties of aqueous blends of 1-(2-aminoethyl) piperazine and N-methyldiethanolamine, Fluid Phase Equilib. 463 (2018) 91-105.

[41] A. Dey , S.K. Dash, S. Balchandani, B.P. Mandal, Investigation on the inclusion of 1-(2-aminoethyl)piperazine as a promoter on the equilibrium CO_2 solubility of aqueous 2-amino-2-methyl-1-propanol, J. Mol. Liq. (2019) doi.org/10.1016/j.molliq.2019.111036.

[42] S. Paul, B.P. Mandal, 2006, Density and viscosity of aqueous solutions of 2-piperidineethanol, (2-piperidinethanol + monoethanolamine), and (2-piperidinethanol + diethanolamine) from (288 to 333) K, J. Chem. Eng. Data 51 (2006) 1406-1410.

[43] A. Henni, J.J. Hromek, P. Tontiwachwuthikul, A. Chakma, Volumetric properties and viscosities for aqueous AMP solutions from 25 °C to 70 °C, J. Chem. Eng. Data 48 (2003) 551-556.

[44] B. Das, B. Deogam, Y. Agrawal, B.P. Mandal, 2016. Measurement and correlation of the physicochemical properties of novel aqueous bis(3-aminopropyl)amine and its blend with N-methyldiethanolamine for CO_2 capture, J. Chem. Eng. Data 61 (2016) 2226-2235.

[45] A. J. Treszczanowicz, G. C. Benson, Excess volumes for n-alkanols + n-alkanes II. Binary mixtures of n-pentanol, n-hexanol, n-octanol, and n-decanol + n-heptane, J. Chem. Thermodyn. 10 (1978) 967–974.

[46] H. Eyring, Viscosity, plasticity, and diffusion as examples of absolute reaction rates, J. Chem. Phy. 4 (1936) 283–291

[47] H. Eyring, M.S. Jhon, 1960. Significant liquid structure, Wiley, New York.

[48] L. Li, J. Zhang, Q. Li, B. Guo, T. Zhao, F. Sha, Density, viscosity, surface tension, and spectroscopic properties for binary system of 1,2-ethanediamine+diethylene glycol, Thermochimica Acta 590 (2014) 91-99.

[49] J.A. Hernandez, A. Trejo, J.G. Fadrique, Surface tension of aqueous solutions of alkanolamines: single amines, blended amines and systems with nonionic surfactants, Fluid phase Equilib. 185 (2001) 165-175.

[50] J.A. Rocha, J.L. Bravo, R. Fair, Distillation columns containing structured packings: A comprehensive model for their performance. 1. Hydraulic Models, Ind. Eng. Chem. Res. 32 (1993) 641–651.

[51] N. Asprion, Surface tension models for aqueous amine blends, Ind. Eng. Chem. Res. 44 (2005) 7270-7278.

Chapter 4

EQUILIBRIUM CO_2 SOLUBILITY IN AQUEOUS AEP AND ITS BLEND WITH MDEA AND AMP

This chapter demonstrates the experimental and theoretical study of equilibrium CO_2 solubility in potential absorbent, aqueous 1-(2-aminoethyl) piperazine (AEP) and its blend with N-methyldiethanolamine (MDEA) and 2-amino-2-methyl-2-propanol (AMP). The measurements have been conducted at 303.2 to 323.2 K and within the CO_2 partial pressure range of 2 to 250 kPa. The experimental data are modeled using modified Kent-Eisenberg (KE) equilibrium model and Feed-forward neural network (ANN) model for all the concentration range. Carbamate hydrolysis and AEP deprotonation constants are expressed as a function of pressure, temperature and amine concentration from the modified KE model. The developed model is used to predict the equilibrium liquid phase speciation in the CO_2 loaded amine solution. Qualitative ^{13}C NMR and FTIR-ATR analysis have been performed for CO_2 loaded solvent to understand the reaction scheme and identify the various important reaction product.

4.1 Introduction

The benchmarked monoethanolamine (MEA) solvent used conventionally for CO_2 capture suffers from various disadvantages such as high solvent degradation and regeneration energy requirement, which restricts the wide implementation of carbon capture and sequestration (CCS) technology in power plants [1].

N-methyldiethanolamine (MDEA) which is a tertiary amine and 2-amino-2-methyl-1-propanol (AMP), which is a sterically hindered amine, have been widely used for decades as an energy-efficient solvent for capturing CO_2 from gas streams [2]. MDEA and AMP has several desirable

characteristics such as higher CO_2 absorption capacity and lower reboiler heat duty for the regeneration of CO_2-rich amine solvent compared to other widely used amines such as MEA, diethanolamine (DEA), piperazine (PZ) [3]. However, since the reaction of MDEA and AMP with CO_2 does not lead to the formation of intermediate carbamates, the reaction rate is very slow in this case. Hence, it is desirable to add a rate activator in the said solvent to enhance the CO_2 absorption rate [2]. These blended amines not only enhance the equilibrium solubility but also help in reducing solvent regeneration energy. Various research works have been conducted in the recent history to investigate the CO_2 solubility in aqueous (MDEA + MEA) [4], (AMP + MEA) [4], (MDEA + PZ) [5], (AMP + PZ) [5], (MDEA + DEA) [6] system. As selecting a solvent for CO_2 capture process is crucial, there is an important scope for investigating new solvent for this application.

Recently, 1-(2-aminoethyl) piperazine (AEP), a PZ derivative having one primary, one secondary and one tertiary amine group has been explored as a rate activator for CO_2 capture [7], which also shows higher CO_2 absorption capacity [8]. AEP offers some advantages over PZ such as better water solubility at lower solution temperature and there is no solid precipitation issue at higher CO_2 loading [9]. In addition to this, a recent study shows that PZ can degrade in a CO_2 capture process and one degradation product can be AEP [10]. Presence of AEP in a PZ blended aqueous solvent shows lesser nitrosamine formation; hence more environmentally friendly as compared to PZ based solvent [10]. The CO_2 absorption characteristics of AEP can be explained from its molecular structure which consists of all the three different types of amino groups viz. primary, secondary and tertiary. The AEP molecule has several advantageous inherent properties, such as a high boiling point, low vapor pressure and good solubility in water [8]. Singh et al. [11] in their extensive screening analysis of novel amines have outlined the merits of aqueous AEP solution over the conventional amines solvent for CO_2 capture application. It was further confirmed that compared to alkyl or hydroxyl group, the substitution of an amine group into the saturated diamine increases the CO_2 absorption rate and solubility to a great extent.

Du et al. [9] studied the CO_2 cyclic capacity, distribution of chemical species with significant CO_2 loading in the aqueous (PZ + AEP) solution at a wide temperature range using the electrolyte –Non-random Two-liquid (eNRTL) model. They predicted the cyclic capacity of CO_2 as 0.86 $mol.kg^{-1}$ for 5 mole PZ/2 mole AEP blend, which is quite high compared to 7 mole MEA

which gives CO_2 capacity as 0.50 mol.kg^{-1}. Paul et al. [7] investigated the physicochemical properties of aqueous AEP as well as kinetic rate parameters of AEP-CO_2 reactions over the temperature range of (298.2 to 323.2) K and concentration range of (0.08 to 1.23 kmol.m^{-3}). It has been inferred that the understudy solvent display very high reaction rate with second-order rate constant for AEP-CO_2 reaction is 56354.2 m^3.kmol^{-1}s^{-1} at 313.2 K. These desirable characteristics as well as lack of literature data on the CO_2 solubility measurement of aqueous AEP and (AEP + MDEA/AMP) system persuade us to investigate the following blends for PCC applications. Equilibrium solubility data of CO_2 in aqueous amine systems at a wide temperature and pressure range are required for the process design of CO_2 capture by regenerative chemical absorption from post-combustion gas streams [3]. Solubility measurements and models can lead to the development of accurate process predictions and for the optimization of a CO_2 capture process. Modified Kent-Eisenberg (KE) framework [12] is used to model the experimentally measured solubility data. Since the KE model does not account for non-ideality in the reaction system, it avoids the rigorous calculations and hence reduces the computation time compared to other thermodynamic models such as Deshmukh Mather, e-NRTL, extended UNIQUAC and Pitzer model, respectively [3, 13-14]. Apart from the KE model, feed forward artificial neural network (ANN) model has also been applied to model the CO_2 solubility data of the single and blended amine system. Both the model outputs are compared and reported.

This work mostly focuses on the detail experimental cum theoretical investigation of equilibrium CO_2 solubility in (AEP + H_2O), (AEP + MDEA+ H_2O) and (AEP + AMP + H_2O) within the broad CO_2 partial pressure and temperature range of (2 - 250) kPa and (303.2 – 323.2) K, respectively. The concentration of AEP was varied from 0.10 to 0.40 w, mass fractions (0.8 to 3.2 kmol.m^{-3}) for the binary mixture of (AEP + H_2O). For the ternary mixtures, the total composition of the amine blend has been kept constant at 0.40 mass fraction (4 kmol.m^{-3}) keeping in mind the recent interest in using concentrated amine solution for acid gas separation technology.

4.2 Experimental section

4.2.1 Materials

All the chemicals used in the present work were procured from Sigma-Aldrich (USA). The specifications of all the chemicals are given in Table 4.1. CO_2 gas having purity (> 99.9 %) used for solubility study was procured from Linde India Ltd. Deionized water is used to prepare all the solvent used in the present work.

4.2.2 Experimental methodology

4.2.2.1 Equilibrium solubility measurement

Equilibrium solubility of CO_2 in aqueous amine system was measured in the stainless steel (SS) stirred equilibrium cell (600×10^{-6} m^3) connected to a (1200×10^{-6} m^3) SS buffer cell. The schematic of the experimental set up developed in this work is shown in Fig. 4.1.

The buffer cell is fitted with a pressure transmitter (0-500 psia, Honeywell STA74L, USA) and has an accuracy of ±0.065% of the full scale. The equilibrium cell is fitted with a pressure transmitter (0-100 psia, Rosemount 2051T, Emerson Process Management, USA) and has an accuracy of ±0.065% of the full scale. Temperature sensor (Pt 100, Julabo, FRG) with an accuracy of ± 0.1 K are mounted at the respective cell to measure the temperature. A magnetic stirrer (5MLH, Remi Instruments Ltd., India) was used for liquid phase stirring which is placed under the equilibrium cell. The equilibrium and buffer cell assembly is submerged in a thermostated water bath. The temperature of the water bath is controlled by water circulating temperature controller (F32 HL, Julabo, FRG) with an accuracy of ± 0.1 K. The tubing and needle valves used for regulating the gas flow and solvent inlet to the system are of Swagelok make.

For each experimental run, the equilibrium cell and the buffer cell were allowed to reach the thermal equilibrium with the external temperature controller to attain the experimental temperature condition. Both the cells were evacuated simultaneously by applying high vacuum using a vacuum pump (IV-50, INDVAC, India). The vacuum pump was then kept disconnected. After the evacuation, the buffer cell was made to fill with pure CO_2 from the external CO_2 cylinder till it attains a pressure of about 300 psia. The equilibrium cell was then fed with a known amount of aqueous amine solution (50×10^{-6} m^3) from the solvent injection port with the

help of an attached burette, and the port was fully closed by operating the needle valve. The amine solution was again degassed to remove any dissolved gases in the liquid by applying an instant vacuum and it was kept under this condition for about 20 min so that the liquid inside the cell exists under its own vapor pressure.

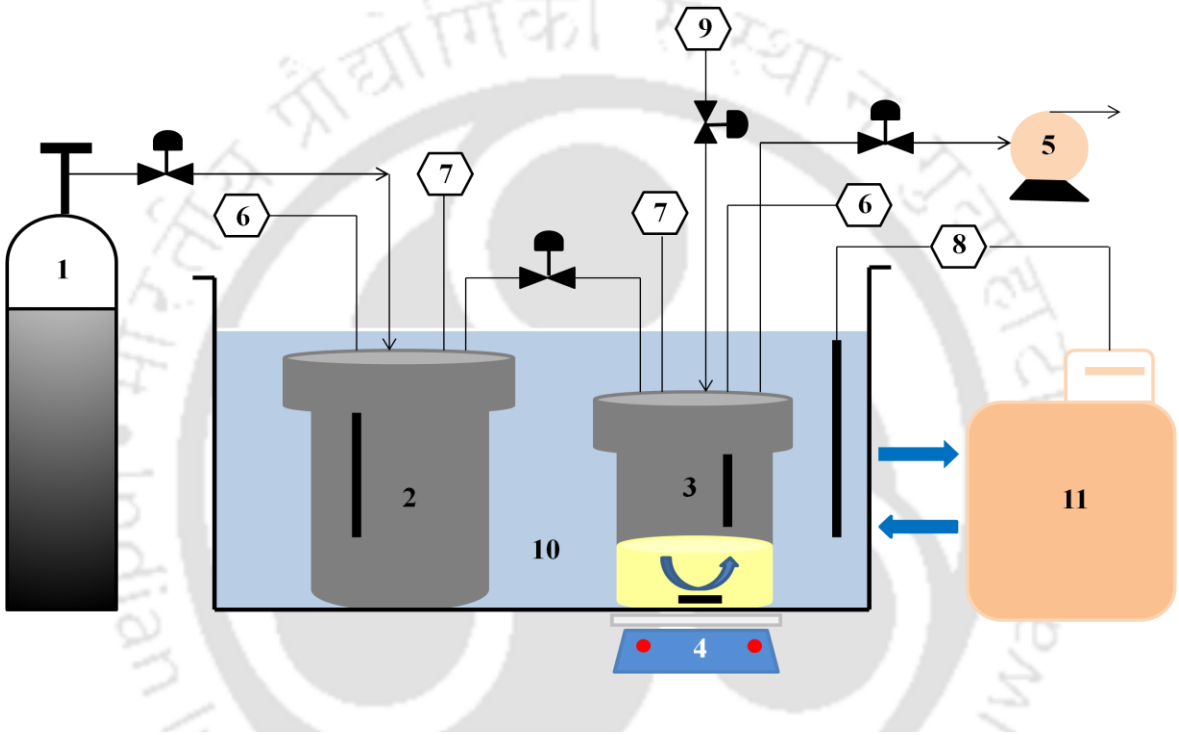

Fig. 4.1 Experimental arrangement for CO_2 solubility measurement: 1- CO_2 Cylinder, 2- Buffer Cell, 3- Equilibrium Cell, 4- Magnetic stirrer, 5- Vacuum Pump, 6- Temperature sensor, 7- Pressure Transducer, 8- Temperature sensor for water bath, 9- Inlet provision for liquid solvent, 10- Water bath, 11- Temperature controller

The vapor pressure corresponding to the experimental temperature inside the equilibrium cell (P^v) and the initial pressure in the buffer cell (P_{b1}) were measured using the pressure transducers mounted on each cell. A certain amount of CO_2 gas from the buffer cell was then transferred to the equilibrium cell by operating the needle valve between them. The magnetic stirrer kept under

the equilibrium cell was kept on for liquid phase stirring. As CO_2 gas is absorbed by the solution inside the equilibrium cell, the total pressure of the cell decreases. Vapor and liquid phase equilibrium of CO_2 gas was attained when there was no change of total pressure in the equilibrium cell noted at least for 1 hr. At this condition total pressure in the equilibrium cell, (P^T) and the final pressure in the buffer cell, (P_{b2}) were recorded simultaneously. The equilibrium partial pressure of CO_2 at the experimental temperature was calculated by taking the difference between total pressure and amine vapor pressure $(P_{CO_2} = P^T - P^v)$. The liquid phase CO_2 loading (α_{CO2}) was calculated using equations (4.1-4.3) as reported in the literature [16]. This procedure was repeated to obtain liquid phase CO_2 loading at different higher CO_2 partial pressures and at different temperatures.

The moles of CO_2, n_{CO_2} transferred from the buffer cell to the equilibrium cell is calculated as [15]:

$$n_{CO2} = \frac{V_b}{RT}\left(\frac{P_{b1}}{Z_1} - \frac{P_{b2}}{Z_2}\right) \tag{4.1}$$

Where, V_b is the volume of the buffer cell, R and T represents the gas constant and the system temperature, Z_1 and Z_2 are the compressibility factors corresponding to the initial pressure (P_{b1}) and final pressure (P_{b2}) of the buffer cell, respectively. At high CO_2 pressure, the gas phase may behave non-ideal and compressibility factor (Z) is required to calculate using an equation of state (EOS). In the present work, Peng-Robinson equation of state is used to calculate 'Z' and used in Eq. (4.1). The moles of CO_2 remaining in the gas phase (n^g_{CO2}) after the attainment of phase equilibrium is calculated by Eq. (4.2).

$$n^g{}_{CO2} = \frac{V^g\ P_{CO2}}{Z_{CO2}RT} \tag{4.2}$$

Where, V^g and Z_{CO2} represent the gas phase volume and the compressibility factor of CO_2 in the equilibrium cell, respectively. The gas phase volume was calculated by subtracting the liquid

volume from the volume of the equilibrium cell. Equilibrium CO_2 loading (α_{CO2}) expressed in moles of CO_2 per moles of total amine corresponding to a CO_2 partial pressure can be determined using a mass balance of CO_2 in liquid and vapor phase. The expression is given by:

$$\alpha_{CO2} = \frac{n_{CO2} - n^{g}{}_{CO2}}{n_{am}} \tag{4.3}$$

Where n_{am} represents the total moles of amine in the liquid phase. The sample calculation corresponding to the calculation of CO_2 loading has been presented in Appendix II.

4.2.2.2 Standard uncertainty in the solubility measurement

The standard uncertainty associated with the estimation of equilibrium CO_2 loading data can be determined by error propagation theory [16-17]. According to this theory, the standard uncertainty $u(y)$ corresponding to the measured output variables can be expressed as a function of the standard uncertainties associated with each input variable $u(x_i)$. The functional relation can be represented as:

$$u^2(y) = \sum_{i=1}^{n} \left(\frac{\partial f}{\partial x_i} u(x_i) \right)^2 \tag{4.4}$$

The standard uncertainty in the measurement of CO_2 loading can be considered as a function of uncertainty in temperature, reactor volume, pressure and composition of the inlet solution. The uncertainties associated with each measured variable as well as the methodology for uncertainty calculation is reported in Appendix III.

4.3 Modeling of CO_2 solubility

The equilibrium CO_2 solubility data in aqueous amine solution has been modeled using modified Kent-Eisenberg model [6] and artificial neural network (ANN) model [18].

4.3.1 Modified Kent-Eisenberg model

The AEP consist of all the three different types of amino groups and thus the reaction chemistry is very complex leading to the formation of a large number of intermediate species. However, the protonation constant of the tertiary amine group present in the AEP molecule is very small and hence the overall contribution to the reaction can be neglected [7-8]. Also, the possibility of di-carbamate formation can be ruled out. In the mixed amine system involving AMP, the overall stability of intermediate AMP-carbamate is very low due to steric hindrance effect and it readily undergoes hydrolysis to form bicarbonate species and freer amine molecule. The phase and chemical equilibrium corresponding to the aqueous binary and ternary amine system can be represented by (R 4.1 – R 4.8) as mentioned below. Phase equilibrium of CO_2 can be expressed by Henry's law model of physical solubility and chemical equilibrium related to all the proposed reversible reactions can be represented by the equilibrium constants (K_1-K_7). The reactions pertaining to the aqueous amine system and CO_2 can be represented as follows:

Physical Solubility

$$CO_2(g) \overset{H_{CO_2}}{\rightleftharpoons} CO_2(aq) \quad \text{(R 4.1)}$$

Dissociation of bicarbonate ion

$$HCO_3^-(g) \overset{K_1}{\rightleftharpoons} CO_3^{2-} + H^+ \quad \text{(R 4.2)}$$

Formation of bicarbonate ion

$$CO_2 + H_2O \overset{K_2}{\rightleftharpoons} HCO_3^- + H^+ \quad \text{(R 4.3)}$$

Dissociation of water

$$H_2O \overset{K_3}{\rightleftharpoons} OH^- + H^+ \quad \text{(R 4.4)}$$

Deprotonation of AEP

$$AEPH^+ \overset{K_4}{\rightleftharpoons} AEP + H^+ \quad \text{(R 4.5)}$$

Carbamate hydrolysis of AEP

$$AEPCOO^- + H_2O \overset{K_5}{\rightleftharpoons} AEP + HCO_3^- \quad \text{(R 4.6)}$$

Deprotonation of MDEA

$$MDEAH^+ \overset{K_6}{\rightleftharpoons} MDEA + H^+ \quad \text{(R 4.7)}$$

Deprotonation of AMP

$$AMPH^+ \overset{K_7}{\rightleftharpoons} AMP + H^+ \quad \text{(R 4.8)}$$

In the modified Kent-Eisenberg model, the activity coefficients of the species in the liquid phase are assumed to be unity. The concentration based apparent equilibrium constants of reactions R_2-R_7 are expressed as:

$$K_1 = \frac{[CO_3^{2-}][H^+]}{[HCO_3^-]} \quad (4.5)$$

$$K_2 = \frac{[HCO^{3-}][H^+]}{[CO_2]} \quad (4.6)$$

$$K_3 = [H^+][OH^-] \quad (4.7)$$

$$K_4 = \frac{[AEP][H^+]}{[AEPH^+]} \quad (4.8)$$

$$K_5 = \frac{[AEP][HCO_3^-]}{[AEPCOO^-]} \quad (4.9)$$

$$K_6 = \frac{[MDEA][H^+]}{[MDEAH^+]} \quad (4.10)$$

$$K_7 = \frac{[AMP][H^+]}{[AMPH^+]} \quad (4.11)$$

Where, $(K_1 - K_7)$ are the equilibrium constants corresponding to the reaction R (4.2) – R (4.8).

The CO_2 partial pressure, P_{CO_2}, at equilibrium is related to the physically dissolved CO_2 concentration, $[CO_2]$, in the solvent phase by Henry's law expression. Vapor phase equilibrium can be expressed as:

$$P_{CO_2} = H_{CO_2}[CO_2] \tag{4.12}$$

The overall mass balance and charge balance of various molecular and ionic species present in the liquid phase can be described as:

AEP balance:

$$[AEP]_t = m_1 = [AEP] + [AEPH^+] + [AEPCOO^-] \tag{4.13}$$

MDEA balance:

$$[MDEA]_t = m_2 = [MDEA] + [MDEAH^+] \tag{4.14}$$

AMP balance:

$$[AMP]_t = m_2 = [AMP] + [AMPH^+] \tag{4.15}$$

CO_2 balance:

$$\alpha_{CO_2} \times (m_1 + m_2) = [CO_2] + [HCO^{3-}] + [CO_3^{2-}] + [AEPCOO^-] \tag{4.16}$$

Where, α_{CO2} is the CO_2 loading and m_1 as well as m_2 represents initial AEP and MDEA or AMP molar concentration, respectively.

Electroneutrality balance for aqueous (AEP + MDEA):

$$[H^+] + [AEPH^+] + [MDEAH^+] - [HCO_3^-] + 2[CO_3^{2-}] + [OH^-] + [AEP(COO^-)] = 0 \tag{4.17}$$

Electroneutrality balance for aqueous (AEP + AMP):

$$[H^+]+[AEPH^+]+[AMPH^+]-[HCO_3^-]+2[CO_3^{2-}]+[OH^-]+[AEP(COO^-)]=0 \quad (4.18)$$

Where the terms in third bracket relates to the concentration of ionic species in the reaction medium. The system of equations (4.5) - (4.15) and either of (4.17) and (4.18) can be used to derive a polynomial equation which is expressed in terms of $[H^+]$. The detailed derivation of model equation is presented in Appendix IV. The linear polynomial equation accompanied with the coefficients can be expressed as follows:

$$A[H^+]^6 + B[H^+]^5 + C[H^+]^4 + D[H^+]^3 + E[H^+]^2 + F[H^+] + G = 0 \quad (4.19)$$

Where,

$$A = K_5$$

$$B = K_5.(K_6 + K_4 + m_1 + m_2)$$

$$C = K_6.K_5(m_1 + K_4) + K_2.[CO_2].(K_4 - K_5) + K_5.(m_2.K_4 - K_3)$$

$$D = K_2.K_4.(K_6.[CO_2] + m_2 - K_5.[CO_2] - m_1[CO_2]) - K_5.(K_2.K_6.[CO_2] - K_2.K_4[CO_2]) - K_3.K_5.(K_6 + K_4)$$

$$E = K_2.[CO_2].(-K_4.K_5.K_6 - K_2.K_4.[CO_2] - 2.K_1.K_5.K_6 - 2.K_1.K_4.K_5 - K_3.K_4 - m_1.K_4.K_6) - K_3.K_4.K_5.K_6$$

$$F = K_2.K_4.[CO_2].(-2.K_1.K_5.K_6 - 2.K_1.K_2.[CO_2] - K_3.K_6 - K_2.K_6.[CO_2])$$

$$G = -2.K_1.K_2^2.K_4.K_6.[CO_2]^2$$

Furthermore, equations (4.5) – (4.19) can be used to get the modified form of loading equation.

$$\alpha_{CO_2} = \frac{P_{CO_2}}{H_{CO_2}(m_1 + m_2)}\left[1 + \frac{K_2}{[H^+]} + \frac{K_1.K_2}{[H^+]^2} + \frac{m_1.K_2.K_4}{K_4.K_5.[H^+] + K_5.[H^+]^2 + K_2.K_4.[P_{CO_2}/H_{CO_2}]}\right] \quad (4.20)$$

Where, α_{CO_2} is the estimated CO_2 loading in the aqueous amine solution and m_1, m_2 represents the concentration of AEP and MDEA in molarity scale respectively.The real root of the equation (4.19) is used to calculate the estimated CO_2 loading value from equation (4.20). In the above model the equilibrium constants $(K_1 - K_3)$ and K_6 can be considered as a function of temperature and expressed as follows:

$$\ln K = a_i + b_i / T + c_i \ln T \tag{4.21}$$

Where, a_i, bi and c_i are the coefficients of the above expression and are reported in Table 4.2 [6]. The Henry's constant for physical solubility, H_{CO_2}, have been taken from the work of Hsu et al. [19] as given below.

$$\ln H_{CO_2} = 20.2669 - \frac{1.38306\times10^4}{T} + \frac{0.06913\times10^8}{T^2} - \frac{0.015589\times10^{11}}{T^3} + \frac{0.012\times10^{13}}{T^4} \tag{4.22}$$

In this work, equilibrium constants K_4 and K_5 which relates to the deprotonation and carbamate hydrolysis reaction of AEP, respectively, are regressed using least square fitting in MATLAB® platform (Appendix V). Since there are multiple roots of equation (4.19), only one value of $[H^+]$ which falls in the range of 10^{-12} -10^{-6} kmol.m^{-3} has been used for loading calculations. The necessary algorithm for the data regression system of the present work is shown in Fig. 4.2. The equilibrium constants estimated by Kent and Eisenberg in their work [20] were correlated in terms of temperature only. Later, on various researchers revised this model and regressed the equilibrium rate constants of important amine reactions in different form [6, 18, 21-22]. In some modified version, equilibrium constants are considered to be a function of CO_2 loading, amine concentration and temperature. In the present work, K_4 and K_5 are expressed in terms of temperature, CO_2 partial pressure and amine concentration [18].

4.3.2 Artificial neural network

The applicability of artificial neural network (ANN) model has been also investigated in the present work to correlate the equilibrium CO_2 solubility in aqueous AEP as well as blended

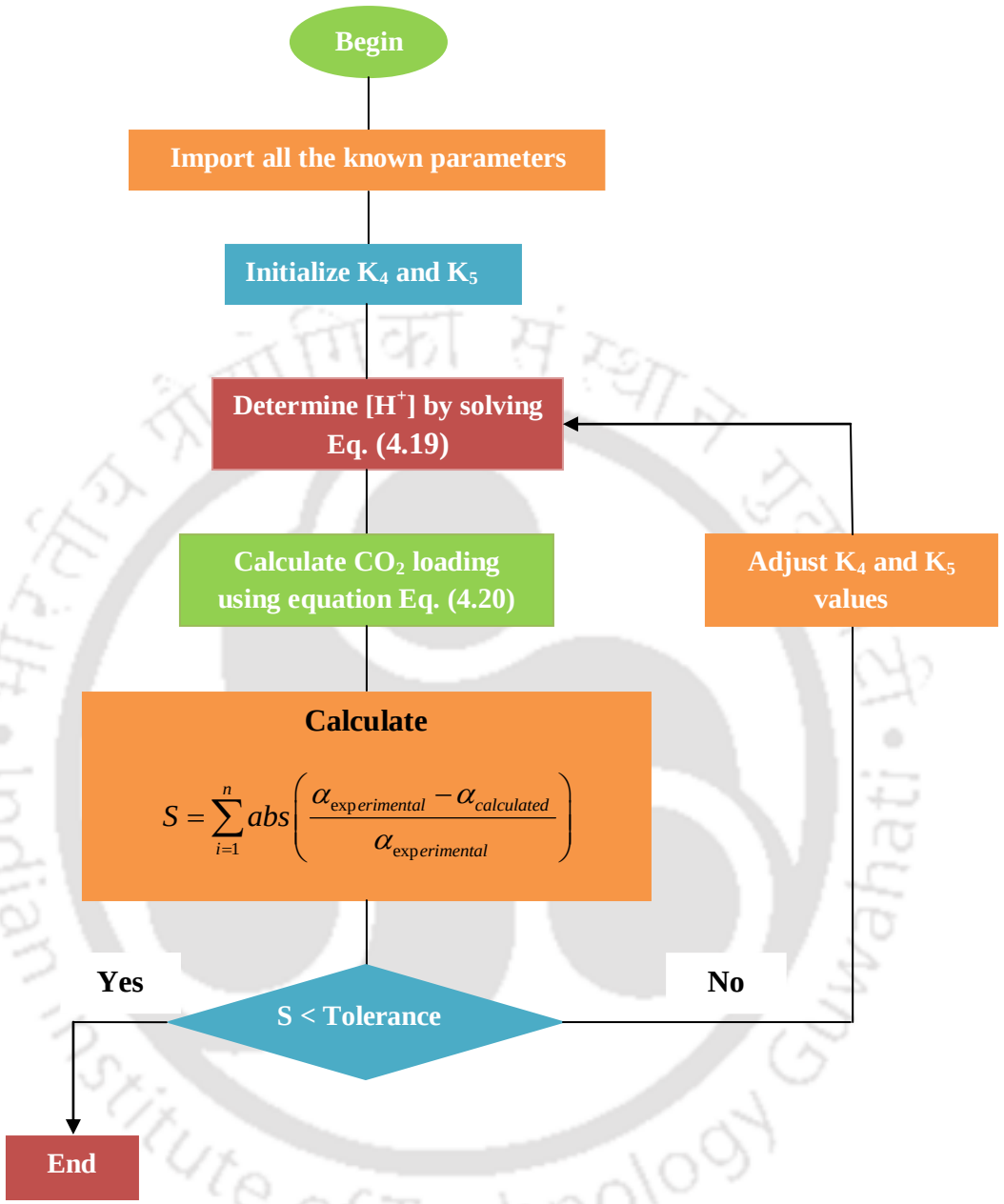

Fig. 4.2 Algorithm for regression of equilibrium constants from experimental data

(AEP + MDEA) and (AEP + AMP) systems. The ANN model can directly relate and develop the linear or nonlinear relationship of the observed experimental data and the variables, which can be considered to overcome the limitations of various theoretical models. Due to its simplicity and better prediction ability, ANN models have already been used in correlating the CO_2 solubility in various solvent systems [23-25].

In this work, a multilayer feed-forward neural network is considered to correlate the solubility data. The performance of the above developed neural network model is tested based on the following parameter as mentioned below:

Mean square error (MSE) = $$\frac{1}{N}\sum_{i=1}^{n}\left(Y_i^{\exp}-Y_i^{\mathrm{mod}}\right)^2 \quad (4.23)$$

Average absolute deviation (AAD) = $$\frac{1}{N}\sum_{i=1}^{N}\frac{\left|Y_i^{\exp}-Y_i^{\mathrm{mod}}\right|}{Y_i^{\exp}} \quad (4.24)$$

Correlation coefficient (R^2) = $$\frac{\sum_{i=1}^{n}\left(Y_i^{\exp}-\bar{Y}\right)^2-\sum_{i=1}^{n}\left(Y_i^{\exp}-Y_i^{\mathrm{mod}}\right)^2}{\sum_{i=1}^{n}\left(Y_i^{\exp}-\bar{Y}\right)^2} \quad (4.25)$$

Where, 'N' represents the number of data points, $Y_i^{\exp}$ and Y_i^{mod} stands for experimental and network predicted value of output variable, respectively and $\bar{Y}$ denotes the average value of the experimental output. The solubility data obtained in the present system are divided into three categories, out of which 70 % is used for training, 15 % is used for validation and 15 % is used for testing the network as suggested in the literature [18, 24-25]. The input parameters used in the network are temperature, equilibrium CO_2 partial pressure and concentration of AEP and MDEA or AMP, respectively. The CO_2 loading (α_{CO_2}) has been chosen as the output variable.

4.4 Results and discussion

4.4.1 Equilibrium solubility of CO_2 in aqueous amine system

The experimental set-up and procedure for solubility measurement have been validated by measuring the equilibrium solubility of CO_2 in aqueous 0.30 mass fractions MDEA at 313.2 K

using the procedure described in the experimental section and compared with the literature data [26-27]. The comparison of data is represented in Fig. 4.3. It can be envisaged from the figure that the measurement of the present work agrees well with the solubility data reported in the literature for aqueous MDEA at same experimental conditions.

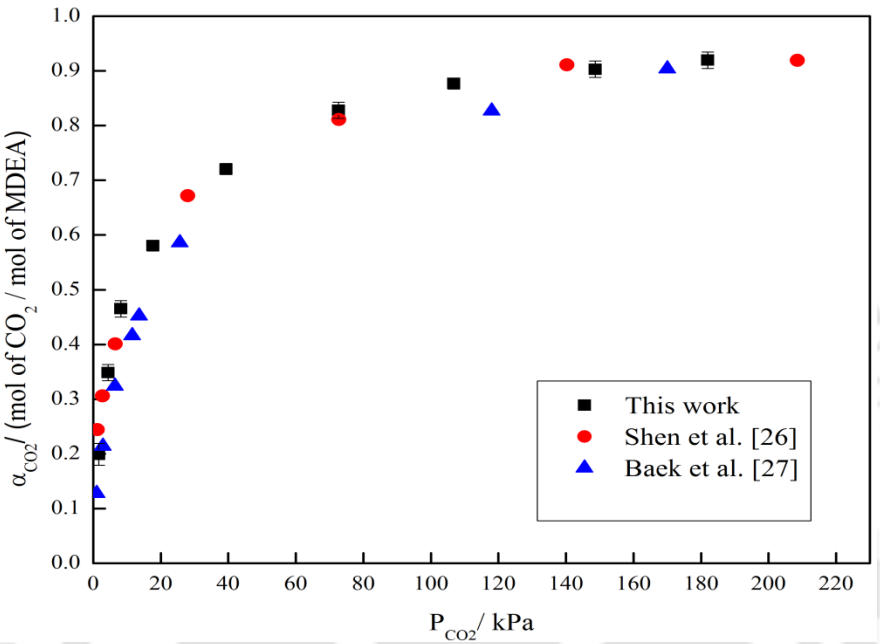

Fig. 4.3 Comparison of solubility data of CO_2 in 0.30 mass fraction aqueous MDEA solution at 313.2 K with literature

The solubility measurement of binary system, have been conducted over AEP concentration of 0.10*w* to 0.40*w* in the aqueous blend. The composition of ternary solution has been taken as (0.05*w*AEP + 0.35*w*MDEA/AMP), (0.10*w*AEP + 0.30*w*MDEA/AMP), (0.15*w*AEP + 0.25*w* MDEA/AMP), (0.20*w*AEP + 0.20*w*MDEA/AMP) and (0.25*w*AEP + 0.15*w*MDEA/AMP). The experimental data related to CO_2 solubility in both binary and ternary aqueous amine systems are represented in Tables 4.3 – 4.19.

4.4.2 Effect of reaction parameters on the equilibrium CO_2 solubility

Various parameters such as CO_2 partial pressure, temperature as well as the concentration of amine play an important role in the solubility of CO_2 in aqueous amine system. It can be

interpreted from the experimental results that at any fixed operating temperature and solvent concentration domain, there is a gradual increase in the α_{CO_2} upon increase in P_{CO_2} till the saturation zone of equilibrium graph (Fig. 4.4). The reason can be attributed to the fact that, an increase in the system pressure results in an increase in kinetic energy of gas molecules which further enhances the rate of diffusion till it attains the maximum limit where further increment of pressure does not lead to any remarkable increase in the CO_2 loading [28]. Also it can be inferred from Figs. 4.4 - 4.6 that since the reaction between aqueous amine solution and CO_2 is considered to be an exothermic reaction [5], the CO_2 loading shows a decreasing trend with an increase in temperature from 303.2 K to 323.2 K at a constant amine concentration and partial pressure of CO_2. Moreover with rise in the AEP concentration from 0.10 to 0.40 mass fractions in the solvent system, CO_2 loading decreases at a constant temperature. The same can be inferred from Fig. 4.7 where the comparison between the various concentration in terms of normalized α_{CO_2} (mol of CO_2 per mol of amine) have been carried out at 323.2 K. Similar trend was also observed by other researcher for different system [14, 18, 29].

Expressing the solubility data in terms of CO_2 partial pressure with the concentration of CO_2 in liquid phase, m_{CO_2} (mol of CO_2 per kg of solvent), is industrially useful. It can be noticed from Fig. 4.8 that with rise in AEP concentration in the aqueous solvent system results in the proportionate increment of absorbed CO_2 in the solvent medium. For a given CO_2 partial pressure, a concentrated amine solution can be an attractive option for industrial gas sweetening operation, thus reducing the need for large solvent handling capacity as well as the size of liquid handling equipment such as pumps and pipelines [30]. The promotion effect of AEP in the aqueous blend can be inferred from the fact that there is a significant rise in the CO_2 loading upon increasing the concentration of AEP in the mixed amine solvent system (Figs. 4.9 - 4.10). Similar observations were also noticed in the earlier AEP based blend (AEP + MEA) system [31].

.

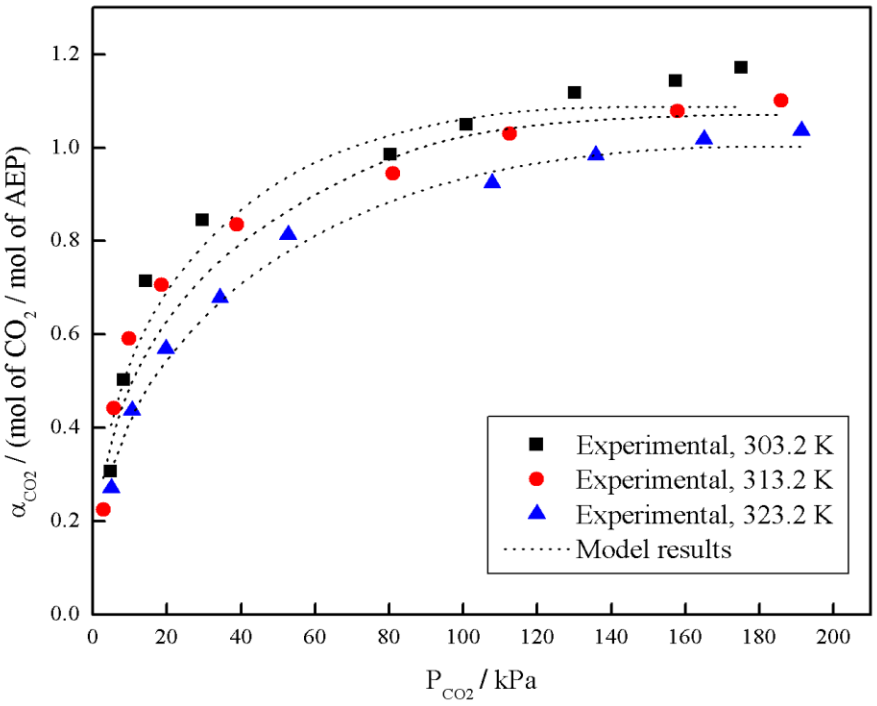

Fig. 4.4 Effect of temperature on the CO_2 solubility in aqueous 0.30*w* AEP

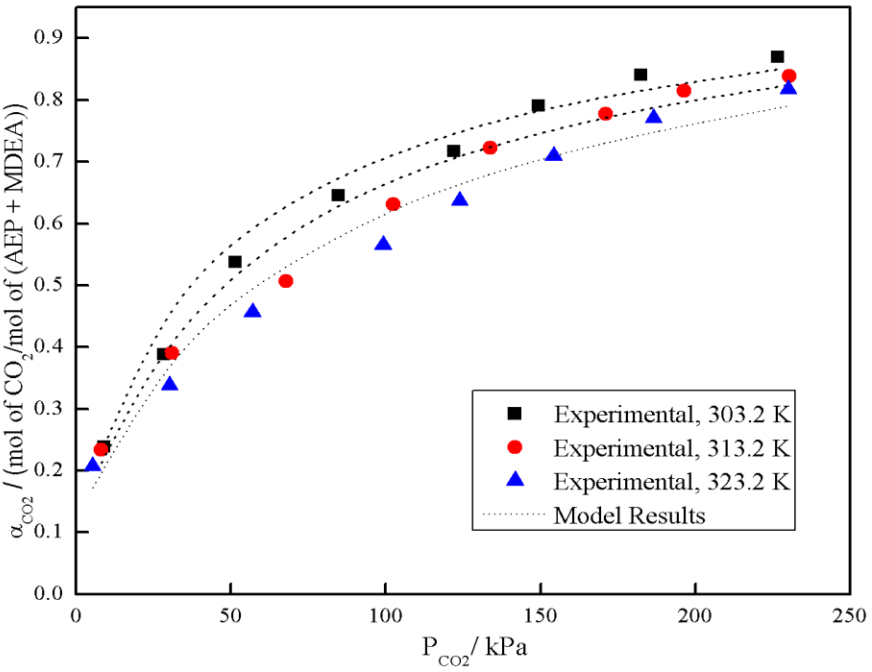

Fig. 4.5 Effect of temperature on the CO_2 solubility in aqueous (0.05*w* AEP + 0.35*w* MDEA)

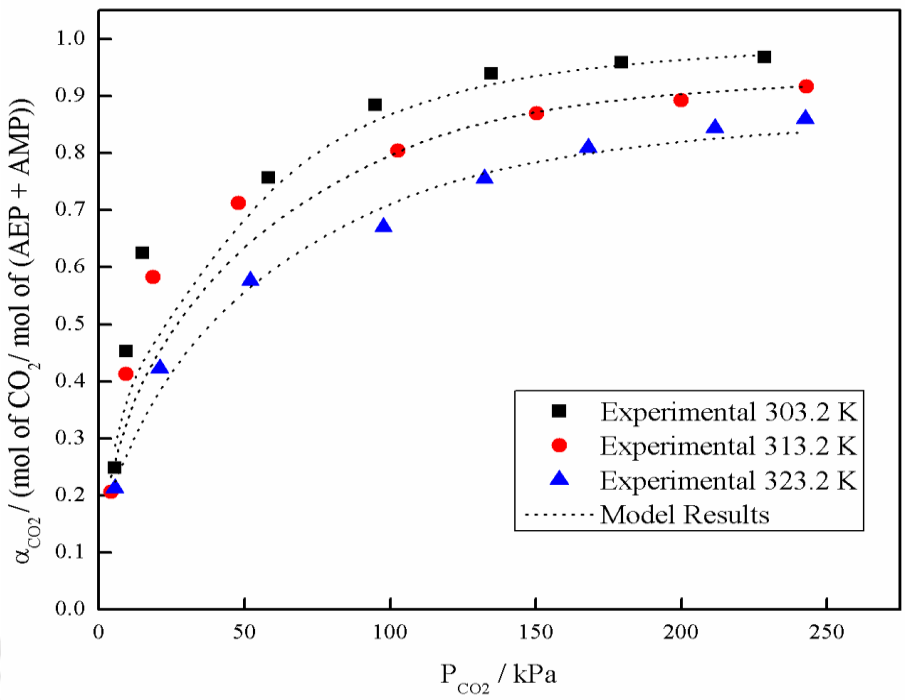

Fig. 4.6 Effect of temperature on the CO_2 solubility in aqueous (0.05*w* AEP + 0.35*w* AMP)

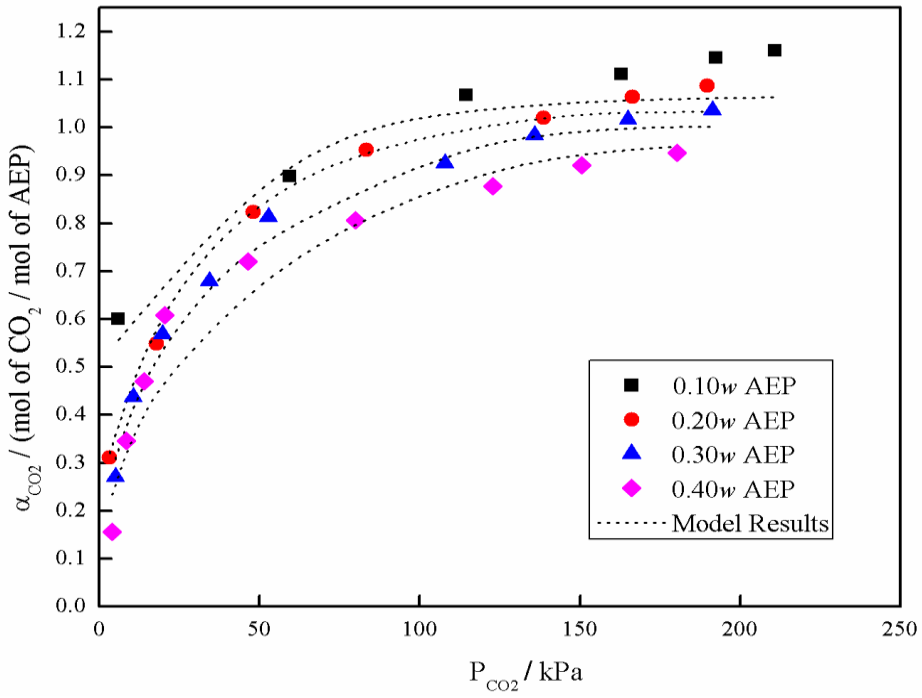

Fig. 4.7 Effect of solvent concentration on the CO_2 solubility in aqueous AEP at 323.2 K.

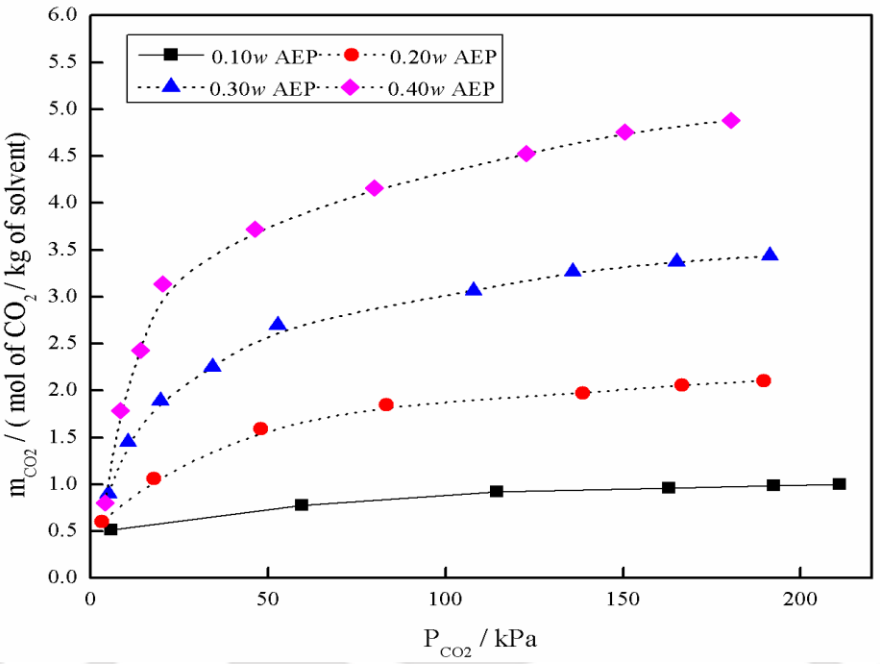

Fig. 4.8 Equilibrium molality based solubility of CO_2 in aqueous AEP of different concentration at 323.2 K

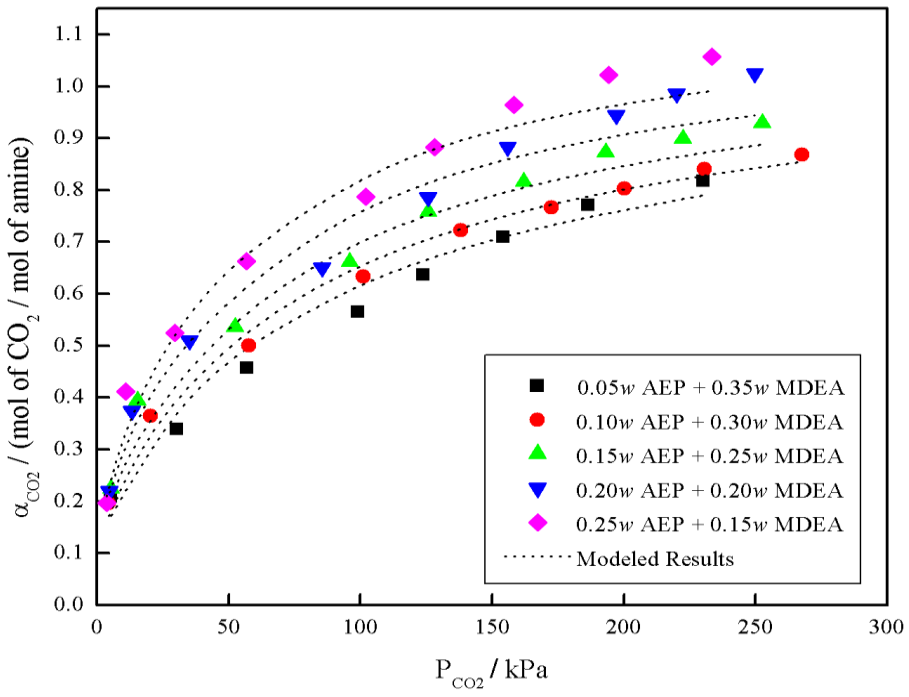

Fig. 4.9 CO_2 solubility in aqueous blend of (AEP + MDEA) having different composition (mass fraction) at temperature T = 323.2 K

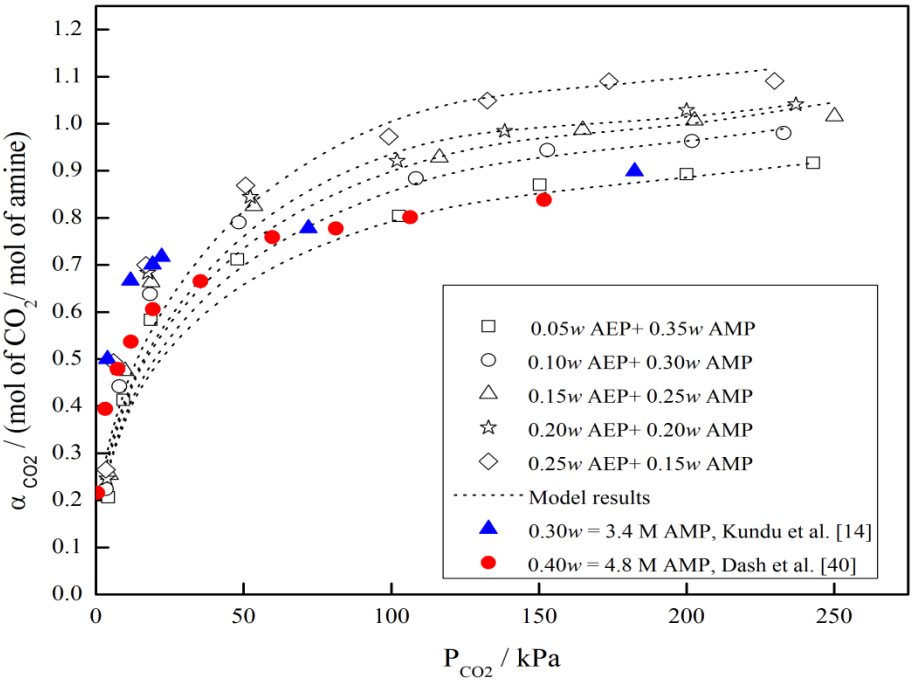

Fig. 4.10 Effect of solvent concentration on the CO_2 solubility in aqueous (AEP + AMP) solvent blend at 313.2 K

4.4.3 Correlation of equilibrium CO_2 solubility

As discussed in the previous section, the experimental solubility data generated in this work has been further used in the modified KE model to regress the equilibrium constant (K_4, K_5) for the binary system of (AEP + H_2O), (K_4', K_5') for (AEP + MDEA + H_2O) and (K_4'', K_5'') for (AEP + AMP + H_2O) system, respectively. In order to decrease the error margin between the caculated and experimental results, a non-linear optimization framework is applied in the present work which uses an objective function as described below:

$$S = \frac{1}{N}\sum_{i=1}^{N}\left|\frac{\alpha_i^{\exp} - \alpha_i^{cal}}{\alpha_i^{\exp}}\right| \qquad (4.26)$$

In the above equation, α_i^{exp} and α_i^{cal} stands for experimental and calculated value of α_{CO_2} respectively and N represents the total number of data sets used in the developed model. The reaction equilibrium constants (K_4 and K_5) can be estimated utilizing equation (4.19) and (4.20) employing the algorithm shown in Fig. 4.2.

$$K_4 = 1.632\times10^{-7} - 1.411\times10^{-9}(m_1) - 1.056\times10^{-9}(T) + 5.187\times10^{-12}(m_1\times T) + 1.714\times10^{-12}(T^2) - 1.809\times10^{-11}(P_{CO_2}) - 5.223\times10^{-14}(P_{CO_2}^2) \quad (4.27)$$

$$K_5 = -5.990\times10^{-2} + 1.892\times10^{-6}(m_1) + 2.587\times10^{-2}(T) - 2.431\times10^{-1}(m_1^{\,2}) - 8.752\times10^{-2}(m_1\times T) - 4.766\times10^{-2}(T^2) - 7.910\times10^{-4}(P_{CO_2}) - 9.672\times10^{-6}(P_{CO_2}^2) \quad (4.28)$$

$$K_4' = -1.5570\times10^{-9} - 8.7982\times10^{-9}(m) + 2.8495\times10^{-11}(T) + 2.6409\times10^{-11}(m\times T) + 5.2805\times10^{-14}(T^2) - 1.8379\times10^{-14}(P_{CO_2}) - 7.4253\times10^{-17}(P_{CO_2}^2) \quad (4.29)$$

$$K_5' = 2.7754\times10^{1} + 2.4126\times10^{-3}(m) - 7.3712\times10^{-2}(T) - 2.2115\times10^{-2}(m^2) + 5.0266\times10^{-3}(m\times T) - 1.0412\times10^{-4}(T^2) - 3.6454\times10^{-5}(P_{CO_2}) - 2.9108\times10^{-7}(P_{CO_2}^2) \quad (4.30)$$

$$K_4'' = 1.2476\times10^{-8} - 3.7795\times10^{-10}(m_1\times m_2) - 7.9590\times10^{-11}(T) + 1.6061\times10^{-12}(m_1\times m_2\times T) + 1.2578\times10^{-13}(T^2) + 5.8432\times10^{-13}(P_{CO_2}) + 1.9001\times10^{-15}(P_{CO_2}^2) \quad (4.31)$$

$$K_5'' = 7.5261\times10^{-2} + 3.4054\times10^{-2}(m_1\times m_2) + 2.8074\times10^{-3}(T) - 4.4914\times10^{-2}(m_1^{\,2}\times m_2^{\,2}) - 5.6421\times10^{-3}(m_1\times m_2\times T) + 1.1742\times10^{-5}(T^2) - 1.5775\times10^{-2}(P_{CO_2}) - 3.2860\times10^{-5}(P_{CO_2}^2) \quad (4.32)$$

The equilibrium constants estimated from equations. (4.26 - 4.31) can be used to estimate α_{CO_2} over the complete experimental range. The average absolute deviation, % AAD between the experimental and model calculated data has been found to be 9.05 % for (AEP + H_2O), 5.94 % for (AEP + MDEA + H_2O) and 9.51 % for (AEP + AMP + H_2O) considering all data sets.

The applicability of the ANN modeling has been also tested to predict the solubility data. The optimized architecture of the ANN model can be obtained by varying the number of neurons. While large error in the network can be the results of incorporating low number of neurons, a large number may lead to over-fitting of the output data [18]. The optimum performance of the network can be considered based on some of the statistical parameter such as, a lower value of

% AAD and MSE. Fig. 4.11 represents the results of variation in the number of neurons on the MSE value of the network output for aqueous AEP system. The optimized neuron for the developed model is 7, which can be also concluded from the lower value of MSE. In addition to this, the best ANN architecture developed in the present work for aqueous AEP system is presented in Fig. 4.12.Using the above developed ANN model, CO_2 loading for all the composition and temperature ranges have been calculated and the % (AAD) between the experimental and estimated data for both the binary and ternary solvent systems of aqueous AEP and aqueous (AEP + AMP) are determined to be 0.16 and 0.09, respectively, while aqueous (AEP + MDEA) shows a relatively lower AAD of 0.08.

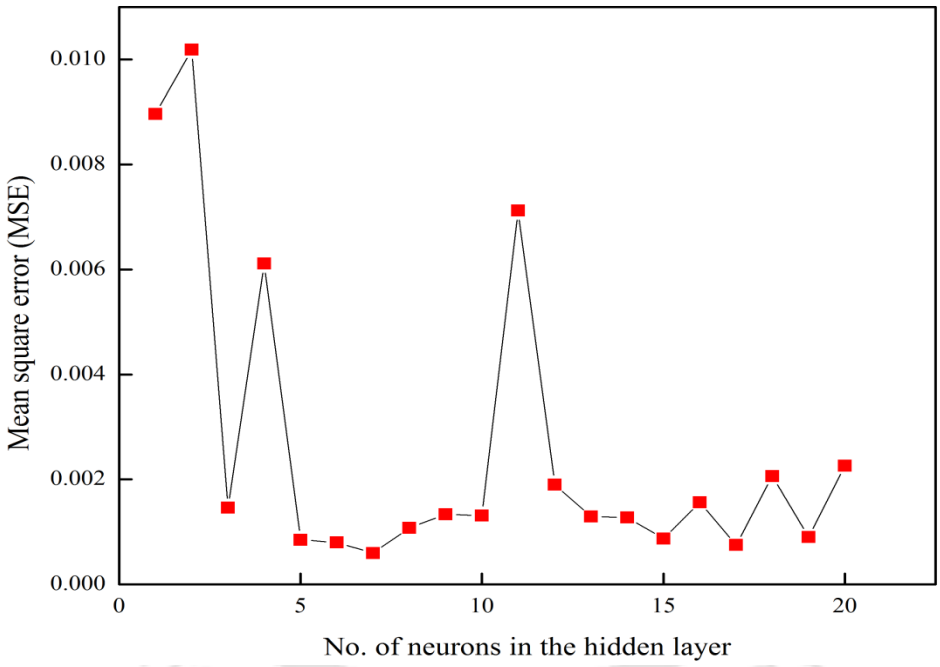

Fig. 4.11 Variation of MSE (Mean square error) with number of neurons in the hidden layer for ANN model for (AEP + H_2O) system

The comparison of both the models developed in the present study for correlating the equilibrium CO_2 solubility data of mixed amine system of (AEP + AMP) have been also assessed against each data point and represented in the form of Cross plot in Fig. 4.13. From the figure it can be clearly observed that the correlated solubility data obtained from both the models matches well

with the experimental data. Also, the prediction capability of ANN model outperforms the modified KE model.

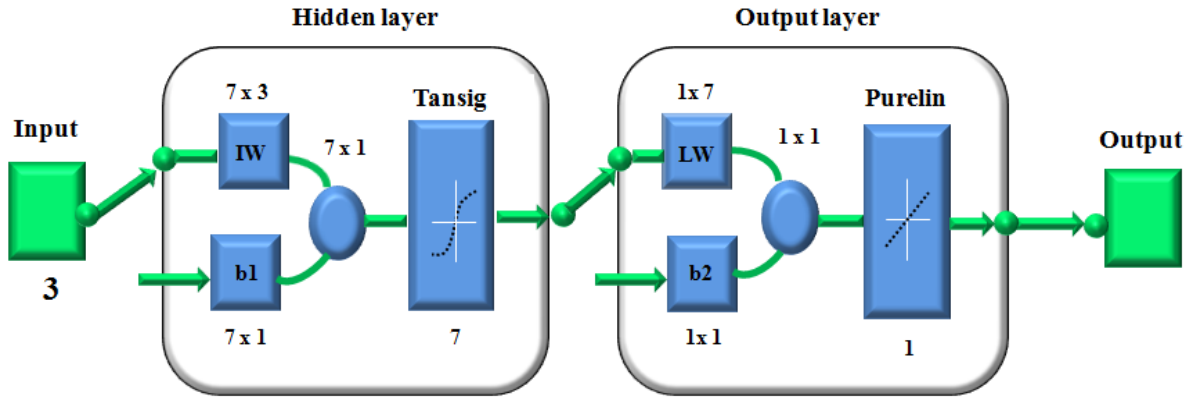

Fig. 4.12 Optimized architecture of the developed ANN model for estimating equilibrium solubility of CO_2 in (AEP + H_2O) system

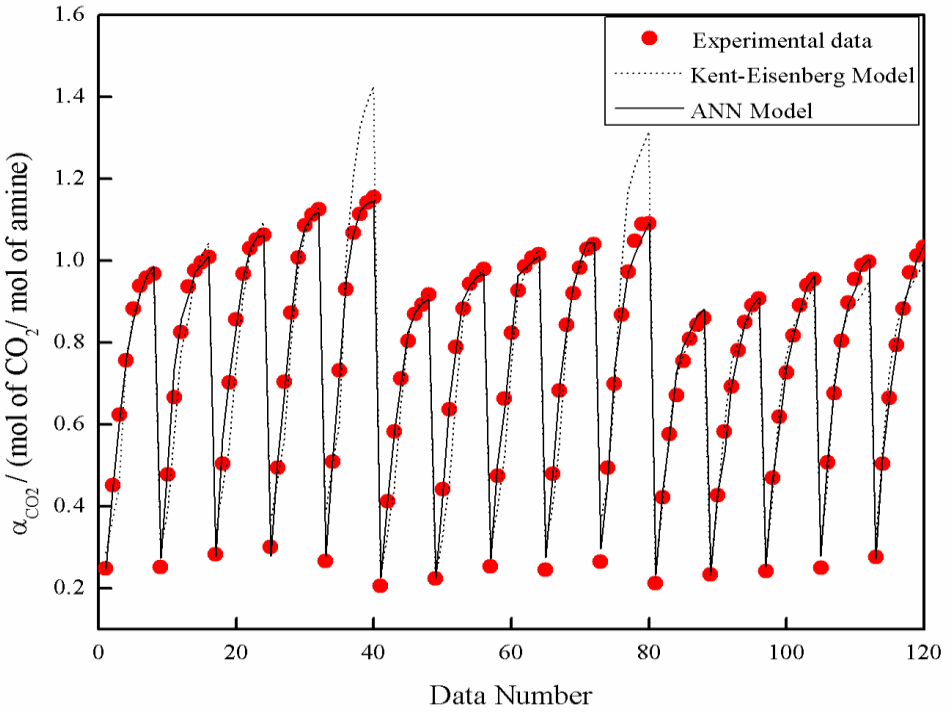

Fig. 4.13 Cross plot for the comparison of experimental solubility data with model data. (AEP + AMP+ H_2O solvent)

4.4.4 Liquid phase speciation profile, pH, solvent capacity

The application of the modified KE model developed in this study can be further extended in estimating the concentrations of various ionic species at equilibrium conditions in the solvent phase. The distribution of various reaction species resulting from CO_2 – (AEP + H_2O) reaction with the variation of α_{CO_2} has been presented in Fig. 4.14. It is inferred from the concentration profiles that rise in CO_2 loading results in the gradual disappearance of AEP molecules in the solvent phase and $AEPH^+$ and HCO_3^- are the major reaction products. The presence of $AEPCOO^-$ also shows a decreasing trend at α_{CO_2} > 0.6 indicating its hydrolysis to form more bicarbonate type species. Fig. 4.15 shows the liquid phase speciation profile of CO_2 with mixed amine solvent system. The general trend of the majority of species with respect to the change in α_{CO_2} is the same. The only major difference is the presence of protonated species $AMPH^+$ at higher loadings.

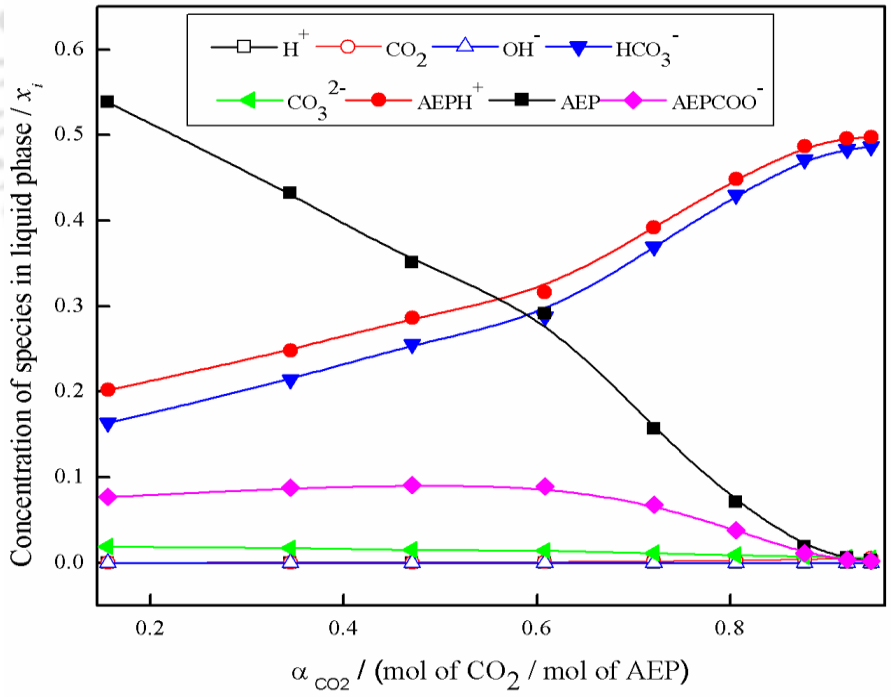

Fig. 4.14 Model (modified KE) estimated speciation profile of aqueous 0.40 w AEP at 323.2 K

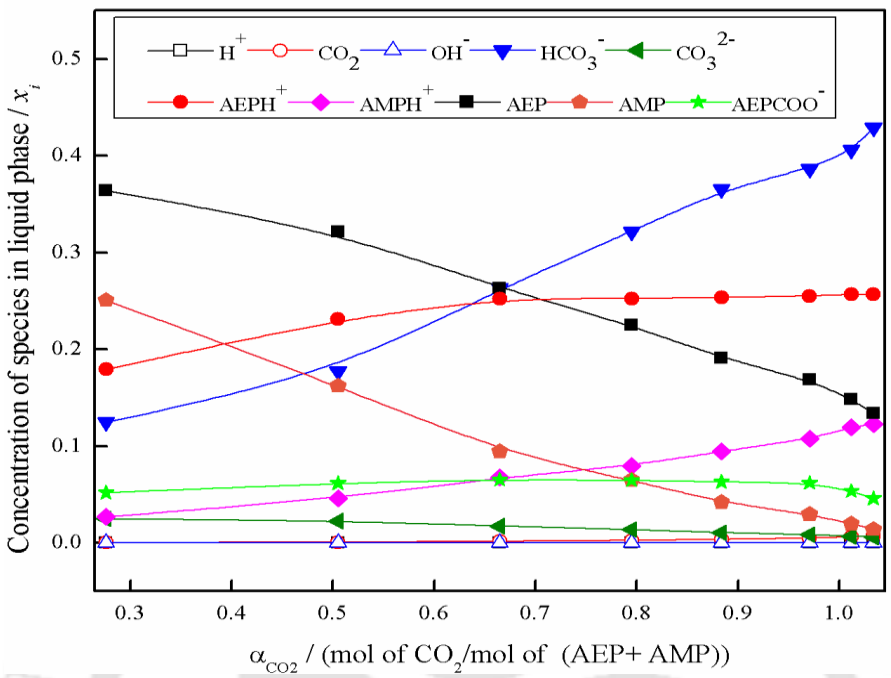

Fig. 4.15 Model (modified KE) estimated speciation profile of aqueous (0.25w AEP + 0.15w AMP) solvent blend at 323.2 K

The KE model can also be used to predict the pH of the CO_2 loaded amine solvents. Appropriate knowledge of pH value of the loaded solvent is very important from the point of view of the design of CO_2 capture processes. According to the literature reported data for other solvent systems, the pH range with respect to the change in α_{CO_2} is between 7 and 12 [21]. The plot corresponding to the modified KE model estimated pH of CO_2 loaded aqueous (0.05 AEP + 0.35 AMP) against the operating experimental temperature is shown in Fig. 4.16. It can be interpreted that for a particular fixed concentration of amine solvent, there is a gradual reduction in the pH with rise in the system temperature and CO_2 loading. This can be explained from the fact that upon increasing the α_{CO_2}, more amount of acidic CO_2 moves into the solution and hence the pH of the solvent system decreases. Also, rise in temperature results in higher ionization which leads to a rise in H^+ ion concentration [21].

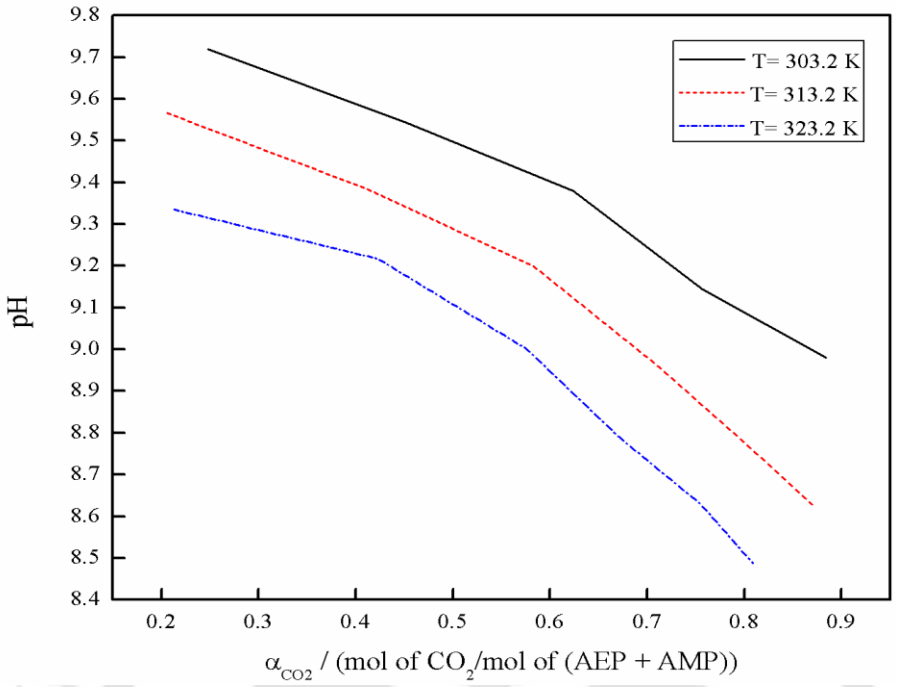

Fig. 4.16 Estimation of pH as a function of CO_2 loading in aqueous (0.05w AEP + 0.35w AMP) using modified KE Model

In addition to this, solubility data can be further analyzed to determine the solvent capacity in present reaction system. The capacity of the solvent, (mol of CO_2 / kg of solvent) over a given partial pressure range is calculated using equation (4.33) expressed as:

$$\text{Capacity (mole of } CO_2 \text{ / kg solvent)} = \left(\alpha_{PCO2,rich} - \alpha_{PCO2,lean}\right) \times [AEP] \quad (4.33)$$

Where, $\alpha_{P_{CO_2},rich}$ and $\alpha_{P_{CO_2},lean}$ can be calculated corresponding to particular $P_{CO_2,rich}$ and $P_{CO_2,lean}$ from the measured solubility data and $[AEP]$ represents the concentration in molal scale. At a particular P_{CO_2} of 5 kPa and 313.2 K, the effect of CO_2 rich loading and aqueous AEP concentration on the solvent capacity has been presented in Fig. 4.17. The solvent capacity enhances significantly with rise in amine concentration from (0.10 to 0.40) mass fraction. It is also concluded that the CO_2 capacity increases with the increase in $P_{CO_2,rich}$ from 30 to 50 kPa.

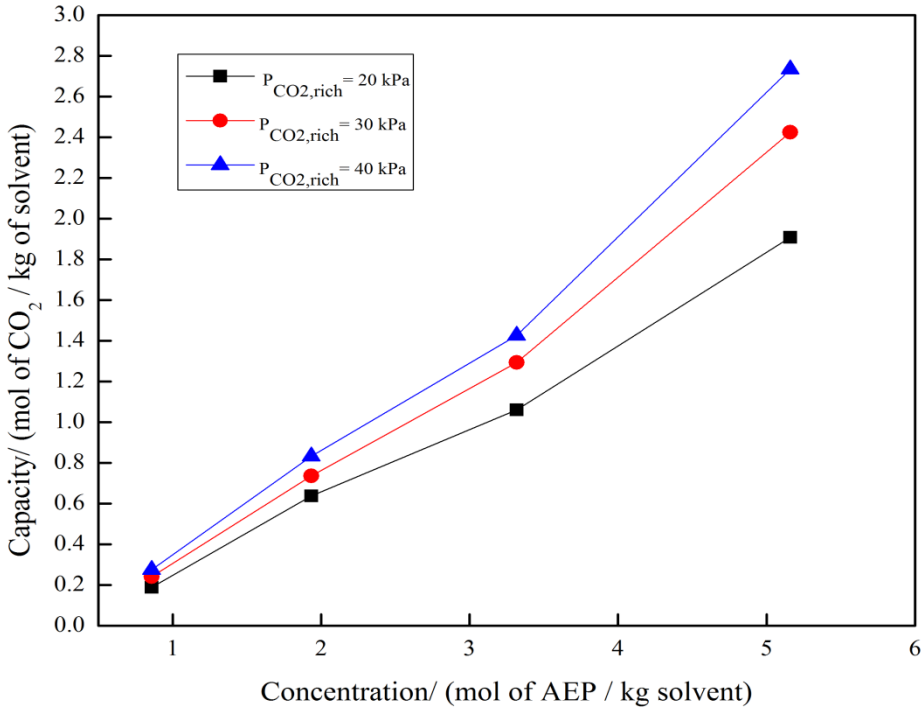

Fig. 4.17 CO_2 cyclic capacity of aqueous AEP system at 313.2 K with P_{CO2}, lean = 5kPa

4.4.5 FTIR-ATR and NMR study

The unloaded and carbonated single and blended amine system are further characterized using FTIR-ATR spectroscopy (Model: Perkin Elmer Inc., Germany). The measurements were conducted within the wavenumber 2000 to 800 cm^{-1}. The spectra of both the single and blended amine systems prior to CO_2 absorption are shown in Fig. 4.18. Both the system shows characteristic peaks at 1645 cm^{-1} and 1600 cm^{-1} which corresponds to (N-H) rocking vibration modes [32-33] . The peaks corresponding to 1324 and 1463 cm^{-1} relates to $–CH_2$ symmetric and asymmetric rocking mode. In addition, the characteristic peaks at 1140, 1065 and 1050 cm^{-1} relate to C-N and C-O stretching vibration modes for aqueous AEP solvent system, while the former peaks are merged at 1045 cm^{-1} for the blended system [32]. Also, $C-NH_2$ twisting mode is predominant at 914 cm^{-1} for (AEP + AMP) system.

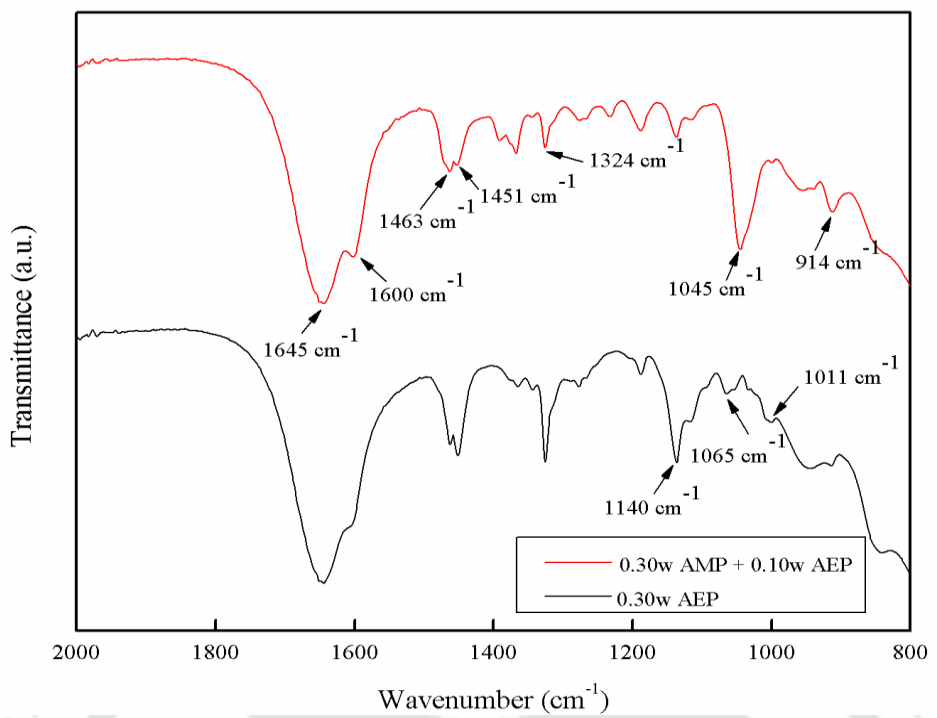

Fig. 4.18 FTIR-ATR spectra of unloaded amine solvent

Fig. 4.19 represents the spectra of amine solvents with CO_2 loading of 0.8. Upon CO_2 absorption, new bands appeared at 1322, 1476 and 1566 cm^{-1} and the same can be assigned to (COO^-) carbamate symmetric and asymmetric stretching [33]. It can be quite apparent from the spectra that there is a gradual shift in the peaks corresponding to stretching modes of C-N and C-OH group from 1065 to 1056 cm^{-1} and 1011 to 1002 cm^{-1} and the same can be anticipated to be the result of protonation of AEP species. The bands corresponding to 1297 cm^{-1} and 1268 cm^{-1} assigned to N-C stretching vibration of the AEP-carbamate. Similarly, the band at 1432 cm^{-1} assigned to the transformation of mono-carbamate to the di-carbamate. The C-O stretching mode which is quite prominent at 1356 cm^{-1} in the loaded (AEP + AMP) blended aqueous solvent system assigned to the formation of bicarbonate species.

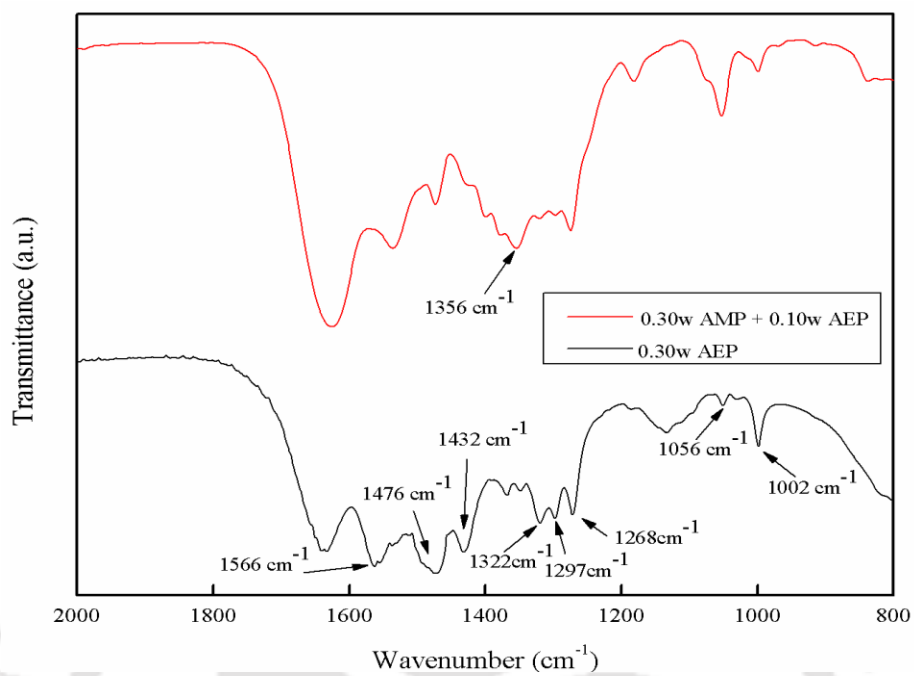

Fig. 4.19 FTIR-ATR spectra of CO_2 loaded amine solvent at $\alpha_{CO_2} = 0.8$

In addition to IR study, qualitative ^{13}C NMR analysis was also performed to establish the proper reaction mechanism in the present study. The NMR measurement was carried out for CO_2 loaded aqueous single and blended amine solvent in D_2O using a 500 MHz NMR spectrometer (Model: Ascend, Bruker). The information related to the observed peaks corresponding to the respective functional groups of the molecules was assigned by using information derived from different literature sources [34-35]. The number of peaks in the ^{13}C NMR spectra of AEP-H_2O-CO_2 (Fig. 4.20 (a)) confirmed the formation of primary and secondary carbamates. The peaks which appeared in the low field region (160-165 ppm) mostly correspond to the peaks of carbonyl carbon of carbamate and HCO^{3-}/CO_3^{2-} species. However, the carbons of amine in the high field region (35-58 ppm) relate to the CH_2 group of various intermediate carbamate species. While from the NMR spectra of blended system (Fig. 4.20 (b)), it can be observed that the carbon peak for bicarbonate ion at 160.66 pm is quite prominent compared to the single amine system, which confirmed the hydrolysis of unstable carbamate of AMP to form bicarbonate as the major reaction product.

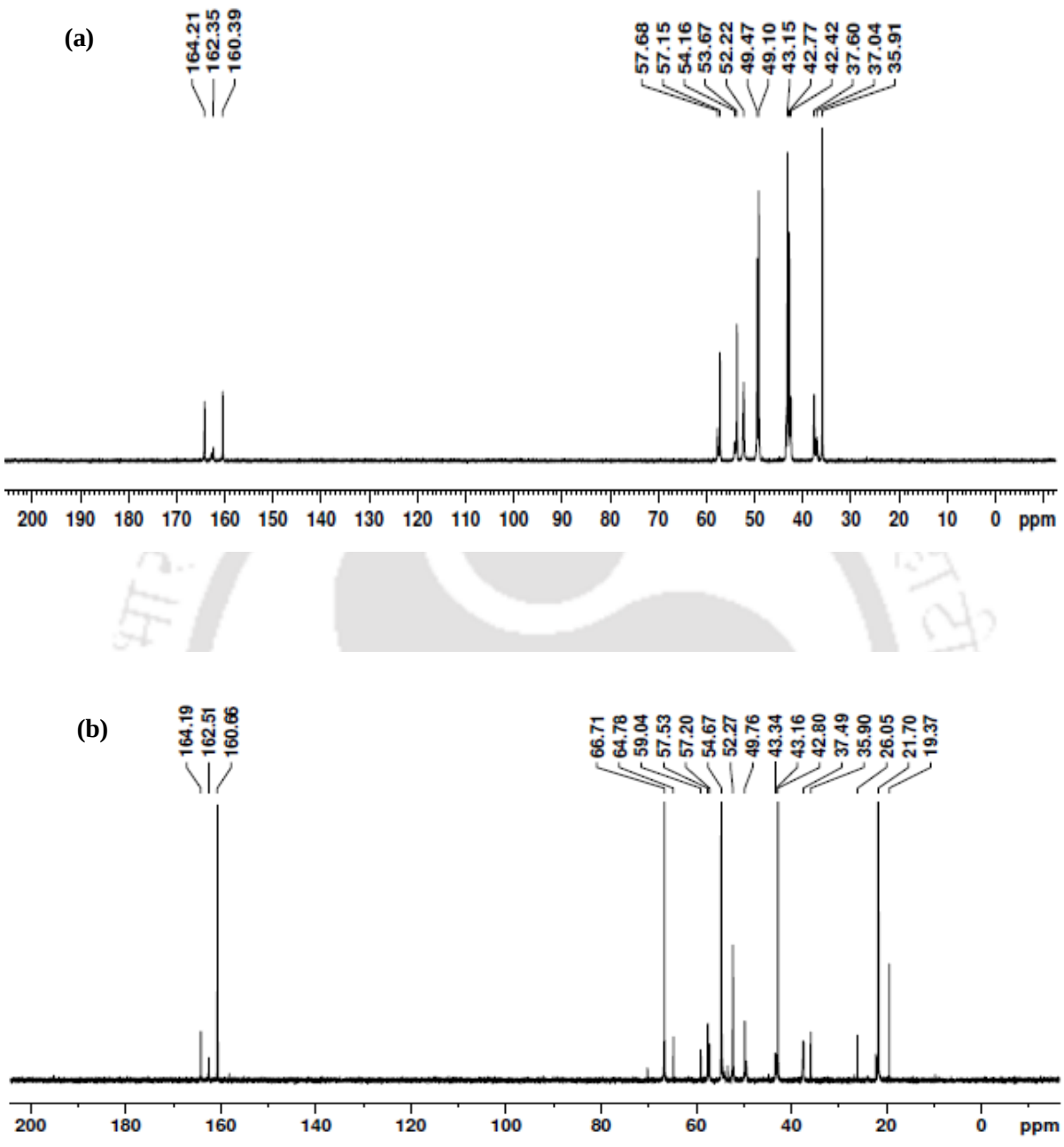

Fig. 4.20 ^{13}C NMR spectra of CO_2 loaded aqueous (a) 0.30 *w* AEP solution (b) (0.30 *w* AMP + 0.10 *w* AEP) solution ($\alpha_{CO_2} = 0.8$)

4.4.6 Comparison of solubility with other conventional single and blended amines

Experimental data corresponding to CO_2 solubility in $0.30w \approx 2.4$ kmol.m^{-3} (AEP + H_2O) system obtained in the present work has been also compared at 313.2 K with the results obtained by Choi et al. [8]. The solubility results obtained in this work matches well with the available literature data. Also generated data corresponding to the present amine systems are also compared with the solubility data of CO_2 in approximate equimolar concentration of conventional solvents such as aqueous MEA, DEA, MDEA, AMP and PZ solution available in the literature [4, 14, 36-38] and represented in Fig. 4.21. At low CO_2 pressure, the CO_2 loading in all these aqueous amines are somewhat comparable with AEP. However at higher pressure range, the CO_2 loading in the aqueous amine solution follows the trend AEP > AMP > MDEA > DEA ≈ MEA. Similar trend can be also observed upon comparison with 3.2 M PZ solution, which clearly indicates the enhancement of absorption capacity with the substitution of amino group in the saturated diamine (PZ).

For aqueous blended amine system, first the equilibrium solubility data corresponding to the entire experimental range for aqueous (AEP + AMP) blend are compared with the different composition of aqueous AMP solution [14, 38] in Fig. 4.10. It can be clearly inferred from the P_{CO_2} *vs* α_{CO_2} plot that the solubility of CO_2 in $0.40w \approx 4.8$ M aqueous AMP is relatively comparable with the solvent blend having lower concentration of AEP, on the other hand the performance of the blend enhances significantly with the increase of AEP concentration from 0.05w to 0.25w. Along with this, the efficiency of the mixed amine blend has been also compared with conventional AMP based solvent blend such as (MEA + AMP) and (PZ + AMP) used extensively for CO_2 capture application. Due to the lack of available literature data on the concentrated mixed amine solvents, the CO_2 solubility data in ($0.05w$ AEP + $0.25w$ AMP) has been generated at 313.2 K and compared with the other solvent blends at the same temperature in Fig. 4.22. The anticipated results clearly confirms that compared to conventional solvent blends viz. ($0.06w$ MEA + $0.24w$ AMP) as well as ($0.12w$ MEA + $0.18w$ AMP) [39], the solubility of CO_2 in ($0.05w$ AEP + $0.25w$ AMP) is quite higher throughout the experimental pressure range.

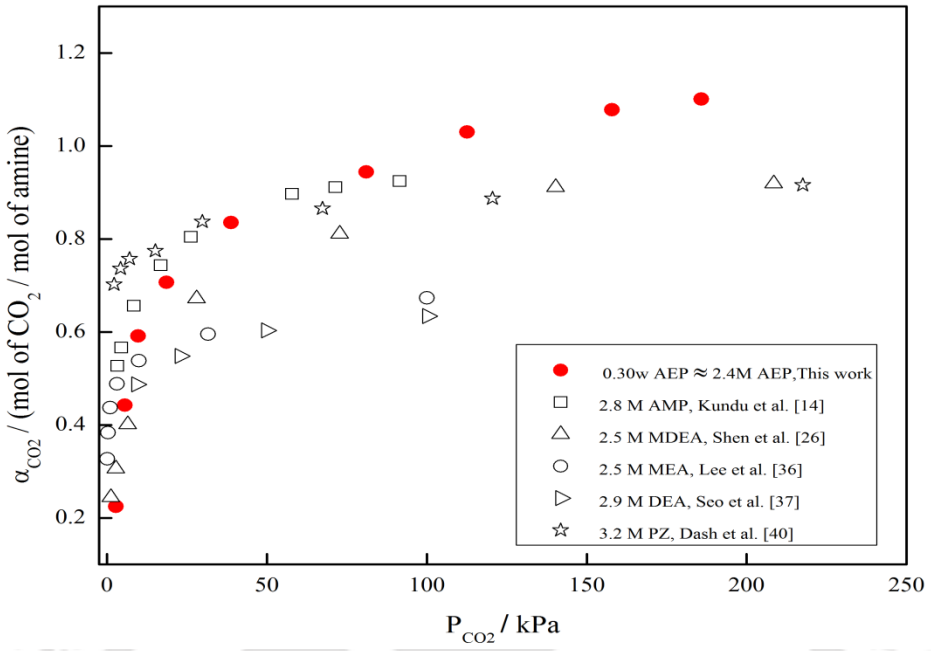

Fig. 4.21 Comparison of equilibrium CO_2 loading data of aqueous 0.30 *w* = 2.4M AEP with that of conventional aqueous amine solution at 313.2 K

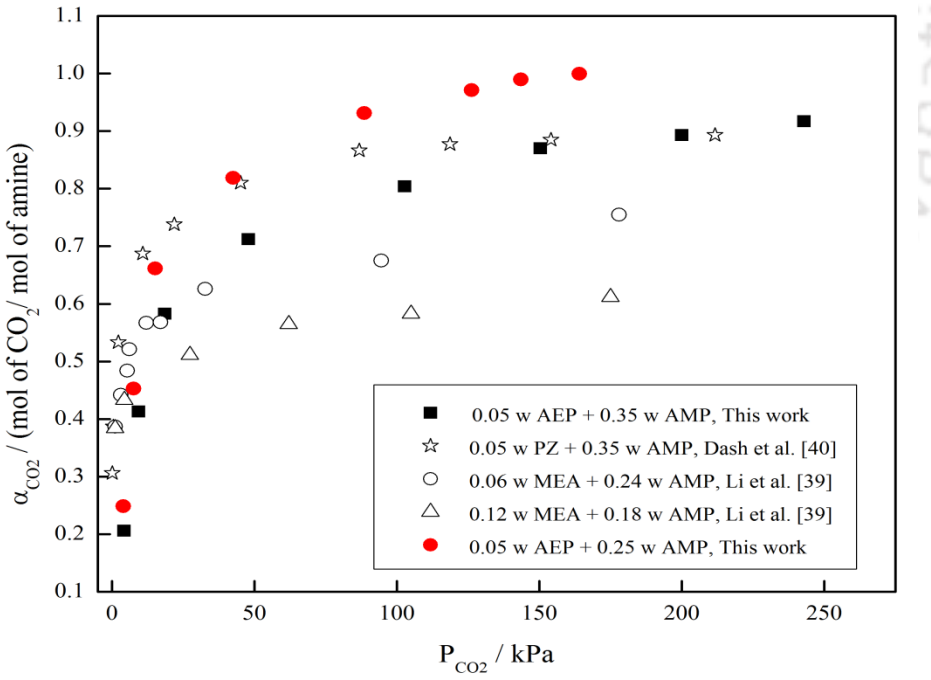

Fig. 4.22 Comparison of equilibrium solubility of (AEP + AMP) with conventional AMP based blends at 313.2 K

On the other hand, CO_2 solubility in concentrated mixed system (0.40 *w*) obtained in the present study is comparable at higher pressure and loading with the benchmarked system (0.05*w* PZ + 0.35*w* AMP) [3]. The enhancement of the solubility can be the result of steric hindrance effect of AMP molecule in addition to the substitution of amine group in the saturated cyclic diamine ring of PZ. This further facilitate the generation of free amine species and bicarbonate ions due to the gradual hydrolysis of unstable intermediate carbamates.

4.5. Conclusions

The study investigated the equilibrium CO_2 solubility in aqueous AEP as well as aqueous blends of (AEP + MDEA) and (AEP + AMP) system over the broad domain of operating pressure and temperature range. The experimental results were successfully correlated with the modified KE model and ANN model. The equilibrium constants corresponding to amine deprotonation and carbamate hydrolysis reaction were calculated in terms of temperature, amine concentration and CO_2 partial pressure from modified KE model. The estimated modeling results indicates that compared to modified KE model, ANN model gives better prediction for CO_2 solubility data. The modified KE model developed for the present system has been also used to predict pH and speciation profile of the intermediate species as well as solvent capacity. IR and ^{13}C NMR analysis further confirms the prevalence of bicarbonate species in the reaction products of blended solvent system. Moreover, it is also quite apparent from the comparative study that at higher CO_2 partial pressure, the CO_2 loading in the understudy solvent system is greater than the CO_2 loading in other conventional aqueous amines used in CO_2 capture processes. Both the solvent blends show similar equilibrium behavior. However since AMP showcases higher reaction rate compared to MDEA, hence it can be anticipated that AMP based system should have higher kinetic selectivity compared to MDEA system. Moreover further analyses in terms of heat of absorption study, amine degradation study, and cyclic capacity are required prior to implementing it in Industrial PCC applications. All these evaluated properties can be helpful in designing CO_2 separation processes using AEP based solvent and its subsequent utilization.

Table 4.1 Provenance and purity of Reagents

Alias	Chemical	Source	Purity (Mass fraction)	Method of Purification
CO_2	Carbondioxide gas	Linde India Ltd.	>99 %	None
AEP	1-(2-aminoethyl) piperazine 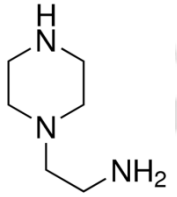	Sigma Aldrich Co.	99 %	None
MDEA	N-Methyldiethanolamine 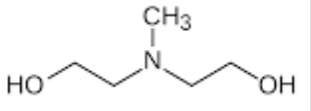	Sigma Aldrich Co.	95 %	None
AMP	2-Amino-2-methyl-1-Propanol 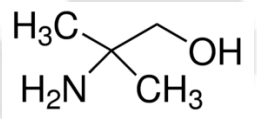	Sigma Aldrich Co.	95 %	None

Table 4.2 Parameters corresponding to equilibrium constant and Henrys constant used in the KE model

$K_1 = \exp\left(220.067 - \frac{12431.7}{T} - 35.482 \ln T\right)$ (kmol.m^{-3})	[3]
$K_2 = \exp\left(235.485 - \frac{12092.1}{T} - 36.782 \ln T\right)$ (kmol.m^{-3})	[3]
$K_3 = \exp\left(140.932 - \frac{13445.9}{T} - 22.477 \ln T\right)$ (kmol.m^{-3})	[3]
$K_6 = \exp\left(87.397 - \frac{8483.95}{T} - 13.832 \ln T\right)$ (kmol.m^{-3})	[12]
$H_{CO2} = \exp\left(20.2669 - \frac{1.38306 \times 10^4}{T} + \frac{0.06913 \times 10^8}{T^2} - \frac{0.015589 \times 10^{11}}{T^3} + \frac{0.012 \times 10^{13}}{T^4}\right)$ (kPa.m^3.kmol^{-1})	[19]

Table 4.3 Solubility data of CO_2 in aqueous 0.10 *w* AEP solution at equilibrium state

T/K	Mass Fraction (AEP)	Mass Fraction (H_2O)	P_{CO_2} / *kPa*	α_{CO_2}
	0.1	0.9	6.688	0.709
	0.1	0.9	50.339	1.029
	0.1	0.9	129.187	1.167
	0.1	0.9	173.162	1.249
303.2	0.1	0.9	205.319	1.322
	0.1	0.9	1.703	0.419
	0.1	0.9	8.391	0.755
	0.1	0.9	59.977	0.984
	0.1	0.9	110.985	1.099
	0.1	0.9	154.96	1.161
	0.1	0.9	183.352	1.201
313.2	0.1	0.9	208.153	1.229
	0.1	0.9	5.861	0.6
	0.1	0.9	59.564	0.898
	0.1	0.9	114.57	1.067
	0.1	0.9	162.902	1.111
	0.1	0.9	192.467	1.145
323.2	0.1	0.9	211	1.16

Table 4.4 Solubility data of CO_2 in aqueous 0.15 *w* AEP solution at equilibrium state

T/K	Mass Fraction (AEP)	Mass Fraction (H_2O)	P_{CO_2} / *kPa*	α_{CO_2}
	0.15	0.85	5.343	0.51
	0.15	0.85	10.59	0.795
	0.15	0.85	28.165	1.016
	0.15	0.85	75.036	1.182
	0.15	0.85	118.714	1.273
303.2	0.15	0.85	161.544	1.293
	0.15	0.85	2.551	0.404
	0.15	0.85	6.55	0.731
	0.15	0.85	36.404	0.883
	0.15	0.85	77.842	1.045
	0.15	0.85	124.864	1.13
	0.15	0.85	160.51	1.162
313.2	0.15	0.85	192.915	1.185
	0.15	0.85	5.212	0.382
	0.15	0.85	28.551	0.672
	0.15	0.85	52.442	0.873
	0.15	0.85	99.119	0.994
	0.15	0.85	125.947	1.072
	0.15	0.85	161.144	1.122
323.2	0.15	0.85	193.343	1.147

Table 4.5 Solubility data of CO_2 in aqueous 0.20 *w* AEP solution at equilibrium state

T/K	Mass Fraction (AEP)	Mass Fraction (H_2O)	P_{CO_2} / *kPa*	α_{CO_2}
	0.2	0.8	4.033	0.286
	0.2	0.8	7.612	0.558
	0.2	0.8	17.416	0.785
	0.2	0.8	63.259	0.983
	0.2	0.8	111.599	1.093
	0.2	0.8	140.577	1.151
	0.2	0.8	156.87	1.197
303.2	0.2	0.8	183.987	1.221
	0.2	0.8	2.765	0.274
	0.2	0.8	5.523	0.505
	0.2	0.8	12.617	0.731
	0.2	0.8	35.115	0.877
	0.2	0.8	60.439	0.971
	0.2	0.8	102.877	1.041
	0.2	0.8	138.674	1.091
	0.2	0.8	162.247	1.133
313.2	0.2	0.8	185.965	1.153
	0.2	0.8	3.178	0.312
	0.2	0.8	17.823	0.549
	0.2	0.8	47.925	0.823
	0.2	0.8	83.399	0.953
	0.2	0.8	138.729	1.02
	0.2	0.8	166.536	1.064
323.2	0.2	0.8	189.716	1.087

Table 4.6 Solubility data of CO_2 in aqueous 0.25 *w* AEP solution at equilibrium state

T/K	Mass Fraction (AEP)	Mass Fraction (H_2O)	P_{CO_2} / *kPa*	α_{CO_2}
	0.25	0.75	4.937	0.278
	0.25	0.75	8.446	0.51
	0.25	0.75	16.182	0.729
	0.25	0.75	41.362	0.91
	0.25	0.75	80.538	1.033
	0.25	0.75	122.444	1.118
	0.25	0.75	160.076	1.164
303.2	0.25	0.75	183.807	1.188
	0.25	0.75	2.861	0.241
	0.25	0.75	6.191	0.477
	0.25	0.75	10.749	0.658
	0.25	0.75	25.421	0.797
	0.25	0.75	38.321	0.929
	0.25	0.75	79.628	1.006
	0.25	0.75	116.694	1.047
	0.25	0.75	153.381	1.108
313.2	0.25	0.75	192.433	1.125
	0.25	0.75	3.323	0.23
	0.25	0.75	9.046	0.427
	0.25	0.75	20.553	0.618
	0.25	0.75	39.273	0.764
	0.25	0.75	77.207	0.902
	0.25	0.75	125.485	0.989
	0.25	0.75	155.229	1.036
323.2	0.25	0.75	186.062	1.052

Table 4.7 Solubility data of CO_2 in aqueous 0.30 *w* AEP solution at equilibrium state

T/K	Mass Fraction (AEP)	Mass Fraction (H_2O)	P_{CO_2} / *kPa*	α_{CO_2}
	0.3	0.7	4.875	0.306
	0.3	0.7	8.356	0.502
	0.3	0.7	14.376	0.714
	0.3	0.7	29.53	0.844
	0.3	0.7	80.351	0.985
	0.3	0.7	100.829	1.049
	0.3	0.7	130.097	1.117
	0.3	0.7	157.359	1.143
303.2	0.3	0.7	175.21	1.172
	0.3	0.7	2.779	0.225
	0.3	0.7	5.605	0.442
	0.3	0.7	9.729	0.591
	0.3	0.7	18.588	0.707
	0.3	0.7	38.769	0.835
	0.3	0.7	81.117	0.944
	0.3	0.7	112.633	1.03
	0.3	0.7	157.869	1.078
313.2	0.3	0.7	185.855	1.1
	0.3	0.7	4.978	0.271
	0.3	0.7	10.556	0.438
	0.3	0.7	19.678	0.569
	0.3	0.7	34.336	0.679
	0.3	0.7	52.704	0.813
	0.3	0.7	107.862	0.925
	0.3	0.7	135.861	0.984
	0.3	0.7	165.054	1.017
323.2	0.3	0.7	191.336	1.036

Table 4.8 Solubility data of CO_2 in aqueous 0.35 *w* AEP solution at equilibrium state

T/K	Mass Fraction (AEP)	Mass Fraction (H_2O)	P_{CO_2} / *kPa*	α_{CO_2}
	0.35	0.65	4.613	0.276
	0.35	0.65	7.715	0.492
	0.35	0.65	12.383	0.642
	0.35	0.65	24.042	0.77
	0.35	0.65	31.468	0.883
	0.35	0.65	69.003	0.978
	0.35	0.65	99.05	1.031
	0.35	0.65	132.683	1.113
	0.35	0.65	162.634	1.151
303.2	0.35	0.65	189.509	1.161
	0.35	0.65	2.979	0.18
	0.35	0.65	7.067	0.384
	0.35	0.65	10.983	0.543
	0.35	0.65	17.802	0.666
	0.35	0.65	27.317	0.782
	0.35	0.65	52.69	0.877
	0.35	0.65	86.06	0.962
	0.35	0.65	141.081	1.04
313.2	0.35	0.65	158.317	1.056
	0.35	0.65	3.799	0.214
	0.35	0.65	7.308	0.395
	0.35	0.65	14.624	0.544
	0.35	0.65	26.076	0.685
	0.35	0.65	51.325	0.808
	0.35	0.65	71.595	0.901
	0.35	0.65	112.578	0.955
	0.35	0.65	137.151	0.986
323.2	0.35	0.65	169.383	1.003

Table 4.9 Solubility data of CO_2 in aqueous 0.40 *w* AEP solution at equilibrium state

T/K	Mass Fraction (AEP)	Mass Fraction (H_2O)	P_{CO_2} / *kPa*	α_{CO_2}
	0.4	0.6	4.013	0.199
	0.4	0.6	6.605	0.333
	0.4	0.6	9.887	0.464
	0.4	0.6	11.728	0.585
	0.4	0.6	14.3	0.687
	0.4	0.6	26.696	0.812
	0.4	0.6	55.565	0.921
	0.4	0.6	87.867	1.009
	0.4	0.6	119.383	1.064
	0.4	0.6	154.222	1.077
303.2	0.4	0.6	181.029	1.091
	0.4	0.6	3.275	0.163
	0.4	0.6	6.46	0.319
	0.4	0.6	9.591	0.444
	0.4	0.6	16.327	0.575
	0.4	0.6	23.608	0.692
	0.4	0.6	36.473	0.77
	0.4	0.6	61.191	0.866
	0.4	0.6	83.392	0.943
	0.4	0.6	119.734	0.989
	0.4	0.6	140.984	1.023
313.2	0.4	0.6	156.966	1.036
	0.4	0.6	3.999	0.156
	0.4	0.6	8.287	0.345
	0.4	0.6	14.003	0.471
	0.4	0.6	20.34	0.608
	0.4	0.6	46.291	0.721
	0.4	0.6	79.841	0.82
	0.4	0.6	122.761	0.892
	0.4	0.6	150.478	0.936
323.2	0.4	0.6	180.339	0.961

Table 4.10 Solubility data of CO_2 in aqueous (0.05*w* AEP + 0.35*w* MDEA) solution at equilibrium state

T/K	Mass Fraction (AEP)	Mass Fraction (MDEA)	Mass Fraction (H_2O)	P_{CO_2} / *kPa*	α_{CO_2}
	0.05	0.35	0.6	8.96	0.239
	0.05	0.35	0.6	28.27	0.388
	0.05	0.35	0.6	51.5	0.537
	0.05	0.35	0.6	84.81	0.645
	0.05	0.35	0.6	122.11	0.716
	0.05	0.35	0.6	149.48	0.79
	0.05	0.35	0.6	182.57	0.84
303.2	0.05	0.35	0.6	226.77	0.869
	0.05	0.35	0.6	8.07	0.233
	0.05	0.35	0.6	30.96	0.39
	0.05	0.35	0.6	67.71	0.507
	0.05	0.35	0.6	102.53	0.631
	0.05	0.35	0.6	133.83	0.723
	0.05	0.35	0.6	170.99	0.778
	0.05	0.35	0.6	196.43	0.815
313.2	0.05	0.35	0.6	230.35	0.839
	0.05	0.35	0.6	5.38	0.208
	0.05	0.35	0.6	30.2	0.338
	0.05	0.35	0.6	56.95	0.456
	0.05	0.35	0.6	99.15	0.565
	0.05	0.35	0.6	123.97	0.637
	0.05	0.35	0.6	154.24	0.709
	0.05	0.35	0.6	186.57	0.771
323.2	0.05	0.35	0.6	230.15	0.818

Table 4.11 Solubility data of CO_2 in aqueous (0.10*w* AEP + 0.30*w* MDEA) solution at equilibrium state

T/K	Mass Fraction (AEP)	Mass Fraction (MDEA)	Mass Fraction (H_2O)	P_{CO_2} / *kPa*	α_{CO_2}
	0.1	0.3	0.6	8.48	0.255
	0.1	0.3	0.6	26.41	0.467
	0.1	0.3	0.6	72.12	0.64
	0.1	0.3	0.6	115.35	0.757
	0.1	0.3	0.6	171.68	0.853
	0.1	0.3	0.6	206.15	0.918
	0.1	0.3	0.6	253.24	0.968
303.2	0.1	0.3	0.6	280.34	0.998
	0.1	0.3	0.6	8.34	0.257
	0.1	0.3	0.6	29.92	0.431
	0.1	0.3	0.6	79.5	0.615
	0.1	0.3	0.6	130.93	0.721
	0.1	0.3	0.6	171.13	0.795
	0.1	0.3	0.6	200.78	0.85
	0.1	0.3	0.6	220.98	0.886
313.2	0.1	0.3	0.6	255.38	0.917
	0.1	0.3	0.6	4.41	0.196
	0.1	0.3	0.6	20.34	0.364
	0.1	0.3	0.6	57.57	0.5
	0.1	0.3	0.6	101.08	0.633
	0.1	0.3	0.6	138.24	0.723
	0.1	0.3	0.6	172.64	0.767
	0.1	0.3	0.6	200.36	0.803
	0.1	0.3	0.6	230.7	0.84
323.2	0.1	0.3	0.6	267.65	0.868

Table 4.12 Solubility data of CO_2 in aqueous (0.15*w* AEP + 0.25*w* MDEA) solution at equilibrium state

T/K	Mass Fraction (AEP)	Mass Fraction (MDEA)	Mass Fraction (H_2O)	P_{CO_2} / *kPa*	α_{CO_2}
	0.15	0.25	0.6	9.45	0.304
	0.15	0.25	0.6	20.75	0.53
	0.15	0.25	0.6	60.19	0.68
	0.15	0.25	0.6	115.28	0.818
	0.15	0.25	0.6	174.99	0.9
	0.15	0.25	0.6	218.7	0.978
	0.15	0.25	0.6	261.66	1.043
303.2	0.15	0.25	0.6	286.68	1.075
	0.15	0.25	0.6	7.03	0.263
	0.15	0.25	0.6	18.89	0.434
	0.15	0.25	0.6	40.82	0.554
	0.15	0.25	0.6	76.39	0.65
	0.15	0.25	0.6	114.66	0.766
	0.15	0.25	0.6	160.17	0.829
	0.15	0.25	0.6	189.54	0.886
	0.15	0.25	0.6	222.63	0.935
313.2	0.15	0.25	0.6	253.18	0.966
	0.15	0.25	0.6	5.31	0.224
	0.15	0.25	0.6	15.38	0.394
	0.15	0.25	0.6	52.4	0.536
	0.15	0.25	0.6	95.91	0.661
	0.15	0.25	0.6	125.76	0.758
	0.15	0.25	0.6	162.1	0.817
	0.15	0.25	0.6	193.05	0.873
	0.15	0.25	0.6	222.42	0.899
323.2	0.15	0.25	0.6	252.55	0.929

Table 4.13 Solubility data of CO_2 in aqueous (0.20*w* AEP + 0.20*w* MDEA) solution at equilibrium state

T/K	Mass Fraction (AEP)	Mass Fraction (MDEA)	Mass Fraction (H_2O)	P_{CO_2} / *kPa*	α_{CO_2}
	0.2	0.2	0.6	6.89	0.272
	0.2	0.2	0.6	14.41	0.504
	0.2	0.2	0.6	59.43	0.724
	0.2	0.2	0.6	112.11	0.896
	0.2	0.2	0.6	168.92	0.988
	0.2	0.2	0.6	204.84	1.074
	0.2	0.2	0.6	240.9	1.107
303.2	0.2	0.2	0.6	272.83	1.147
	0.2	0.2	0.6	5.93	0.238
	0.2	0.2	0.6	14.89	0.422
	0.2	0.2	0.6	36.4	0.579
	0.2	0.2	0.6	82.87	0.734
	0.2	0.2	0.6	119.21	0.841
	0.2	0.2	0.6	158.92	0.91
	0.2	0.2	0.6	195.33	0.977
	0.2	0.2	0.6	215.53	1.025
313.2	0.2	0.2	0.6	245.25	1.046
	0.2	0.2	0.6	4.69	0.22
	0.2	0.2	0.6	13.17	0.374
	0.2	0.2	0.6	35.03	0.509
	0.2	0.2	0.6	85.49	0.651
	0.2	0.2	0.6	125.62	0.786
	0.2	0.2	0.6	155.96	0.882
	0.2	0.2	0.6	197.12	0.944
	0.2	0.2	0.6	220.08	0.986
323.2	0.2	0.2	0.6	249.73	1.024

Table 4.14 Solubility data of CO_2 in aqueous (0.25*w* AEP + 0.15*w* MDEA) solution at equilibrium state

T/K	Mass Fraction (AEP)	Mass Fraction (MDEA)	Mass Fraction (H_2O)	P_{CO_2} / *kPa*	α_{CO_2}
	0.25	0.15	0.6	4.9	0.285
	0.25	0.15	0.6	8.69	0.495
	0.25	0.15	0.6	27.79	0.66
	0.25	0.15	0.6	69.09	0.897
	0.25	0.15	0.6	115.83	1.016
	0.25	0.15	0.6	184.02	1.09
	0.25	0.15	0.6	217.74	1.153
303.2	0.25	0.15	0.6	251.52	1.187
	0.25	0.15	0.6	5.45	0.259
	0.25	0.15	0.6	8	0.45
	0.25	0.15	0.6	29.99	0.601
	0.25	0.15	0.6	55.23	0.747
	0.25	0.15	0.6	98.32	0.864
	0.25	0.15	0.6	125.21	0.95
	0.25	0.15	0.6	154.79	1.023
	0.25	0.15	0.6	186.99	1.062
313.2	0.25	0.15	0.6	229.11	1.096
	0.25	0.15	0.6	3.59	0.197
	0.25	0.15	0.6	10.82	0.411
	0.25	0.15	0.6	29.58	0.525
	0.25	0.15	0.6	56.61	0.663
	0.25	0.15	0.6	101.97	0.787
	0.25	0.15	0.6	128.24	0.882
	0.25	0.15	0.6	158.37	0.964
	0.25	0.15	0.6	194.29	1.022
323.2	0.25	0.15	0.6	233.53	1.058

Table 4.15 Solubility data of CO_2 in aqueous (0.05*w* AEP + 0.35*w* AMP) solution at equilibrium state

T/K	Mass Fraction (AEP)	Mass Fraction (AMP)	Mass Fraction (H_2O)	P_{CO_2} / *kPa*	α_{CO_2}
	0.05	0.35	0.6	5.35	0.248
	0.05	0.35	0.6	9.45	0.452
	0.05	0.35	0.6	15.03	0.624
	0.05	0.35	0.6	58.4	0.757
	0.05	0.35	0.6	94.87	0.884
	0.05	0.35	0.6	134.72	0.939
	0.05	0.35	0.6	179.54	0.958
303.2	0.05	0.35	0.6	228.56	0.968
	0.05	0.35	0.6	4.21	0.206
	0.05	0.35	0.6	9.31	0.413
	0.05	0.35	0.6	18.55	0.583
	0.05	0.35	0.6	47.85	0.712
	0.05	0.35	0.6	102.66	0.804
	0.05	0.35	0.6	150.31	0.87
	0.05	0.35	0.6	200.02	0.893
313.2	0.05	0.35	0.6	242.9	0.917
	0.05	0.35	0.6	5.45	0.213
	0.05	0.35	0.6	20.89	0.423
	0.05	0.35	0.6	52.06	0.576
	0.05	0.35	0.6	97.7	0.671
	0.05	0.35	0.6	132.38	0.755
	0.05	0.35	0.6	167.96	0.809
	0.05	0.35	0.6	211.46	0.844
323.2	0.05	0.35	0.6	242.56	0.86

Table 4.16 Solubility data of CO_2 in aqueous (0.10*w* AEP + 0.30*w* AMP) solution at equilibrium state

T/K	Mass Fraction (AEP)	Mass Fraction (AMP)	Mass Fraction (H_2O)	P_{CO_2} / *kPa*	α_{CO_2}
	0.1	0.3	0.6	5.38	0.252
	0.1	0.3	0.6	9.38	0.479
	0.1	0.3	0.6	24.41	0.666
	0.1	0.3	0.6	57.71	0.826
	0.1	0.3	0.6	77.7	0.938
	0.1	0.3	0.6	130.04	0.977
	0.1	0.3	0.6	168.99	0.997
303.2	0.1	0.3	0.6	217.74	1.009
	0.1	0.3	0.6	3.45	0.224
	0.1	0.3	0.6	8	0.442
	0.1	0.3	0.6	18.27	0.638
	0.1	0.3	0.6	48.33	0.79
	0.1	0.3	0.6	108.32	0.884
	0.1	0.3	0.6	152.86	0.944
	0.1	0.3	0.6	201.88	0.963
313.2	0.1	0.3	0.6	232.9	0.98
	0.1	0.3	0.6	5.03	0.234
	0.1	0.3	0.6	18.55	0.428
	0.1	0.3	0.6	48.33	0.584
	0.1	0.3	0.6	100.25	0.693
	0.1	0.3	0.6	131	0.781
	0.1	0.3	0.6	165.89	0.85
	0.1	0.3	0.6	201.46	0.892
323.2	0.1	0.3	0.6	241.39	0.908

Table 4.17 Solubility data of CO_2 in aqueous (0.15*w* AEP + 0.25*w* AMP) solution at equilibrium state

T/K	Mass Fraction (AEP)	Mass Fraction (AMP)	Mass Fraction (H_2O)	P_{CO_2} / *kPa*	α_{CO_2}
	0.15	0.25	0.6	4.9	0.284
	0.15	0.25	0.6	10.2	0.505
	0.15	0.25	0.6	16.82	0.703
	0.15	0.25	0.6	40.47	0.857
	0.15	0.25	0.6	76.26	0.968
	0.15	0.25	0.6	125.35	1.031
	0.15	0.25	0.6	164.92	1.052
303.2	0.15	0.25	0.6	224.42	1.063
	0.15	0.25	0.6	4.62	0.254
	0.15	0.25	0.6	9.86	0.475
	0.15	0.25	0.6	18.75	0.663
	0.15	0.25	0.6	53.57	0.825
	0.15	0.25	0.6	116.25	0.928
	0.15	0.25	0.6	164.85	0.987
	0.15	0.25	0.6	202.71	1.007
313.2	0.15	0.25	0.6	250.07	1.016
	0.15	0.25	0.6	4.55	0.242
	0.15	0.25	0.6	13.86	0.47
	0.15	0.25	0.6	47.57	0.62
	0.15	0.25	0.6	94.53	0.728
	0.15	0.25	0.6	126.17	0.817
	0.15	0.25	0.6	160.79	0.892
	0.15	0.25	0.6	205.05	0.94
323.2	0.15	0.25	0.6	254	0.956

Table 4.18 Solubility data of CO_2 in aqueous (0.20*w* AEP + 0.20*w* AMP) solution at equilibrium state

T/K	Mass Fraction (AEP)	Mass Fraction (AMP)	Mass Fraction (H_2O)	P_{CO_2} / *kPa*	α_{CO_2}
	0.2	0.2	0.6	4.62	0.301
	0.2	0.2	0.6	8.89	0.494
	0.2	0.2	0.6	14.2	0.704
	0.2	0.2	0.6	39.23	0.874
	0.2	0.2	0.6	79.08	1.008
	0.2	0.2	0.6	132.93	1.087
	0.2	0.2	0.6	186.37	1.113
303.2	0.2	0.2	0.6	230.35	1.126
	0.2	0.2	0.6	3.79	0.246
	0.2	0.2	0.6	7.31	0.48
	0.2	0.2	0.6	17.58	0.683
	0.2	0.2	0.6	52.26	0.844
	0.2	0.2	0.6	102.04	0.921
	0.2	0.2	0.6	138.38	0.984
	0.2	0.2	0.6	199.95	1.029
313.2	0.2	0.2	0.6	237.04	1.041
	0.2	0.2	0.6	4.69	0.25
	0.2	0.2	0.6	14.62	0.508
	0.2	0.2	0.6	52.33	0.676
	0.2	0.2	0.6	88.46	0.804
	0.2	0.2	0.6	131.35	0.898
	0.2	0.2	0.6	153.13	0.956
	0.2	0.2	0.6	196.02	0.989
323.2	0.2	0.2	0.6	249.59	0.998

Table 4.19 Solubility data of CO_2 in aqueous (0.25*w* AEP + 0.15*w* AMP) solution at equilibrium state

T/K	Mass Fraction (AEP)	Mass Fraction (AMP)	Mass Fraction (H_2O)	P_{CO_2} / *kPa*	α_{CO_2}
	0.25	0.15	0.6	3.1	0.267
	0.25	0.15	0.6	6.07	0.51
	0.25	0.15	0.6	10	0.733
	0.25	0.15	0.6	41.37	0.931
	0.25	0.15	0.6	75.91	1.068
	0.25	0.15	0.6	127.83	1.114
	0.25	0.15	0.6	178.02	1.142
303.2	0.25	0.15	0.6	236.63	1.155
	0.25	0.15	0.6	3.45	0.265
	0.25	0.15	0.6	5.93	0.494
	0.25	0.15	0.6	17.03	0.7
	0.25	0.15	0.6	50.68	0.869
	0.25	0.15	0.6	99.15	0.973
	0.25	0.15	0.6	132.52	1.049
	0.25	0.15	0.6	173.68	1.09
313.2	0.25	0.15	0.6	229.8	1.091
	0.25	0.15	0.6	4.14	0.276
	0.25	0.15	0.6	15.24	0.505
	0.25	0.15	0.6	41.51	0.665
	0.25	0.15	0.6	67.84	0.795
	0.25	0.15	0.6	108.39	0.884
	0.25	0.15	0.6	148.17	0.971
	0.25	0.15	0.6	197.95	1.012
323.2	0.25	0.15	0.6	242.9	1.034

References

[1] G. Fytianos, A. Grimstvedt, H. Knuutila, H.F. Svendsen, Effect of MEA's degradation products on corrosion at CO_2 capture plants, Energy Procedia 63 (2014) 1869–1875.

[2] H. Najibi, N. Maleki, Equilibrium solubility of carbon dioxide in N methyldiethanolamine+piperazine aqueous solution: Experimental measurement and prediction, Fluid Phase Equilib. 354 (2013) 298–303.

[3] S.K. Dash, A.N. Samanta S.S. Bandyopadhyay, Simulation and parametric study of the post combustion CO_2 capture using aqueous 2-amino-2-methyl-1-propanol and piperazine, Int. J. Greenh. Gas Control 21(2014) 130-139.

[4] K.P. Shen, M.H. Li, Solubility of carbon dioxide in aqueous mixtures of monoethanolamine with methyldiethanolamine, J. Chem. Eng. Data 37 (1992) 96–100.

[5] S.K. Dash, S.S. Bandyopadhyay, Studies on the effect of addition of piperazine and sulfolane into aqueous solution of N-methyldiethanolamine for CO_2 capture and VLE modelling using eNRTL equation, Int. J. Greenh. Gas Control 44 (2016) 227–237.

[6] M.Z. Haji-Sulaiman, M.K. Aroua, A. Benamor, Analysis of equilibrium data of CO_2 in aqueous solutions of diethanolamine (DEA), methyldiethanolamine (MDEA) and their mixtures using the modified Kent Eisenberg model, Chem. Eng. Res. Des. 76 (1998) 961–968.

[7] S. Paul, A.K. Ghoshal, B. Mandal, Kinetics of absorption of carbon dioxide into aqueous solution of 2-(1-piperazinyl)-ethylamine, Chem. Eng. Sci. 64 (2009) 313–321.

[8] J. Choi, Y. Kim, S. Nam, S. Yun, Y. Yoon, J. Lee, CO_2 absorption characteristics of a piperazine derivative with primary, secondary, and tertiary amino groups, Kor. J Chem. Engg. 33 (2016) 3222-3230.

[9] Y. Du, L. Li, O. Namjoshi, K.A. Voice, A.N. Fine, G.T. Rochelle, Aqueous piperazine/N-(2-Aminoethyl)piperazine for CO_2 capture, Energy Procedia 37 (2013) 1621-1638.

[10] Y. Du, Y. Wang, G.T. Rochelle, Thermal degradation of novel piperazine-based amine blends for CO_2 capture, Int. J. Greenh. Gas Control 49 (2016) 239–249.

[11] P. Singh, J.P.M. Niederer, G.F. Versteeg, Structure and activity relationships for amine-based CO_2 absorbents-II, Chem. Eng. Res. Des. 7 (2008) 135–144.

[12] A. Dey, S.K. Dash, B.P. Mandal, Equilibrium CO_2 solubility and thermophysical properties of aqueous blends of 1-(2-aminoethyl) piperazine and N-methyldiethanolamine, Fluid Phase Equilib. 463(2018) 91-105.

[13] B. Khosravi, F. Feyzi, M. R. Dehghani, S. Kaviani, Experimental measurement and thermodynamic modeling of CO_2 solubility in aqueous solutions of morpholine, J. Mol. Liq. 214 (2016) 411-417.

[14] M. Kundu, B.P. Mandal, and S.S. Bandyopadhyay, Vapor-liquid equilibrium of CO_2 in aqueous solutions of 2-amino-2-methyl-1-propanol, J. Chem. Engg. Data 48 (2003) 789-796.

[15] M.K. Park, O.C. Sandall, Solubility of carbon dioxide and nitrous oxide in 50 mass % methyldiethanolamine, J. Chem. Engg. Data 46 (2001) 166-168.

[16] D.P. Shoemaker, C.W. Garland, J.I. Steinfeld, J.W. Nibler, Experiments in physical chemistry, fourth ed., McGraw-Hill, New York, 1981.

[17] A.T. Zoghi, F. Feyzi, S. Zarrinpashneh, Equilibrium solubility of carbon dioxide in a 30wt.% aqueous solution of 2-((2-aminoethyl)amino)ethanol at pressures between atmospheric and 4400kPa: An experimental and modelling study, J. Chem. Thermodyn. 44 (2012) 66-74.

[18] S. Garg, A.M. Shariff, M.S. Shaikh, B. Lal, H. Suleman, N. Faiqa, Experimental data , thermodynamic and neural network modeling of CO_2 solubility in aqueous sodium salt of L -phenylalanine, J. CO_2 Util. 19 (2017) 146–156.

[19] Y.H. Hsu, R.B. Leron, M.H. Li, Solubility of carbon dioxide in aqueous mixtures of (reline + monoethanolamine) at T = (313.2 to 353.2) K, J. Chem. Thermodyn. 72 (2014) 94–99.

[20] R.L. Kent, B. Eisenberg, Better data for amine treating, Hydrocarbon Proces 55 (1976) 87-90.

[21] B.K. Mondal, S.S. Bandyopadhyay, A.N. Samanta, Experimental measurement and Kent-Eisenberg modelling of CO_2 solubility in aqueous mixture of 2-amino-2-methyl-1-propanol and hexamethylenediamine, Fluid Phase Equilib. 437 (2017) 118–126.

[22] M. Khodadadi, S. Riahi, M. Abbasi, Experimental modeling of the solubility of carbon dioxide in aqueous solution of monoethanolamine +1, 3-diaminopropane. J. Mol. Liq. 2019.

[23] H. Saghafia, M. Arabloob, Modeling of CO_2 solubility in MEA, DEA, TEA, and MDEA aqueoussolutions using AdaBoost-Decision Tree and Artificial Neural Network, Int. J. Greenh. Gas Control 58 (2017) 256-265.

[24] M.E. Hamzehie , S. Mazinani , F. Davardoost , A. Mokhtare , H. Najibi , B. Van der Bruggen , S. Darvishmanesh, Developing a feed forward multilayer neural network model

for prediction of CO_2 solubility in blended aqueous amine solutions, J. Nat. Gas Sci. Eng. 21(2014) 19-25.

[25] H. Pahlavanzadeh, S. Nourani, M. Saber, Experimental analysis and modeling of CO_2 solubility in AMP (2-amino-2-methyl-1-propanol) at low CO_2 partial pressure using the models of Deshmukh-Mather and the artificial neural network, J. Chem. Thermodyn. 43 (2011) 1775–1783.

[26] K.P. Shen, M.H. Li, Solubility of carbon Dioxide in aqueous mixtures of monoethanolamine with methyldiethanolamine, J. Chem. Eng. Data 37 (1992) 96–100.

[27] J.I. Baek, J.H. Yoon, Solubility of carbon dioxide in aqueous solutions of 2-Amino-2-methyl-1,3-propanediol, J. Chem. Eng. Data 43 (1998) 635-637.

[28] M.K. Wong, M.A. Bustam, A.M. Shariff, Chemical speciation of CO_2 absorption in aqueous monoethanolamine investigated by in situ Raman spectroscopy, Int. J. Greenh. Gas Control 39 (2015) 139–147.

[29] Y.C. Chang, R.B. Leron, M.H. Li, Equilibrium solubility of carbon dioxide in aqueous solutions of (diethylenetriamine + piperazine), J. Chem. Thermodyn. 64 (2013) 106–113.

[30] F. Bougie, M.C. Iliuta, Solubility of CO_2 in and density, viscosity, and surface tension of aqueous 2-amino-1,3-propanediol (serinol) solutions, J. Chem. Eng. Data 59 (2014) 355–361.

[31] R. Ramazani, S. Mazinani, A. Hafizi, A. Jahanmiri, Equilibrium solubility of carbon dioxide in aqueous blend of monoethanolamine (MEA) and 2-1-piperazinyl-ethylamine (PZEA) solutions: Experimental and optimization study, Process Saf. Environ. Prot. 98 (2015) 325–332.

[32] G. Richner, G. Puxty, Assessing the chemical speciation during CO_2 absorption by aqueous amines using in Situ FTIR, Ind. Eng. Chem. Res. 51 (2012) 14317-14324.

[33] C. Sun, P.K. Dutta, Infrared spectroscopic study of reaction of carbon dioxide with aqueous Monoethanolamine solutions, Ind. Eng. Chem. Res. 55 (2016) 6276-6283.

[34] W. Bottinger, M. Maiwald, H. Hasse, Online NMR spectroscopic study of species distribution in MEA-H_2O-CO_2 and DEA-H_2O-CO_2, Fluid Phase Equilib. 263 (2008) 131-143

[35] A.K. Chakraborty, G. Astarita, K.B. Bischoff, CO_2 Absorption in aqueous solutions of hindered amines, Chem. Eng. Sci., 41 (1986) 997–1003

[36] J.I. Lee, F.D. Otto, A.E. Mather, Equilibrium between carbon dioxide and aqueous monoethanolamine solutions, J. appl. Chem. Biotechnol. 26 (1976) 541-549.

[37] D.J. Seo and W.H. Hong, Solubilities of carbon dioxide in aqueous mixtures of diethanolamine and 2-amino-2-methyl-1-Propanol, J. Chem. Eng. Data 41 (1996) 258-260.

[38] S.K. Dash, A.N. Samanta, S.S. Bandyopadhyay, (vapor+ liquid) equilibria (VLE) of CO_2 in aqueous solutions of 2-amino-2-methyl-1-propanol: New data and modelling using eNRTL-equation, J. Chem. Thermo. 43 (2011) 1278-1285.

[39] M. Li, B. Chang, Solubilities of carbon dioxide in water + monoethanolamine + 2- amino-2-methyl-1-propanol, J. Chem. Eng. Data 39 (1994).

[40] S.K. Dash, A.N. Samanta, S.S. Bandyopadhyay, Experimental and theoretical investigation of solubility of carbon dioxide in concentrated aqueous solution of 2-amino-2-methyl-1-propanol and piperazine, J. Chem. Thermo. 51 (2012) 120-125.

Chapter 5

INVESTIGATION ON THE ADDITION OF APDA AS A PROMOTER ON THE EQUILIBRIUM CO_2 SOLUBILITY OF AQUEOUS MDEA /AMP/1DMAP

The utility of polyamine-based solvent-activators for the possible application in post-combustion CO_2 capture technology has drawn considerable attention recently owing to its higher loading capacity as well as superior kinetics. This chapter presents a comprehensive experimental cum theoretical investigation on the equilibrium solubility of CO_2 pertaining to aqueous (APDA) and its blends with MDEA, AMP, and 1-DMAP. 1-DMAP has been chosen as another potential tertiary amine because of its superior kinetics and lower regeneration energy penalty compared to MDEA.

5.1 Introduction

Tertiary amines such as MDEA / 1DMAP or sterically hindered amine (AMP) has several desirable characteristics such as higher CO_2 absorption capacity and lower reboiler heat duty for regeneration of CO_2-rich amine solvent compared to other widely used amines such as MEA. The major drawbacks associated with the tertiary/sterically amines are their unfavorable kinetics and low reaction rates upon absorption with CO_2 which results in increasing the size of absorption column used in the PCC process [1]. To overcome these limitations of non-carbamate forming conventional amines, the strategy which has been widely adopted by researchers globally is the blending of suitable rate activator with the conventional amine group. Polyamines consisting of more than one amine groups are considered as the potential activator in the acid gas removal technology. Researchers got very promising results in earlier instances especially with most commonly used Piperazine (PZ) activated N-methyldiethanolamine (MDEA) or 2-amino-2-methyl-1-propanol (AMP) solvent system [2, 3]. Also, as can be inferred from Chapter 4 that the incorporation of 1-(2-aminoethyl) piperazine (AEP), a piperazine derivative into an aqueous

solution of MDEA/AMP not only enhances the kinetics but also increases the equilibrium CO_2 solubility over a wide range of experimental conditions [4, 5].

Recently, N-(3-aminopropyl)-1,3-propanediamine (APDA) a polyamine containing two primary amine group and one secondary group has been explored as a potential activator for CO_2 removal application. It possesses some favorable traits such as low vapor pressure along with high pKa value, which further results in higher reaction rates and absorption capacity [6, 7]. Das et al. [8] investigated the kinetics of APDA-CO_2 reaction over a wide range of experimental conditions. The second-order rate constant k_2 for aqueous APDA is 35775 $m^3kmol^{-1}s^{-1}$ which is substantially higher compared to conventional activator piperazine and another polyamine-based activator such as AEP. Following its superior kinetic characteristics, it can be also anticipated that since APDA consists of three amino groups viz. two primary and one secondary, it is expected to contribute for higher loading capacity in single and blended solvent system. The CO_2 loading capacity can be determined from detail experimental equilibrium solubility study. Solubility data at a wide temperature and pressure range is very much essential for the process design and optimization of industrial gas separation unit [9, 10]. Despite its potential as a promising candidate for acid gas removal technology, there are very limited solubility data related to APDA-CO_2 system are available in the open literature. APDA shows very high loading capacity upon reacting with CO_2, three times high compared to benchmark MEA at 15 kPa [11]. These desirable traits of APDA, as well as lack of literature data, encourage us to investigate CO_2 solubility in aqueous APDA as well as its potential blends with MDEA and AMP. In addition to this another new tertiary amine, 1-dimethylamino-2-propanol (1DMAP) has drawn considerable attention because of its superior performance over MDEA in terms of higher reaction rate constant and lower heat of absorption [12, 13] which prompted us to investigate this novel blend (APDA + DMAP) in our present work along with the two former potential blends. Accurate process modeling is also very much essential to assess the thermodynamic applicability as well as to systematically interpolate between or extrapolate the data beyond the operating conditions [14]. Equilibrium based modified Kent-Eisenberg model has been used to correlate the solubility data by estimating the equilibrium constants of important amine-CO_2-H_2O reactions as a function of important operating parameters [15-16]. Multilayer feed-forward network involving Levenberg-Marquardt (LM) back-propagation algorithm has been also employed to predict the equilibrium CO_2 absorption data over the different experimental conditions [17-19]

In this chapter, equilibrium CO_2 solubility in aqueous APDA as well as aqueous blends of (APDA + AMP), (APDA + MDEA) and (APDA + DMAP) have been measured and modeled over the CO_2 partial pressure range of (2-200) kPa and at 303.2, 313.2 and 323.2 K. The concentration of aqueous binary solvent has been varied from 0.10 *w* to 0.40 *w*, while the ternary systems are analyzed for 0.30 *w*.

5.2 Experimental

5.2.1 Materials

Reagent grade N-(3-aminopropyl)-1,3-propanediamine (APDA, 99 % pure), N-methyldiethanolamine (MDEA, 99 % pure) and 2-amino-2-methyl-1-Propanol (AMP, 99 % pure) were procured from Sigma–Aldrich and was used without further purification. CO_2 gas (> 99 % pure) was obtained from Linde India Ltd. All the amine solutions were prepared with double distilled deionized water. The detailed chemical specification is reported in Table 5.1.

5.2.2 Experimental methodology

The experimental set-up described in Chapter 4 has been used for solubility measurements reported in Chapter 5. The details of the experimental setup and the procedure have been described in previous chapter and also reported elsewhere [4, 5].

5.3 Equilibrium based modeling of CO_2 solubility

The equilibrium CO_2 solubility data in all the four systems viz. (APDA+H_2O), (APDA+AMP+H_2O), (APDA+MDEA+H_2O) and (APDA + DMAP + H_2O) have been modeled using modified Kent-Eisenberg model

5.3.1 Modified Kent-Eisenberg model

Absorption of CO_2 in aqueous (APDA) as well as its blend with AMP, MDEA and DMAP system consists of both phase and chemical equilibrium. Physical solubility of CO_2 is represented by Henry's law whereas reaction equilibrium constants are used to represent the

chemical equilibrium considering reversible reactions in liquid phase. The liquid phase reaction consisting of protonation of amines, carbamate formation by APDA and other reactions. The bicarbamate formation of APDA has not been considered here following the scheme adopted by Das et al. [7]. The equilibrium reactions for all the three system can be expressed using reactions R 5.1 to R 5.9:

Physical Solubility

$$CO_2(g) \overset{H_{CO_2}}{\rightleftharpoons} CO_2(aq) \qquad \text{(R 5.1)}$$

Dissociation of bicarbonate ion

$$HCO_3^-(g) \overset{K_1}{\rightleftharpoons} CO_3^{2-} + H^+ \qquad \text{(R 5.2)}$$

Formation of bicarbonate ion

$$CO_2 + H_2O \overset{K_2}{\rightleftharpoons} HCO_3^- + H^+ \qquad \text{(R 5.3)}$$

Dissociation of water

$$H_2O \overset{K_3}{\rightleftharpoons} OH^- + H^+ \qquad \text{(R 5.4)}$$

Deprotonation of APDA

$$APDAH^+ \overset{K_4}{\rightleftharpoons} APDA + H^+ \qquad \text{(R 5.5)}$$

Carbamate hydrolysis of APDA

$$APDACOO^- + H_2O \overset{K_5}{\rightleftharpoons} APDA + HCO_3^- \qquad \text{(R 5.6)}$$

Deprotonation of MDEA

$$MDEAH^+ \overset{K_6}{\rightleftharpoons} MDEA + H^+ \qquad \text{(R 5.7)}$$

Deprotonation of AMP

$$AMPH^+ \overset{K_7}{\rightleftharpoons} AMP + H^+ \qquad \text{(R 5.8)}$$

Deprotonation of DMAP

$$DMAPH^+ \overset{K_8}{\rightleftharpoons} DMAP + H^+ \qquad \text{(R 5.9)}$$

While Kent-Eisenberg, in their work [21] expressed the equilibrium constants in terms of temperature only, there are various modifications proposed so far by different researchers [15, 22-23] in the estimation of equilibrium constants. In the present work, equilibrium constants K_4 and K_5 of important reactions related to deprotonation reaction of AEP as well as hydrolysis of carbamate are expressed in terms of composition of amine, Partial pressure of CO_2 and temperature. They are further estimated by regression analysis in MATLAB® platform. The equilibrium constant corresponding to reactions (R 5.2 – R 5.4) and (R 5.7- R 5.9) can be taken from the literature as reported in Table 5.2

5.4 Results and discussion

5.4.1. CO_2 solubility measurement

The standardization of experimental set up used in the present work and the methodology has been already presented in Chapter 4 and reported elsewhere [4, 5]. The solubility measurement of binary system, have been conducted over APDA concentration of 0.10*w* to 040*w* ≈ 0.8 to 3 kmol.m^{-3} in the aqueous blend. The composition of ternary solution has been taken as (0.04*w*APDA + 0.26*w*AMP/MDEA), (0.07*w*APDA + 0.23*w*AMP/MDEA), (0.10*w*APDA + 0.20*w* AMP/MDEA) keeping the total composition fixed at 0.30*w*.While for the APDA activated DMAP blends, the composition are taken as (0.02*w*APDA + 0.28*w*DMAP), (0.04*w*APDA + 0.26*w*DMAP), (0.06*w*APDA + 0.24*w*DMAP), (0.08*w*APDA + 0.22*w*DMAP) and (0.10*w*APDA + 0.20*w*DMAP). The experimental data related to CO_2 solubility in both binary and ternary aqueous amine systems are represented in Tables 5.3 – 5.19.

Various important reaction parameters ranging from pressure, temperature and the concentration of amines plays an important role in CO_2 solubility. From the experimental results, it can be

clearly observed that solubility increases with increment in P_{CO_2} across the entire experimental domain. This is due to the fact that intermolecular collision increases in the gas phase as the system pressure increases which results in the net increase of driving force for the absorption of gas molecules in the solution [24]. While once the solution saturated with CO_2, any further increment in the system pressure does not contribute much to the increment of CO_2 loading defined as moles of CO_2/moles of amine, α_{CO_2}. A steep rise in the α_{CO_2} till 1.5 is noticed within the experimental P_{CO_2} of 20 kPa for aqueous APDA solution which further signifies its applicability as a potential candidate for CO_2 capture from flue gas streams of thermal power plants. In the contrary, on account of exothermic reaction between CO_2 – amine system, α_{CO_2} decreases with a rise in system temperature from (303.2 to 323.2) K [3]. The influence of temperature on the equilibrium solubility has been presented in Figs. 5.1-5.2 for aqueous APDA and (APDA + AMP) systems. From Fig. 5.1, it can be observed that at a fixed composition of 0.30 w and CO_2 partial pressure of 50 kPa, aqueous APDA shows highest CO_2 loading of 1.78 at 303.2 K while it undergoes non-linear decrement to 1.65 at a temperature of 323.2 K. Moreover, at a fixed temperature of 313.2 K, upon increasing the concentration of APDA from 0.10 w to 0.40 w, the CO_2 loading shows a decreasing trend (Fig. 5.3). The reason can be attributed to the fact that the CO_2 solubility is expressed in the normalized form α_{CO_2} (*mol of CO_2/ mol of amine*) and upon an increase in the solution concentration, the increment in the mole of CO_2 absorbed in the amine system is less as compared to the increment in the moles of amine resulting in the loading factor to get reduced [13, 20, 22]. The effect of addition of APDA into the blended system of MDEA, AMP and 1DMAP can be observed from Figs. 5.4-5.6. For the blended solvent system, a gradual increase is noticed with a rise in APDA concentration while keeping the total blend concentration constant at 0.30w.

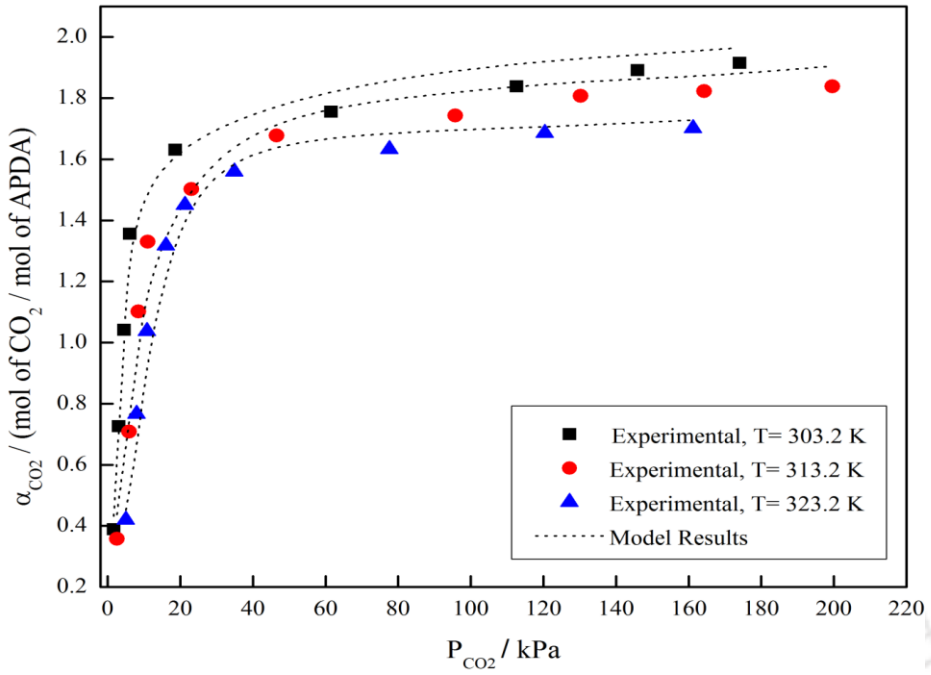

Fig. 5.1 CO_2 solubility as a function of different experimental temperature corresponding to 0.30 *w* APDA

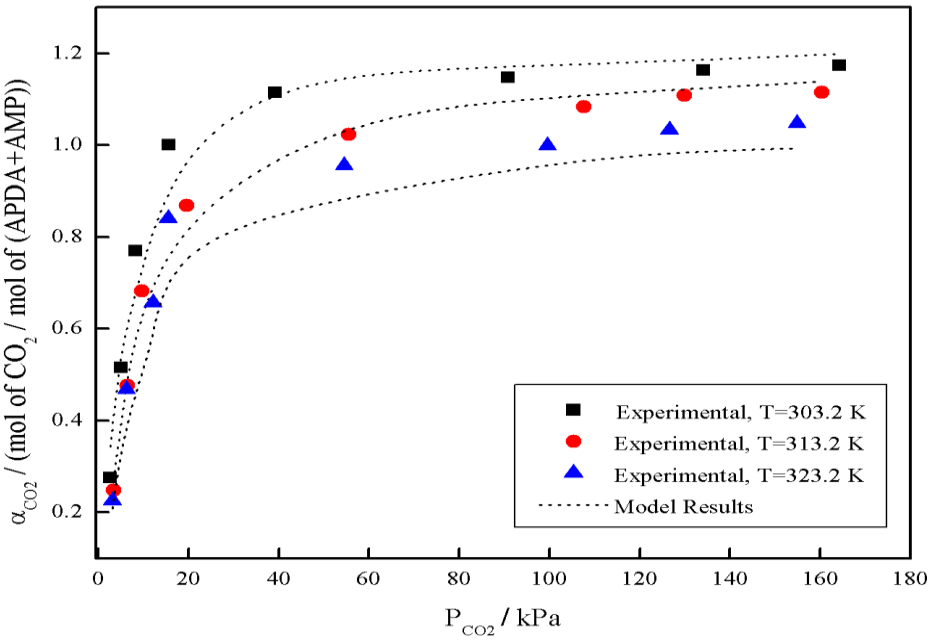

Fig. 5.2 CO_2 solubility as a function of different experimental temperature corresponding to (0.20 *w* AMP + 0.10 *w* APDA)

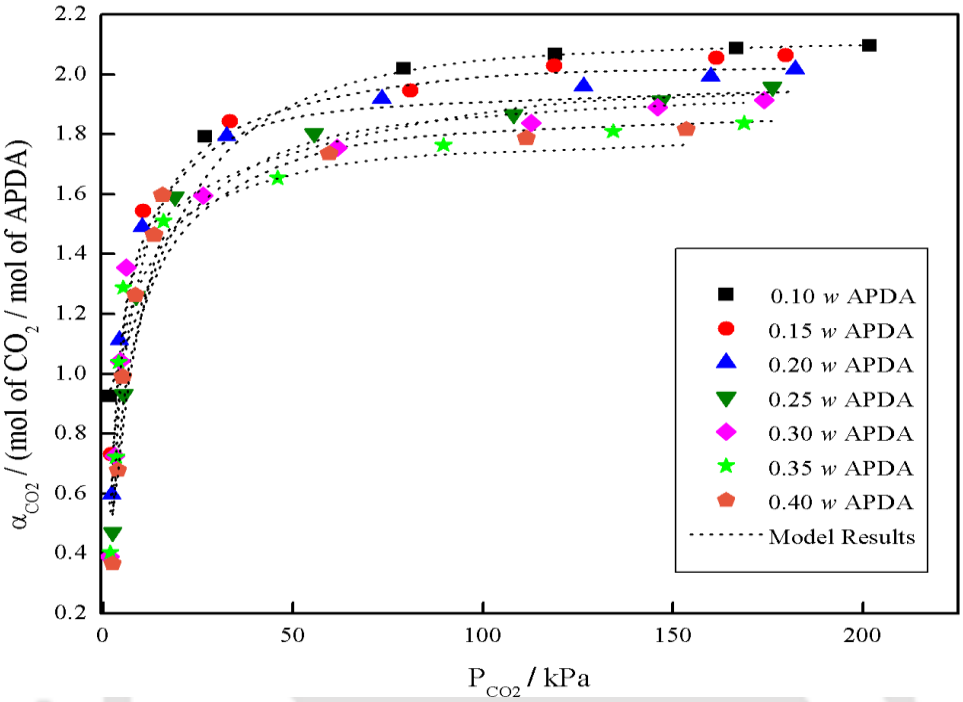

Fig. 5.3 CO_2 solubility as a function of different concentration of aqueous APDA system corresponding to temperature T= 313.2 K

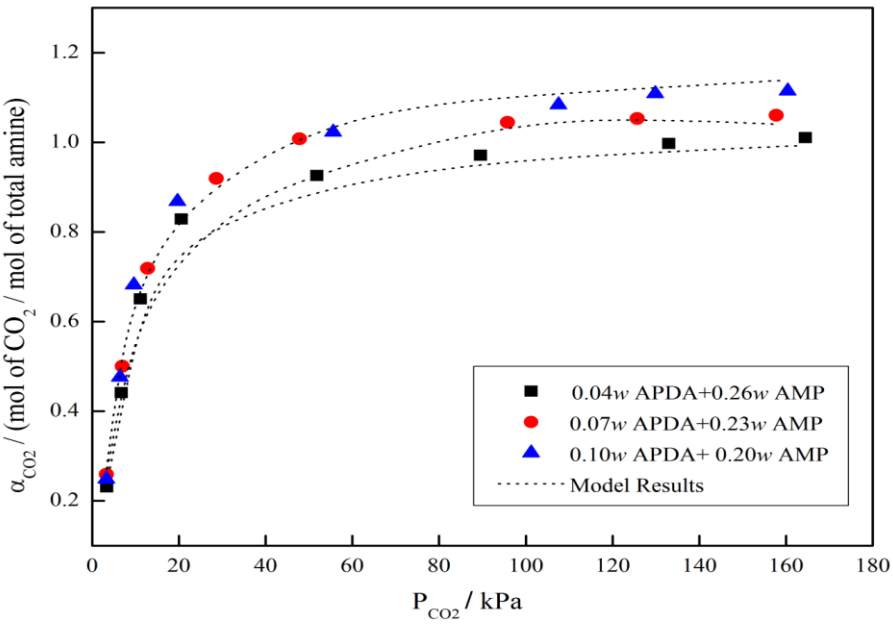

Fig. 5.4 CO_2 solubility as a function of different concentration of aqueous (APDA + AMP) system corresponding to temperature T= 313.2 K

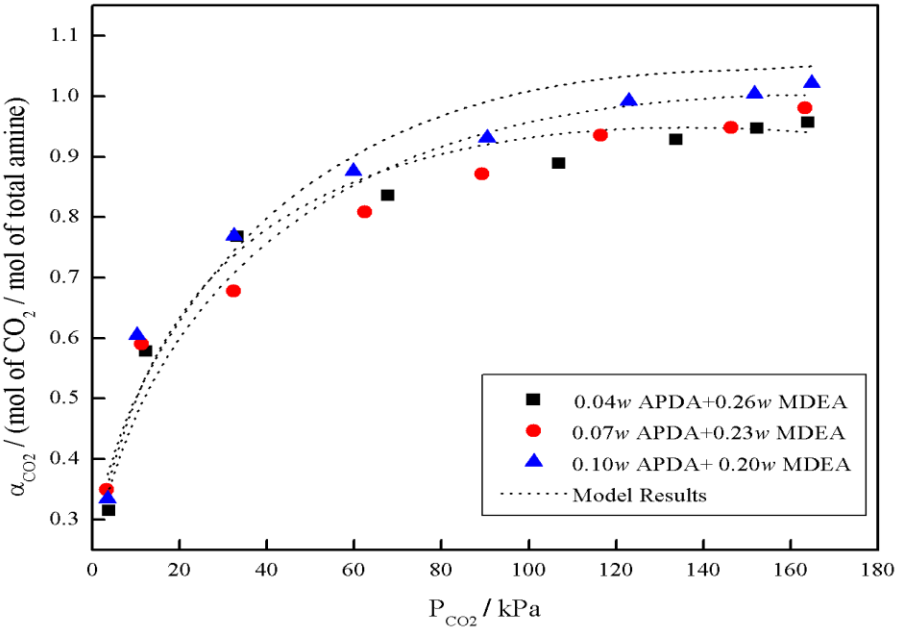

Fig. 5.5 CO_2 solubility as a function of different concentration of aqueous (APDA + MDEA) system corresponding to temperature T= 313.2 K

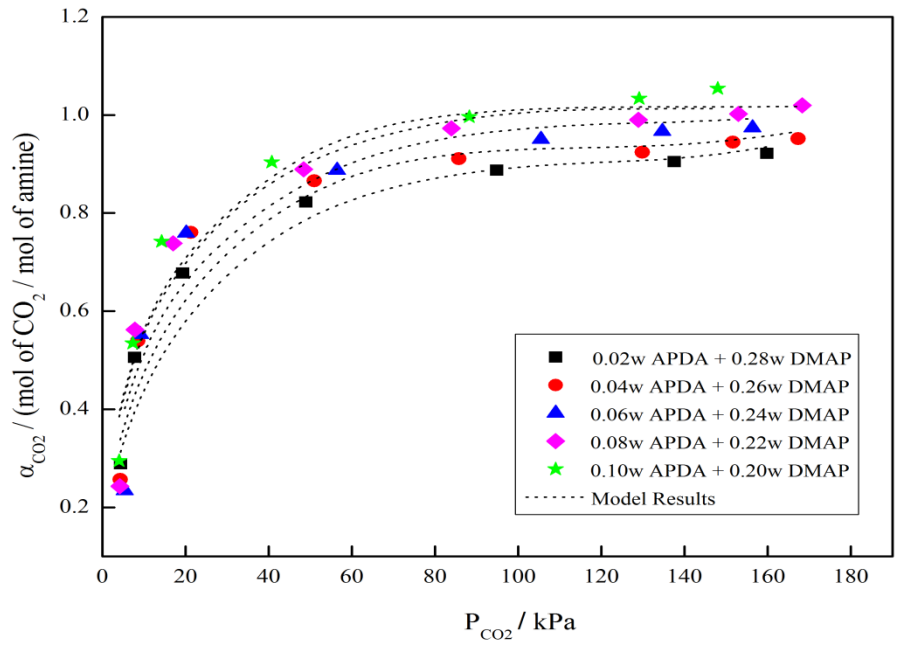

Fig.5.6 CO_2 solubility as a function of different concentration of aqueous (APDA + DMAP) system corresponding to temperature T= 313.2 K

In this work, solubility data has been modeled using different approaches described in the previous sections. In the modified KE approach, the coefficients of the equilibrium constants, (R 5.5) and (R 5.6) have been regressed to fit the experimental CO_2 loading data to obtain the estimated data. To reduce the error gap between the experimental and estimated data, a non-linear optimization technique is used. The corresponding objective function which is used for optimization in the present work can be defined as:

$$S = \frac{1}{N}\sum_{i=1}^{N}\left|\frac{\alpha_i^{\exp} - \alpha_i^{\mathrm{mod}}}{\alpha_i^{\exp}}\right| \tag{5.4}$$

Where, α_i^{exp} and α_i^{mod} represents experimental and model predicted CO_2 loading data and N stands for total set of data points. Also, equation (4.18) has been taken as the constraint equation for the above model. The reaction equilibrium constants (K_4 and K_5) can be estimated using equation (4.19) and (4.20) and employing the algorithm shown in Fig. 4.2. The equilibrium constants expressed in terms of temperature, CO_2 partial pressure and amine concentration can be estimated as:

For (APDA + H_2O) system:

$$K_4 = 1.637\times10^{-7} - 1.488\times10^{-9}(m_1) - 1.057\times10^{-9}(T) + 5.143\times10^{-12}(m_1\times T) + 1.713\times10^{-12}(T^2) - 2.435\times10^{-11}(P_{CO_2}) + 5.269\times10^{-14}(P_{CO_2}^2)$$

$$K_5 = -8.614\times10^{-2} + 2.225\times10^{-6}(m_1) - 2.707\times10^{-2}(T) - 2.882\times10^{--1}(m_1^{\,2}) - 3.903\times10^{-1}(m_1\times T) - 4.756\times10^{-2}(T^2) - 1.112\times10^{-3}(P_{CO_2}) - 1.873\times10^{-5}(P^2{}_{CO_2})$$

For (APDA + MDEA + H_2O) system:

$$K_4' = 5.238\times10^{-9} - 3.696\times10^{-10}(m_1\times m_2) - 3.205\times10^{-11}(T) + 1.224\times10^{-12}(m_1\times m_2\times T) + 4.899\times10^{-14}(T^2) - 4.848\times10^{-14}(P_{CO_2}) + 2.474\times10^{-15}(P_{CO_2}^2)$$

$$K_5' = 2.862\times10^{-1} + 5.668\times10^{-3}(m_1\times m_2) - 5.388\times10^{-4}(T) - 7.143\times10^{-4}(m_1^{\,2}\times m_2^{\,2}) + 4.376\times10^{-4}(m_1\times m_2\times T) + 2.596\times10^{-5}(T^2) + 1.755\times10^{-5}(P_{CO_2}) + 6.098\times10^{-7}(P^2{}_{CO_2})$$

For (APDA+ AMP + H_2O) system:

$$K_4'' = 1.264\times10^{-8} - 1.549\times10^{-10}(m_1\times m_2) - 8.084\times10^{-11}(T) + 8.382\times10^{-13}(m_1\times m_2\times T)$$
$$+1.286\times10^{-13}(T^2) + 3.810\times10^{-13}(P_{CO_2}) + 1.985\times10^{-16}(P_{CO_2}^2)$$

$$K_5'' = -1.481\times10^{-1} + 1.619\times10^{-1}(m_1\times m_2) - 1.732\times10^{-3}(T) + 4.267\times10^{-2}(m_1{}^2\times m_2{}^2)$$
$$-6.836\times10^{-4}(m_1\times m_2\times T) + 1.043\times10^{-5}(T^2) - 1.007\times10^{-5}(P_{CO_2}) + 2.829\times10^{-6}(P^2{}_{CO_2})$$

For (APDA+ DMAP + H_2O) system:

$$K_4'' = 1.23\times10^{-8} - 4.81\times10^{-9}(m_1\times m_2) - 7.62\times10^{-11}(T) + 1.04\times10^{-11}(m_1\times m_2\times T)$$
$$+1.42\times10^{-13}(T^2) + 1.54\times10^{-11}(P_{CO_2}) + 6.09\times10^{-14}(P_{CO_2}^2)$$

$$K_5'' = 3.084\times10^{-2} + -7.807\times10^{-1}(m_1\times m_2) - 7.46\times10^{-2}(T) + 2.233\times10^{-2}(m_1{}^2\times m_2{}^2)$$
$$-3.059\times10^{-2}(m_1\times m_2\times T) - 7.12\times10^{-7}(T^2) - 3.254\times10^{-1}(P_{CO_2}) + 1.231\times10^{-2}(P^2{}_{CO_2})$$

Applying all these equilibrium constants, the model estimated α_{CO_2} can be calculated and compared with the experimental results. The average absolute deviation (% AAD) between the model and experimental results are 11.09 % for (APDA + H_2O), 10.14 % for (APDA + AMP + H_2O), 7.47 % (APDA + MDEA + H_2O) and 8.35% for (APDA + 1DMAP + H_2O) system considering all data points which reflects the good prediction capability of the developed model of the present work.

The modified KE model proposed in the present work is also capable of predicting the equilibrium concentrations of various species present in the liquid phase as a function of CO_2 loading. The concentration profiles of various species for CO_2 loaded 0.30 mass fractions APDA, (0.07 mass fraction APDA + 0.23 mass fraction AMP) and (0.08 mass fraction APDA + 0.22 mass fraction DMAP) at 323.2 K have been represented in Figs. 5.7-5.9. It is evident from the speciation plot that the concentration of both APDA and AMP decreases gradually with CO_2 loading in both the binary and ternary system and the main reaction products are protonated APDA, protonated AMP, and bicarbonate ion. While the general trend of [CO_3^{2-}] in the reaction medium depicts its gradual decrease with increase in CO_2 loading, since at higher loadings there is a decrease in the free amine molecules resulting in the weak basic solution which further

facilitates the conversion of CO_3^{2-} to HCO_3^- through the reverse reaction of (R 5.2). Also the concentration of [$APDACOO^-$] species also shows a gradual reduction at higher loading indicating its conversion to more bicarbonate species.

The feed-forward neural network model employed in the present work has been also implemented to estimate the CO_2 loading over the entire experimental range of pressure and temperature. In the present work, the networks are developed keeping 70 % data for training and 30 % respectively for validation and testing, respectively [17]. The optimized network architecture for aqueous APDA system has been presented in Fig. 5.10 .The calculated % AAD between the estimated and investigational α_{CO2} has been found to be 6.95 and 2.38 % for aqueous APDA and (APDA + MDEA) systems. The comparison has been represented in the form of parity plot and shown in Fig 5.11. The lower value of % AAD indicates that ANN model outperforms equilibrium based model for predicting CO_2 solubility.

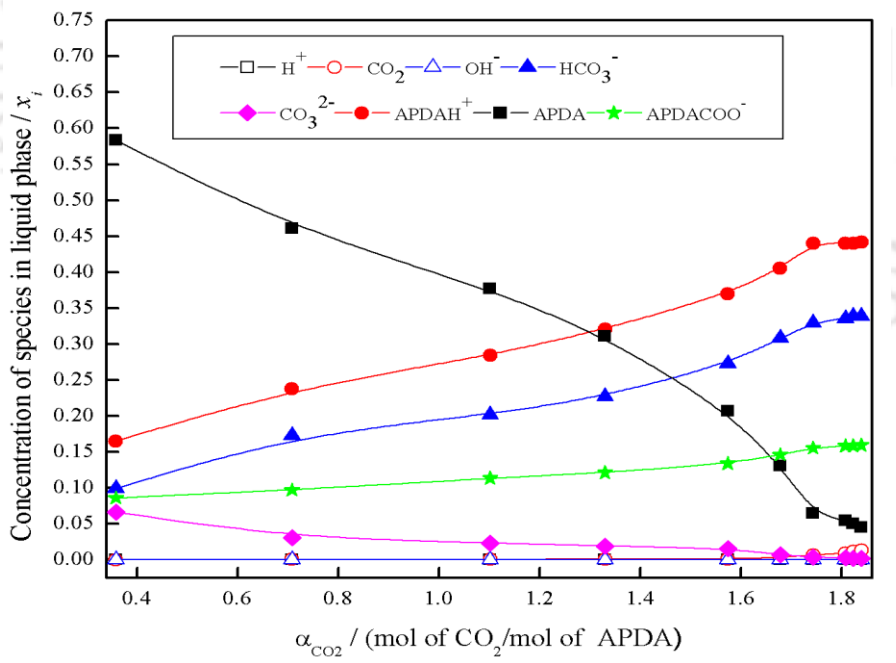

Fig. 5.7 Modified KE model predicted liquid phase ionic species profile as a function of in aqueous 0.30 w APDA solvent at T = 323.2 K

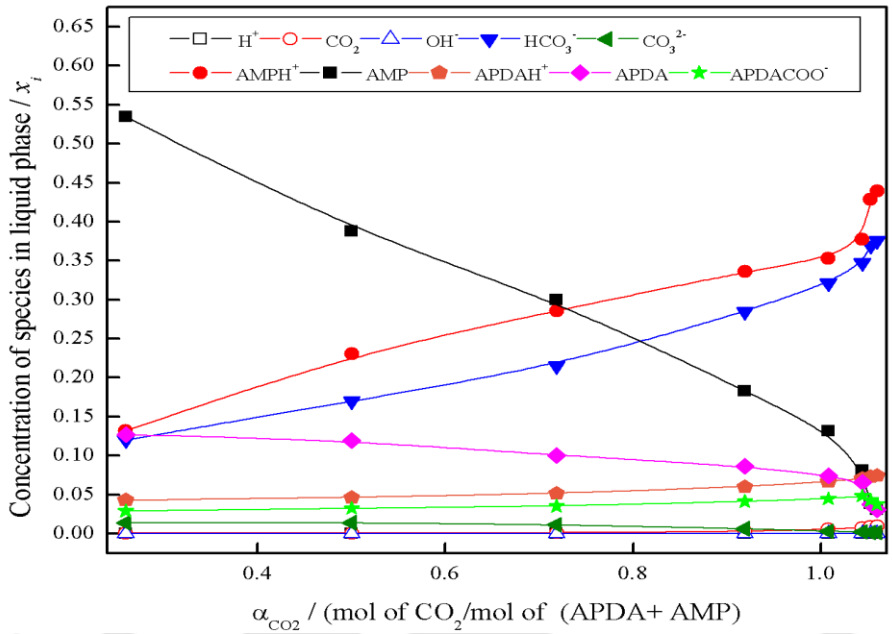

Fig. 5.8 Modified KE model predicted liquid phase ionic species profile as a function of in aqueous (0.07w APDA + 0.23w AMP) at T = 323.2 K

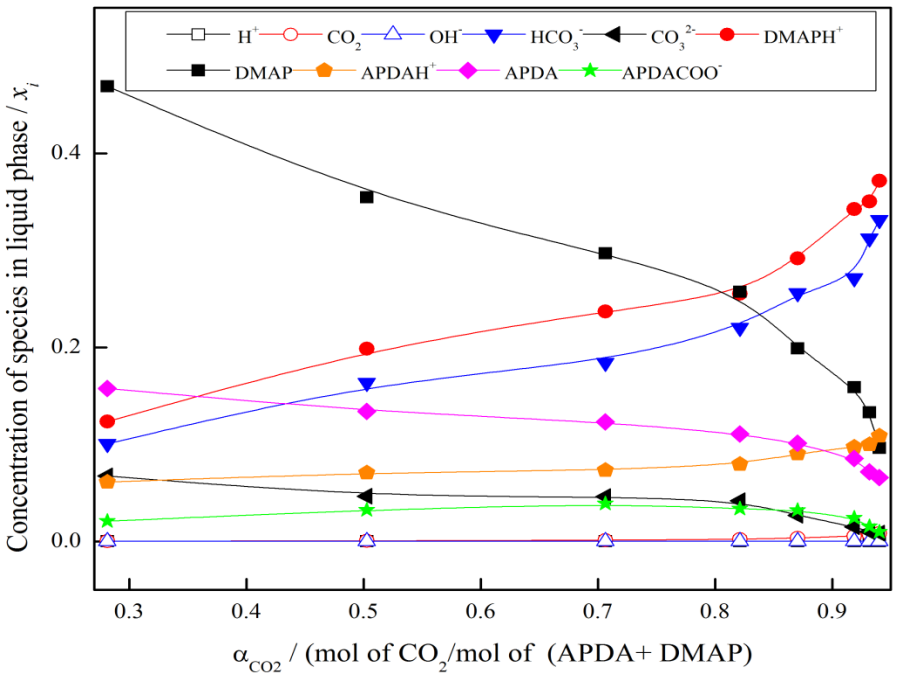

Fig. 5.9 Modified KE model predicted liquid phase ionic species profile as a function of in aqueous (0.08w APDA + 0.22w DMAP) at T = 323.2 K

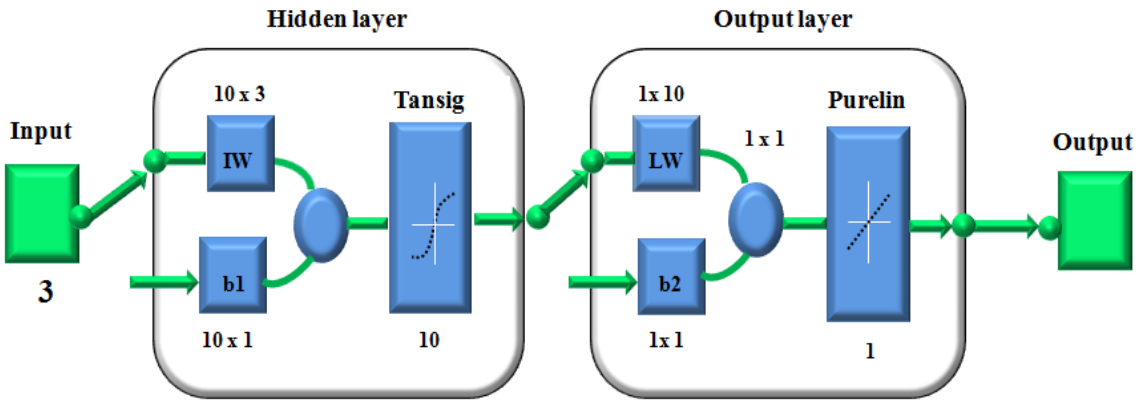

Fig. 5.10 Optimized ANN architecture used for the prediction of CO_2 solubility in aqueous APDA solution

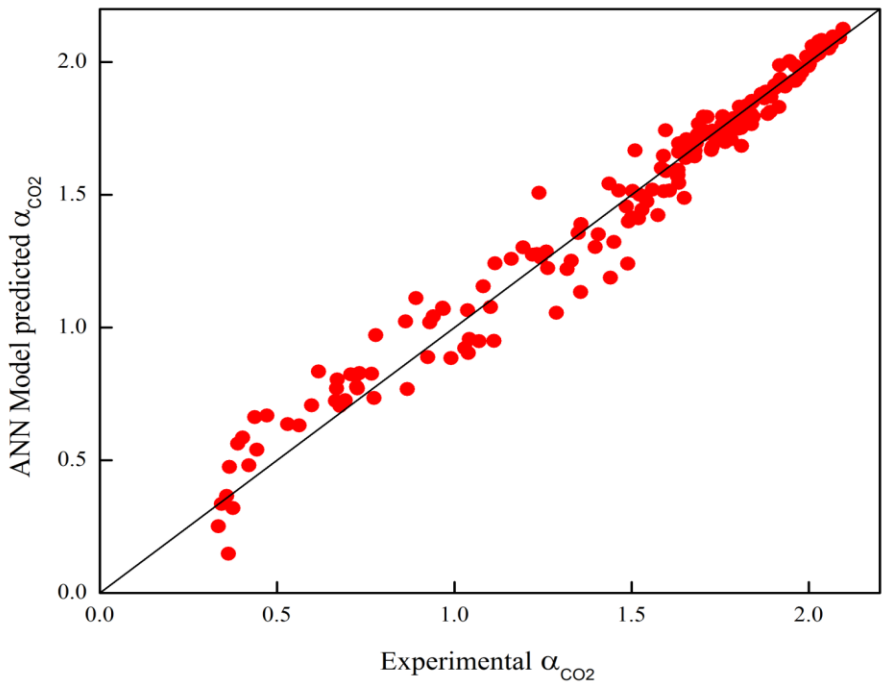

Fig. 5.11 Comparison plot of experimental vs ANN model predicted CO2 solubility data of aqueous APDA system

5.4.2 FTIR and ^{13}C NMR study

The FTIR spectra of CO_2 unloaded amine solvents are presented in Fig. 5.12. The primary amine group present in the APDA molecule shows characteristic vibration modes of N–H rocking at 1646.49 cm^{-1} and 1601.08 cm^{-1}. The intense peak at 1113.62 cm^{-1} represents C–N Stretching mode which is a characteristic of the secondary group present in the amine molecule. Along with this, the corresponding spectra at 1469.87 cm^{-1} and 961 cm^{-1} relates to out of plane wagging vibration of C-H and C-N-H bonds of aqueous APDA system. A significant contribution from symmetric and asymmetric stretching of $–CH_2$, $–CH_3$ and C–C bonds of AMP absorbs at 1371 and 1474 cm^{-1}, respectively for (APDA + AMP) system. While the prominent peak at 1027.36 cm^{-1} corresponding to (APDA +MDEA) system relates to C–O stretching mode, for AMP based blends the C–N and C–O stretching modes are closely overlapping at 1043 cm^{-1}. The significant peak observed at 914 cm^{-1} can be attributed to the $C–NH_2$ twisting mode [25]. The spectrum of the amine solvents corresponding to $\alpha_{CO2} = 0.8$ are presented in Fig. 5.13.

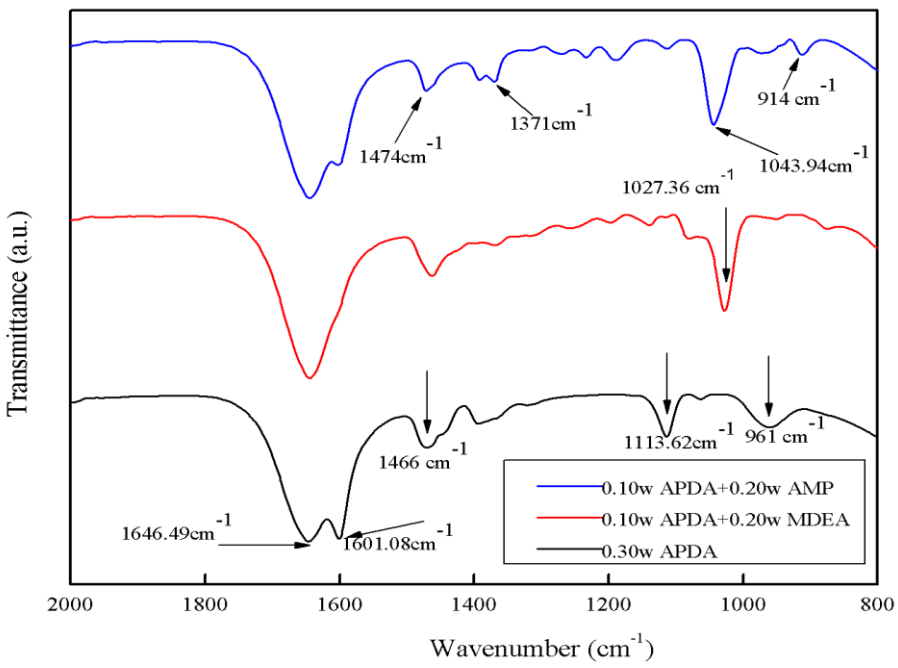

Fig. 5.12 FTIR-ATR Spectra of unloaded single and blended amine solvent

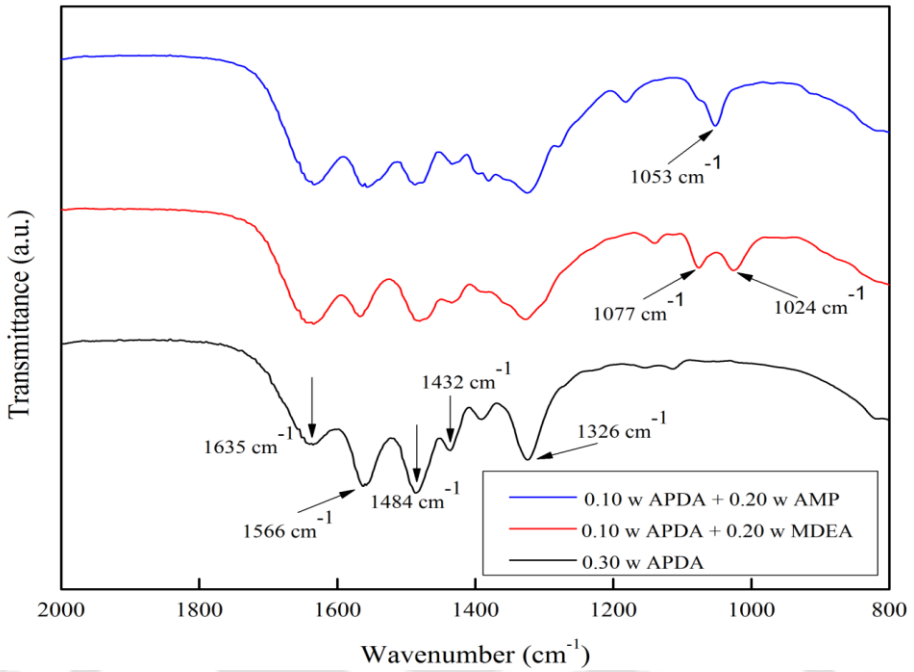

Fig. 5.13 FTIR-ATR Spectra of CO_2 loaded single and blended amine solvent at $\alpha_{CO_2} = 0.80$

New peaks observed at 1432, 1484 and 1566 cm^{-1} corresponds to the symmetric and asymmetric stretching vibration of COO^- and relates to the formation of carbamate species corresponding to APDA. While the intense peak at 1326 cm^{-1} has been conferred to N-COO^- stretching vibration of carbamate ions, all other peaks are more prominent in a single aqueous APDA system (Fig. 5.13). However, for the blended system, in addition to these peaks, the corresponding peaks at 1053, 1077 and 1024 cm^{-1} corresponds to the generation of protonated amine species [26].

A qualitative ^{13}C NMR has been also used to identify the various important reaction products of the blended systems of (APDA + MDEA) and (APDA + AMP) system. The analyses were carried out in D_2O solvent using 500 MHz NMR spectrometer (Ascend, Bruker). From both the spectra shown in Fig. 5.14, it can be envisaged that along with APDA carbamate, bicarbonate as well as carbonate species, are also prevalent in the blended system. In general, the peaks at (26-45 ppm) correspond to the various CH_2 groups of intermediate reactive carbamate species whereas the chemical shifts at (160-165 ppm) indicates the presence of bicarbonate/carbonate

species [8, 27-28]. This confirms the fact that, the blended system which involves non-carbamate forming base amines (MDEA/AMP) forms bicarbonate as the important reaction products.

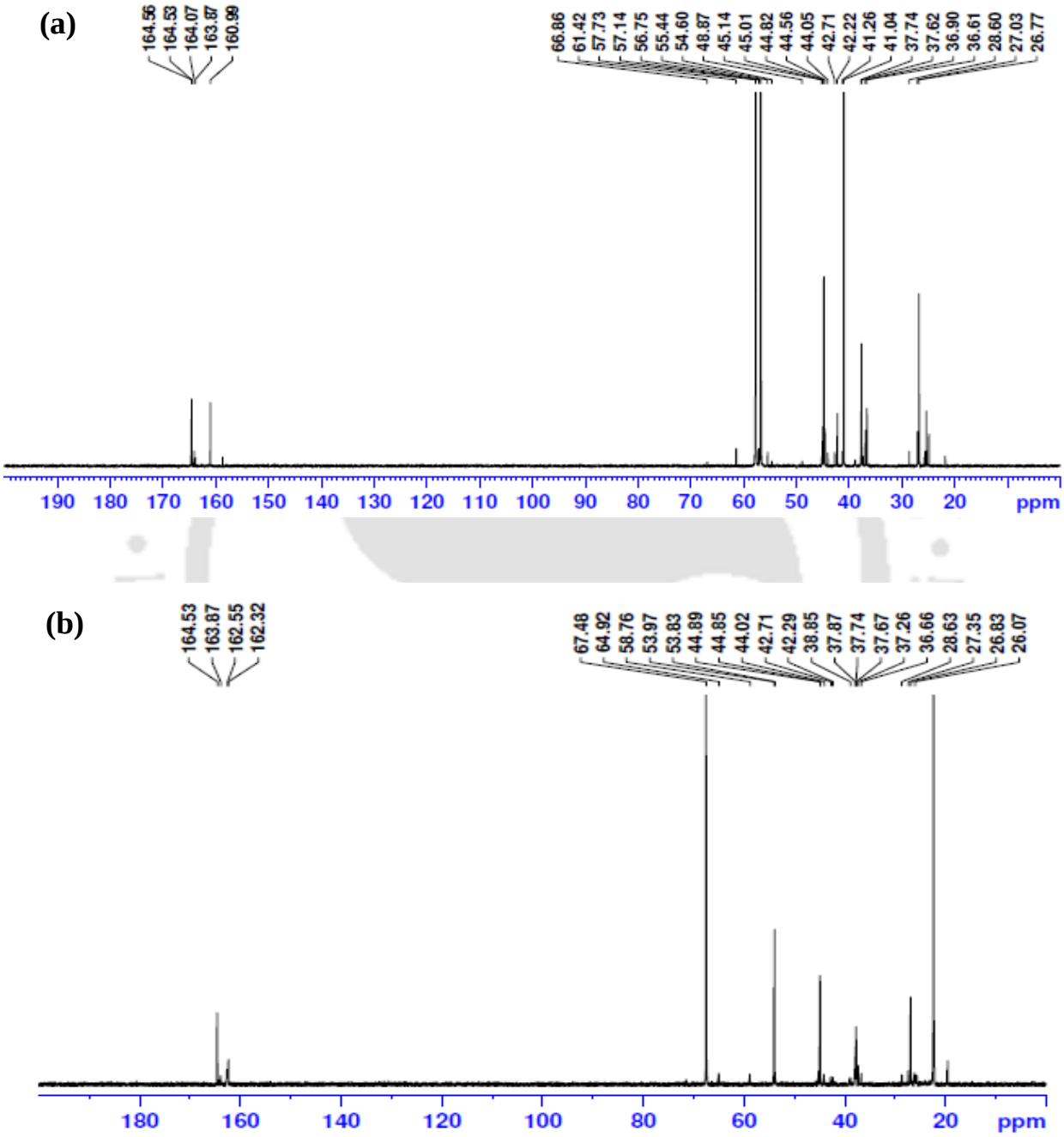

Fig. 5.14 ^{13}C NMR spectra of CO_2 absorbed aqueous blended (a) (0.10w APDA + 0.20w MDEA) (b) (0.10w APDA + 0.20w AMP) solvent system ($\alpha_{CO_2} = 0.80$)

In the case of AMP-based system, the HCO^{3-} and CO_3^{2-} can be mostly identified from the peaks at (162–164 ppm). The reaction scheme mainly follows the zwitterion mechanism which results in the formation of unstable carbamate owing to the steric hindrance effect posed by the bulkier methyl groups associated with it. These carbamates gradually undergo hydrolysis to get converted into bicarbonate and free amine molecules resulting in higher CO_2 loading.

5.4.3 Comparison of solvent performance with other conventional amines/blends

The CO_2 solubility in aqueous 0.30 mass fraction APDA has been compared with the other conventional amines as well as activators at two pressures 50 kPa and 100 kPa and temperature T= 313 K (Fig. 5.15). The results indicate that the equilibrium solubility of CO_2 in aqueous APDA is 3 times higher than the solubility of benchmarked MEA [33] at both the pressure. Also, it showcases higher solubility compared to other popular polyamine-based activators [5, 10, 20].

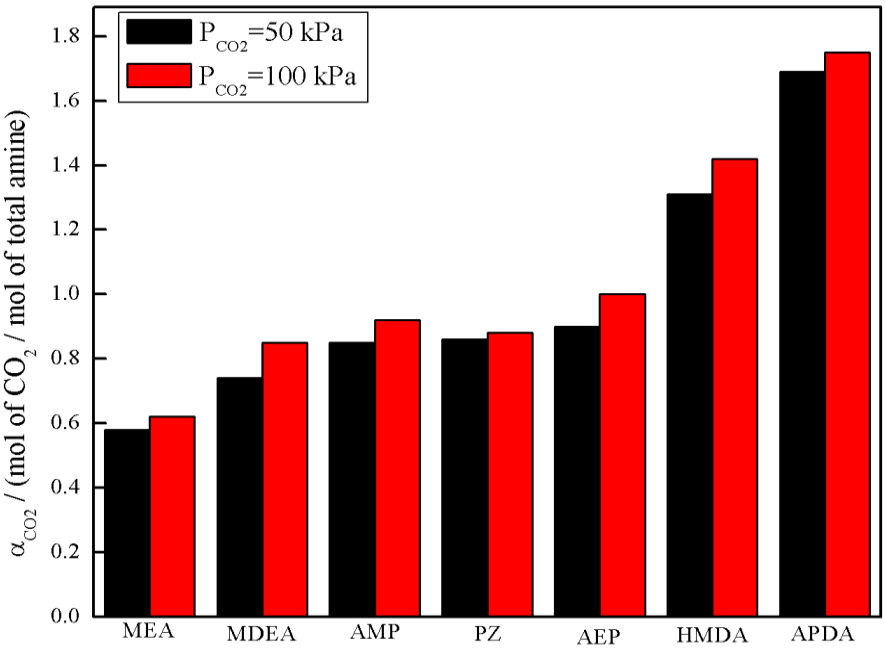

Fig. 5.15 Comparison of APDA solvent with other conventional amines at T= 313.2 K and composition of 0.30 w

The results show that at 50 kPa, the CO_2 loading capacity of APDA is 22% higher than hexamethylenediamine (HMDA), 46 % higher than 1-(2-aminoethyl) piperazine (AEP) and 49 % higher than piperazine (PZ) at similar conditions. The higher loading can be the result of six electron donating alkyl group present in the APDA molecule, two amine groups at either end cannot affect each other and are equally reactive with higher pKa value (10.85). Also the basicity of APDA is higher compared to other conventional amines and hence undergoes the zwitterion deprotonation faster resulting in higher equilibrium solubility [11].

The CO_2 solubility in aqueous (0.04 APDA+ 0.26 MDEA/AMP/DMAP) have also been compared with some of the benchmarked solvent blends viz. (0.05 PZ + 0.25 MDEA/AMP) [29-30] and (0.04 MEA + 0.26 MDEA/AMP) [31-32] at 313.2 K and are shown in Fig. 5.16.

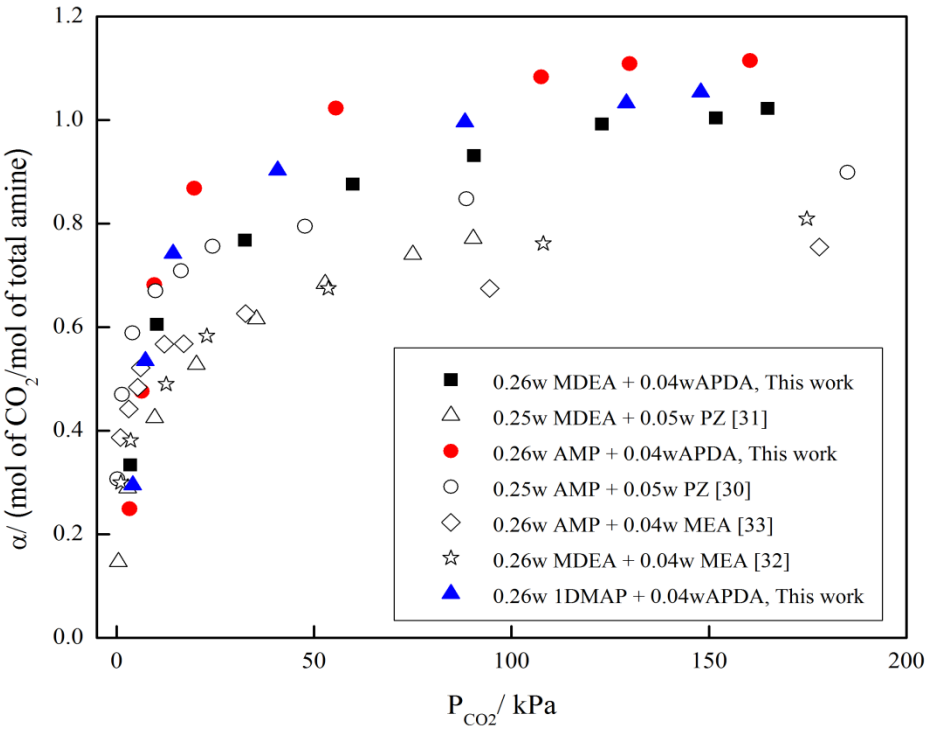

Fig. 5.16 Comparison of APDA based blend with other conventional solvent blend at T= 313.2 K and total composition of 0.30 w

It can be inferred from the figure that the blend of (APDA+AMP) outperforms all the solvent blends while the (PZ+AMP) blend is somewhat comparable with (APDA + MDEA) at pressure up to 80 kPa and CO_2 loading of 0.80. However at higher P_{CO_2}, the equilibrium CO_2 solubility in (0.04*w* APDA+ 0.26*w* MDEA) is substantially higher than the α_{CO_2} in (0.05*w* PZ + 0.25*w* MDEA/AMP). The equilibrium CO_2 solubility in the aqueous blended system is compared with the base solvent AMP, MDEA and DMAP in Fig. 5.17. It can be inferred from the figure that upon substitution of 0.10 mass fraction APDA in the total solvent blend of 0.30 mass fraction, the equilibrium solubility enhanced by 22 % for (APDA + AMP) and 15 % for (APDA+ MDEA) compared to single aqueous amines.

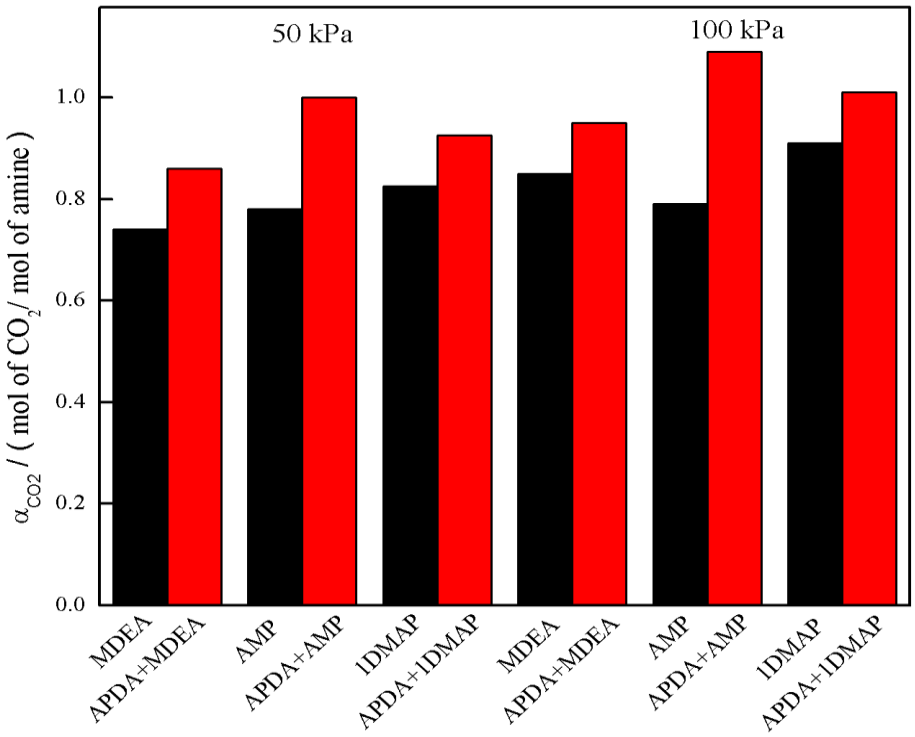

Fig. 5.17 Comparison of APDA activated solvent with base solvent at T= 313.2 K

5.5 Conclusions

The equilibrium CO_2 solubility in four potential amine system viz., aqueous APDA as well as its potential blends with MDEA, AMP and DMAP having overall eighteen different relative compositions were investigated over a broad temperature and pressure range. From the results, it can be clearly inferred that, the loading capacity enhances substantially upon the addition of APDA as an activator. The experimental results are well validated using both equilibrium based KE model as well as back propagation based ANN model. The estimated equilibrium constants of important amine based reactions have been used to predict the CO_2 solubility over the whole domain of experimentation. The significant prediction ability of the model can be inferred from the reasonable (% AAD) value of 11.09 % for aqueous APDA and 10.14 %, 7.47 %, 8.35 % for APDA activated aqueous AMP, MDEA and DMAP systems. Furthermore, the optimized ANN model developed for the present amine system could be useful in predicting the CO_2 solubility in the entire experimental domain. FTIR-ATR and qualitative ^{13}C NMR analysis of the blended solvent systems confirmed the existence of protonated species, carbamate as well as bicarbonate ions in the reaction medium. As per the CO_2 solubility study, the blends of (APDA + AMP) shows highest CO_2 loading of 1.173 at 164.3 kPa and 303.2 K compared to 1.097 at 174.1 kPa and 303.2 kPa for (APDA + MDEA) system. Hence based on superior solubility as well as kinetics of (APDA + AMP) blends, it can be further investigated for determining other parameters such as regeneration energy requirement, amine degradation study etc. Finally, comprehensive comparison with other conventional benchmark solvent reveals that both the single and blended system exhibits higher loading capacity compared to other solvent systems.

Table 5.1 Technical specification of the reagents used in the present work

Alias	Chemical	Source	Purity (Mass fraction)	Method of Purification
CO_2	Carbondioxide gas	Linde India Ltd.	>99 %	None
APDA	*N*-(3-Aminopropyl)-1,3-propanediamine 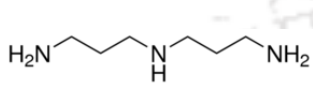	Sigma Aldrich Co.	98 %	None
MDEA	*N*-methyldiethanolamine 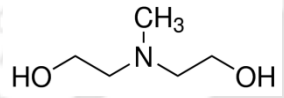	Sigma Aldrich Co.	99 %	None
AMP	2-Amino-2-methyl-1-Propanol 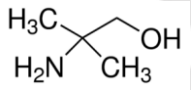	Sigma Aldrich Co.	95 %	None

Table 5.2 Modified KE model based equilibrium constant parameters and Henrys constant parameter

$\ln K_3 = \left(87.397 - \frac{8483.95}{T} - 13.833 \ln T\right)$ (kmol.m^{-3})	[9]
$\ln K_4 = \left(\frac{-7261.78}{T} - 22.477 \ln T + 142.58\right)$ (kmol.m^{-3})	[10]
$\ln K_5 = \left(220.067 - \frac{12431.7}{T} - 35.482 \ln T\right)$ (kmol.m^{-3})	[10]
$\ln K_6 = \left(235.485 - \frac{12092.1}{T} - 36.782 \ln T\right)$ (kmol.m^{-3})	[10]
$\ln K_7 = \left(140.932 - \frac{13445.9}{T} - 22.477 \ln T\right)$ (kmol.m^{-3})	[10]
$\ln H_{CO2} = \left(20.2669 - \frac{1.38306 \times 10^4}{T} + \frac{0.06913 \times 10^8}{T^2} - \frac{0.015589 \times 10^{11}}{T^3} + \frac{0.012 \times 10^{13}}{T^4}\right)$ (kPa.m^3.kmol^{-1})	[10]

Table 5.3 Solubility data of CO_2 in aqueous 0.10*w* APDA solution at equilibrium state

T/K	Mass Fraction (AEP)	Mass Fraction (H_2O)	P_{CO_2} / *kPa*	α_{CO_2}
	0.1	0.9	1.931	0.925
	0.1	0.9	26.958	1.791
	0.1	0.9	79.221	2.019
	0.1	0.9	119.141	2.068
	0.1	0.9	166.784	2.087
303.2	0.1	0.9	201.878	2.096
	0.1	0.9	2.896	0.867
	0.1	0.9	23.511	1.584
	0.1	0.9	83.702	1.98
	0.1	0.9	136.516	2.009
	0.1	0.9	170.507	2.028
313.2	0.1	0.9	198.5	2.036
	0.1	0.9	3.516	0.773
	0.1	0.9	46.471	1.522
	0.1	0.9	115.142	1.81
	0.1	0.9	146.238	1.884
323.2	0.1	0.9	179.746	1.904

Table 5.4 Solubility data of CO_2 in aqueous 0.15*w* APDA solution at equilibrium state

T/K	Mass Fraction (AEP)	Mass Fraction (H_2O)	P_{CO_2} / *kPa*	α_{CO_2}
	0.15	0.85	2.206	0.732
	0.15	0.85	10.549	1.543
	0.15	0.85	33.44	1.843
	0.15	0.85	80.807	1.946
	0.15	0.85	118.797	2.028
	0.15	0.85	161.337	2.056
303.2	0.15	0.85	179.677	2.063
	0.15	0.85	3.241	0.725
	0.15	0.85	15.306	1.239
	0.15	0.85	49.366	1.702
	0.15	0.85	103.283	1.917
	0.15	0.85	137.964	1.978
	0.15	0.85	164.923	1.999
313.2	0.15	0.85	201.051	2.002
	0.15	0.85	3.93	0.665
	0.15	0.85	11.307	1.194
	0.15	0.85	33.853	1.436
	0.15	0.85	77.911	1.631
	0.15	0.85	133.069	1.772
	0.15	0.85	160.51	1.84
323.2	0.15	0.85	185.4	1.878

Table 5.5 Solubility data of CO_2 in aqueous 0.20*w* APDA solution at equilibrium state

T/K	Mass Fraction (AEP)	Mass Fraction (H_2O)	P_{CO_2} / *kPa*	α_{CO_2}
	0.2	0.8	2.275	0.597
	0.2	0.8	4.275	1.112
	0.2	0.8	10.342	1.491
	0.2	0.8	32.543	1.795
	0.2	0.8	73.36	1.919
	0.2	0.8	126.381	1.961
	0.2	0.8	159.889	1.994
303.2	0.2	0.8	182.091	2.017
	0.2	0.8	2.689	0.562
	0.2	0.8	5.309	1.07
	0.2	0.8	8.894	1.489
	0.2	0.8	50.194	1.757
	0.2	0.8	114.453	1.893
	0.2	0.8	152.374	1.933
	0.2	0.8	170.99	1.962
313.2	0.2	0.8	199.396	1.972
	0.2	0.8	4.206	0.53
	0.2	0.8	6.826	1.03
	0.2	0.8	10.549	1.44
	0.2	0.8	34.681	1.633
	0.2	0.8	111.419	1.728
	0.2	0.8	141.549	1.809
323.2	0.2	0.8	167.06	1.823

Table 5.6 Solubility data of CO_2 in aqueous 0.25*w* APDA solution at equilibrium state

T/K	Mass Fraction (AEP)	Mass Fraction (H_2O)	P_{CO_2} / *kPa*	α_{CO_2}
	0.25	0.75	2.482	0.471
	0.25	0.75	5.378	0.931
	0.25	0.75	8.618	1.259
	0.25	0.75	18.823	1.59
	0.25	0.75	55.503	1.804
	0.25	0.75	108.041	1.866
	0.25	0.75	146.858	1.913
303.2	0.25	0.75	176.161	1.957
	0.25	0.75	2.827	0.443
	0.25	0.75	6.826	0.862
	0.25	0.75	10.135	1.22
	0.25	0.75	15.996	1.503
	0.25	0.75	57.64	1.705
	0.25	0.75	104.938	1.814
	0.25	0.75	136.585	1.874
	0.25	0.75	166.439	1.906
313.2	0.25	0.75	191.261	1.922
	0.25	0.75	5.792	0.437
	0.25	0.75	9.032	0.778
	0.25	0.75	11.928	1.081
	0.25	0.75	15.651	1.397
	0.25	0.75	26.821	1.649
	0.25	0.75	80.531	1.725
	0.25	0.75	134.034	1.781
323.2	0.25	0.75	163.544	1.802

Table 5.7 Solubility data of CO_2 in aqueous 0.30*w* APDA solution at equilibrium state

T/K	Mass Fraction (AEP)	Mass Fraction (H_2O)	P_{CO_2} / *kPa*	α_{CO_2}
	0.30	0.70	1.655	0.389
	0.30	0.70	3.034	0.726
	0.30	0.70	4.482	1.042
	0.30	0.70	6.136	1.356
	0.30	0.70	26.338	1.596
	0.30	0.70	61.501	1.755
	0.30	0.70	112.591	1.838
	0.30	0.70	145.893	1.891
303.2	0.30	0.70	174.024	1.915
	0.30	0.70	2.551	0.358
	0.30	0.70	5.861	0.708
	0.30	0.70	8.481	1.102
	0.30	0.70	11.032	1.330
	0.30	0.70	15.031	1.574
	0.30	0.70	44.195	1.678
	0.30	0.70	95.699	1.743
	0.30	0.70	130.242	1.807
	0.30	0.70	164.302	1.823
313.2	0.30	0.70	199.603	1.839
	0.30	0.70	5.033	0.420
	0.30	0.70	7.929	0.767
	0.30	0.70	10.825	1.037
	0.30	0.70	13.583	1.318
	0.30	0.70	16.203	1.450
	0.30	0.70	27.993	1.559
	0.30	0.70	74.119	1.633
	0.30	0.70	120.382	1.686
323.2	0.30	0.70	161.199	1.702

Table 5.8 Solubility data of CO_2 in aqueous 0.35*w* APDA solution at equilibrium state

T/K	Mass Fraction (AEP)	Mass Fraction (H_2O)	P_{CO_2} / *kPa*	α_{CO_2}
	0.35	0.65	1.931	0.403
	0.35	0.65	3.447	0.722
	0.35	0.65	4.068	1.039
	0.35	0.65	5.309	1.288
	0.35	0.65	15.927	1.51
	0.35	0.65	45.988	1.654
	0.35	0.65	89.563	1.764
	0.35	0.65	134.241	1.81
303.2	0.35	0.65	168.715	1.837
	0.35	0.65	3.103	0.375
	0.35	0.65	6.619	0.67
	0.35	0.65	9.515	0.967
	0.35	0.65	12.824	1.233
	0.35	0.65	16.685	1.5
	0.35	0.65	29.027	1.629
	0.35	0.65	72.257	1.683
	0.35	0.65	93.838	1.732
	0.35	0.65	129.966	1.754
313.2	0.35	0.65	165.405	1.765
	0.35	0.65	3.999	0.334
	0.35	0.65	8.412	0.617
	0.35	0.65	11.859	0.892
	0.35	0.65	14.341	1.115
	0.35	0.65	17.582	1.349
	0.35	0.65	21.856	1.529
	0.35	0.65	29.096	1.606
	0.35	0.65	60.95	1.652
	0.35	0.65	132.241	1.669
323.2	0.35	0.65	154.512	1.679

Table 5.9 Solubility data of CO_2 in aqueous 0.40*w* APDA solution at equilibrium state

T/K	Mass Fraction (AEP)	Mass Fraction (H_2O)	P_{CO_2} / *kPa*	α_{CO_2}
	0.4	0.6	2.482	0.366
	0.4	0.6	3.93	0.678
	0.4	0.6	5.24	0.99
	0.4	0.6	8.481	1.263
	0.4	0.6	13.376	1.464
	0.4	0.6	15.582	1.597
	0.4	0.6	59.502	1.736
	0.4	0.6	111.419	1.787
303.2	0.4	0.6	153.477	1.817
	0.4	0.6	3.861	0.343
	0.4	0.6	6.55	0.692
	0.4	0.6	9.928	0.969
	0.4	0.6	12.824	1.244
	0.4	0.6	14.686	1.406
	0.4	0.6	16.341	1.519
	0.4	0.6	25.235	1.631
	0.4	0.6	67.431	1.689
	0.4	0.6	116.59	1.713
313.2	0.4	0.6	158.235	1.728
	0.4	0.6	3.792	0.363
	0.4	0.6	7.998	0.668
	0.4	0.6	10.756	0.941
	0.4	0.6	14.065	1.161
	0.4	0.6	17.306	1.357
	0.4	0.6	19.788	1.485
	0.4	0.6	23.028	1.591
	0.4	0.6	57.364	1.633
323.2	0.4	0.6	135.827	1.645

Table 5.10 Solubility data of CO_2 in aqueous (0.04*w* APDA+ 0.26*w* AMP) solution at equilibrium state

T/K	Mass Fraction (APDA)	Mass Fraction (AMP)	Mass Fraction (H_2O)	P_{CO_2} / *kPa*	α_{CO_2}
	0.04	0.26	0.7	4.413	0.26
	0.04	0.26	0.7	8.067	0.458
	0.04	0.26	0.7	12.48	0.639
	0.04	0.26	0.7	23.511	0.81
	0.04	0.26	0.7	61.915	0.97
	0.04	0.26	0.7	99.56	1.021
	0.04	0.26	0.7	140.033	1.063
303.2	0.04	0.26	0.7	161.613	1.077
	0.04	0.26	0.7	3.378	0.231
	0.04	0.26	0.7	6.688	0.441
	0.04	0.26	0.7	11.101	0.651
	0.04	0.26	0.7	20.546	0.829
	0.04	0.26	0.7	51.849	0.926
	0.04	0.26	0.7	89.563	0.971
	0.04	0.26	0.7	133	0.997
313.2	0.04	0.26	0.7	164.509	1.01
	0.04	0.26	0.7	3.93	0.22
	0.04	0.26	0.7	7.86	0.417
	0.04	0.26	0.7	14.893	0.6
	0.04	0.26	0.7	35.991	0.759
	0.04	0.26	0.7	77.704	0.855
	0.04	0.26	0.7	106.317	0.904
	0.04	0.26	0.7	135.068	0.928
323.2	0.04	0.26	0.7	152.788	0.939

Table 5.11 Solubility data of CO_2 in aqueous (0.07*w* APDA+ 0.23*w* AMP) solution at equilibrium state

T/K	Mass Fraction (APDA)	Mass Fraction (AMP)	Mass Fraction (H_2O)	P_{CO_2} / *kPa*	α_{CO_2}
	0.07	0.23	0.7	3.241	0.259
	0.07	0.23	0.7	6.205	0.483
	0.07	0.23	0.7	9.86	0.682
	0.07	0.23	0.7	19.581	0.869
	0.07	0.23	0.7	54.882	0.996
	0.07	0.23	0.7	104.662	1.073
	0.07	0.23	0.7	126.726	1.101
303.2	0.07	0.23	0.7	158.993	1.113
	0.07	0.23	0.7	3.309	0.259
	0.07	0.23	0.7	6.964	0.5
	0.07	0.23	0.7	12.755	0.719
	0.07	0.23	0.7	28.613	0.919
	0.07	0.23	0.7	47.85	1.008
	0.07	0.23	0.7	95.837	1.044
	0.07	0.23	0.7	125.691	1.053
313.2	0.07	0.23	0.7	157.752	1.06
	0.07	0.23	0.7	2.827	0.244
	0.07	0.23	0.7	6.826	0.445
	0.07	0.23	0.7	11.928	0.614
	0.07	0.23	0.7	29.923	0.781
	0.07	0.23	0.7	66.603	0.863
	0.07	0.23	0.7	105.076	0.925
	0.07	0.23	0.7	140.584	0.961
323.2	0.07	0.23	0.7	160.027	0.986

Table 5.12 Solubility data of CO_2 in aqueous (0.10*w* APDA+ 0.20*w* AMP) solution at equilibrium state

T/K	Mass Fraction (APDA)	Mass Fraction (AMP)	Mass Fraction (H_2O)	P_{CO_2} / *kPa*	α_{CO_2}
	0.1	0.2	0.7	2.62	0.275
	0.1	0.2	0.7	5.033	0.515
	0.1	0.2	0.7	8.205	0.769
	0.1	0.2	0.7	15.582	1
	0.1	0.2	0.7	39.231	1.114
	0.1	0.2	0.7	90.804	1.147
	0.1	0.2	0.7	134.103	1.163
303.2	0.1	0.2	0.7	164.302	1.173
	0.1	0.2	0.7	3.309	0.249
	0.1	0.2	0.7	6.412	0.476
	0.1	0.2	0.7	9.584	0.682
	0.1	0.2	0.7	19.65	0.868
	0.1	0.2	0.7	55.572	1.023
	0.1	0.2	0.7	107.558	1.083
	0.1	0.2	0.7	129.897	1.109
313.2	0.1	0.2	0.7	160.441	1.115
	0.1	0.2	0.7	3.103	0.225
	0.1	0.2	0.7	6.274	0.468
	0.1	0.2	0.7	12.066	0.657
	0.1	0.2	0.7	15.444	0.841
	0.1	0.2	0.7	54.538	0.956
	0.1	0.2	0.7	99.56	0.998
	0.1	0.2	0.7	126.588	1.034
323.2	0.1	0.2	0.7	154.925	1.047

Table 5.13 Solubility data of CO_2 in aqueous (0.04*w* APDA+ 0.26*w* MDEA) solution at equilibrium state

T/K	Mass Fraction (APDA)	Mass Fraction (MDEA)	Mass Fraction (H_2O)	P_{CO_2} / *kPa*	α_{CO_2}
	0.04	0.26	0.7	4.275	0.354
	0.04	0.26	0.7	12.548	0.602
	0.04	0.26	0.7	28.751	0.804
	0.04	0.26	0.7	59.433	0.938
	0.04	0.26	0.7	99.353	0.986
	0.04	0.26	0.7	133.689	1.01
	0.04	0.26	0.7	153.546	1.026
303.2	0.04	0.26	0.7	175.127	1.04
	0.04	0.26	0.7	3.723	0.315
	0.04	0.26	0.7	12.273	0.578
	0.04	0.26	0.7	33.164	0.768
	0.04	0.26	0.7	67.775	0.836
	0.04	0.26	0.7	107.007	0.889
	0.04	0.26	0.7	133.827	0.929
	0.04	0.26	0.7	152.374	0.947
313.2	0.04	0.26	0.7	164.026	0.956
	0.04	0.26	0.7	4.275	0.301
	0.04	0.26	0.7	16.754	0.554
	0.04	0.26	0.7	45.161	0.749
	0.04	0.26	0.7	77.773	0.839
	0.04	0.26	0.7	107.696	0.869
	0.04	0.26	0.7	134.586	0.883
	0.04	0.26	0.7	161.199	0.892
323.2	0.04	0.26	0.7	174.162	0.903

Table 5.14 Solubility data of CO_2 in aqueous (0.07*w* APDA+ 0.23*w* MDEA) solution at equilibrium state

T/K	Mass Fraction (APDA)	Mass Fraction (MDEA)	Mass Fraction (H_2O)	P_{CO_2} / *kPa*	α_{CO_2}
	0.07	0.23	0.7	3.447	0.373
	0.07	0.23	0.7	8.963	0.608
	0.07	0.23	0.7	22.477	0.817
	0.07	0.23	0.7	56.33	0.949
	0.07	0.23	0.7	89.701	1.01
	0.07	0.23	0.7	126.174	1.041
	0.07	0.23	0.7	155.408	1.063
303.2	0.07	0.23	0.7	173.334	1.08
	0.07	0.23	0.7	3.309	0.35
	0.07	0.23	0.7	11.307	0.59
	0.07	0.23	0.7	32.267	0.678
	0.07	0.23	0.7	62.398	0.809
	0.07	0.23	0.7	89.218	0.872
	0.07	0.23	0.7	116.521	0.935
	0.07	0.23	0.7	146.376	0.949
313.2	0.07	0.23	0.7	163.268	0.981
	0.07	0.23	0.7	3.999	0.328
	0.07	0.23	0.7	12.411	0.587
	0.07	0.23	0.7	32.13	0.701
	0.07	0.23	0.7	67.844	0.804
	0.07	0.23	0.7	104.938	0.876
	0.07	0.23	0.7	126.657	0.92
	0.07	0.23	0.7	148.375	0.94
323.2	0.07	0.23	0.7	167.543	0.941

Table 5.15 Solubility data of CO_2 in aqueous (0.10*w* APDA+ 0.20*w* MDEA) solution at equilibrium state

T/K	Mass Fraction (APDA)	Mass Fraction (MDEA)	Mass Fraction (H_2O)	P_{CO_2} / *kPa*	α_{CO_2}
	0.1	0.2	0.7	3.034	0.359
	0.1	0.2	0.7	6.964	0.625
	0.1	0.2	0.7	20.822	0.881
	0.1	0.2	0.7	54.469	1.028
	0.1	0.2	0.7	87.081	1.066
	0.1	0.2	0.7	131.897	1.08
	0.1	0.2	0.7	154.374	1.092
303.2	0.1	0.2	0.7	174.093	1.097
	0.1	0.2	0.7	3.447	0.334
	0.1	0.2	0.7	10.204	0.605
	0.1	0.2	0.7	32.474	0.768
	0.1	0.2	0.7	59.778	0.876
	0.1	0.2	0.7	90.459	0.931
	0.1	0.2	0.7	122.934	0.992
	0.1	0.2	0.7	151.754	1.004
313.2	0.1	0.2	0.7	164.854	1.022
	0.1	0.2	0.7	3.447	0.306
	0.1	0.2	0.7	9.446	0.579
	0.1	0.2	0.7	28.406	0.731
	0.1	0.2	0.7	64.397	0.813
	0.1	0.2	0.7	90.39	0.903
	0.1	0.2	0.7	119.21	0.947
	0.1	0.2	0.7	147.272	0.954
323.2	0.1	0.2	0.7	166.991	0.97

Table 5.16 Solubility data of CO_2 in aqueous (0.02*w* APDA+ 0.28*w* DMAP) solution at equilibrium state

T/K	Mass Fraction (APDA)	Mass Fraction (DMAP)	Mass Fraction (H_2O)	P_{CO_2} / *kPa*	α_{CO_2}
	0.02	0.28	0.7	4.826	0.332
	0.02	0.28	0.7	7.998	0.583
	0.02	0.28	0.7	15.1	0.826
	0.02	0.28	0.7	42.541	0.924
	0.02	0.28	0.7	85.15	0.966
	0.02	0.28	0.7	131.966	1
303.2	0.02	0.28	0.7	147.341	1.009
	0.02	0.28	0.7	4.413	0.289
	0.02	0.28	0.7	7.722	0.506
	0.02	0.28	0.7	19.305	0.678
	0.02	0.28	0.7	48.953	0.822
	0.02	0.28	0.7	94.803	0.888
	0.02	0.28	0.7	137.55	0.905
313.2	0.02	0.28	0.7	159.82	0.922
	0.02	0.28	0.7	5.171	0.271
	0.02	0.28	0.7	9.653	0.454
	0.02	0.28	0.7	27.234	0.638
	0.02	0.28	0.7	52.469	0.739
	0.02	0.28	0.7	100.87	0.807
	0.02	0.28	0.7	123.278	0.838
	0.02	0.28	0.7	152.581	0.845
323.2	0.02	0.28	0.7	164.095	0.857

Table 5.17 Solubility data of CO_2 in aqueous (0.04*w* APDA+ 0.26*w* DMAP) solution at equilibrium state

T/K	Mass Fraction (APDA)	Mass Fraction (DMAP)	Mass Fraction (H_2O)	P_{CO_2} / *kPa*	α_{CO_2}
	0.04	0.26	0.7	3.93	0.305
	0.04	0.26	0.7	7.86	0.542
	0.04	0.26	0.7	16.616	0.803
	0.04	0.26	0.7	48.884	0.937
	0.04	0.26	0.7	87.219	1.001
	0.04	0.26	0.7	126.726	1.028
303.2	0.04	0.26	0.7	152.098	1.058
	0.04	0.26	0.7	4.344	0.257
	0.04	0.26	0.7	8.549	0.539
	0.04	0.26	0.7	21.236	0.761
	0.04	0.26	0.7	50.952	0.866
	0.04	0.26	0.7	85.702	0.911
	0.04	0.26	0.7	129.828	0.924
	0.04	0.26	0.7	151.616	0.945
313.2	0.04	0.26	0.7	167.267	0.952
	0.04	0.26	0.7	5.998	0.248
	0.04	0.26	0.7	8.687	0.47
	0.04	0.26	0.7	24.27	0.664
	0.04	0.26	0.7	45.919	0.76
	0.04	0.26	0.7	92.321	0.802
	0.04	0.26	0.7	117.694	0.862
	0.04	0.26	0.7	147.755	0.879
323.2	0.04	0.26	0.7	156.925	0.899

Table 5.18 Solubility data of CO_2 in aqueous (0.06*w* APDA+ 0.24*w* DMAP) solution at equilibrium state

T/K	Mass Fraction (APDA)	Mass Fraction (DMAP)	Mass Fraction (H_2O)	P_{CO_2} / *kPa*	α_{CO_2}
	0.06	0.24	0.7	4.344	0.323
	0.06	0.24	0.7	7.653	0.575
	0.06	0.24	0.7	12.617	0.828
	0.06	0.24	0.7	31.509	0.957
	0.06	0.24	0.7	75.084	1.029
	0.06	0.24	0.7	110.937	1.055
303.2	0.06	0.24	0.7	140.929	1.06
	0.06	0.24	0.7	5.378	0.234
	0.06	0.24	0.7	9.101	0.552
	0.06	0.24	0.7	20.133	0.759
	0.06	0.24	0.7	56.468	0.887
	0.06	0.24	0.7	105.49	0.95
	0.06	0.24	0.7	134.655	0.967
313.2	0.06	0.24	0.7	156.304	0.974
	0.06	0.24	0.7	5.516	0.27
	0.06	0.24	0.7	10.411	0.5
	0.06	0.24	0.7	18.823	0.698
	0.06	0.24	0.7	38.611	0.807
	0.06	0.24	0.7	73.498	0.867
	0.06	0.24	0.7	115.142	0.902
	0.06	0.24	0.7	132.31	0.915
323.2	0.06	0.24	0.7	153.822	0.922

Table 5.19 Solubility data of CO_2 in aqueous (0.08*w* APDA+ 0.22*w* DMAP) solution at equilibrium state

T/K	Mass Fraction (APDA)	Mass Fraction (DMAP)	Mass Fraction (H_2O)	P_{CO_2} / *kPa*	α_{CO_2}
	0.08	0.22	0.7	3.103	0.334
	0.08	0.22	0.7	6.343	0.588
	0.08	0.22	0.7	14.617	0.788
	0.08	0.22	0.7	34.336	0.971
	0.08	0.22	0.7	73.291	1.044
	0.08	0.22	0.7	108.799	1.071
303.2	0.08	0.22	0.7	133.62	1.093
	0.08	0.22	0.7	4.206	0.243
	0.08	0.22	0.7	7.86	0.562
	0.08	0.22	0.7	17.03	0.738
	0.08	0.22	0.7	48.47	0.889
	0.08	0.22	0.7	83.978	0.973
	0.08	0.22	0.7	128.932	0.99
	0.08	0.22	0.7	152.995	1.002
313.2	0.08	0.22	0.7	168.301	1.02
	0.08	0.22	0.7	4.757	0.281
	0.08	0.22	0.7	8.205	0.503
	0.08	0.22	0.7	18.271	0.706
	0.08	0.22	0.7	37.025	0.821
	0.08	0.22	0.7	59.157	0.87
	0.08	0.22	0.7	96.458	0.919
	0.08	0.22	0.7	127.898	0.932
323.2	0.08	0.22	0.7	149.892	0.94

Table 5.20 Solubility data of CO_2 in aqueous (0.10*w* APDA+ 0.20*w* DMAP) solution at equilibrium state

T/K	Mass Fraction (APDA)	Mass Fraction (DMAP)	Mass Fraction (H_2O)	P_{CO_2} / *kPa*	α_{CO_2}
	0.1	0.2	0.7	3.861	0.334
	0.1	0.2	0.7	6.274	0.586
	0.1	0.2	0.7	13.996	0.793
	0.1	0.2	0.7	30.957	1.007
	0.1	0.2	0.7	75.842	1.089
	0.1	0.2	0.7	107.007	1.114
303.2	0.1	0.2	0.7	131.483	1.134
	0.1	0.2	0.7	4.068	0.295
	0.1	0.2	0.7	7.308	0.535
	0.1	0.2	0.7	14.272	0.742
	0.1	0.2	0.7	40.748	0.903
	0.1	0.2	0.7	88.253	0.996
	0.1	0.2	0.7	129.07	1.033
313.2	0.1	0.2	0.7	147.961	1.054
	0.1	0.2	0.7	3.861	0.267
	0.1	0.2	0.7	7.239	0.493
	0.1	0.2	0.7	15.237	0.7
	0.1	0.2	0.7	41.92	0.856
	0.1	0.2	0.7	89.908	0.926
	0.1	0.2	0.7	124.244	0.951
323.2	0.1	0.2	0.7	148.582	0.963

References

[1] A.A. Olajire, CO_2 capture and separation technologies for end-of-pipe applications-A review, Energy 35 (2010) 2610-2628.

[2] H. Najibi, N. Malek, Equilibrium solubility of carbon dioxide in N-methyldiethanolamine + piperazine aqueous solution: Experimental measurement and prediction, Fluid Phase Equilib. 354 (2013) 298–303.

[3] S.K. Dash, A.N. Samanta, S.S. Bandyopadhyay, Simulation and parametric study of the post combustion CO_2 capture using aqueous 2-amino-2-methyl-1propanol and piperazine, Int. J. Greenh. Gas Control 21 (2014) 130-139.

[4] A. Dey, S.K. Dash, B.P. Mandal, Equilibrium CO_2 solubility and thermophysical properties of aqueous blends of 1-(2-aminoethyl) piperazine and N-methyldiethanolamine, Fluid Phase Equilib. 463 (2018) 91-105.

[5] A. Dey, S.K. Dash, S. Balchandani, B. Mandal, Investigation on the inclusion of 1-(2-aminoethyl)piperazine as a promoter on the equilibrium CO_2 solubility of aqueous 2-amino-2-methyl-1-propanol, J. Mol. Liq. (2019).

[6] Z. Bouzina, F. Dergal, I. Mokbel, A. Negadi, J. Saab, J. Jose, L. Negadi, Liquid-vapor equilibria of pure and aqueous solutions of diethylenetriamine or dipropylenetriamine, Fluid phase Equilib. 414 (2016) 164-169.

[7] B. Das, B. Deogam, B. Mandal, Experimental and theoretical studies on efficient carbon dioxide capture using novel bis(3-aminopropyl)amine (APA)-activated aqueous 2-amino-2-methyl-1-propanol (AMP) solutions, Rsc Adv. 7 (2017) 21518–21530.

[8] B. Das, B. Deogam, B. Mandal, Absorption of CO_2 into novel aqueous bis (3-aminopropyl) amine and enhancement of CO_2 absorption into its blends with N-methyldiethanolamine, Int. J. Greenh. Gas Control 60 (2017) 172–185.

[9] X. Luo, N. Chen, S. Liu, W. Rongwong, R.O. Idema, P. Tontiwachwuthikul, Z. Liang, Experiments and modeling of vapor-liquid equilibrium data in DEEA-CO_2-H_2O system, Int. J. Greenh. Gas Control 53 (2016) 160–168.

[10] S.K. Dash, A.N. Samanta, S.S. Bandyopadhyay, Vapour liquid equilibria of carbon dioxide in dilute and concentrated aqueous solutions of piperazine at low to high pressure, Fluid Phase Equilib. 300 (2011) 145-154.

[11] B.K. Mondal, S.S. Bandyopadhyay, A.N. Samanta, Equilibrium solubility and enthalpy of CO_2 absorption in aqueous bis (3-aminopropyl) amine and its mixture with MEA, MDEA, AMP and K_2CO_3, Chem. Eng. Sci. 170 (2017) 58–67.

[12] S. Kadiwala, A.V. Rayer, A. Henni, Kinetics of carbon dioxide (CO_2) with ethylenediamine, 3-amino-1-propanol in methanol and ethanol, and with 1-dimethylamino-2-propanol and 3- dimethylamino-1-propanol in water using stopped-flow technique, Chem. Eng. J. 179 (2012) 262-271.

[13] Y. Liang, H. Liu, W. Rongwong, Z. Liang, R. Idem, P. Tontiwachwuthikul, Solubility, absorption heat and mass transfer studies of CO_2 absorption into aqueous solution of 1-dimethylamino-2-propanol, Fuel 144 (2015) 121-129.

[14] M. Afkhamipour, M. Mofarahi, A. Rezaei, R. Mahmoodi, C.H. Lee, Experimental and theoretical investigation of equilibrium absorption performance of CO_2 using a mixed 1-dimethylamino-2-propanol (1DMA2P) and monoethanolamine (MEA) solution, Fuel, 256 (2019) doi.org/10.1016/j.fuel.2019. 115877.

[15] Y.H. Hsu, R.B. Leron, M.H. Li, Solubility of carbon dioxide in aqueous mixtures of (reline + monoethanolamine) at T = (313.2 to 353.2) K, J. Chem. Thermodyn. 72 (2014) 94–99.

[16] H. Liu, C. Chan, P. Tontiwachwuthikul, R. Idem, Analysis of CO_2 equilibrium solubility of seven tertiary amine solvents using thermodynamic and ANN models, Fuel 249 (2019) 61-72.

[17] M.E. Hamzehie, S. Mazinani, F. Davardoost, A. Mokhtare, H. Najibi, B. Van der Bruggen, S. Darvishmanesh, Developing a feed forward multilayer neural network model for prediction of CO_2 solubility in blended aqueous amine solutions, J. Nat. Gas Sci. Eng. 21 (2014) 19-25.

[18] H. Pahlavanzadeh, S. Nourani, M. Saber, Experimental analysis and modeling of CO_2 solubility in AMP (2-amino-2-methyl-1-propanol) at low CO_2 partial pressure using the models of Deshmukh-Mather and the artificial neural network, J. Chem. Thermodyn. 43 (2011) 1775–1783.

[19] H. Saghafia, M. Arabloob , Modeling of CO_2 solubility in MEA, DEA, TEA, and MDEA aqueous solutions using AdaBoost-Decision Tree and Artificial Neural Network, Int. J. Greenh. Gas Cont. 58 (2017) 256-265.

[20] R.L.Kent, B. Eisenberg, Better data for amine treating, Hydrocarbon Process. 55 (1976) 87-90.

[21] B.K. Mondal, S.S. Bandyopadhyay, A.N. Samanta, Vapor–liquid equilibrium measurement and ENRTL modeling of CO_2 absorption in aqueous hexamethylenediamine, Fluid Phase Equilib. 402 (2015) 102–112.

[22] R.L. Kent, B. Eisenberg, Better data for amine treating, Hydrocarbon Process. 55 (1976) 87-90

[23] S. Garg, A.M. Shariff, M.S. Shaikh, B. Lal, H. Suleman, N. Faiqa, Experimental data , thermodynamic and neural network modeling of CO_2 solubility in aqueous sodium salt of L-phenylalanine, J. CO_2 Util. 19 (2017) 146–156.

[24] D. Tong, G.C. Maitland, M.J.P. Trusler, P.S. Fennell, Solubility of carbon dioxide in aqueous blends of 2-amino-2-methyl-1-propanol and piperazine, Chem. Eng. Sci. 101 (2013) 851–864.

[25] M.K. Wong, M.A. Bustam, A.M. Shariff, Chemical speciation of CO_2 absorption in aqueous monoethanolamine investigated by in situ Raman spectroscopy, Int. J. Greenh. Gas Control 39 (2015) 139–147.

[26] G. Richner, G. Puxty, Assessing the chemical speciation during CO_2 absorption by aqueous amines using in Situ FTIR, Ind. Eng. Chem. Res. 51 (2012) 14317-14324.

[27] C. Sun, P.K. Dutta, Infrared spectroscopic study of reaction of carbon dioxide with aqueous monoethanolamine solutions, Ind. Eng. Chem. Res. 55 (2016) 6276-6283.

[28] W. Bottinger, M. Maiwald, H. Hasse, Online NMR spectroscopic study of species distribution in MEA-H_2O-CO_2 and DEA-H_2O-CO_2, Fluid Phase Equilib. 263 (2008) 131-143

[29] Q. Ye, X. Wang, Y. Lu, Screening and evaluation of novel biphasic solvents for energy-efficient post –combustion CO_2 capture, Int. J. Greenh. Gas Control 39 (2015) 205-214.

[30] S.K. Dash, A.N. Samanta, S.S Bandyopadhyay, Solubility of carbon dioxide in aqueous solution of 2-amino-2-methyl-1-propanol and piperazine, Fluid Phase Equilib. 307 (2011), 166-174

[31] S.K. Dash, S.S. Bandyopadhyay, Studies on the effect of addition of piperazine and sulfolane into aqueous solution of N-methyldiethanolamine for CO_2 capture and VLE modelling using eNRTL equation, Int. J. Greenh. Gas Control 44 (2016) 227–237.

[32] K.P. Shen, M.H. Li, Solubility of carbon dioxide in aqueous mixtures of monoethanolamine with methyldiethanolamine, J. Chem. Eng. Data 37 (1992) 96–100.

[33] M. Li, B. Chang, Solubilities of carbon dioxide in water + monoethanolamine + 2- amino-2-methyl-1-propanol, J. Chem. Eng. Data 39 (1994) 448-452.

Chapter 6

CONCLUSIONS AND DIRECTION FOR FUTURE WORK

This chapter summarizes the major inferences drawn from the research work investigated and presented in this dissertation and recommendation toward the future scope of research.

6.1 Conclusions

A comprehensive experimental and theoretical investigation on the equilibrium CO_2 solubility as well as thermophysical property measurements of 35 different relative composition of solvent blends pertaining to 1-(2-aminoethyl) piperazine (AEP) and N-(3-aminopropyl)-1,3-propanediamine (APDA) activated N-methyldiethanolamine (MDEA) / 2-amino-2-methyl-1-Propanol (AMP) / 1-dimethylamino-2-propanol (1DMAP) solvents have been carried out over wide experimental conditions. A summary of the important findings and further suggestions of work in the investigated domain are also included in this Chapter.

- In the present work a precise experimental facility consisting of static equilibrium and buffer cell for measuring equilibrium CO_2 solubility has been developed. The developed system as well as experimental procedure has been validated with the initial solubility measurement in 0.30 mass fractions aqueous MDEA and aqueous MEA system. The results are in good agreement with the literature data.
- Equilibrium CO_2 solubility in aqueous (AEP), aqueous (APDA), (AEP + MDEA + H_2O), (AEP + AMP + H_2O), (APDA + MDEA + H_2O), (APDA + AMP + H_2O) and (APDA + 1DMAP + H_2O) with different relative amine compositions over the temperature range of (303.2 -333.2 K) and the CO_2 partial pressure up to 250 kPa have been experimentally determined in a temperature controlled static equilibrium cell. It is expected that the generated CO_2 solubility data in terms of P_{CO_2} vs α_{CO_2} of this work will be useful as a solubility database for the design of gas treating units.

- Among the aqueous solvents of AEP and APDA, the CO_2 solubility are higher in the APDA throughout the experimental range. From the results, it can be inferred for all the solvent blends investigated that CO_2 loading increases with the increase in P_{CO_2} at any particular temperature and amine concentration. Also the CO_2 loading decreases with rise in temperature at a constant pressure and amine concentration. While in blended solvents, the α_{CO_2} significantly rises upon addition of activators (AEP/APDA). For aqueous (AEP + MDEA) system, the α_{CO_2} enhanced by 54 % when the AEP concentration is increased from 0.05 to 0.25 mass fractions. APDA activated mixed solvent blends also shows a substantial enhancement in the α_{CO_2} upon increment in the concentration of APDA. Among APDA activated blends, AMP based blend records highest solubility of 1.17 at P_{CO_2} = 164 kPa and 303.2 K
- Modified Kent-Eisenberg model has been used to correlate and predict the CO_2 solubility in aqueous single as well as blended amine solvent. The equilibrium constants corresponding to the AEP and APDA deprotonation reaction and carbamate hydrolysis reaction are regressed as a function of CO_2 partial pressure, amine concentration and temperature by least square fitting method. Out of all the system studied, the lowest average absolute deviation between the experimental and model predicted results has been estimated to be 5.94 % for (AEP + MDEA+H_2O) blend, and 7.47 % for (APDA + MDEA + H_2O) while AAD corresponding to other system are also restricted within 10 %. This again proves that the modified KE equilibrium based thermodynamic model can be used for predicting the solubility of CO_2 in aqueous amine system with better accuracy.
- The equilibrium based model can be further extended to predict the pH of the CO_2 loaded amine solution, liquid phase speciation profile of all the probable ionic species with the variation in CO_2 loading. Qualitative ^{13}CNMR and ATR-FTIR analysis reveals the fact that bicarbonate formation dominates in the blended amine system which results in the higher CO_2 loading.
- Multilayer feed forward neural network model has also been employed to model and correlate the solubility data of CO_2 in aqueous amine system. The network architecture has been trained using Levenberg-Marquardt back propagation algorithm as a training function. The optimal design of the ANN was figured out by the trial and error method with the variation in the number of neuron. The developed model

predicted results are in good agreement with % AAD between the experimental and correlated solubility data has been found to be less than 8 % for the entire system understudy.

- In addition, important thermophysical properties such as density, viscosity and the surface tension of the unloaded aqueous amine solvents have been measured and reported over wide temperature range of (303.2 to 343.2) K. The density and viscosity data are correlated with Redlich-Kister and Grunberg –Nissan Models respectively. Surface tensions of the aqueous amine system are modeled using multiple linear regression technique as well as temperature-based correlation. The experimental results are at par with the model calculated results.
- The experimental viscosity data were utilized to analyze various thermodynamic properties such as enthalpy (ΔH^o), entropy (ΔS^o) and Gibbs energies (ΔG^o) of activation of viscous flow. These properties are determined by applying Andrade's theory. It can be inferred from the results that ΔG^o and ΔH^o values are +ve as ΔS^o are –ve across the entire composition and temperature range which reflects a strong interaction between the individual components of the solution mixture and the absence of any disorders in the viscous flow.
- At the end a comprehensive comparison with the conventional solvent blends indicates that the performance of both the single aqueous AEP/APDA as well their potential blends with MDEA/AMP are superior in terms of equilibrium solubility.

6.1.1 Environmental Impacts of current amine system

Amines and degraded compounds react under atmospheric conditions by photo oxidation to form several compounds called nitrosamines, nitramines, nitramides and amides. These compounds can also be produced by NOx derivate reactions with amines in the absorber.

N-nitrosamines cannot be formed directly from primary amine solvents. They can only be formed from other degradation products. Solvents with secondary and tertiary amine functionalities can directly form N-nitrosamines. The sterically hindered amine, AMP is considered to be more stable than MEA. Steric hindrance of AMP prevents dealkylation and avoids the formation of volatile compounds. Hence the proposed solvent used in the current study can be anticipated to form lesser nitrosamine.

Several alternatives have been proposed to mitigate amine and derivates emissions from CO_2 chemical absorption units. Recent studies showed that thermal decomposition of nitro-compounds is a promising technique to reduce nitrosamines and nitramines levels in the exhaust gas. Washing treatment with both water and acid aqueous solutions and UV radiation are the most common techniques. They can reduce those emissions up to 90%.

6.2 Recommendations for Future Work

- The present work mostly devoted to the generation of solubility data within 250 kPa CO_2 partial pressure. An essential next step should be the generation of solubility data at regeneration pressure and temperature.
- Heat of absorption (ΔH) is the major important parameter since it provides the magnitude of total heat released during the absorption and also to estimate the regeneration energy required to strip CO_2 from solvent. Hence this property should be measured experimentally using reaction calorimeter.
- Along with unloaded solvents the thermophysical properties of the CO_2 loaded amine solvents are also very much important for the accurate design of absorber cum regeneration unit. Hence, these properties need to be accurately measured along different temperature as well as CO_2 loading range.
- Simulation study of absorber-regenerator unit for the aqueous amine solvent studied in these work needs to be carried out in commercial simulator such as Aspen Plus®. Parametric effects need to be analyzed such as relative amine composition, temperature, absorber/regenerator pressure, liquid to gas ratio (L/G), reboiler duty, etc.
- Corrosion and solvent degradation are the major concern in the wide implementation of amine technology. Studies on oxidative and thermal degradation of all the activated as well as aqueous amine solvents should be taken in the future.

Appendix-I

Tabulated representation of thermo physical properties

Table I.1 Summary of the literature review of the density measurement of various aqueous single amine solvents

Solvent	Amine mass %	Temperature range (K)	Reference
Monoethanolamine (MEA)	20	303 – 333	Mandal et al. [5]
	30	293 – 323	Li et al. [6]
Diethanolamine (DEA)	10 – 30	293 - 373	Rinker et al. [9]
	30	293 - 323	Mandal et al. [5]
	20 – 30	313 – 353	Hsu et al. [10]
N-Methyldiethanolamine (MDEA)	10 – 50	293 - 373	Rinker et al. [9]
	30	293 - 323	Mandal et al. [5]
	20 – 30	303 - 333	Li et al. [6]
	10 – 50	288 - 323	Al-Ghawas et al. [12]
2- Amino-2-methyl-1-propanol (AMP)	30	293 - 323	Mandal et al. [5]
	20 - 30	303 - 333	Li et al. [6]
	9 – 100	293 - 363	Xu et al. [15]
Piperazine (PZ)	5.35 – 14.5	293 - 323	Derks et al. [16]
	1.74 – 30	298 – 333	Samanta et al. [17]
	1.98 – 7.91	303 - 313	Sun et al. [18]
	1.74 – 10.35	298 – 333	Murshid et al. [19]
2- Piperidineethanol (2-PE)	10 - 100	298 – 357.2	Xu et al. [21]
	1.38 – 12.9	313	Shen et al. [22]
2-Amino-2-ethyl-1,3-propanediol (AEPD)	4.94 – 25.63	303 – 318	Yoon et al. [23]
Dimethylpropanolamine (DMPA)	0 – 100 %	293 – 333	Narayana et al. [24]
Dimethylethylenediamine (DMEDA)	0 – 100 %	25 – 50 ^{o}C	Blanco et al. [25]

Table I.2 Summary of the literature review of the density measurement of various aqueous blended amine solvents

Solvent	Amine mass %	Temperature range (K)	Researcher
Monoethanolamine + N-Methyldiethanolamine	MEA: 1.5 – 9 MDEA: 21 – 28.5	293 – 323	Mandal et al. [5]
	MEA: 10 MDEA: 10	303 – 353	Hsu et al. [10]
	MEA : 5 – 24 MDEA : 5 – 24	303 – 353	Li et al. [27]
Monoethanolamine + 2 – Amino-2-methyl-1-propanol	MEA : 1.5 – 7.5 AMP : 22.5 – 28.5	293 – 323	Mandal et al. [5]
	MEA: 10 AMP : 10	303 – 353	Hsu et al. [10]
	MEA : 5 – 24 AMP: 5 – 24	303 - 353	Li et al. [27]
Diethanolamine + N-Methyldiethnaoalmine	DEA : 2.11 – 18.5 MDEA: 31.5 – 47.89	293 - 373	Mandal et al. [5]
	DEA: 1.5 – 9 MDEA: 21 – 28.5	293 - 323	Rinker et al. [9]
	DEA: 5 – 24 MDEA: 5 – 24	303 – 353	Hsu et al. [10]
Diethanolamine + 2-Amino-2-methyl-1-propanol	DEA : 1.5 – 9 AMP : 21 – 28.5	293 - 323	Mandal et al. [5]
	DEA: 5 – 24 AMP: 5 – 24	303 - 353	Hsu et al. [10]
Piperazine + 2- Amino-2-methyl-1-propanol	PZ : 2 – 8 AMP: 22 – 28	298 - 333	Samanta et al. [29]
	PZ : 0.86 – 3.44 AMP: 8.9	303 – 313	Sun et al. [18]
	PZ : 1.74 – 10.35 AMP : 19.65 – 28.26	298 – 333	Murshid et al. [19]
Piperazine + N-Methyldiethanolamine	PZ : 1 – 8.6 MDEA : 3.23 – 12.9	293 - 323	Derks et al. [30]
	PZ : 1.74 – 10.35 MDEA: 32.28 – 48.80	298 - 338	Mohammad et al. [20]
Monoethanolamine + Triethanolamine	MEA : 0.61 – 3.05 TEA : 7.45	303 – 313	Horng et al. [31]

Table I.3 Summary of the literature review of the viscosity measurement of various aqueous single amine solvents

Solvent	Amine mass %	Temperature range (K)	Researcher
Monoethanolamine (MEA)	30	293 – 323	Li et al. [6]
Diethanolamine (DEA)	10 – 30	293 - 373	Rinker et al. [9]
	30	293 - 323	Mandal et al. [5]
	20 – 30	313 – 353	Hsu et al. [10]
N-Methyldiethanolamine (MDEA)	10 – 50	293 - 373	Rinker et al. [9]
	30	293 - 323	Mandal et al. [5]
	20 – 30	303 - 333	Li et al. [6]
	10 – 50	288 - 323	Al-Ghawas et al. [12]
2- Amino-2-methyl-1-propanol (AMP)	30	293 - 323	Mandal et al. [5]
	17.8 – 26.7	296 - 318	Xu et al. [15]
Piperazine (PZ)	5.35 – 14.5	293 - 323	Derks et al. [16]
	1.74 – 6.88	298 – 333	Samanta et al. [17]
	1.98 – 7.91	303 - 313	Sun et al. [18]
	1.74 – 10.35	298 – 333	Murshid et al. [19]
2- Piperidineethanol (PE)	10 - 100	298 – 358.2	Xu et al. [21]
	1.38 – 12.9	313	Shen et al. [22]
2-Amino-2-ethyl-1,3-propanediol (AEPD)	4.94 – 25.63	303 – 318	Yoon et al. [23]
Dimethylpropanolamine (DMPA)	0 – 100 %	293 – 333	Narayan et al. [24]
Dimethylethylenediamine (DMEDA)	0 – 100 %	298 – 323	Blanco et al. [25]

Table I.4 Summary of the literature review of the viscosity measurement of various aqueous blended amine solvents

Solvent	Amine mass %	Temperature range (K)	Researcher
Monoethanolamine + N-Methyldiethanolamine	MEA: 1.5 – 9 MDEA: 21 – 28.5	293 – 323	Mandal et al. [5]
	MEA: 10 MDEA: 10	303 – 353	Hsu et al. [10]
	MEA : 5 – 24 MDEA : 5 – 24	303 – 353	Li et al. [27]
Monoethanolamine + 2 – Amino-2-methyl-1-propanol	MEA : 1.5 – 7.5 AMP : 22.5 – 28.5	293 – 323	Mandal et al. [5]
	MEA: 10 AMP : 10	303 – 353	Hsu et al. [10]
	MEA : 5 – 24 AMP: 5 – 24	303 - 353	Li et al. [27]
Diethanolamine + N-Methyldiethnaoalmine	DEA : 2.11 – 18.5 MDEA: 31.5 – 47.89	293 - 373	Mandal et al. [5]
	DEA: 1.5 – 9 MDEA: 21 – 28.5	293 - 323	Rinker et al. [9]
	DEA: 5 – 24 MDEA: 5 – 24	303 – 353	Hsu et al. [10]
Diethanolamine + 2-Amino-2-methyl-1-propanol	DEA : 1.5 – 9 AMP : 21 – 28.5	293 - 323	Mandal et al. [5]
	DEA: 5 – 24 AMP: 5 – 24	303 - 353	Hsu et al. [28]
Piperazine + 2- Amino-2-methyl-1-propanol	PZ : 2 – 8 AMP: 22 – 28	298 - 333	Samanta et al. [29]
	PZ : 0.86 – 3.44 AMP: 8.9	303 – 313	Sun et al. [18]
	PZ : 1.74 – 10.35 AMP : 19.65 – 28.26	298 – 333	Murshid et al. [19]
Piperazine + N-Methyldiethanolamine	PZ : 1 – 8.6 MDEA : 3.23 – 12.9	293 - 323	Derks et al. [30]
	PZ : 1.74 – 10.35 MDEA: 32.28 – 48.80	298 - 338	Mohammad et al. [20]

Table I.5 Summary of the literature review of the surface tension measurement of various aqueous single amine solvent

Solvent	Amine mass %	Temperature range (K)	Researcher
Monoethanoalmine (MEA)	0 – 100	298 – 323	Vazquez et al. [7]
	0 – 100	303 – 333	Han et al. [8]
Diethanoalmine (DEA)	0 – 100	298 – 323	Vazquez et al. [11]
N-Methyldiethanolamine (MDEA)	0 – 100	298 – 323	Alvarez et al. [13]
	32 – 48	303 – 333	Muhammad et al. [14]
Triethanolamine (TEA)	0 – 100	298 – 323	Vazquez et al. [11]
2-Amino-2-methyl-1-propanol (AMP)	0 – 100	298 – 323	Vazquez et al. [7]
Piperazine (PZ)	4.3 – 12.5	293 – 313	Derks et al. [16]
	1.74 – 10.35	298 – 338	Muhammad et al. [20]
	3.45 – 10.35	298 – 333	Murshid et al. [19]
2-Amino-2-ethyl-1,3-propanediol (AEPD)	20 – 80	303 – 343	Yoon et al. [23]
Dimethylpropanolamine (DMPA)	0 – 100	293 – 333	Narayan et al. [24]
Dimethylethylenediamine (DMEDA)	0 – 100	298 – 323	Blanco et al. [25]
2-Diethylaminoethanol (DEEA)	10 – 100	303 – 323	Fu et al. [26]

Table I.6 Summary of the literature review of the surface tension measurement of various aqueous blended amine solvents

Solvent	Amine mass %	Temperature range (K)	Researcher
Monoethanolamine + 2-Amino-2-methyl-1-propanol	MEA : 0 – 50 AMP : 0 – 50	298 – 323	Vazquez et al. [7]
N-Methyldiethanolamine + Monoethanolamine	MDEA : 0 – 50 MEA : 0 – 50	298 – 323	Alvarez et al. [13]
N-Methyldiethanolamine + Diethanolamine	MDEA : 0 – 50 DEA : 0 – 50	298 – 323	Alvarez et al. [13]
N-Methyldiethanolamine + 2-amino-2-methyl-1-propanol	MDEA : 0 – 50 AMP : 0 – 50	298 – 323	Alvarez et al. [13]
2-Diethylaminoethanol + Monoethanolamine	DEAE : 30 – 50 MEA : 5 – 15	303 – 323	Fu et al. [26]
2-Diethylaminoethanol + Piperazine	DEAE : 30 – 50 PZ : 5 – 15	303 – 323	Fu et al. [26]
N-Methyldiethanolamine + Piperazine	MDEA : 32 – 48 PZ : 1.74 – 10.35	298 – 338	Muhammad et al. [20]
	MDEA : 18 – 27 PZ : 3 – 12	293 – 333	Paul et al. [32]
2-Amino-2-methyl-1-propanol + Piperazine	AMP : 19.65 – 28.26 PZ : 1.74 – 10.35	298 – 333	Murshid et al. [19]
	AMP : 18 – 27 PZ : 3 – 12	293 – 333	Paul et al. [32]
(2-Methylamino)-ethanol + 2-Amino-2-methyl-1-propanol	MAE : 3 – 12 AMP : 18 – 27	298 – 323	Venkat et al. [33]
(2-Methylamino)-ethanol + N-Methyldiethanolamine	MAE : 3 – 12 MDEA : 18 – 27	298 – 323	Venkat et al. [33]

Appendix – II

Sample calculation

AII.1 Determination of solvent phase CO_2 loading (Chapters 4 and 5):

Liquid phase CO_2 loading (α_{CO_2}) can be defined as:

α_{CO_2} = mol of CO_2/ mol of amine

The concentration of CO_2 in the solvent phase have been determined by the methodology described in Chapter 4, Section 4.2.2

The total moles of CO_2 transferred to the equilibrium cell from buffer cell can be calculated as:

$$n_{CO2} = \frac{V_b}{RT}\left(\frac{P_{b1}}{Z_1} - \frac{P_{b2}}{Z_2}\right) \quad (1)$$

Where,

P_{b1} : Initial buffer cell pressure
P_{b2} : Final buffer cell pressure
V_b : Volume of buffer cell
R : Gas constant
T : Experimental temperature
Z_1 : Compressibility factor of CO_2 at T and P_{b1}
Z_2 : Compressibility factor of CO_2 at T and P_{b2}

Example: **Table 4.7** (Solubility data of 0.30 w aqueous AEP)

P_{b1} = 656.726 kPa P_{b2} = 556.544 kPa
V_b = 1200 ml R = 8.314 m^3kPa.$(kmole)^{-1}.K^{-1}$
T = 303.2 K Z_1= 0.9653
Z_2= 0.9703
Using all these given data, we can calculate n_{CO_2} from Eq. 1, n_{CO_2} = 0.051 mol

The moles of CO_2 remaining in the gas phase (n^g_{CO2}) after the attainment of phase equilibrium can be determined by:

$$n^g{}_{CO2} = \frac{V^g\ P_{CO2}}{Z_{CO2}RT} \quad (2)$$

Vg : Volume of gas phase in the equilibrium cell
P_{CO2} : Partial pressure of CO_2 = (P_T - P_v)
P_T : Total pressure in the equilibrium cell
P_v : Vapour pressure of aqueous amine solution
Z_{CO2} : Compressibility factor of CO_2 at T and P_{CO2}

Vg = 550 ml P_T = 8.880 kPa

Pv = 4.005 kPa P_{CO2} = 4.874 kPa Z_{CO2} = 0.9998

Using all these given data, we can calculate $n^g_{CO_2}$ from Eq. 2, $n^g_{CO_2}$ = 0.001064 mol

The moles of CO_2 absorbed in the solvent are then determined from the following equation

$$n^l_{CO_2} = n_{CO_2} - n^g_{CO_2} \quad (3)$$

$n^l_{CO_2}$ = 0.04975

The CO_2 loading in the solvent phase is defined as:

$$\alpha_{CO_2} = \frac{n^l_{CO_2}}{n_{am}} \quad (4)$$

Where, n_{am} is the total mole of amine in the solvent phase.

n_{am} = 0.1625

Hence, α_{CO_2} = 0.306 (mol of CO_2 / mol of amine)

Appendix- III

Error analysis

AIII.1 Estimation of error in the determination of CO_2 loading in solvent phase

$$\alpha_{CO_2} = \frac{n^{l}{}_{CO_2}}{n_{am}} = \frac{n_{CO_2} - n^{g}{}_{CO_2}}{n_{am}} = \frac{n_{CO_2} - \left(V_g P_{CO_2} \Big/ Z_{CO_2}.RT \right)}{n_{am}}$$

$$\alpha_{CO_2} = \frac{\frac{V_b}{RT}\left[\frac{P_1}{Z_1} - \frac{P_2}{Z_2}\right] - \frac{V_g P_3}{Z_3 RT}}{m_1 \times V_l} \qquad (P_3 = \text{Cell Pressure})$$

$$\alpha = \frac{V_b P_1}{RTZ_1 m_1 V_l} - \frac{V_b P_2}{RTZ_2 m_1 V_l} - \frac{V_g P_3}{RTZ_3 m_1 V_l}$$

$$\alpha = f(P_1, P_2, P_3, T, V_g, V_b, V_l, m_1)$$

$$\frac{\partial \alpha}{\partial P_1} = \frac{V_b}{RTZ_1 m_1 V_l}$$

$$\frac{\partial \alpha}{\partial V_b} = \frac{P_1}{RTZ_1 m_1 V_l} - \frac{P_2}{RTZ_2 m_1 V_l} = \frac{1}{RTm_1 V_l}\left[\frac{P_1}{Z_1} - \frac{P_2}{Z_2}\right]$$

$$\frac{\partial \alpha}{\partial P_1} = \frac{V_b}{RTZ_1 m_1 V_l}$$

$$\frac{\partial \alpha}{\partial m_1} = \frac{\frac{V_b}{RT}\left[\frac{P_1}{Z_1} - \frac{P_2}{Z_2}\right] - \frac{V_g P_3}{Z_3 RT}}{V_l} \cdot \left(\frac{-1}{m_1^{\,2}}\right)$$

$$\frac{\partial \alpha}{\partial V_l} = \frac{\frac{V_b}{RT}\left[\frac{P_1}{Z_1} - \frac{P_2}{Z_2}\right] - \frac{V_g P_3}{Z_3 RT}}{m_1} \cdot \left(\frac{-1}{V_l^{\,2}}\right), \qquad \frac{\partial \alpha}{\partial P_2} = -\frac{V_b}{RTZ_2 m_1 V_l}$$

$$\frac{\partial \alpha}{\partial P_3} = -\frac{V_g}{RTZ_3 m_1 V_l}, \qquad \frac{\partial \alpha}{\partial V_g} = -\frac{P_3}{RTZ_3 m_1 V_l}, \qquad \frac{\partial \alpha}{\partial T} = \frac{\frac{V_b}{RT}\left[\frac{P_1}{Z_1} - \frac{P_2}{Z_2}\right] - \frac{V_g P_3}{Z_3 R}}{m_1 \times V_l}\left(-\frac{1}{T^2}\right)$$

The absolute error associated with the calculation of CO_2 loading can be calculated as:

$$E_a = \left|\Delta P_1 \frac{\partial \alpha}{\partial P_1}\right| + \left|\Delta P_2 \frac{\partial \alpha}{\partial P_2}\right| + \left|\Delta P_3 \frac{\partial \alpha}{\partial P_3}\right| + \left|\Delta T \frac{\partial \alpha}{\partial T}\right| + \left|\Delta V_g \frac{\partial \alpha}{\partial V_g}\right| + \left|\Delta V_b \frac{\partial \alpha}{\partial V_b}\right| + \left|\Delta V_l \frac{\partial \alpha}{\partial V_l}\right| + \left|\Delta m_1 \frac{\partial \alpha}{\partial m_1}\right|$$

AIII.2 Sample calculation of estimated error in liquid phase CO_2 loading (Solubility data of 0.30 w aqueous AEP)

Temperature, T = 303.2 K
Initial Buffer cell pressure, P_1 = 656.725 kPa

Final Buffer cell pressure, P_2 = 556.544 kPa

Compressibility factor, Z_1= 0.9653

Compressibility factor, Z_2= 0.9703

Volume of Buffer cell, V_b m^3 = 0.0012 m^3

R, Universal gas constant, kPa.m^3/ kmol.K = 8.314

Volume of equilibrium cell = 0.0006 m^3

Volume of solvent in the equilibrium cell= 0.000050 m^3

Volume of gas phase in cell = 0.00055 m^3

Concentration of solution = 2.378 kmol.m^{-3}

ΔP_1 = 0.05 ΔP_2= 0.05 ΔP_3=0.05 ΔT = 0.1 K ΔVg = 0.000005 m^3

ΔV_b = 0.000005 m^3 ΔV_l = 1E-06 m_1 = 2.378 Δm_1 = 0.00025 Z_1 = 0.9653

Z_2 = 0.9703 Z_3 = 0.9998

$\frac{\partial \alpha}{\partial P_1}$ = 0.00401 $\frac{\partial \alpha}{\partial V_b}$ = 351.78 $\frac{\partial \alpha}{\partial P_2}$ = -0.00398 $\frac{\partial \alpha}{\partial m_1}$ = 0.1737

$\frac{\partial \alpha}{\partial V_l}$ = -8269.75 $\frac{\partial \alpha}{\partial P_2}$ = -0.00398 $\frac{\partial \alpha}{\partial P_3}$ = -0.00178 $\frac{\partial \alpha}{\partial T}$ = 2.33E-05

$\frac{\partial \alpha}{\partial V^g}$ = -15.734

Calculated Error in α_{CO2}= 0.011, % Error = 3.65 %

AIII.3 Estimation of standard uncertainty associated with thermo physical property measurement

Since all the experimental measurements of present work were conducted 3 times and the average value has been reported in the manuscript, so the revised value of Standard uncertainty has been calculated as per **NIST** definition:

The standard uncertainty $u\,(x_i)$ to be associated with x_i is the estimated standard deviation of the mean

$$u(x_i) = s(\overline{X_i}) = \left(\frac{1}{n(n-1)} \sum_{k=1}^{n} \left(X_{i,k} - \overline{X_i} \right)^2 \right)^{0.5}$$

The value of standard uncertainity of aqueous (**AEP + MDEA**) has been calculated based on each individual data set (Density, viscosity, and surface tension) over all concentration and temperature range and based on revised calculation the maximum standard uncertainity for the measured properties are:

Density measurement (**u (ρ) = 0.435 Kg.m^{-3}**)

Viscosity measurement (**u (μ) = 0.055 mPa.s**)

Surface tension measurement (**u (ϒ) = 0.266 mN.m^{-1}**)

Appendix – IV

Derivation of model equation for modified Kent – Eisenberg model

AIV.1 Derivation of equation (4.19) for (AEP + MDEA+H_2O) system

The equilibrium reaction taking place in the blended amine system and CO_2 can be expressed as:

Physical Solubility

$$CO_2(g) \overset{H_{CO_2}}{\rightleftharpoons} CO_2(aq) \quad \text{(R IV.1)}$$

Dissociation of bicarbonate ion

$$HCO_3^-(g) \overset{K_1}{\rightleftharpoons} CO_3^{2-} + H^+ \quad \text{(R IV.2)}$$

Formation of bicarbonate ion

$$CO_2 + H_2O \overset{K_2}{\rightleftharpoons} HCO_3^- + H^+ \quad \text{(R IV.3)}$$

Dissociation of water

$$H_2O \overset{K_3}{\rightleftharpoons} OH^- + H^+ \quad \text{(R IV.4)}$$

Deprotonation of AEP

$$AEPH^+ \overset{K_4}{\rightleftharpoons} AEP + H^+ \quad \text{(R IV.5)}$$

Carbamate hydrolysis of AEP

$$AEPCOO^- + H_2O \overset{K_5}{\rightleftharpoons} AEP + HCO_3^- \quad \text{(R IV.6)}$$

Deprotonation of MDEA

$$MDEAH^+ \overset{K_6}{\rightleftharpoons} MDEA + H^+ \quad \text{(R IV.7)}$$

The concentration based apparent equilibrium constants of reactions can be represented as:

$$K_1 = \frac{[CO_3^{2-}][H^+]}{[HCO_3^-]} \quad (1)$$

$$K_2 = \frac{[HCO^{3-}][H^+]}{[CO_2]} \quad (2)$$

$$K_3 = [H^+][OH^-] \quad (3)$$

$$K_4 = \frac{[AEP][H^+]}{[AEPH^+]} \quad (4)$$

$$K_5 = \frac{[AEP][HCO_3^-]}{[AEPCOO^-]} \quad (5)$$

$$K_6 = \frac{[MDEA][H^+]}{[MDEAH^+]} \quad (6)$$

The CO_2 partial pressure, P_{CO_2}, at equilibrium is related to the physically dissolved CO_2 concentration, $[CO_2]$, in the solvent phase by Henry's law expression.

$$P_{CO2} = H_{CO2}[CO_2] \quad (7)$$

Amine Balance:

AEP balance:

$$m_1 = [AEP]_t = [AEP] + [AEPH^+] + [AEPCOO^-] \quad (8)$$

MDEA balance:

$$m_2 = [MDEA]t = [MDEA] + [MDEAH^+] \quad (9)$$

CO_2 Balance:

$$\alpha_{CO2} \times ([AEP]_t + [MDEA]_t) = [CO_2] + [HCO_3^-] + [CO_3^{2-}] + [AEPCOO^-] \quad (10)$$

Electroneutrality balance:

$$[H^+] + [AEPH^+] + [MDEAH^+] - [HCO_3^-] - 2[CO_3^{2-}] - [OH^-] - [AEPCOO^-] = 0 \quad (11)$$

Let us denote all the species with following notations:

[AEP] = a, $[AEPH^+]$ = b, [MDEA] = c, $[MDEAH^+]$ = d, $[HCO_3^-]$ = e, $[CO_3^{2-}]$ = f, OH^- = g $[AEPCOO^-]$ = h,

From equation (3),

$$[OH^-] = \frac{K_3}{[H^+]}$$

$$g = \frac{K_3}{[H^+]} \quad (12)$$

From equation (2),

$$e = \frac{K_2.[CO_2]}{[H^+]} \quad (13)$$

Equation (1) can be further expressed as:

$K_1.e = [CO_3^{2-}]\,[H^+]$

$$K_1.K_2.\frac{CO_2}{[H^+]} = f[H^+]$$

$$f = \frac{K_1.K_2.[CO_2]}{[H^+]^2} \quad (14)$$

From equation (6),

$$K_6 = \frac{c.[H^+]}{d}$$

$$c = \frac{K_6.d}{[H^+]} \quad (15)$$

From equation (4),

$$K_4 = \frac{[H^+].a}{b}$$

$$a = \frac{K_4.b}{[H^+]} \quad (16)$$

From equation (5),

$$K_5 = \frac{a.e}{h}$$

$$h = \frac{a.e}{K_5} = \frac{K_4.b}{[H^+]}.\frac{K_2.[CO_2]}{[H^+].K_5}$$

$$h = \frac{K_2.K_4.[CO_2].b}{K_5.[H^+]^2} \qquad (17)$$

From equation (8),

$$m_1 = a + b + h$$

$$\Rightarrow m_1 = \frac{K_4.b}{\left[H^+\right]} + b + \frac{K_2.K_4.\left[CO_2\right].b}{K_5.\left[H^+\right]^2}$$

$$\Rightarrow m_1 = b.\left\{\frac{K_4}{\left[H^+\right]} + 1 + \frac{K_2.K_4.\left[CO_2\right]}{K_5.\left[H^+\right]^2}\right\}$$

$$\Rightarrow b = \frac{m_1}{\left\{\frac{K_4}{\left[H^+\right]} + 1 + \frac{K_2.K_4.\left[CO_2\right]}{K_5.\left[H^+\right]^2}\right\}}$$

$$\Rightarrow b = \frac{m_1}{\frac{K_4.K_5.\left[H^+\right] + K_5.\left[H^+\right]^2 + K_2.K_4.\left[CO_2\right]}{K_5.\left[H^+\right]^2}}$$

$$b = \frac{m_1.K_5.\left[H^+\right]^2}{K_4.K_5.\left[H^+\right] + K_5.\left[H^+\right]^2 + K_2.K_4.\left[CO_2\right]} \qquad (18)$$

From equation (9)

$$m_2 = c + d = \frac{K_6.d}{\left[H^+\right]} + d$$

$$d = \frac{m_2.\left[H^+\right]}{K_6 + \left[H^+\right]}$$

From electro neutrality balance:

$$\left[H^+\right]+b+d-e-2f-g-h=0$$

$$\Rightarrow\left[H^+\right]+\frac{m_1.K_5.\left[H^+\right]^2}{K_4.K_5.\left[H^+\right]+K_5.\left[H^+\right]^2+K_2.K_4.\left[CO_2\right]}+\frac{m_2.\left[H^+\right]}{K_6+\left[H^+\right]}-\frac{K_2.\left[CO_2\right]}{\left[H^+\right]}$$

$$-2.\frac{K_1.K_2.\left[CO_2\right]}{\left[H^+\right]^2}-\frac{K_3}{\left[H^+\right]}-\frac{K_2.K_4.\left[CO_2\right].b}{K_5.\left[H^+\right]^2}=0$$

$$\Rightarrow\left[H^+\right]+\frac{m_1.K_5.\left[H^+\right]^2}{K_4.K_5.\left[H^+\right]+K_5.\left[H^+\right]^2+K_2.K_4.\left[CO_2\right]}+\frac{m_2.\left[H^+\right]}{K_6+\left[H^+\right]}-\frac{K_2.\left[CO_2\right]}{\left[H^+\right]}-2.\frac{K_1.K_2.\left[CO_2\right]}{\left[H^+\right]^2}-\frac{K_3}{\left[H^+\right]}$$

$$-\frac{K_2.K_4.\left[CO_2\right].m_1}{K_4.K_5.\left[H^+\right]+K_5.\left[H^+\right]^2+K_2.K_4.\left[CO_2\right]}=0$$

After solving the above polynomial equation:

$$\left[H^+\right]^6.\left\{K_5\right\}$$

$$+\left[H^+\right]^5.\left\{K_5.K_6+K_4.K_5+m_1.K_5+m_2.K_5\right\}$$

$$+\left[H^+\right]^4.\left\{K_4.K_5.K_6\left[CO_2\right]+K_2.K_4.\left[CO_2\right]+m_1.K_5.K_6+m_2.K_4.K_5-K_2.K_5.\left[CO_2\right]-K_3.K_5\right\}$$

$$+\left[H^+\right]^3.\left\{\begin{matrix}K_2.K_4.K_6.\left[CO_2\right]+m_2.K_2.K_4.\left[CO_2\right]-K_2.K_5.K_6.\left[CO_2\right]-K_2.K_4.K_5.\left[CO_2\right]\\-2.K_1.K_2.K_5.\left[CO_2\right]-K_3.K_6.K_5-K_3.K_4.K_5-K_2.K_4.m_1.\left[CO_2\right]\end{matrix}\right\}$$

$$+\left[H^+\right]^2.\left\{\begin{matrix}-K_2.K_4.K_5.K_6.\left[CO_2\right]-K_2{}^2K_4.\left[CO_2\right]^2-2.K_1.K_2.K_5.K_6.\left[CO_2\right]-2K_1.K_2.K_4.K_5.\left[CO_2\right]-K_3.K_4.K_5.K_6\\-K_2.K_3.K_4.\left[CO_2\right]-m_1.K_2.K_4.K_6.\left[CO_2\right]\end{matrix}\right\}$$

$$+\left[H^+\right].\left\{-2.K_1.K_2.K_4.K_5.K_6.\left[CO_2\right]-2.K_1.K_2{}^2K_4.\left[CO_2\right]^2-K_2.K_3.K_4.K_6.\left[CO_2\right]-K_2{}^2.K_4.K_6.\left[CO_2\right]^2\right\}$$

$$-2K_1.K_2{}^2.K_4.K_6.\left[CO_2\right]^2=0$$

$$\Rightarrow A.[H^+]^6+B.[H^+]^5+C.\left[H^+\right]^4+D.\left[H^+\right]^3+E.\left[H^+\right]^2+F.\left[H^+\right]+G=0$$

Similarly, the equation corresponding to the estimation of CO_2 loading in aqueous blends of (AEP + MDEA) can be expressed as:

$$\alpha = \frac{1}{m}\left\{\left[CO_2\right]+\left[HCO_3^{-}\right]+\left[CO_3^{2-}\right]+\left[AEP\left(COO^{-}\right)\right]\right\}$$

$$\Rightarrow \alpha = \frac{1}{m}\left\{\left[CO_2\right]+\frac{K_2.\left[CO_2\right]}{\left[H^{+}\right]}+\frac{K_1.K_2.\left[CO_2\right]}{\left[H^{+}\right]^2}+\frac{K_2.K_4.\left[CO_2\right]}{K_5.\left[H^{+}\right]^2}.\frac{m_1.K_5.\left[H^{+}\right]^2}{K_4.K_5.\left[H^{+}\right]+K_5.\left[H^{+}\right]^2+K_2.K_4.\left[CO_2\right]}\right\}$$

$$\Rightarrow \alpha = \frac{1}{m}\left\{\left[CO_2\right]+\frac{K_2.\left[CO_2\right]}{\left[H^{+}\right]}+\frac{K_1.K_2.\left[CO_2\right]}{\left[H^{+}\right]^2}+\frac{m_1.K_2.K_4.\left[CO_2\right]}{K_4.K_5.\left[H^{+}\right]+K_5.\left[H^{+}\right]^2+K_2.K_4.\left[CO_2\right]}\right\}$$

$$\boxed{\alpha = \frac{P_{CO_2}}{H_{CO_2}.m_1}\left[1+\frac{K_2}{\left[H^{+}\right]}+\frac{K_1.K_2}{\left[H^{+}\right]^2}+\frac{m_1.K_2.K_4}{K_4.K_5.\left[H^{+}\right]+K_5.\left[H^{+}\right]^2+K_2.K_4.\left[CO_2\right]}\right]}$$

Appendix- V

Typical M-File and Program output

AV.1 Determining Density using Redlich – Kister equation for APDA + MDEA +Water using nonlinear regression method

```
clc
clear
format long e
%1 is for APDA, 2 for MDEA and 3 for H2O
 %calculation of densities of pure components
rho =[924.7 916.5 908.3 900.1 897.2;1033.7 1026.7 1019.4 1012.3 1006.2 ; 995.69 992.27
988.10  983.27 977.85] ;
%rhom is experimental densities of mixtures in kg/m3
%-------------------------------------------------------------------
T= [303.15 313.15 323.15 333.15 343.15];
 M= [131.22 119.16 18]; %M is molecular weights
% row indicates composition and column indicates temperature
rhom=[1019.77 1014.66 1009.01 1002.86 996.15
         1016.45  1011.47 1005.91 999.86   993.32
         1014.17  1009.03 1003.34  997.19 991.58]
 n=length (T);
%calculation of pure component volume at set of experimental temperatures from density above
for j=1:5
     v01 (j) = M(1) / rho(1,j);
     v02 (j) = M(2) / rho(2,j);
     v03 (j) = M(3) / rho(3,j);
     v0= [v01; v02; v03]*(1/1000); % v0 is in cm3/g.mol
 end
 % x1, x2, x3 are weight percentage 1 is for APDA , 2 for MDEA and 3 for H2O
```

```
x1=[4 7 10];
x2=[26 23 20];
x3=[70 70 70];
 %-------------------------------------------------------------------------
 % mole fractions are found using mass percentages

For ii=1:3 % 3 indicates the number of composition taken
xf1 (ii) =(x1(ii)/M(1)) / ((x1(ii)/M(1)) + (x2(ii)/M(2)) + (x3(ii)/M(3))); %mole fraction of APDA
xf2 (ii) =(x2(ii)/M(2)) / ((x1(ii)/M(1)) + (x2(ii)/M(2)) + (x3(ii)/M(3))); %mole fraction of MDEA
xf3 (ii) =(x3(ii)/M(3)) / ((x1(ii)/M(1)) + (x2(ii)/M(2)) + (x3(ii)/M(3))); %mole fraction of Water
xm (ii) =xf1(ii)*M(1) + xf2(ii)*M(2)+xf3(ii)*M(3); % xm is the average molecular weight of
components
 xf1;
 xf2;
 xf3;
 xm;
    for j = 1:5
s1(ii,j) = xf1(ii)*v0(1,j)+ xf2(ii)*v0(2,j)+xf3(ii)*v0(3,j);
% s1 is summation (sigma) of (mole fractions *pure component volume)
 % excess volume of liquid mixtures VE=Vm- sigma(x*Vio)
% vm is the molar volume of the liquid mixture and vi0 is the molar volume of the pure fluids at
the system temperature
 end
end
s1;
xm;
%-------------------------------------------------------------
for jj=1:5 %vm is molar volume calculate using mole fractions and density
    vm1(jj) = xm(1)/rhom(1,jj);
    vm2(jj) = xm(2)/rhom(2,jj);
    vm3(jj) = xm(3) / rhom(3,jj);
```

```
end
 vm=[vm1;vm2;vm3];
     VE=VM-s1;
 % VE is experimental excess molar volumes----------------------
%-------------calculation of Ai (pair temperature dependent parameter)---------
 %--------------v12, v23, v31 are excess volumes of pairs of AEP, MDEA and water respectively
  for ii=1:3
         p1(ii)=xf1(ii)*xf2(ii);
         p2(ii)=p1(ii)*(xf1(ii)-xf2(ii));
         p3(ii)=p1(ii)*(xf1(ii)-xf2(ii))^2;
         p11(ii)=xf2(ii)*xf3(ii);
         p21(ii)=p11(ii)*(xf2(ii)-xf3(ii));
         p31(ii)=p11(ii)*(xf2(ii)-xf3(ii))^2;
         p12(ii)=xf1(ii)*xf3(ii);
         p22(ii)=p12(ii)*(xf1(ii)-xf3(ii));
         p32(ii)=p12(ii)*(xf1(ii)-xf3(ii))^2;
  end
     v12= [p1; p2; p3]';
     v23= [p11; p21; p31]';
     v31= [p12; p22; p32]';
     v= [v12 v23 v31];
     r= pinv(v);
    A=r*ve;
    A1=A';
 for j=1:5
        t(j)=T(j);
        t2(j)=T(j)^2;
    end
    t1=t;
    t12 = t2;
    T2 = [ones (1,5); t1; t12];
```

```
T3 = T2';
B= pinv(T3);
coef=B*A1

a=coef(1,:)
b=coef(2,:)
c=coef(3,:)

for kk=1:5
  for nn=1:9
bb(nn,kk)=b(nn)*T(kk);
cc(nn,kk)=c(nn)*(T(kk))^2;
  end
end
for mm=1:5
  Ai1(mm)=a(1)+bb(1,mm)+cc(1,mm);
  Ai2(mm)=a(2)+bb(2,mm)+cc(2,mm);
  Ai3(mm)=a(3)+bb(3,mm)+cc(3,mm);
  Ai4(mm)=a(4)+bb(4,mm)+cc(4,mm);
  Ai5(mm)=a(5)+bb(5,mm)+cc(5,mm);
  Ai6(mm)=a(6)+bb(6,mm)+cc(6,mm);
  Ai7(mm)=a(7)+bb(7,mm)+cc(7,mm);
  Ai8(mm)=a(8)+bb(8,mm)+cc(8,mm);
  Ai9(mm)=a(9)+bb(9,mm)+cc(9,mm);

  AiAPDAMDEA= [Ai1; Ai2; Ai3];
  AiAPDAH2O  = [Ai4; Ai5; Ai6];
  AiMDEAH2O  = [Ai7; Ai8; Ai9];
end

for rr=1:5
```

```
ve121(rr)=p1(1,1)*AiAPDAMDEA(1,rr)+p2(1,1)*AiAPDAMDEA(2,rr)+p3(1,1)*AiAPDAMD
EA (3,rr);
ve122(rr)=p1(1,2)*AiAPDAMDEA(1,rr)+p2(1,2)*AiAPDAMDEA(2,rr)+p3(1,2)*AiAPDAMD
EA (3,rr);
ve123(rr)=p1(1,3)*AiAPDAMDEA(1,rr)+p2(1,3)*AiAPDAMDEA(2,rr)+p3(1,3)*AiAPDAMD
EA (3,rr);
ve12 = [ve121; ve122; ve123];

ve231(rr)=p11(1,1)*AiAPDAH2O(1,rr)+p21(1,1)*AiAPDAH2O(2,rr)+p31(1,1)*AiAPDAH2O(3,
rr);
ve232(rr)=p11(1,2)*AiAPDAH2O(1,rr)+p21(1,2)*AiAPDAH2O(2,rr)+p31(1,2)*AiAPDAH2O(3,
rr);
ve233(rr)=p11(1,3)*AiAPDAH2O(1,rr)+p21(1,3)*AiAPDAH2O(2,rr)+p31(1,3)*AiAPDAH2O(3,
rr);
ve23 = [ve231; ve232; ve233];
ve131(rr)=p12(1,1)*AiMDEAH2O(1,rr)+p22(1,1)*AiMDEAH2O(2,rr)+p32(1,1)*AiMDEAH2O(
3,rr);
ve132(rr)=p12(1,2)*AiMDEAH2O(1,rr)+p22(1,2)*AiMDEAH2O(2,rr)+p32(1,2)*AiMDEAH2O(
3,rr);
ve133(rr)=p12(1,3)*AiMDEAH2O(1,rr)+p22(1,3)*AiMDEAH2O(2,rr)+p32(1,3)*AiMDEAH2O(
3,rr);

ve13= [ve131; ve132; ve133];
 ve =ve12+ve23+ve13;
end
vm = ve+s1;
for zz=1:5
    Rhom1(zz)=xm(1,1)/Vm(1,zz);
    Rhom2(zz)=xm(1,2)/Vm(2,zz);
    Rhom3(zz)=xm(1,3)/Vm(3,zz);
```

```
Rhom=[Rhom1;Rhom2;Rhom3];
end
 %rhom is experimental densities of mixtures
 rhom;
 %Rhom is calculated densities of mixtures
 Rhom;
 %standard deviation calculation
x=Rhom-rhom;
x1=x.^2;
x2=sum(x1);
x3=sum(x2');
sd=sqrt(x3/(15-1))
%average absolute absolute deviation calculation
b_tr=abs(x);
P=b_tr./rhom;
P1=sum(P);
P2=sum(P1');
aad=(P2*100)/15
```

Network output:

```
rhom=[1019.77000000000    1014.66000000000    1009.01000000000    1002.8600000000
996.150000000000
1016.45000000000    1011.47000000000    1005.91000000000    999.860000000000
993.320000000000
1014.17000000000    1009.03000000000    1003.34000000000    997.190000000000
991.580000000000]

coeff=[12.4273732514720    -1.22278774993216    0.0391855691948203              -
12.8345970888763    -2.59159882702190    14.1572022331191    -10.1726753774314   -
0.584933122585369   9.72016103283800
```

-0.0774969056087128 0.00762868240757814 -0.000244490115417756
0.0810261572939696 0.0152915422637433 -0.0875178890109308 0.0644776308229622
0.00272212137307462 -0.0597930614844425

0.000119518769298435 -1.17647964826474e-05 3.77045083613173e-07 -
0.000124797694208213 -2.37273204797795e-05 0.000135100416245251 -
9.92992621930723e-05 -4.32322873392514e-06 9.23262461406447e-05]

ve= 0.0236762376529101 0.0237952296092341 0.0239284214417813 0.0240758131505522
0.0242374047355459

0.0237665957341258 0.0238841397077210 0.0240156069936801 0.0241609975920034
0.0243203115026904

0.0238312197481741 0.0239587982306839 0.0240926880634529 0.0242328892464817
0.0243794017797694

sd = 9.558515031399434e-002

aad = 5.370666586314290e-003

AV.2 Determining Viscosity using Grunberg-Nissan Equation for APDA + MDEA +Water

% viscosity regression using Nissan-Grunberg corelation

format short e

%1 is for AEP, 2 for MDEA and 3 for H_2O

M=[131.22 119 18]

%x1,x2,x3 are weight percentage 1 is for AEP, 2 for MDEA and 3 for H_2O

x1=[4 7 10]

x2=[26 23 20]

x3=[70 70 70]

T=[303 313 323 333 343]

```
%-------------------------------------------------------------------------

 % mole fractions are found using mass percentages
for i=1:3
   xf1(i)=(x1(i)/M(1))/((x1(i)/M(1))+(x2(i)/M(2))+(x3(i)/M(3)))
   xf2(i)=(x2(i)/M(2))/((x1(i)/M(1))+(x2(i)/M(2))+(x3(i)/M(3)))
   xf3(i)=(x3(i)/M(3))/((x1(i)/M(1))+(x2(i)/M(2))+(x3(i)/M(3)))
end
%-------------------------------------------------------------------------

% eta1, eta2 and eta3 are the viscosities of the pure components

   eta1=[7.87 5.4131 3.9673 3.0079 2.6337]
   eta2=[57.57 34.78 21.98 14.5 7.14]
   eta3=[0.845 0.668 0.559 0.476 0.412]

   %     etam is the experimental viscosities
etam=[3.48900396    2.493497477 1.894327285 1.364051734 1.040852885
3.620994449 2.70073976  2.071521185 1.547695472 1.170729302
3.899800351 3.08923545  2.241225164 1.667764232 1.201132315]

  % Viscosities of pure component
     for j=1:5
       lneta1(j)=log(eta1(j))
       lneta2(j)=log(eta2(j))
       lneta3(j)=log(eta3(j))
     end

    %-----------Viscosities of measured viscosities-------
     for ii=1:3 %ii indicates composition
```

```
    for n=1:5 %n indicates temperature
        lnetam(ii,n)=log(etam(ii,n));
    end
  end

%-------------------------------------------------------------------
 %ln etam=sigma(xlnetai)  + doublesigma (xixjiGij)
 %A=sigma(xlnetai)
 %B=doublesigma (xixjiGij)
    lnetam1=lnetam
  for m=1:3
    for k=1:5
      A(m,k)=(xf1(m))*(lneta1(k))+(xf2(m))*(lneta2(k))+(xf3(m))*(lneta3(k))
    end
  end

%-------------------------------------------------------------------
  B=lnetam1-A;
  for kk=1:3
  x12(kk)=xf1(kk)*xf2(kk); % calculation of coefficient attached to G
    x13(kk)=xf1(kk)*xf3(kk)
    x23(kk)=xf2(kk)*xf3(kk)
  end
    x123=[x12;x23;x13]
  C=x123
  B1=B'
  D=pinv(C)
  G123=B1*D
 %-------------------------------------------------------------------
 %----------Gij=a+bT+cT^2----------------------------------------
  for j=1:5
```

```
        t(j)=T(j)
        t2(j)=T(j)^2
    end
    t1=t
    t12=t2
    T2=[ones(1,5); t1; t12]
    T3=T2'
    B=pinv(T3)
    coef=B*G123

 %------------------------calculation of viscosity using the coefficients
   a=coef(1,:);
   b=coef(2,:);
   c=coef(3,:);
   for ii=1:5
      for jj=1:3
      bb(ii,jj)=b(jj)*T(ii);
      cc(ii,jj)=c(jj)*T(ii)^2;
      end
   end
G12=coef(1,1)*ones(5,1)+bb(:,1)+cc(:,1);
G23=coef(1,2)*ones(5,1)+bb(:,2)+cc(:,2);
G13=coef(1,3)*ones(5,1)+bb(:,3)+cc(:,3);
for mm=1:3
   for nn=1:5

Lnetam(mm,nn)=xf1(mm)*lneta1(nn)+xf2(mm)*lneta2(nn)+xf3(mm)*lneta3(nn)+x12(mm)*G1
2(nn)+x23(mm)*G23(nn)+x13(mm)*G13(nn);
   end
end
  % Etam is the calculated viscosity
```

```
Etam=exp(Lnetam)
% etam is the experimental viscosity
etam
%calculation of standard deviation
error=Etam-etam;
m=error.^2;
m1=sum(m);
m2=sum(m1)';
sd=sqrt(m2/14)
%calculation of average absolute deviation
b=abs(error);
P=b./etam;
P1=sum(P);
P2=sum(P1');
aad=(P2*100)/15
```

Network output:

```
coef = [8.3306e+004 -4.5149e+001 -4.7251e+003
 -5.6988e+002 7.0139e-001 3.1701e+001
  9.6581e-001 -1.5970e-003 -5.2492e-002]

Etam =
  [3.4969e+000 2.4969e+000  1.8611e+000  1.3948e+000  1.0324e+000
  3.6309e+000  2.6915e+000  2.0590e+000  1.5656e+000  1.1652e+000
  3.9523e+000 2.9909e+000  2.2793e+000  1.6844e+000  1.1919e+000]
sd = 3.4973e-002

aad =1.0684e+000
```

AV.3 Determination of surface tension using temperature based correlation for aqueous (APDA + AMP)

```
clc
clear
format long e
T = [303.15   313.15 323.15 333.15 343.15];
st = [ 48.88  48.12   47.78   47.19   46.56];
n= length(T)

for i=1:n
   T_sq(i)=T(i)*T(i);
   st_T(i)=st(i)*T(i);
end
a=sum(T);
b=sum(st_T);
c=sum(st);
d=sum(T_sq);
A=[n a; a d];
B=[c;b]
C=inv(A)*B;
k1=C(1)
k2=C(2)
for i=1:n
st_mod(i)=k1+(k2*T(i));
err1(i)=abs(st(i)-st_mod(i))/st(i);
end
AAD=100*sum(err1)/n
```

Network output:

```
St_mod(i) =[48.8199999999989       48.2629999999988     47.7059999999988
         47.1489999999988     46.5919999999988]
```

k1 = 6.570545499999935e+001

k2 = -5.570000000000164e-002

AAD = 1.460822354072891e-001

AV.4 Correlation of CO_2 solubility data using Modified Kent-Eisenberg Model

```
function [AAD] = VLE_AEP(xo)

g=xo(1);
h=xo(2);
q=xo(3);
r=xo(4);
s=xo(5);
y=xo(6);
z=xo(7);
g1=xo(8);
h1=xo(9);
q1=xo(10);
r1=xo(11);
s1=xo(12);
y1=xo(13);
z1=xo(14);
d1=xo(15);
```

P_exp= [6.688 50.339 129.187 173.162 205.319 5.343 10.590 28.165 75.036 118.714 161.544 4.033 7.612 17.416 63.259 111.599 140.577 156.87 183.987 4.937 8.446 16.182 41.362 80.538 122.444 160.076 183.807 4.875 8.356 14.376 29.53 80.351 100.829 130.097 157.359 175.21 4.613 7.715 12.383 24.042 31.468 69.003 99.050 132.683 162.634 189.509 4.013 6.605 9.887 11.728 14.3 26.696 55.565 87.867 119.383 154.222

181.029 1.703 8.391 59.977 110.985 154.96 183.352 208.153 2.551 6.550 36.404 77.842 124.864 160.510 192.915 2.765 5.523 12.617 35.115 60.439 102.877 138.674 162.247 185.965 2.861 6.191 10.749 25.421 38.321 79.628 116.694 153.381 192.433 2.779 5.605 9.729 18.588 38.769 81.117 112.633 157.869 185.855 2.979 7.067 10.983 17.802 27.317 52.690 86.060 141.081 158.317 3.275 6.46 9.591 16.327 23.608 36.473 61.191 83.392 119.734 140.984 156.966 5.861 59.564 114.57 162.902 192.467 211 5.212 28.551 52.442 99.119 125.947 161.144 193.343 3.178 17.823 47.925 83.399 138.729 166.536 189.716 3.323 9.046 20.553 39.273 77.207 125.485 155.229 186.062 4.978 10.556 19.678 34.336 52.704 107.862 135.861 165.054 191.336 3.799 7.308 14.624 26.076 51.325 71.595 112.578 137.151 169.383 3.999 8.287 14.003 20.340 46.291 79.841 122.761 150.478 180.339];

m1_exp= [0.770 0.770 0.770 0.770 0.770 1.170 1.170 1.170 1.170 1.170 1.170 1.57 1.57 1.57 1.57 1.57 1.57 1.57 1.57 1.972 1.972 1.972 1.972 1.972 1.972 1.972 1.972 2.378 2.378 2.378 2.378 2.378 2.378 2.378 2.378 2.378 2.786 2.786 2.786 2.786 2.786 2.786 2.786 2.786 2.786 2.786 3.195 3.195 3.195 3.195 3.195 3.195 3.195 3.195 3.195 3.195 3.195 0.770 0.770 0.770 0.770 0.770 0.770 0.770 1.170 1.170 1.170 1.170 1.170 1.170 1.170 1.570 1.570 1.570 1.570 1.570 1.570 1.570 1.570 1.570 1.972 1.972 1.972 1.972 1.972 1.972 1.972 1.972 1.972 2.378 2.378 2.378 2.378 2.378 2.378 2.378 2.378 2.378 2.786 2.786 2.786 2.786 2.786 2.786 2.786 2.786 2.786 3.195 3.195 3.195 3.195 3.195 3.195 3.195 3.195 3.195 3.195 3.195 0.77 0.77 0.77 0.77 0.77 0.77 1.170 1.170 1.170 1.170 1.170 1.170 1.170 1.570 1.570 1.570 1.570 1.570 1.570 1.570 1.972 1.972 1.972 1.972 1.972 1.972 1.972 1.972 2.378 2.378 2.378 2.378 2.378 2.378 2.378 2.378 2.378 2.786 2.786 2.786 2.786 2.786 2.786 2.786 2.786 2.786 3.195 3.195 3.195 3.195 3.195 3.195 3.195 3.195 3.195];

T_exp=[303.15 313.15 313.15

313.15 313.15 313.15 313.15 313.15 313.15 313.15 313.15 313.15 313.15 313.15 313.15
313.15 313.15 313.15 313.15 313.15 313.15 313.15 313.15 313.15 313.15 313.15 313.15
313.15 313.15 313.15 313.15 313.15 313.15 313.15 313.15 313.15 313.15 313.15 313.15
313.15 313.15 313.15 313.15 313.15 313.15 313.15 313.15 313.15 313.15 313.15 313.15
313.15 313.15 313.15 313.15 313.15 313.15 313.15 313.15 313.15 313.15 313.15 323.15
323.15 323.15 323.15 323.15 323.15 323.15 323.15 323.15 323.15 323.15 323.15 323.15
323.15 323.15 323.15 323.15 323.15 323.15 323.15 323.15 323.15 323.15 323.15 323.15
323.15 323.15 323.15 323.15 323.15 323.15 323.15 323.15 323.15 323.15 323.15 323.15
323.15 323.15 323.15 323.15 323.15 323.15 323.15 323.15 323.15 323.15 323.15 323.15
323.15 323.15 323.15 323.15 323.15 323.15];

alpha_exp=[0.709 1.029 1.167 1.249 1.322 0.510 0.795 1.016 1.182 1.273 1.293
0.286 0.558 0.785 0.983 1.093 1.151 1.197 1.221 0.278 0.510 0.729 0.910 1.033
1.118 1.164 1.188 0.306 0.502 0.714 0.844 0.985 1.049 1.117 1.143 1.172 0.276
0.492 0.642 0.770 0.883 0.978 1.031 1.113 1.151 1.161 0.199 0.333 0.464 0.585
0.687 0.812 0.921 1.009 1.064 1.077 1.091 0.419 0.755 0.984 1.099 1.161 1.201
1.229 0.404 0.731 0.883 1.045 1.130 1.162 1.185 0.274 0.505 0.731 0.877 0.971
1.041 1.091 1.133 1.153 0.241 0.477 0.658 0.797 0.929 1.006 1.047 1.108 1.125
0.225 0.442 0.591 0.707 0.835 0.944 1.03 1.078 1.1 0.180 0.384 0.543 0.666
0.782 0.877 0.962 1.040 1.056 0.163 0.319 0.444 0.575 0.692 0.77 0.866 0.943
0.989 1.023 1.036 0.6 0.898 1.067 1.111 1.145 1.16 0.382 0.672 0.873 0.994
1.072 1.122 1.147 0.312 0.549 0.823 0.953 1.020 1.064 1.087 0.230 0.427 0.618
0.764 0.902 0.989 1.036 1.052 0.271 0.438 0.569 0.679 0.813 0.925 0.984 1.017
1.036 0.214 0.395 0.544 0.685 0.808 0.901 0.955 0.986 1.003 0.156 0.345 0.471
0.608 0.721 0.820 0.892 0.936 0.961];

data=[P_exp' m1_exp' T_exp' alpha_exp'];

for i=1:length(data)
    P_{CO2}=data(i,1);
    m1=data(i,2);

```
T=data(i,3);
alpha=data (i,4);

%constants

% find the values of K1, K2, K3 from the litrature data
% using eq. ln Ki= ai + (bi/T) + ci lnT----------
%--------HCO3^3- <---> CO3^2- + H^+, K1 is the equilibrium constant
a1=220.067;
b1=-12431.7;
c1=-35.4819;
lnk1=a1+(b1/T) + (c1*log(T));
k1=exp(lnk1);
%----CO2+H2O <---> HCO3^- + H^+, K2 is the equilibrium constant
 a2=235.485;
 b2=-12092.1;
 c2= -36.7816;

 lnk2=a2+(b2/T) + (c2*log(T));
k2=exp(lnk2);

%------ H2O <---> OH^- + H^+, K3 is the equilibrium constant
 a3=140.932;
 b3=-13445.9;
 c3=-22.4773;
lnk3=a3+(b3/T) + (c3*log(T));
k3=exp(lnk3);

% ah=-6789.04; % for henry's law
% bh=-11.4519;
% ch=-0.010454;
```

```
% dh=94.4914;
% HCO2=exp((ah/T)+(bh*log(T))+(ch*T)+dh);

HCO2=exp ((20.2669)-(1.3806*(10^4)/T)+(0.06913*(10^8)/(T^2))-
(0.015589*(10^11)/(T^3))+(0.012*(10^13)/(T^4)));

% Henry's constant is in k Pa.m3/kmol

k4=g+ h*m1+q*T+ r*T*m1+s*T^2+y*PCO2+z*PCO2^2;
k5=g1+h1*m1+q1*T+r1*m1^2+s1*T*m1+y1*T^2+z1*PCO2+d1*PCO2^2;

Cx=PCO2/HCO2;

A=k5;
B=k5*(k4 + m1);
C=k2*k4*Cx - k2*k5*Cx - k3*k5;
D=-k2*k4*k5*Cx - 2*k1*k2*k5*Cx - k3*k4*k5 - k2*k4*m1*Cx;
E=-k2*k2*k4*Cx*Cx-2*k1*k2*k4*k5*Cx-k2*k3*k4*Cx;
F=-2*k1*k2*k2*k4*Cx*Cx;

eq=[A B C D E F];
HR=roots(eq);
HA=HR(HR>=1e-12&HR<=1e-5); %select the valid value of [H+]
H=real(HA(1)); %in case there are 2 values of [H+]
alpha= (Cx + (k2*Cx/H) + (k1*k2*Cx/H^2) + ((m1*k2*k4*Cx)/(k4*k5*H + k5*H*H +
k2*k4*Cx)))/m1;
%Cx/AM*(1+(AM*k2/(kc*H+kc*H^2/k1+k2*Cx))+k2*k3/H^2+k2/H);
error=((alpha-data(i,4)));
cal1(i,1)=alpha;
cal2(i,1)=abs(alpha-data(i,4))/data(i,4)*100;
end
```

```
 results=[cal1,cal2]
AAD=sum(cal2)/numel(cal2)
end


format long e
xo=[1.63216305577835e-07,-1.40742163773554e-09,-1.05614097156734e 09,
5.19644480603817e-12,1.71434124444015e-12,-1.80928130191410e-11,5.22635305912758e-
14,-0.0598412276108764,1.88794830176147e-06,0.0258574308090291,0.243218539534684,-
8.76185431016384e-2,0.0455080999298005,-0.000791655089781519,-9.67264052681091e-06]

options=optimset('MaxFunEvals',4000,'TolX',1e-500,'TolFun',1e-
50,'MaxIter',4000,'PlotFcns',{@optimplotx,@optimplotfunccount,@optimplotfval,@optimplotst
epsize});

[AAD,fval]=fminsearch(@VLE_AEP(xo),options)


Network output =

[1.63219861330434e-07     -1.41114159755379e-09     -1.05613879497514e-09
5.18714919726732e-12      1.71434798519520e-12      -1.80925455412281e-11
-5.22281453639149e-14     -0.0599320279993429       1.89163781030658e-06
0.0258709924236074         0.243136063917769        -0.0875200976020888
0.0476620006944974        -0.000791043970324173     -9.67230734092031e-06]

AAD = 9.05 %
```